KATHOLIEKE UNIVERSITEIT LEUVEN
FACULTY OF SCIENCES

DEPARTMENT OF EARTH AND ENVIRONMENTAL SCIENCES

A downscaling approach for air quality at a mid-latitude site using circulation patterns and surface meteorology

Matthias Demuzere

Promotor:
Prof. Dr. Nicole van Lipzig

Co-Promotor:
Dr. Koen De Ridder

Proefschrift voorgedragen tot het behalen van het doctoraat in de wetenschappen

Academiejaar 2008-2009

Leden van de examencommissie:

Prof. Dr. N.P.M. van Lipzig, promotor, Department Earth and Environmental Sciences, K.U.Leuven

Dr. K. De Ridder, co-promotor, Vlaamse Instelling voor Technologisch Onderzoek (VITO), Mol, Belgium.

Prof. Dr. G. Govers, Department Earth and Environmental Sciences, K.U.Leuven

Prof. Dr. G. Verstraeten, Department Earth and Environmental Sciences, K.U.Leuven

Prof. Dr. A. Van Rompaey, Department Earth and Environmental Sciences, K.U.Leuven

Prof. Dr. S. Carl, Quantum Chemistry and Physical Chemistry Section, K.U.Leuven

Dr. M. Werner, Alfred Wegener Institute for Polar- and Marine Research, Division Climate Science | Paleoclimate Dynamics, Bremerhaven, Germany

Dr. C. Mensink, Vlaamse Instelling voor Technologisch Onderzoek (VITO), Mol, Belgium.

Notice

Parts of this dissertation have been published in or are submitted to international scientific journals:

Chapter 3	Demuzere, M., Trigo, R. M., Vila-Guerau de Arellano, J. and van Lipzig, N. P. M., 2008. The impact of weather and atmospheric circulation on O3 and PM10 levels at a mid-latitude site. Atmos. Chem. Phys. Discuss. 8, 21037-21088.
Chapter 4	Demuzere, M., van Lipzig, N.P.M., 2008. A new method to assess air quality levels using a synoptic-regression approach. Part I: Present analysis for O_3 and PM_{10}. Atmospheric environment (submitted).
Chapter 5	Demuzere, M., Werner, M., van Lipzig, N. P. M. and Roeckner, E., 2008. An analysis of present and future ECHAM5 pressure fields using a classification of circulation patterns. International Journal of Climatology 29, 10.1002/joc.1821.
Chapter 6	Demuzere, M., van Lipzig, N.P.M., 2008. A new method to assess air quality levels using a synoptic-regression approach. Part II: Future O_3 projections. Atmospheric environment (submitted).
Chapter 7	Demuzere, M., De Ridder, K. and Van Lipzig, N. P. M., 2008. Modeling the energy balance in Marseille: Sensitivity to roughness length parameterizations and thermal admittance. Journal of Geophysical Research-Atmospheres 113, 1-19.

When referring to this dissertation, please refer to the references above.

Voorwoord

“There is not a tree in heaven higher than the tree of patience” zegt een Iers gezegde vrolijk, en voor mij vat deze zin de weg van deze dissertatie dan ook mooi samen. Vier jaar heb je de tijd om je eigen specifieke doctoraats onderwerp tot in de diepste dalen te verkennen, bloot te leggen en te beheersen. Dit proces doe je natuurlijk niet alleen, onderweg kruisen tal van mensen je pad, waarbij de een al meer dan de andere een bijdrage aan het totaal tracht te leveren. Vandaar dit korte voorwoord, om mijn oprechte dank te betuigen aan tal van personen, die me zowel mentaal als inhoudelijk hebben gesteund bij het realiseren van dit werk. Zoals mijn master thesis begeleider Frank een aantal jaar terug al opmerkte, hoop ik dat mijn vaak onnauwkeurige en te snelle manier van handelen ook hier niet zal leiden tot een veevuldig vergeten van een aantal personen. Om dit laatste obstakel te omzeilen zal ik proberen de logica van de chronologie te respecteren, te beginnen bij het indienen van het doctoraatsvoorstel tot het schrijven van dit voorwoord.

In de eerste plaats gaat mijn dank uit naar mijn promotor en co-promotor Nicole van Lipzig en Koen De Ridder respectievelijk. Eerst en vooral heeft Koen me (waarschijnlijk onbewust op dat moment) enorm gemotiveerd tijdens de master thesissen geografie en milieuwetenschappen om dingen in vraag te stellen, wat me de ogen heeft geopend naar de vele mogelijkheden van zelfstandig wetenschappelijk onderzoek. Dit doctoraatsvoorstel is dan ook door Koen geïnitieerd, en ondanks de lichte wijzigingen in het onderzoeksplan ben ik hem dan ook enorm dankbaar in mij te geloven en te steunen tijdens de periode van de IWT aanvraag. Na een jaar nam Nicole de taak op zich als promotor en heeft me gedurende de laatste drie jaar uitvoerig en met veel oog voor detail begeleid. Het enthousiasme, een vlotte samenwerking, continue mogelijkheid tot open dialoog en de grote (onderzoeks) vrijheid zorgde ervoor dat de weg tot het

schrijven van dit voorwoord zonder noemenswaardige problemen is verlopen. Hoogstens een dikke kiezel op een pas geasfalteerde boulevard, maar ook dit werd snel omzeild. Niet alleen heeft de vlotte samenwerking een stempel op dit onderzoeksschrift gedrukt, ook heeft het aanzienlijk bijgedragen tot een verdere persoonlijke ontplooiing en ondernemendheid, wat op zijn beurt heeft geleid tot tal van niet-doctoraat gerelateerde verwezenlijkingen.

Furthermore I would like to thank all members of the COST 733 action on the Harmonization of weather types in Europe, for providing a broad platform of discussion and knowledge concerning one of the key topics of my research. Especially, I would like to thank Ole Einar Tveito, Radan Huth, Christoph Frei, Zbigniew Ustrnul, Reinhard Schiemann, Christel Prudhomme, Anne Fleig, Christoph Beck, Arne Spekat, Pere Esteban, Javier Martin-Vide, Pavlos Kassomenos, Massimiliano Pasqui and Andreas Philipps for their continuous enthousiasm and help. Last but not least, the whole management committee is acknowlegded for accepting my proposals for my various scientific missions abroad.

During these scientific missions, I had the opportunity to experience research life in other universities or research centres. First, Martin Werner accepted to supervise me during a three months stay in the Max Planck Institute in Jena. During this stay, I set my first step in the world of climate models, climate data operating and lots of other elements which were indispensable during the remainder of my Ph.D. Secondly, Jordi Vila supported me during my stay at the meteorology and air quality department of the University of Wageningen. During these three months, I was taken through the world of air quality modelling, and since my visit we continued our cooperation, resulting (for now?) in a common publication. Thirdly, COST supported my third long-term scientific visit to the Department of Geophysics at the University of Lisbon, guided by Ricardo Trigo. Here, I was introduced to a large spectrum of statistical downscaling methods, and the appropriate ways to evaluate the downscaled results. It shouldn’t be mentioned that this visit, at the end of my Ph. D., provided me a clear overview on the possibilities and newest tendencies in statistical downscaling, but also provided me a interesting and quiet environment to finalize a great deal of my doctoral dissertation.

Velen hebben me ook in Leuven gesteund tijdens de jaren van onderzoek. Graag draag ik iedereen een warm hart toe, maar een aantal mensen wil ik toch graag persoonlijk bedanken. Toon heeft me gedurende de laatste drie jaar gezelschap gehouden op ons bureau in het GEO instituut. Als bureaugenoot was hij het eerste slachtoffer om mijn frustraties te aanhoren, maar steeds beantwoorde hij deze op zijn eigen gereide, sterk relativerende manier. Kwinten heb ik voor de eerste keer (echt) leren kennen toen ik hem gedeeltelijk mocht

begeleiden tijdens zijn master thesis en het schrijven van zijn doctoraatsvoorstel. Onze interesses liggen kort bij elkaar, zowel professioneel als privé, en we vonden elkaar dan ook snel om samen EGEA te introduceren in Leuven. Dit project bracht ons (en velen na ons) naar verschillende Europese uithoeken onder leiding van buitenlandse collega-geografie (doctoraat) studenten. Een periode om nooit te vergeten, en een basis voor een erg vertrouwde vriendschap die we hopelijk nog lang in stand kunnen houden.

Alle medewerkers van de onderzoeksgroep Fysische en Regionale Geografie zijn hartelijk bedankt voor de vriendschap, boeiende gesprekken en goede sfeer tijdens de (vele) pauzes. Ondanks het feit dat het intieme Instituut voor Aardwetenschappen in de Redingenstraat na een jaar werd ingeruild voor het killere en bombastische GEO instituut, bleef de sfeer opgewekt, gedragen door de donkerrode warme binnenmuur op ons verdiep. Meer specifiek bedank ik nog graag de leden van de onderzoeksgroep regionale klimaatsmodellering, in het bijzonder Dirk, Erwan, Tim en Irina, voor hun steun en hulp bij tal van technische en inhoudelijke klimatologische (en andere) problemen. Graag vermeld ik nog Wim Obbels en Jan de Laet van het LUDIT, voor hun hulp bij het opzetten van de modelsimulaties op de VIC supercomputer.

Verder bedank ik ook nog graag mijn ouders, die me altijd hebben gesteund en interesse toonden voor mijn studies en onderzoek. En hoewel ik het hen niet altijd gemakkelijk heb gemaakt gedurende mijn negen jaar durende loopbaan aan de K.U.Leuven, hebben hun constante motivatie en geloof in mij er toch voor gezorgd dat alles, zei het vaak op het laatste nippertje, steeds op zijn poten terecht kwam.

Als laatste, wil ik mijn grootste schat, fan, steun en toeverlaat Suus bloemen met nectar bedekte dankbetuigingen toewerpen! Samen hebben we dit doctoraatsbeestje klein gekregen, samen hebben we het ganse onderzoeksgebeuren de hemel ingeprezen en naar de diepste kerkers verwezen. Onze vele avonturen samen in het buitenland, zowel de werk- als plezierverblijven, de lange discussies over de zin en onzin van het onderzoek, het voortdurend enthousiasme en haar geloof in mij maakten het leven als doctoraatstudent mooi, eenvoudig en interessant. Beter kan je je niet wensen om een vier jaar durend doctoraatsonderzoek met een brede glimlach tot een goed einde te brengen.

Matthias

Abstract [English]

Clean air is essential to our own health and that of the environment. Since the industrial revolution, the quality of the air we breathe has deteriorated considerably for some chemical species (e.g. ozone (O_3) and particulate matter (PM)), which can lead to serious health problems. One the one hand, this is caused by a change in human activities, characterized by e.g. rising industrial and energy production, the burning of fossil fuels and especially a dramatic rise in traffic. On the other hand, the effect of a changing climate itself has the potential to increase average ambient concentrations and the frequency of pollution episodes. At present, levels of PM and the photochemical pollutant O_3 continue to exceed the thresholds set by the European Air Quality Directives, albeit various mitigation strategies are introduced since the late 70s to reduce (precursor) emissions. In this respect, most of the European emission reduction strategies do not take into account a change in climate conditions. As in the future O3 and PM are likely to remain of concern, this doctoral research aims to estimate the effect of future climate change on O3 (and PM) concentrations, assuming that future emissions remain at the present-day level.

This research develops a statistical downscaling method as a combination of two key techniques: 1) the objective Lamb circulation pattern classification describing the large-scale synoptic conditions and 2) a linear multiple regression analyses, relating surface meteorology to ozone concentrations. First, the circulation technique based on sea level pressure data describes for a given day the location of the high and low-pressure centres. After the classification, all members of each circulation-type class are ascribed to a linear regression equation, this for each season separately, taking into account a range of meteorological surface variables for a rural mid-latitude site in the Netherlands. The combination of the Lamb circulation pattern approach prior to a multiple

linear regression is a new approach in the statistical downscaling community and analyses have shown to significantly improve the observed O_3 non-linear characteristics. On the other hand, our research shows that PM_{10} is less influenced by the considered meteorological variables. Therefore, this technique is only applied on future climate scenarios for ozone.

The application of this technique on various climate change scenarios from a single global climate model shows an overall increase of maximum 8 hourly mean O_3 concentration with 2.5 to 6.5 and 6.1 to 10.9 µg/m³, for the 2051-2060 and 2091-2100 period respectively, against the present-day 10-year average of 55.2 µg/m³. This increase is even stronger when considering the summer season only. An increase in maximum temperature and shortwave radiation, associated with a decrease in cloud cover under the various future scenario assumptions are the main drivers of ozone increase. In order to verify whether these findings are physically plausible, our results are compared with the observed heat wave in August 2003, characterized by a poor air quality (especially in terms of O_3) and excess of mortalities in large parts of Western and Central Europe. Here, the observed O_3 concentration during August 2003 exceeded the European Air Quality Guidelines in Cabauw for 9 days, which lies in the upper range of our estimated number of exceedences for the 2050s and corresponds closely to the mean number of exceedences by the end of this century (9.7 days $month^{-1}$). This is confirmed by the exceptional warm and dry weather during August 2003, which characteristics corresponds to the climate change scenarios by the end of this century. This suggests, that, not only in terms of temperature, but also in terms of O_3, the August 2003 conditions could become representative for our future climate.

Abstract [Nederlands]

Zuivere lucht is essentieel voor onze gezondheid en dat van onze omgeving. Sedert het begin van de industriële revolutie nam de kwaliteit van de lucht drastisch af voor een aantal chemische componenten (zoals bijv. ozon (O_3) en fijn stof (PM)), wat aanleiding geeft tot aanzienlijke gezondheidsproblemen. Deze evolutie wordt enerzijds veroorzaakt door menselijke activiteiten en anderzijds beïnvloedt een veranderend klimaat zelf ook de concentraties van atmosferische polluenten en de frequentie van periodes met slechte luchtkwaliteit. Tot op heden overschrijden de concentraties van PM en de fotochemische polluent O_3 de limieten voorgeschreven door de EU, ondanks het feit dat sinds eind de jaren ’70 verschillende aanpassingsstrategieën werden ingevoerd met als doel de (precursor) emissies te verminderen. In dit opzicht houden de meeste van de Europese reductiestrategieën geen rekening met een verandering van de klimatologische omstandigheden. Net als in het heden verwacht men dat ook in de toekomst O_3 en PM de belangrijkste polluenten zullen blijven. Daarom beoogt dit doctoraatsonderzoek een schatting te maken van het effect van ons toekomstige klimaat op de O_3 (en PM) concentraties, onder de aanname dat in de toekomst concentraties gelijk blijven aan deze van vandaag.

Dit onderzoek ontwikkelt een statistische schaalverkleiningsmethode bestaande uit twee belangrijke benaderingen: 1) de Lamb circulatietype classificatietechniek die de grootschalige synoptische karakteristieken beschrijft en 2) een meervoudige lineaire regressie analyse die oppervlakte meteorologische variabelen met ozonconcentraties relateert. De classificatie techniek maakt gebruik van de druk op zeeniveau en geeft voor een bepaalde dag de locatie van de hoge en lage druk centra weer. Na deze classificatie

worden alle leden van een specifiek circulatietype toegeschreven aan een lineaire regressie vergelijking, dit voor elk seizoen afzonderlijk, waarbij verschillende meteorologische variabelen in rekening worden gebracht die kenmerkend zijn voor een landelijke locatie in Nederland. De combinatie van de Lamb circulatietypes voorafgaand aan een meervoudige lineaire regressie vertegenwoordigt een nieuwe aanpak wat betreft statistische schaalverkleiningsmethodes, waarbij analyses wijzen op een aanzienlijke verbetering van de waargenomen niet-lineaire eigenschappen van O_3. Anderzijds heeft dit onderzoek aangetoond dat PM concentraties in mindere mate te verklaren zijn aan de hand van meteorologische factoren die in deze studie in rekening gebracht. Daarom wordt de hier ontwikkelde techniek enkel toegepast op klimaatscenario's voor ozon.

De toepassing van bovenstaande techniek op klimaatscenario's van één klimaatmodel toont een algemene toename van de maximum 8-uurlijks gemiddelde ozonconcentraties met 2.5 tot 6.5 en 6.1 tot 10.9 µg/m³, voor de periode 2051-2060 en 2091-2100 respectievelijk, tegenover een huidig 10-jaar klimaatgemiddelde van 55.2 µg/m³. Dit effect is sterker in de zomer. De toename van de maximum temperatuur en kortgolvige neerwaartse zonnestraling, gepaard gaande met een afname van de wolkenbedekking in toekomstige klimaatscenario's zijn de belangrijkste drijfveren voor deze toename in ozon. Om na te gaan of onze bevindingen fysisch mogelijk zijn, vergelijken we onze resultaten met de waargenomen hittegolf tijdens augustus 2003, gekenmerkt door een slechte luchtkwaliteit en een sterke toename van het sterftecijfer in grote delen van West- en Centraal Europa. De geobserveerde ozon concentraties in augustus 2003 overschreden de Europese richtlijnen inzake luchtkwaliteit gedurende 9 dagen, hetgeen overeenkomt met het gemiddeld geschatte aantal overschrijdingen tegen het einde van deze eeuw (9.7 dagen per jaar). Dit onderzoek suggereert dan ook dat niet alleen in termen van temperatuur, maar ook in termen van ozon, de condities gedurende augustus 2003 representatief kunnen worden voor ons toekomstig klimaat.

Table of contents

List of commonly used symbols and abbreviations

Symbol/Abbreviation	Explanation
a	Constant (=0.13) from Zilitinkevich (1990) [-]
ANN	Artificial Neural Network
(AO)GCM/CGCM	(Atmospheric-Ocean) Coupled Global Climate Model
ARPS	Advanced Regional Prediction System
CC	Cloud Cover [Octas (1-8)]
C_R	Geometric coefficient [-]
Cd_0	Surface drag coefficient [-]
COST	European Cooperation in the field of Scientific and Technical research
CTM	Chemistry Transport models
C_p	Volumetric heat capacity [J m^{-3} K^{-1}]
DD / D010	Mean 10 meter wind direction [° from N]
e	Vapour pressure [hPa]
ECHAM5-MPI/OM	The coupled atmosphere-ocean model from the MPI of meteorology in Hamburg
ECMWF	European Center for Medium-range Weather Forecasting
ERA40	ECMWF reanalysis data (1957-2002)
EV / R^2	Explained Variance

F010	Mean 10 meter wind speed [m s^{-1}]
GWL	Grosswetterlagen
IPCC	Intergovernmental Panel on Climate Change
k	von Kármán's constant (=0.4) [-]
k	Thermal conductivity [W m^{-1} K^{-1}]
KNMI	Royal Dutch :Meteorological Institute
MLP	Multilayer perceptron (ANN technique)
MLR	Multiple linear regression model
MSE	Mean Square Error
(M)SLP	(Mean) sea level pressure [hPa]
NAO	North Atlantic Oscillation [-]
NCEP/NCAR	National Center for Environmental Prediction and the National Center for Atmospheric Research
Neff	Effective sample size
NO	Nitric oxide [μg/m^3]
NO_2	Nitrogen dioxide [μg/m^3]
O_3	Ground level ozone [μg/m^3]
P/P0	Surface Pressure [hPa]
PCA	Principal Component Analysis
PM	Particulate Matter [μg/m^3]
Pr	Prandtl number [-]
PRUDENCE	Prediction of Regional scenario and Uncertainties for Defining EuropeaN climate change risks and Effects project
q	Specific humidity [g kg^{-1}]
Q*	Incoming net radiation [W m^{-2}]
Q_E	Latent heat flux [W m^{-2}]
Q_F	Anthropogenic heat flux [W m^{-2}]
Q_{Fh}	Anthropogenic heat flux from households & services [W m^{-2}]
Q_{Fv}	Anthropogenic heat flux from traffic [W m^{-2}]
Q_H	Sensible heat flux [W m^{-2}]
ΔQ_s	Storage heat flux [W m^{-2}]
R	Pearson correlation coefficient
Rain	Daily mean precipitation [mm/day]
Rdur	Rain Duration [s]
RCM	Regional climate model
RE*	Roughness Reynolds number $(= u_{*0} z_0 / \nu)$

RH	Relative Humidity [%]
RIVM	National Institute of Public Health and Environment
RMSE	Root Mean Square Error
SDSM	Statistical DownScaling Model (Wilby et al., 2002)
SO_2	Sulphur dioxide [$\mu g/m^3$]
SOM	Self Organizing Maps
SRES	Second Report on Emission Scenarios (by IPCC)
$SS_{c,\,p}$	Skill score against climatology (c), persistence (p)
STARDEX	STAtistical and Regional dynamical Downscaling of Extremes for European regions project
St_0	Stanton number [-]
SWD	Shortwave Downward Radiation [W m^{-2}]
T	2m Air Temperature [K]
Tmax	Daily maximum 2m Air Temperature [K]
Tmin	Daily minimum 2m Air Temperature [K]
CC	Cloud cover [Octas (1-8)]
TD	2m Dew point Temperature [K]
Tprec	Daily mean precipitation [mm/day]
Ts	Surface temperature [K]
U	Wind speed [ms^{-1}]
$\bar{u}$	Mean wind speed [ms^{-1}]
u_*	Friction velocity [ms^{-1}]
VOC	Volatile Organic Compound [$\mu g/m^3$]
VPD	Vapour pressure deficit [hPa]
Z_{0h}	Roughness length for heat [m]
Z_{0m}	Roughness length for momentum [m]
β	Tuning parameter from eddy renewal model (Brutsaert, 1982) [-]
γ	Tuning parameter from eddy renewal model (Brutsaert, 1982) [-]
μ	Thermal admittance ($=\sqrt{kC_p}$) [J m^{-2} $s^{1/2}$ K^{-1}]
ν	Kinematic molecular viscosity for air ($=1.461\ 10^{-5}$) [m^2s^{-1}]
ρ	Density [Kgm^{-3}]

Chapter 1

Introduction

1.1 Background

1.1.1 Air quality in Europe: O_3 and PM_{10}

Air pollution produced by modern society is well known to cause damage to the environment and ill health for human beings. Rising industrial and energy production, the burning of fossil fuels and especially the dramatic rise in traffic on our roads all contribute to air pollution in the European (and other) region(s), which, in turn, can lead to serious health problems. For example, air pollution is increasingly being cited as the main cause of lung diseases such as asthma - twice as many people suffer from asthma today compared to 20 years ago.

Recognition of this in the European Union has resulted in legislation measures since the early 1970s, aimed at curtailing emissions of the most damaging of these pollutants, such as sulphur dioxide, lead, nitrogen oxides, carbon monoxide and benzene. However, despite a reduction in some harmful emissions, air quality continues to cause problems. Summer smog - originating in potentially harmful ground-level ozone (O_3) - regularly exceeds safe limits. Moreover, also high levels of particulate matter (PM) are a health risk that raises concern. As an example here, the EU has estimated “a statistical loss of life expectancy” for the Benelux region by one to three years, owing to the effects of particulate matter alone.

Ground-level ozone, unlike many other pollutants, is not emitted directly into the atmosphere, but is a secondary pollutant produced by the reaction between nitrogen oxides (NO_x), CO, volatile organic compounds (VOCs), hydrocarbons and incoming solar radiation. VOCs are emitted from a variety of manmade and natural sources. The former include motor vehicles, chemical plants, factories, consumer and commercial products and industrial sources. Plants are responsible for biogenic VOCs emissions in the form of isoprenes and monoterpenes, and more so with increasing temperature and light intensity. NO_x are emitted from motor vehicles, power plants and other sources of combustion, whereas its natural sources include lightning and emissions from the soil due to denitrification processes. Incoming solar radiation provides the energy to initiate ozone formation; consequently, high levels of ozone are generally observed during hot and sunny summertime weather. The sources of particulate matter, and conditions under which it is formed, are varied, resulting in a large spectrum of size, shape and chemical composition. PM consists of solid or liquid particles in the air, including dust, pollens and soot and aerosols from combustion activities. They can be emitted directly into the atmosphere and can form when gaseous pollutants such as SO_2 and NO_x undergo transformation to small particles. PM_{10} and $PM_{2.5}$ particles (particles with an aerodynamic diameter less than 10 µm) are of major current concern, as they are small enough to penetrate deep into the lungs and so potentially pose significant health risks (Bernard et al., 2001a, b).

In Europe, several Directives have been initiated to improve air quality, such as the 6th Environmental Action Plan that is in part a policy response these problems. The Clean Air for Europe programme (CAFE) within the 6th Environmental Action Plan has developed the thematic strategy for further reduction of air pollution and has recently prepared a proposal for a revised Air Quality Directive (EU, 2005). The Thematic Strategy on the Urban Environment has the objective to reduce the emissions in urban areas and to secure a healthy living environment for Europe's urban citizens. The Framework Directive and Daughter Directives are addressing regular assessment of air quality through monitoring and modelling in agglomerations with more than 250000 inhabitants. This requires the development of Action Plans for the improvement of air quality and defines obligations to inform the public on the air quality situation (EU, 2005).

1.1.2 Climate change prospects in Europe

During the 20th century, most of the European territory is characterized by an increase in average annual surface temperature (average increase over the continent 0.8 °C), with stronger warming over most regions in winter than in summer (Alcamo et al., 2007). The 1990s and 2000s were the warmest in the instrumental record. As an example, observed air temperature time series in Uccle (Belgium) show that, since the start of the measurements in 1833, the warmest

fourteen summers have occurred in the last nineteen years (1989-2008)(www.kmi.be). Precipitation during the 20th century showed an increase in northern Europe (10 to 40%) and a decrease in southern Europe (up to 20%). The most recent climate models predict an increase in annual temperature in Europe of 0.1 to 0.4 °C/decade over the 21st century. By the end of 2100, the temperature is predicted to be greater by 1.7 - 4.9 °C in winter and by 2.4 - 6.6 °C for summer compared to the end of the 20th century (Alcamo et al., 2007). Also, a very likely increase in the intensity and frequency of summer heat waves throughout Europe is predicted, as e.g. the summer heat wave of 2003 over large parts of (Central) Europe. Moreover, the models predict a widespread increase in precipitation in the north, small decreases in the south, and small or ambiguous change in central Europe. It is likely that the seasonality of precipitation will change and the frequency of intense precipitation events will increase, especially in winter.

The large spatial variability in the European climate change projections makes it necessary to develop regional (national) climate model projections in order to develop suitable mitigation or adaptation strategies for, among others, air quality abatement strategies and human health effects of climate change (Figure 1.1). Although this thesis doesn't aim to develop regional climate scenarios, it is important to have some background information on the current status of the developments in regional climate modelling. In the following sections, this information is narrowed down toward its role in future air quality levels.

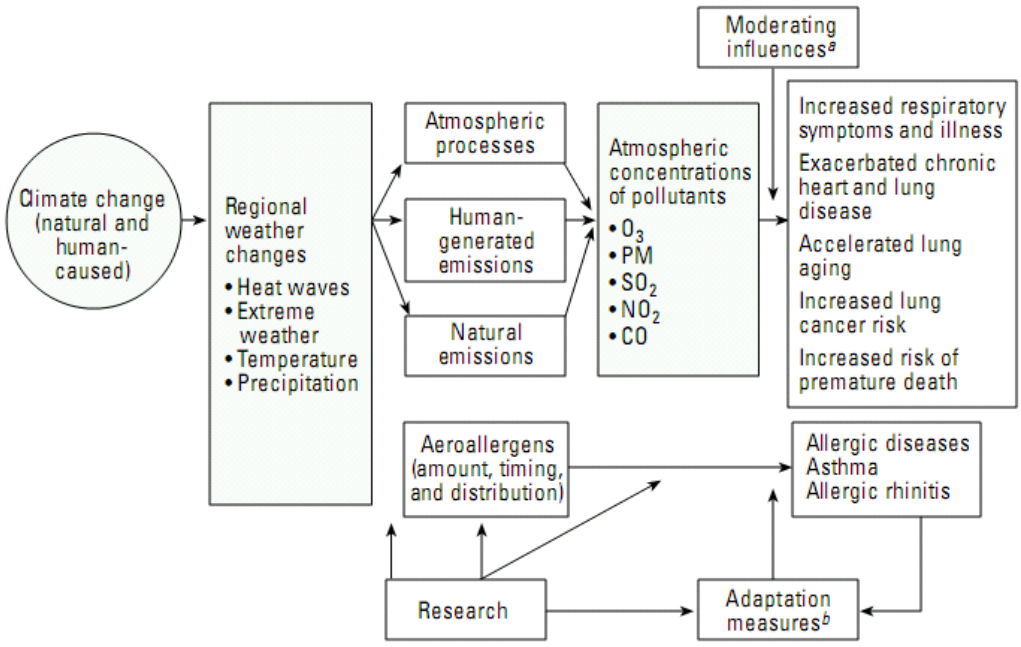

Figure 1.1: Climate change effects on air pollution and potential human health effects (Bernard et al., 2001)

Currently, a great deal of information on the variety of impacts of climate change is available for the whole of Europe through the efforts of the Intergovernmental Panel of Climate Change and all researchers involved. Nevertheless, the spatial variability in climate change predictions doesn't allow a uniform European climate policy adopted on e.g. the national level. Moreover, it is not only important to know how to react on climate change issues within the national boundaries, but also how neighboring countries have developed their scenarios and maybe more important; how they will manage to deal with these climate change scenarios. In Europe, a number of European countries have developed specific national climate scenarios with respect to adaptation strategies. For example, in Belgium, regional climate scenarios are developed by Boukhris et al. (2007), combining a statistical downscaling approach with frequency perturbation factors from the existing high-resolution model integrations from the European PRUDENCE project (Déqué et al., 2005). The KNMI (Royal Dutch Meteorological Institute) developed four climate scenarios; two scenarios based on an unchanged large-scale flow over The Netherlands and two scenarios based on a changed circulation patterns over The Netherlands, which then largely influence other meteorological variables as e.g. temperature and precipitation. For this purpose, they used global climate models from IPCC 4AR (Randall et al., 2007), regional climate models from the PRUDENCE project and historical Dutch measurement series. The U.K. developed regional climate scenarios over Great Britain based on the Hadley Centre Climate model (HadRM3) for four different emission scenarios (Jenkins et al., 2007). France developed climate scenarios using the ARPEGE model under the IMFREX project and Germany has set up a number of experiments for different regions in Germany based on the REMO, ECHAM and WETTREG models under various scenarios and spatial resolutions. Also, the German World Wildlife Fund ordered national German climate scenarios from the Hadley Centre, using their HADRM3 model (Bessembinder, J., 2007).

The above-mentioned paragraph reveals the current interest in, and the importance of, more region-specific impacts of future climate change. Moreover, the implications for our natural and anthropogenic (global and local) environment are crucial. It is apparent that regional climate variability and change already affects features and functions of Europe's production systems (e.g. agriculture), key economic sectors (e.g. tourism, energy) and its natural and anthropogenic environment. As an example of the latter, the impact of an increasing temperature on mortality is described extensively in the international literature (e.g. Wagner, 1999; Chan et al., 2001; Hayhoe et al., 2004). As heat waves are very likely to become more common and severe, heat-related deaths are likely to increase. Similarly, many authors have shown that climate change is likely to affect air quality in Europe (see sections 1.1.2 and 1.1.3). Nevertheless, air quality

measures are often disregarded or only marginally referred to in (inter)national policies on climate change scenarios.

1.1.3 Climate change effects on air pollution

Global warming has the potential to increase average ambient concentrations of pollutants and the frequency and intensity of pollution episodes. Local temperature, precipitation, clouds and atmospheric water vapor influence atmospheric chemical processes and interactions occur between regional-scale environments. Bernard et al. (2001) and Hogrefe et al. (2004) summarize three reasons why air quality is affected by a warmer and more variable climate:

1. Synoptic conditions: weather influences the dispersal and ambient concentrations of many air pollutants, while synoptic flow patterns govern pollutant transport. For example, subsidence during high-pressure situations often creates temperature inversions that can trap air pollutants in the boundary layer.
2. Rate constants of many chemical reactions increase with temperature, in so that higher temperatures are likely to increase the production of O_3 and PM levels when precursors are present.
3. Modification of biogenic emissions: increasing temperatures can lead to an increase of natural precursor emissions. For example, woody plants emit biogenic VOCs called isoprenes, which production is in first instance controlled by leaf temperature and light. These VOCs are, besides NO_x, an important precursor in the ozone formation process.

In the future, the pollutants of concern are likely to remain, as now, PM and the photochemical pollutant O_3 (Bernard et al., 2001). Emissions of sulfur oxides and NO_x due to power generation might increase, but control technologies are available and can control such emissions. At present, most of the emission strategies referred to in section 1.1.1 do not take into account a change in climate-driven variables such as atmospheric temperature and humidity. Before these effects can be introduced, it is of considerable importance to understand the relation between meteorology and air-quality (especially O_3 and PM_{10}) in a present-day climate, before applying this information on a future climate.

Therefore, the first aim of this dissertation is to describe the individual relations between the meteorological predictor variables and O_3 and PM_{10} levels in a present-day climate. Secondly, this information is used to develop a statistical air-quality downscaling tool that considers the combined effect of the large-scale atmospheric circulation and surface meteorology on air-quality levels. The methodology is first calibrated and validated for the present-day climate using observations of meteorological variables. Afterwards, the validation is extended

using operational low-resolution present-day model information. Doing so, one can quantify the limitations of the statistical downscaling tool itself and the possible effect of model deficiencies and scale-dependencies of the surface meteorological predictor variables on modelled air-quality levels.

Afterwards, the statistical downscaling tool is applied to future climate scenarios in order to estimate the effect of the latter on future O_3 and PM_{10} concentrations, under the assumption of constant future emissions. In this respect it is important to point out that this step is a first attempt to assess future air quality levels on a local/regional scale. In order to develop more detailed relevant information towards policy makers in the framework of future Air quality Directives, this research has to be extended and performed in a broader community or project. A first continuation of this is foreseen in the CLIMAQS project (CLimate IMpact and Air Quality modelling for policy Support), intended to, amongst others, conduct long-term regional climate impact and air-quality simulations for the Flemish region.

1.2 Key research questions

For Europe, major uncertainties in future climate projections include the uncertainties associated with the still insufficient resolution of AOGCMs (Atmospheric Ocean coupled Global Climate Models), with the downscaling techniques and with regional climate models. In this respect, the 4th IPCC assessment report states that *"Although numerous studies have tackled a great deal of expected climate change impacts and vulnerabilities, studies on present and future air quality trends are still of indisputable importance"* (Alcamo et al., 2007).

In general, this dissertation follows a downscaling approach to bridge the gap between the information gained from AOGCMs and the information required by the impact assessors (Wilby & Wigley, 1997). In the remaining of this dissertation, we follow a simple categorization of the downscaling techniques (Hewitson and Crane, 1996, 2001): statistical and dynamical downscaling. Both techniques are discussed in more detail in sections 2.2 and 2.3 respectively. From a practical point-of-view, the dynamical downscaling techniques are computationally expensive and time consuming, whereas a statistical downscaling is a computationally more efficient and practical approach in addressing the current needs of high-resolution climate modelling results for impact and assessment studies. From a physical point-of-view, the dynamical approach dynamically derives local (or regional) atmospheric variability from large-scale forcings. Thereby, the model itself resolves the physical properties of the atmosphere, whilst the statistical approach derives quantitative relations between

large-scale circulation indices and local climate or environmental variables from observations or reanalysis data using mathematical or statistical relationships (Figure 1.2). This dissertation first develops a statistical downscaling approach based on a circulation pattern (section 2.2.1) and a multiple regression (section 2.2.2) approach in order to statistically derive point-specific information on air quality for the rural background station of Cabauw. Afterwards, a first step in dynamical downscaling approach (section 2.3) is undertaken. In this respect, the regional atmospheric model ARPS (Advanced Regional Prediction System) is evaluated in terms of some meteorological variables important for air quality modelling (Chapter 7).

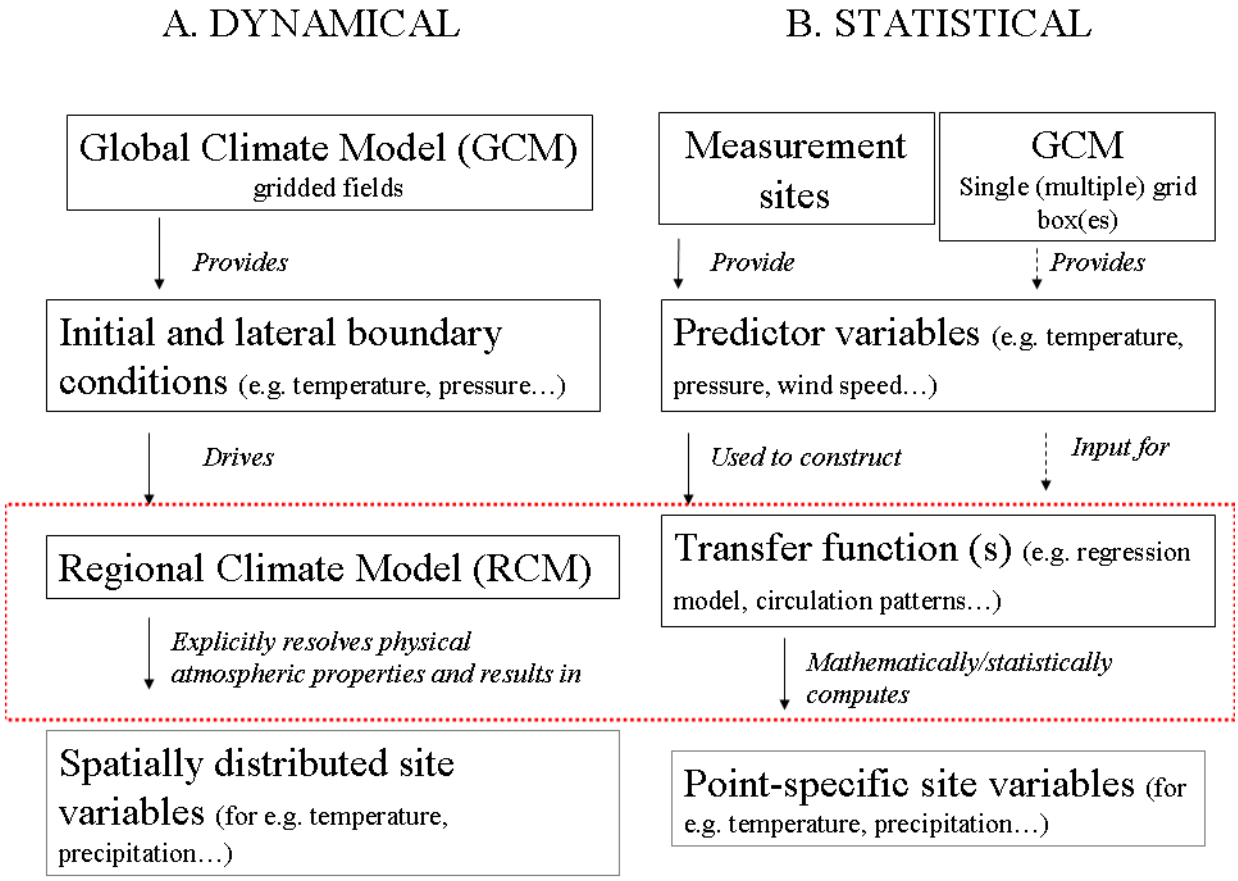

Figure 1.2: A general conceptual representation of the dynamical (A.) and statistical (B.) downscaling approaches. The red dotted box shows the downscaling step itself.

Based on these techniques, the main objective of this dissertation is to understand the effect of the variations in large-scale circulation and surface meteorology on O_3 and PM_{10} levels. In order to reach that goal, the following strategy is used:

- Derivation of the statistical relations between meteorological variables and several air quality variables (with a focus on O_3 and PM_{10}) for a rural mid-latitude site.

- Development and evaluation of a novel approach to downscale large-scale meteorological data from (low-resolution) models with the intention to derive future regional-scale O_3 and PM_{10} projections.

- Evaluation of the low-resolution global ECHAM5-MPI/OM model in terms of large-scale circulation patterns for present-day and future climate.

- Application and quantification of this novel approach on future climate scenarios from ECHAM5-MPI/OM with respect to the European Guidelines for air quality and air quality assessment.

1.3 Outline of this thesis

The thesis consists out of 6 chapters, with a preceding introductory chapter (Chapter 1), followed by a general discussion and final conclusion in Chapter 8 (Figure 1.3). Three appendices are added and present: A) an overview and recent advances in circulation classification methodologies, B) comments on the objective Lamb classification scheme and C) a possible strategy to extend the spatial applicability of this approach. Chapters 3-7 and Appendix A have been written as research papers, published or submitted to international scientific journals. At the beginning of each chapter that is based on published (or publication intended) data, a footnote indicates the paper on which the information is based and mentions the current status of the paper. Since each paper was intended to be read independently, some overlap may occur between the various chapters, especially in the introduction and data sections.

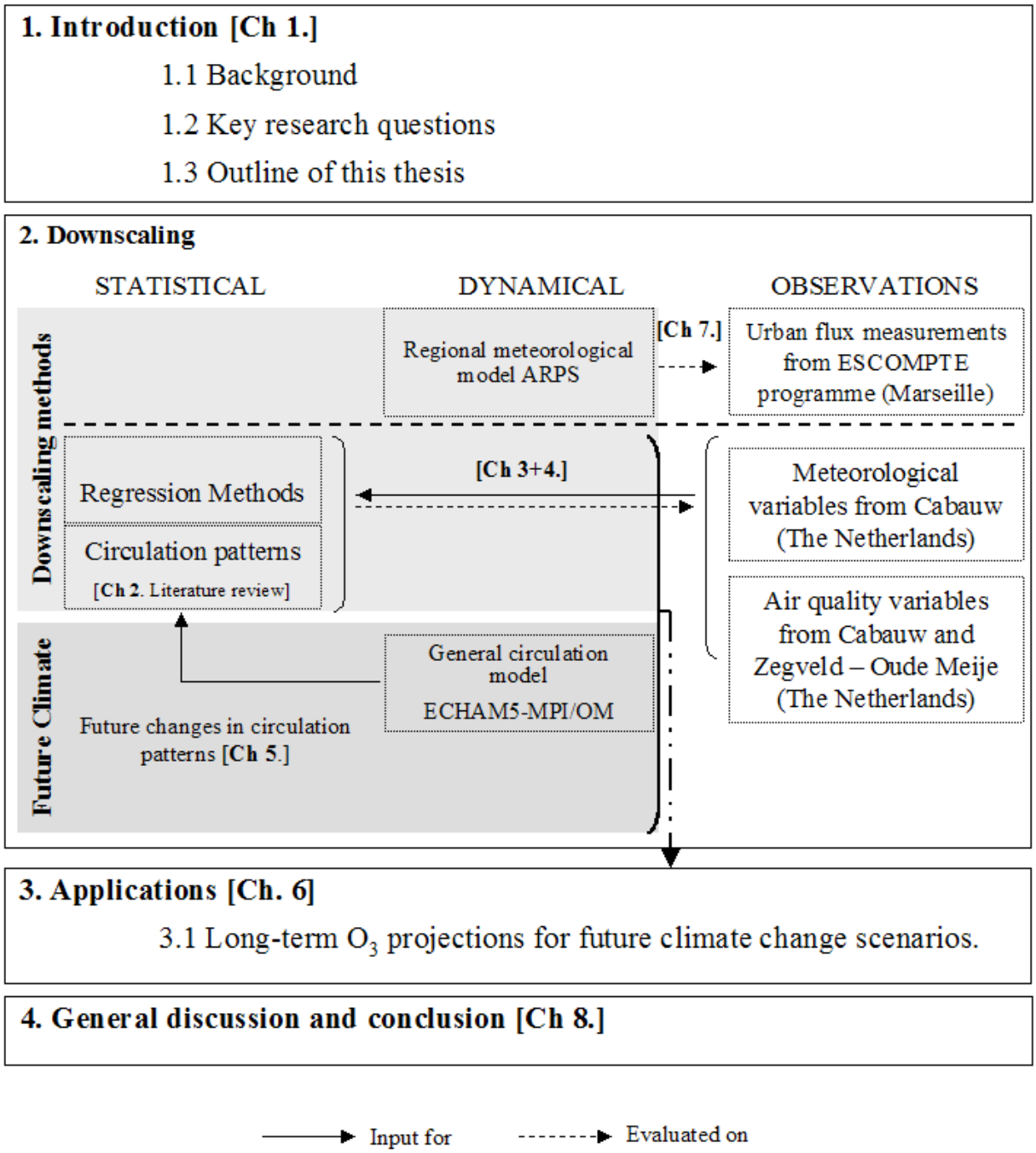

Figure 1.3: Dissertation research approach.

As an introduction to this research theme, chapter 1 describes, in short, present air- quality related issues and climate change impacts (with a focus on air quality) for Europe. This chapter briefly discusses the current research status on global and regional climate modelling, air quality research and the key uncertainties related to this topic. It concludes with formulating the specific objectives of this study.

Chapter 2 gives a review of the current status of dynamical and statistical downscaling methods used for current and future regional impact studies and air quality applications. Conclusively, it describes an intercomparison between both dynamical and statistical applications and provides more insight in the state-of-the-art air-quality applications.

In the following chapters 3 and 4, the physico-chemical relations between meteorology and air quality variables are described. This is first addressed in chapter 3. Secondly, an effort is done to develop a method that is able to downscale regional observed and low-resolution meteorological variables with respect to the air quality variables. This is done for the rural mid-latitude sites in The Netherlands. Chapters 3 and 4 describe the novel approach combining large-scale circulation patterns and a stepwise multiple regression technique.

Chapter 5 subsequently evaluates an AOGCM in terms of its circulation characteristics and explores a possible change of these large-scale circulation patterns under future climate change scenarios.

As global circulation models do not provide any information on surface air quality levels, one has to downscale them indirectly from other modelled (meteorological) variables. Therefore, chapter 6 applies the novel approach developed in chapters 3-5 to estimate the effect of changing meteorological conditions on O_3 levels under changing climate scenarios. For the latter, it is important to mention that these implications assume emission scenarios as described in SRES from IPCC, without any further information or tendencies for O_3 precursor emissions itself. Therefore, this research only explains this part of the O_3 variability explained by changes in meteorology. Furthermore, this chapter does not provide a clear insight in future tendencies in O_3 levels, but describes only a first step in estimating local future levels of O_3, as is mentioned in section 1.1.

Chapter 7 describes the evaluation of the mesoscale meteorological model ARPS (Advanced Regional Prediction System) for the urban energy balance in Marseille. A large intensive measurement campaign in the larger Marseille area provided a great deal of interesting data to test the model in terms of roughness length parameterizations and thermal admittance. These elements largely influence the urban surface fluxes that alternatively affects the boundary layer characteristics that play a major role in air quality dispersion. This study aims to contribute to the often-disregarded implementation of urban-specific thermal characteristics into mesoscale models, and a further implementation of this approach in densely populated areas, often associated with large air quality problems.

Finally, chapter 8 synthesis results in a general discussion and conclusion.

In addition, three appendices are added tackling some aspects of the objective classifications methods. Appendix A presents a more detailed overview on the objective classification of atmospheric circulation patterns. As this statistical downscaling method dominates a large part of this dissertation, this section introduces in more detail the available classification methods and describes the recent developments and tendencies in applications. Appendix B illuminates some inconsistencies between Chapters 5 and 6 using the objective Lamb classification method for different areas and grid configurations. Appendix C describes a possible strategy to extend the spatial applicability of the synoptic-regression based approach. This is not done in the current status of the research, but provides possible strategies for future work on this topic.

Chapter 2

The principle of downscaling: a literature review

2.1 Introduction

The climate change information required for many impact studies is of a spatial scale much finer than that provided by atmospheric ocean coupled global climate models (AOGCMs). Global climate models today still have resolutions of hundreds of kilometers, whilst regional climate models may be as fine as tens of kilometers. However, a great deal of impact assessment studies requires information equivalent to point observations, which are highly sensitive to local-scale climate variations not taken into account in coarse-scale models. Therefore, one can use a downscaling approach to bridge the gap between what AOGCMs produce (large-scale) and what impact assessors require (equivalent to point observations) (Wilby & Wigley, 1997). It consists in seeking relationships between variables simulated by AOGCMs and regional or local surface climate (or environmental) variables. A first attempt to classify the different approaches for regional climate modelling was done by Giorgi and Mearns (1991), by identifying three basic methodologies: empirical, using information from past climate analogues, semi-empirical, based on the statistical downscaling of GCM fields and modelling approaches, using physical models such as regional climate models (RCMs). Hewitson and Crane (1996) revised this classification by describing only two categories of downscaling methods: process-based techniques, involving the explicit solving of the physical dynamics of the system and empirical techniques that use the identified

relationships derived from observational data. Afterwards, Wilby & Wigley (1997) suggested four categories of downscaling methods: regression methods, weather-pattern based approaches, stochastic weather generators and limited-area models. This literature review follows Hewitson and Crane (1996, 2001), using a downscaling categorization that differentiates between the empirical based (statistical) and process-based (dynamical) downscaling techniques. Each approach is discussed in more detail in the following sections 2.2 and 2.3 respectively. A short description of each method and their advantages and disadvantages are summarized in Table 2.1 below. Hereby, the stochastic weather generators (Richardson, 1981; Rackso et al., 1991) described as a statistical downscaling method by Wilby et al. (2004), are excluded from this literature overview. This tool produces artificial time series of weather data for a location based on the statistical characteristics of the observed weather at that location (Richardson, 1981; Rackso et al., 1991). As this technique requires long continuous time series of observed daily weather (at least 10 years), which are often not available for air quality observational records, this technique is not suitable for our purposes and therefore is not included in this literature review.

Table 2.1: Overview of the advantages and disadvantages of dynamical and statistical downscaling tools (compiled from Mearns et al., 2003, Wilby et al., 2004).

Tool	Description	Method	Advantages	Disadvantages
Dynamical models	Providing information at a high spatial/ temporal resolution	Regional/ Mesoscale climate models	Provides very high resolved spatial and temporal information Information is derived from physically-based models Many variables available Better representation of some weather extremes than in GCMs	Computationally expensive, and thus few multiple scenarios Lack of two-way nesting may raise concern regarding completeness Additive errors due to model configuration, parameterizations, domain size and model resolution Dependent on (usually biased) inputs from driving AOGCM

Statistical models	Providing information at a point/high spatial resolution	Circulation patterns e.g. analogue method, hybrid approaches, fuzzy classification, PCA, Self Organizing Maps (SOM),…	Provides very highly resolved spatial and temporal information Potential to address a diverse range of variables Rapid application to multiple GCMs Suitable for locations with limited computational resources Yields physically interpretable linkages to surface climate Compositing for analysis of extreme events	Assumes constancy of empirical relationships in the future Demands access to daily observational surface and/or upper air data that spans range of variability Dependent on (usually biased) inputs from driving AOGCM May not capture intra-type variations in surface climate
		Regression methods e.g. linear regression, neural networks, kriging, canonical correlation analysis, …	Provides very high resolved spatial and temporal information Potential to address a diverse range of variables Rapid application to multiple GCMs Suitable for locations with limited computational resources Straightforward to apply 'Off-the-shelf' solutions and software available	Assumes constancy of empirical relationships in the future Demands access to daily observational surface and/or upper air data that spans range of variability Dependent on (usually biased) inputs from driving AOGCM Poor representation of observed variance and extreme events May assume linearity and/or normality of data

2.2 Statistical downscaling

In this approach, one seeks to derive quantitative relations between large-scale circulation indices and local climate or environmental variables. This transfer function is derived from observations using a mathematical or statistical relationship. Statistical downscaling is, compared to dynamical downscaling, computationally efficient, and is a practical approach in addressing the current needs of high-resolution climate modelling results for impact and assessment studies. This technique is analogous to the "perfect prog" and "model output statistics (MOS)" approaches used for short-range numerical weather prediction (Klein and Glahn, 1974).

Within this statistical downscaling group, one can appoint three subdivisions, as was also suggested by Wilby & Wigley (1997): circulation types, regression methods and stochastic weather generators. As the latter demands long observational records (10 years or more), which are not available in the field of air quality, we opt to test and evaluate the former two methods, and therefore, only these methods are described in more detail below (sections 2.2.1 and 2.2.2).

2.2.1 Classification of circulation patterns

In general terms, classification is a task of grouping entities (cases) so that they share common features (are similar) within each group, while being dissimilar between groups. In the context of the thesis, the word ‘group’ has a meaning similar to ‘class’, ‘cluster’ or ‘type’; all these terms are used interchangeably. The degree of (dis)similarity may be quantified by a variety of metrics, usually based on distance (e.g. Euclidean distance). Classifications have had a long history in meteorology and climatology. At the dawn of meteorology when it was established as an independent science, classifications (in those days called usually ‘catalogues of synoptic types’) were used mainly in weather forecasting.

The usage of classifications has widened in recent decades, especially after the advent of computers, which made it possible to develop and routinely apply objective methods, based on processing large amounts of data. The advance of computers, led at the same time, to a change in the methodology of weather prediction, which lost its interest in classifications. As a consequence, the main driver of the progress in classifications in the atmospheric sciences turned from weather prediction to climatology. At present, various classification methods are used in many fields of the atmospheric sciences for a large spectrum of purposes, making classification one of the most important fields in synoptic and statistical climatology.

Since the field of classifications in meteorology and climatology is quite wide and difficult to cover in total, this section is limited to the applications of classifications of atmospheric circulation patterns (based on sea level pressure), an approach that is used in the following chapters of this thesis. Classifications of other atmospheric entities and phenomena are mentioned only briefly with the intention of providing a broader context. Furthermore, a more detailed description of the availability of different classification approaches, their basic algorithms, input variables and the recent advances are given in Appendix A.

2.2.1.1 Current climate applications

Circulation pattern classifications have a long history in synoptic meteorology, and therefore have a large range of applications for the present-day and future climate. In this section, some of these approaches are addressed in more detail, in order to provide insight in the possible applications and capabilities of the circulation pattern classification schemes.

The development of an improved data set of reconstructed, gridded, monthly SLP data for the period 1780-1995 (Jones et al. 1999) within the framework of

the EU funded research Project ADVICE (Annual to Decadal Variability In Climate in Europe) offers the opportunity to expand synoptic climatological analyses well beyond the 20th century. Moreover, as the SLP data were reconstructed using solely station pressure data and can thus be assumed to be independent of surface climate variables (temperature, precipitation). It enables analysis of variations in the relationship between large-scale atmospheric circulation and regional-scale surface climate over these periods for which climate forcing is negligible (such as the latter decades of the Little Ice Age) and thus having anthropogenic activities of global concern (i.e., the present industrial period).

Beck et al. (2007) analyzed the the importance of low-frequency and within-type changes of atmospheric circulation types for Central European climate variations based on the automated circulation classification scheme from Beck (2000). Using classification results and mean central European temperature and precipitation time series, both available for more than 200 years, temperature and precipitation changes in central Europe were broken down into frequency changes of circulation types and changes attributable to within-type changes of the circulation types. The decomposition was performed for moving 31-year time windows with annual time steps by comparing each 31-year period to its adjacent 31-year periods shifted by 1 year, thereby using the decomposition scheme according to Barry and Perry (1973). This approach resulted in time series of the total, the frequency induced, and within-type related variations in central European temperature and precipitation over the whole 1780–1995 period. From this, the most remarkable overall finding is that only about half of the climatic variations can be explained by varying circulation type frequencies. Remaining parts are due to changing within-type characteristics of several major circulation types. Percentages of frequency-related and within-type induced changes do not only differ between seasons and climate variables (substantially higher importance of within-type variability during summer and concerning precipitation) but are also varying over many decades, the latter pointing to non-stationarities in circulation-climate relationships which are relevant for the application of downscaling approaches.

In the course of examination of historical circulation variability, the development of a gridded SLP reconstruction dataset for the European and North Atlantic domain on a daily basis back to the year 1850 (Ansell et al., 2006) was an important milestone. Within the EU-funded project EMULATE (European and North Atlantic Daily to Multidecadal Climate Variability), intensive studies on circulation changes covered in this dataset have been untertaken making intensive use of circulation type classification. Within the course of EMULATE conventional k-means clustering was found to be unstable and an enhanced clustering algorithm has been developed utilising Simulated

ANnealing and Diversified RAndomisation (called SANDRA), which is much more stable especially for large datasets (for details see Philipp et al. 2007).

Based on the SANDRA technique, significant changes in circulation showed that significant trends in interannual variability of cluster frequencies between 1850 and 2003 can be observed in all seasons. In winter a remarkable result is that a significant overall increase in the frequency of westerly patterns is manifested mainly for a pattern describing cyclones north of the British Isles, while a North Atlantic Oscillation (NAO)-like circulation type, which has been increasing in frequency since 1985, also showed high frequencies in the relatively cold period between 1850 and 1870. This means that there is no significant increasing trend in frequency for the positive NAO state over these 150 years, contrary to what was assumed before (e.g. Hurrel and van Loon, 1997). At the same time, a significant decrease in frequency of continental cold highs is confirmed for the whole period 1850–2003.

Altogether the classification approach shows that changes in the daily circulation-type frequencies have clearly contributed to the long-term warming in Europe. The NAO does not seem to be the only driver of circulation-dependent warming in central Europe but has mainly contributed to the enhanced warming since about 1985. All in all, the exact contribution of changes in atmospheric circulation to the observed climate change in historical times is still an open question, but circulation-type classifications have been proven to be a useful tool to narrow down the lack of knowledge and therefore are subject to ongoing improvements. However, the data quality for the early instrumental period, even if remarkable advances in reconstructions are made, is still limited. More reliable conclusions are possible when using more recent data of a higher quality. In this respect, two examples of such “advanced” applications are given. In the first, the changes in the lifetime of circulation types are analyzed, together with their implications for the severity of temperature extremes, while in the second, the effect of changes in the frequency of circulation types on trends in surface climate elements is examined.

The increasing lifetime of circulation types, which would be indicative of increasing persistence of atmospheric circulation in general, was reported for zonal Hess-Brezowsky types (see Appendix A) in winter by Werner et al. (2000). Kyselý (2002) extended the analysis and showed that the increasing lifetime of the Hess-Brezowsky types is observed for all the types and in all seasons. Kyselý and Domonkos (2006) examined persistence separately in individual seasons and for 10 groups of types (Hess-Brezowsky types) and found out that, using the standard normal homogeneity test (Alexandersson and Moberg, 1997), 67% of the timeseries of lifetimes have a significant change

point during the 1980's, while change points in period 1881-1980 were detected in 8% of the series only. Furthermore, Kyselý and Huth (2006) analyzed the lifetime changes for types in the Hess-Brezowsky catalogue and in an objective classification based on T-mode PCA combined with k-means cluster analysis. The lifetime of Hess-Brezowsky types increases rapidly from about 1980 and peaks about 1990 for both winter and summer, being about two days longer than any time since 1881. The objective types persist longer in winter, although the change is not as pronounced as for the Hess-Brezowsky catalogue and the values reached are fairly close to high values from the 1960's and 1970's, but change very little since 1980 (in summer). The difference in the lifetime changes between the Hess-Brezowsky and objective types can have several causes (Kyselý and Huth 2006): first, there may be an inhomogeneity in the subjective catalogue, although it is stated to be homogeneous (Gerstengarbe et al. 1999); second, the Hess-Brezowsky catalogue poses a limitation on the minimum duration of types (3 days), while for the objective one, short events of one or two days are typical; third, the objective catalogue possesses a large number of unclassified days (about 20% in winter and 35% in summer), contrary to about 1% in Hess-Brezowsky; and fourth, the objective catalogue is based solely on 500 hPa heights, whereas Hess-Brezowsky reflects both mid-tropospheric and near-surface circulation characteristics.

An enhanced persistence of atmospheric circulation appears to contribute to the severity of extreme temperature events of both signs (Kyselý 2002; Domonkos et al. 2003; Kyselý 2007). In this respect, Kyselý (2007) confirms that there are two main causes of the formation of heat waves: warm advection (originating in eastern and southerly types) and anticyclonic conditions (as in types with central European high). Whereas the persistence of an anticyclone leads to an increase of temperature in the course of its duration, the warm advection does not have such an effect. This means that an enhanced severity of heat waves would result from increased lifetimes of situations with stationary anticyclones, where positive radiation balance and air mass stagnation (the absence or reduction of the removal of locally heated air, e.g., by passages of atmospheric fronts) acts as a physical mechanism. On the other hand, changes in the lifetime of advective types would not affect the severity of heat waves.

The importance of atmospheric circulation on recent climate change is frequently considered. Several recent studies examined the impact of changes in the frequency of circulation types on trends in surface climate elements. In such studies, conditional mean values of climatic elements are calculated for circulation types, their trends (which imply that the circulation changes are the only source of the long-term changes) are evaluated, and these 'hypothetical' trends are compared to the observed ones (e.g, Leathers and Ellis 1996; Huth 2001; Keevalik and Russak 2001). Changes in the frequency of circulation types

were found to contribute to spring drying in Portugal (Corte-Real et al. 1998), drought in Spain (Vicente-Serrano and López-Moreno 2006), and a dramatic precipitation decrease in southwestern Australia (Hope et al. 2006). The effects of atmospheric circulation on climate trends in the Czech Republic were analyzed using the Hess-Brezowsky catalogue for eleven climate variables: daily mean, minimum, and maximum temperature, precipitation amount and occurrence, relative humidity, cloudiness, sunshine duration, zonal and meridional wind components, and wind speed. The analysis was conducted at 21 stations for the period 1961-1998. The 'hypothetical' trends, reflecting only changes in the frequency of Hess-Brezowsky types, were calculated for all variables at all stations and divided by the actual trends. The more this ratio approaches one, the more long-term circulation changes affect the trend in the particular surface element. Negative values of the ratio indicate that circulation changes act in the direction opposite to the observed changes. Here, it is shown that changes in the frequency of Hess-Brezowsky circulation types explain about half of the temperature trends and non-negligible portions of relative humidity, cloudiness, and sunshine duration trends in winter. In spring, circulation changes are partially effective in explaining trends in relative humidity, cloudiness, and sunshine duration, whereas for temperature variables, the share of explained trends is about 20% and less. In summer, circulation trends contribute to surface climate trends fairly negligibly. In autumn, circulation explains considerable amounts of cooling trends (between 20% and 50%), as well as the trends in precipitation occurrence, cloudiness, and sunshine duration. Note also that the ratio of trend explained by circulation changes has a large spread across stations for precipitation occurrence and wind speed. For precipitation amount and wind components, the number of stations with significant trends is very low and no conclusions can be made for them.

2.2.1.2 Future climate applications

With more AOGCM runs becoming available, the analyses of changes of circulation types under future climate conditions are increasing. Changes in the frequency of circulation types from the current climate conditions to future (usually to the end of the 21st century) are examined as a first step in all studies of this kind (Cassano, 2006a, Corte-real et al., 1998, Chapter 5 - Demuzere et al., 2008a , Hope, 2006, Huth, 1996, 1997, Kidson and Watterson, 1995, Lynch et al., 2006, McKendry et al., 2006, Saunders and Byrne, 1996, Schoof and Pryor, 2006). A few of these studies also examine changes in the circulation patterns themselves (e.g., weakening or strengthening of troughs / ridges and shifts of a jet stream axis) and related changes in precipitation. Any generalization of the results is unfortunately impossible because of the wide variety of GCMs used and regions covered (Europe, North America, Australia, New Zealand, Arctic, Antarctic).

Circulation classifications have also been applied to statistical downscaling in three different ways. First, data are stratified by circulation classification and the downscaling model is built within each class separately, e.g., Cavazos (1999), Enke and Spekat (1997) and Li and Sailor (2000). In this approach, the relationship between the large-scale predictor and local predictand may vary depending on the type of synoptic pattern. Second, the mean value of a type is calculated and attributed to each member of that class (Saunders and Byrne, 1996, 1999). This approach implicitly assumes that future changes in the climate element considered are solely due to changes in atmospheric circulation, which is unrealistic; therefore, its outputs are at least questionable. Third, the monthly or seasonal frequencies of daily circulation types serve as predictors of monthly / seasonal mean values of a climatic variable (Goodess and Jones, 2002). As for all statistical downscaling methods applied on future climate scenarios, their application assumes constancy of empirical relationships in the future (Table 2.1). In order to derive the empirical relationships between the synoptic patterns and the predictand variable, access to daily observational data that spans the range of variability is necessary. Moreover, this method may not capture the intra-type variations in surface climate. Nevertheless, it is useful because it produces highly-resolved temporal and spatial information using only limited computational resources. Furthermore, it is applied rapidly on multiple AOGCMs, which supports the application on ensemble prediction instead of using one single AOGCM output dataset. Compared to other statistical downscaling approaches, this method yields physically interpretable linkages to surface climate and environmental elements, which is also shown in Chapter 3 (Demuzere et al., 2008b).

2.2.1.3 Air-quality applications

Over the last few decades, several studies have focused on the relationship between air pollution and synoptic circulation patterns. Hereby, circulation patterns are derived for a specific time and region of interest from different predictor variables (e.g. SLP, wind, 850 hPa) and are used afterwards as an indicator of high air pollution episodes. Thereby, a large number of studies relate these large-scale synoptic patterns to mean levels of surface O_3 (e.g. Schjoldager et al., 1981; van Dop et al., 1987), whereby an attempt is done to mark these findings in relation to the associated meteorological characteristics. In general, regimes with high-pressure systems associated with high temperatures and low wind speeds are common on days with high ozone (mixing) ratios (Hogrefe et al., 2004; Ainslie & Steyn, 2007). For exemple, Comrie et al. (1992) manually derived nine synoptic types from daily surface weather maps to examine basic associations between surface ozone pollution and the atmospheric circulation. He concludes that for the Pennsylvania area

(USA), high ozone concentrations occur in summer with slow-moving anticyclones, while in winter, low concentrations occur with cyclonic storms moving in from the North and bringing cold, cloudy and windy conditions with precipitation. Differences in winter and summer ozone conditions were further marked and described by Davies et al. (1992), using a wind speed index indicative for the sub-regional surface pressure gradients in Europe. The importance of wind speed in air-quality research is also shown by Kassomenos et al. (1998) and Ainslie & Steyn (2007). The former classified eleven distinct mesoscale patterns derived from 850 hPa levels by analyzing meteorological sources gathered between 1983-1995 over Athens (Greece) and found that severe and bad air quality conditions were highly related to southerly sea breeze and calm wind. The latter performed a cluster analysis of wind measurements in the Lower Fraser Valley, British Columbia (Canada), to identify mesoscale circulation regimes that are common on days with high ozone mixing ratios. Composite synoptic patterns associated with each regime all showed high pressure over the eastern Pacific Ocean with a thermal trough over Washington State and southwestern British Columbia, whereby the composite ozone patterns, corresponding to each mesoscale circulation regime, show similar general features. They conclude that not only meteorological variables, but also precursor build-up prior to the exceedance day, play an important role in the spatial ozone pattern on exceedences days.

Furthermore, other research focuses on various other atmospheric chemical components. Several classification techniques as described in Appendix A (k-means clustering, tree-based recursive partitioning models, Lamb weather types), using different meteorological input variables (750 hPa and 850 hPa, SLP, temperature…) are applied in order to find general relations between the large-scale synoptic features and surface or upper-tropospheric concentrations of atmospheric chemical species. In this respect, Farmer et al. (1989) showed that on a monthly basis, specific sea-level atmospheric pressure patterns can be found conducive to high excess sulphate concentrations in precipitation over Scotland. Similarly, Davies et al. (1990) used the Lamb classification approach (Lamb, 1972) to categorize precipitation composition associated with the different circulation types. Kassomenos et al. (2003) established a correlation between a circulation scheme using surface and isobaric levels of 850 hPa and both gaseous and particulate pollutant concentrations measured in different sectors of the Athens municipality during 1954-1999. Bridgeman and O'Connor (2007) categorized synoptic charts according to the quadrant where the dominant pressure centre was located and found several significant relationships between their synoptic types and PM_{10}, NO_x and ozone concentrations for Newcastle, located on the SE coast of Australia. Finally, Chuang et al. (2008) identified seven weather patterns from synoptic weather maps for aerosol events, which occurred between March 2002 to February 2005. This

classification of the pollution origin of the air masses shows that 15% of event days were contributed by long-range transport (LRT), 20% by local pollution, and 65% by long-range transport/local pollution mix.

These examples show that circulation patterns have used successfully in air-quality applications, with a wide range of classification methods, input variables, geographical regions and chemical species. Hence, this overview shows a possible capability of circulation patterns (and their related meteorological characteristics) to discriminate between low and high concentrations of a large range of chemical pollutants.

2.2.2 Regression methods

There are various regression techniques available to convert coarse resolution climate model outputs into daily meteorological and environmental variables. The most widely used statistical downscaling methods include linear methods such as, multiple linear regression (MLR), canonical correlation analysis or singular value decomposition (Conway et al., 1996), or non-linear regression methods, such as artificial neural networks (ANNs), which are nowadays increasing in use because of their great potential for complex, nonlinear and time-varying input–output mapping. Most studies deal with the variability of temperature and precipitation, while only recently more effort is done applying these techniques on environmental issues. A limitation of this technique is the poor representation of the observed variance and extreme events, as for example in precipitation (Trigo and Palutikof, 2001) or maximum temperatures (Huth, 1999) (Table 2.1). To deal with this, some authors suggested a number of techniques to increase the downscaled variance, such as “inflated” (Karl et al. 1990; Huth et al. 2001), “expanded” (Bürger 1996) or adding “noise” (Wilby et al. 1999, Zorita & Von Storch 1999, Huth et al. 2001) downscaling approaches. Although these techniques remain debatable (Von Storch, 1999), they have been applied often in regression studies. Besides the fact that variance-increasing techniques are physically questionable, one also has to take into account that such techniques applied to future climates introduce additional assumptions/questions on the validity of present-day relationships extrapolated to the future. Furthermore, regression techniques, similar to other empirical downscaling techniques, assume constancy of the present-day derived relationships under a future climate (also know as the stationarity assumption), a characteristic that cannot be evaluated at present. In contrast, this technique is easily applicable on multiple AOGCMs, can address a wide range of variables and provides highly-resolved spatial and temporal information, and can be applied in areas when computational resources are limited (Table 2.1).

2.2.2.1 Current climate applications

Regression methods have often been applied for the downscaling of (extreme) precipitation and other related hydrological aspects in various parts of the globe, such as, e.g. for the southeast of Brazil using linear and nonlinear methods (Ramirez et al., 2006), for Northern Canada (Dibike and Coulibaly, 2007; Dibike et al., 2008), Ireland (Fealy and Sweeney, 2007), the European Alps (Schmidli et al., 2007) and for Southern Africa (Shongwe et al., 2006). In addition, Gosh and Mujumdar (2007) tackled drought impact assessment in India with results from GCM mean sea level pressure simulations using, next to other techniques, statistical regression as a downscaling tool to retrieve precipitation at a smaller spatial scale. Linderson et al. (2004) employed a multiple linear regression approach for precipitation in Sweden, concluding that the models were only capable for estimating the mean precipitation and the frequency of wet days.

Several studies compared and evaluated the results of different regression downscaling techniques for precipitation and temperature with observational data and between models to assess their validity and/or consistency (Hewitson and Crane, 1996; Huth, 1999; Trigo and Palutikof, 2001). In general, they reveal that there is only little difference in the capabilities of the various methods. As numerous studies apply different sets of methods on different areas, for different variables and specific skill scores, some examples are provided below.

Schoof and Pryor (2001) found little difference between regression-based methods and ANN for the downscaling of temperature and precipitation in Indianapolis (USA). Khan et al. (2006) tested the Statistical Downscaling Model (SDSM) developed by Wilby et al. (2002) (https://co-public.lboro.ac.uk/cocwd/SDSM/), together with a neural network approach and the Long Ashton Research Station Weather Generator (LARS-WG) in terms of various uncertainty attributes on daily precipitation, daily maximum and minimum temperature. For daily maximum and minimum temperature, the performance of all three models is similar in terms of model errors evaluation at the 95% confidence level. But, according to the evaluation of variability and uncertainty in the estimates of means and variances of downscaled precipitation and temperature, the performances of the LARS-WG model and the SDSM are almost similar, whereas the ANN model performance is found to be poor in that consideration. Similarly, Wetterhal et al. (2006, 2007) employed four statistical downscaling methods for precipitation downscaling in Northern Europe and China, whereby the weather patterns and SDSM outperformed the other methods and that no method could well capture the difference between dry and wet summers. Kostopolou et al. (2007) tested three downscaling approaches,

Multiple Linear Regression using a circulation type approach (MLRct), canonical correlation analyses and ANN, to assess their performance skills. None of the methods were found to be superior to the others. Harpam and Wilby (2005) compared three statistical models for downscaling heavy daily precipitation occurrence and amounts at multiple sites. Three models (multi layer perceptron (MLP), ANN and SDSM) were applied to area-average and station daily precipitation amounts in northwest and southeast of England. Thereby, each model approach showed individual advantages and disadvantages whereby all models had greatest capabilities for indices reflecting persistence of large-scale winter precipitation (such as maximum 5-day totals) or dry-spell duration in summer.

Another large comparison study on the downscaling of daily mean temperatures in 39 european sites has been performed by Huth (1999). The methods include canonical correlation analysis, single value decomposition and three multiple regression models. The performance of the methods is evaluated using cross-validation and root-mean-squared error as a measure of accuracy. The pointwise regression proved to be best. Moreover, Huth (1999) suggested that, as GCMs are likely to simulate different predictors with different accuracy as well as to be more confident in simulating large-scale features (teleconnections, modes of variability) than individual grid point values, the rating of methods could change when applied to a GCM run simulating present or future climate conditions (e.g. Huth, 2004).

This overview suggests that there is no clear preference between the various available regression methods. Nevertheless, some of these studies suggest that the use of non-linear downscaling methods does not necessarily improve the downscaling results (Wilby et al., 2002; Huth et al., 1999, Huth et al., 2008b). In this respect, the linear multiple regression technique is often brought forward as a straightforward tool, known for its simplicity, practical feasibility and for being more readily interpretable in comparison to non-linear methods as ANN, for example.

2.2.2.2 Future climate applications

Although downscaling of future climate scenarios using regression analysis is applied in many fields, the majority of them deal with hydrology applications, with results differing depending on AOGCM, the choice of SRES climate scenarios, the downscaling method, time of the year and the geographical region. For example, Linderson et al. (2004) showed a significant increase of the annual mean precipitation by about 10% and a slight decrease in the frequency of wet days, indicating an increase in the precipitation amounts as well as in the precipitation intensity. The main increase of precipitation and

intensity occurs during winter, while the summer precipitation slightly decreases. The seasonal changes found in precipitation are attributable to changes in the westerly flow of the atmospheric circulation. Hertig and Jacobeit (2008) found a shorter but wetter wet season for the western and northern Mediterranean regions including precipitation increases in winter and decreases in autumn and spring for the period 2071-2100 compared to 1990-2019. The eastern and southern parts of the Mediterranean area exhibit mainly negative precipitation changes from October to May for an increased greenhouse gas forcing.

Others apply a regression-based downscaling tool with respect to (extreme) temperatures. For example, Tomozeiu et al. (2007) assessed possible changes of mean climate and the frequency of extreme temperature events in Emilia-Romagna (Italy), over the period 2070-2100 compared to 1960-1990. They used a multivariate regression based on canonical correlation analysis to downscale minimum and maximum temperature from AOGCM output using predictors at different geopotential heights. After an optimization and calibration using NCEP/NCAR reanalysis, the downscaling model is applied to all model output experiments to obtain simulated present-day and A2 and B2 scenario information (Nakicenovic and Swart, 2000) at the local scale. Various scenarios predict significant increases in both maximum and minimum temperature, associated with a decrease in the number of frost days and with an increase in the heat wave duration index. The increase is more significant for the A2 scenario than for the B2 scenario. Schubert (1998) showed that a statistical model combining principal component analysis and linear multiple regression is able to explain a considerable part of both short and long frequency variations of local temperature extremes. The downscaling model was applied on an AOGCM under 2 x CO_2 emission scenario conditions. Compared to the extreme temperature changes simulated by the AOGCM directly, the downscaled variations are much weaker. This is a result of the fact that their downscaling technique depends on the large-scale circulation, which only shows minor changes between the 1 x CO_2 and 2 x CO_2 scenario. From this it seems that their statistical methods misses important processes (e.g. radiative processes) that could cause large temperature changes without affecting the synoptic circulation. Nevertheless, they conclude that this approach (adjusted for by including non-circulation related temperature forcings like thickness between 1000 and 850 hPa) can provide more detailed insight in the processes leading to more local extremes in temperatures.

Thus, regression downscaling techniques can provide a more reliable temporal and spatial distribution at the scale of interest useful in impact studies (Gachon and Dibike, 2007). Furthermore, this characteristic often implies a change in magnitude between the downscaled and raw AOGCM data, as was shown for

example for precipitation by Paul et al. (2008) and for extreme temperatures by Gachon and Dibike (2007).

2.2.2.3 Air quality applications

Multiple regression techniques have often been employed in short-term applications of air quality assessment. In contrast, this approach has not, to the author's best knowledge, been used as an air quality downscaling tool using future AOGCM scenarios for air quality applications. Therefore, the section below particularly addresses the short-term application in more detail.

Stadlober *et al.* (2008) show how present-day PM_{10} data combined with the next-day meteorological forecast can help forecasting daily PM_{10} levels for some cities in Austria using multiple-regression analysis. Barrero *et al.* (2006) developed a MLR model for the prediction of daily ozone maxima in the urban area of Errenteria (Spain). They conclude that this model, despite being linear and therefore unable to account for non-linear behavior, is able to forecast O_3 concentration maxima several hours in advance based on the day of the year, the relations between O_3, sunlight and NO_x, and previous day O_3 levels. Hubbard and Cobourn (1998) used the MLR approach to predict daily domain-peak ground level ozone concentrations in the Louisville (U.S.A.) metropolitan area. Cuhadaroglu and Demici (1997) obtained through a multiple-linear-regression analysis that, for some months, there is a moderate level of relation between the SO_2 and suspended particle level and the meteorological factors in the highly urbanized city of Trabzon (Turkey).

Also, in recent years, the artificial neural network in general, and the multilayer perceptron neural network specifically, have extensively been used in air quality applications. ANN techniques are suggested to be computational efficient, able to handle nonlinear characteristics, able to generalize properties and able to work with high-dimensional data (Gardner and Dorling, 1998; Papanastasiou *et al.*, 2007). In contrast, Gardner and Dorling (1998) state that the reason not to use these techniques in practice is that they are difficult to handle and the results are difficult to interpret. Still, many authors opt to use this technique to study environmental problems in various geographical areas and for different applications. For example, Gardner and Dorling (1999) trained MLP neural networks to model hourly NO_x and NO_2 pollutant concentrations in Central London (UK). Nunnari et al. (1998) applied neural techniques to predict atmospheric pollutant concentrations in areas with a high density of industrial plants in the province of Siracusa (Sicily), whereas Benvenuto and Marani (2000) use this approach in data quality control and air pollution nowcasting for the Venice (Italy) region. Kukkonen *et al.* (2003) evaluate neural networks in the prediction of NO_2 and PM_{10} concentrations compared to a deterministic

modelling system for the centre of Helsinki (Finland). Hooyberghs et al. (2005) attempt to predict the next day PM_{10} concentrations for Uccle (Belgium). Reich et al. (1999) proposed to use a three layered feed-forward ANN to identify unknown air pollution sources in the city of San Nicolás in the province of Buenos Aires (Argentina), while the prediction of $PM_{2.5}$ and SO_2 in the downtown area of Santiago (Chili) has been done by respectively Perez et al. (2000) and Perez (2001).

Some research papers apply various regression techniques on a single dataset in order to perform an intercomparison study between the different methods used in air quality applications. Goyal et al. (2005) applied three statistical models in order to forecast respirable suspended particulate matter (RSPM) based on meteorological factors for urban Dheli and Hong Kong. They conclude that a combination of a multiple-regression model and a Box-Jenkins time series auto-regressive, integrated, moving-average model outperforms a combination of the two with respect to observations. Another paper by Agirre-Basurko et al. (2006) present the results obtained using three prognostic models to forecast ozone and nitrogen dioxide levels in real-time up to 8 hours ahead at four urban stations in Bilbao (Spain). Two multilayer perceptron based models and one multiple-linear-regression-based model were developed. Their results indicated improved performance for the multilayer perceptron-based models over the multiple linear regression model. Comrie (1997) investigated the potential for using neural networks to forecast ozone pollution, as compared to traditional regression models under different climate and ozone regimes. Model comparison statistics indicate that neural network techniques are only slightly better than regression models for daily ozone prediction, and that all types of models are sensitive to different weather-ozone regimes. Cobourn et al. (2000) compared nonlinear regression and neural network models for ground-level ozone forecasting in Louisville (U.S.A). They conclude that both models performed essentially the same, as measured by various errors statistics. In contrast, Gardner and Dorling (2000a) conclude that significant increase in performance is possible when using MLP models, whereas the use of regression models are more readily interpretable in terms of the physical mechanisms between meteorological and environmental variables. Their conclusion is based on the comparison of linear regression, regression tree and multilayer perceptron neural network in order to accurately capture ozone behaviour from its relation with meteorological variables.

2.3 Dynamical downscaling

The idea to use regional climate models for regional climate studies was originally proposed by Dickinson et al. (1989) and Giorgi (1990). It was formed

under the concept of a one-way nesting whereby large-scale fields from global model simulations or (re)-analysis products provide the initial conditions and time-dependent lateral meteorological boundary conditions to drive high-resolution RCM simulations for a selected time period of the global model run. The basic strategy underlying this one-way nesting approach is that the GCM is used to simulate the response of the global circulation to large scale forcings and that the RCM is used to account for sub-GCM grid scale forcings (e.g. complex topographical features) in a physically-based way, and to enhance the simulation of atmospheric circulations and climatic variables at fine spatial scales (Giorgi and Mearns, 1999). The nesting technique can also be two-way interactive, whereby the regional domain feeds back on the large scales, thus reducing potential mismatch between the regional model and the nesting model. Although two-way nested runs are already performed between chemical transport (CTM) and regional climate models, to the author's best knowledge, all RCMs to date have employed one-way nesting from GCMs.

The nested regional modelling technique essentially originated from numerical weather prediction models (Seaman, 2000), but is by now extensively used in a wide range of climate applications, ranging from paleoclimate to anthropogenic climate change studies. Over the last two decades, regional climate models have been shown to be flexible tools, capable of reaching high resolution (down to 10 km or even less) and capable of describing climate feedback mechanisms acting at the regional scale. Regional modelling systems have widely been adapted to, or developed for, climate applications. Thereby, the main advantage and disadvantages are listed in Table 2.1. The main theoretical limitations of this technique are the effects of systematic errors in the driving large scale fields provided by global models (which is common to all downscaling methodologies using AOGCM output) and the lack of two-way interactions between regional and global climate. In addition, for each application, careful consideration needs to be given to the model domain size and resolution and to the technique for assimilation of large scale meteorological forcing. Moreover, the climatology described by a regional climate model is determined by a dynamical equilibrium between two factors: the information provided at the boundaries by the GCM and the internal model physics and parameterization schemes (Giorgi and Mearns, 1999).

From a practical point of view, one has to consider that, in order to run an RCM experiment, high-frequency (e.g. 6-hourly), time-dependent GCM fields are needed. These are not routinely stored because of the implied mass-storage requirements, so that careful coordination between global and regional modelers is needed to design nested RCM experiments. Moreover, depending on the domain size and resolution, RCM simulations are computationally demanding (comparable to the costs of AOGCMs). In this respect, results of one-way

coupled GCM-RCM simulations depend on the choice of size and location of the domain, which is not transferable to other regions. Therefore, an alternative technique known as “spectral nesting” or “large-scale nudging” has gained interest recently (von Storch et al., 2000; Biner et al., 2000). With this technique, the large-scale component of the RCM fields is nudged towards the corresponding large-scale component of the nesting fields, within the whole RCM computational domain. Hence the large-scale information of the driving fields is fully used, which is not the case with the lateral boundary nested in a traditional one-way nesting (Figure 2.1). This data assimilation technique is suboptimal and indirect (von Storch et al., 2000). As an example, the CLIMAQS project (see chapter 8) aims to nudge model variables towards large-scale fields, in order to improve air-quality model simulations with ARPS and AURORA (Air quality modelling in Urban Regions using an Optimal Resolution Approach).

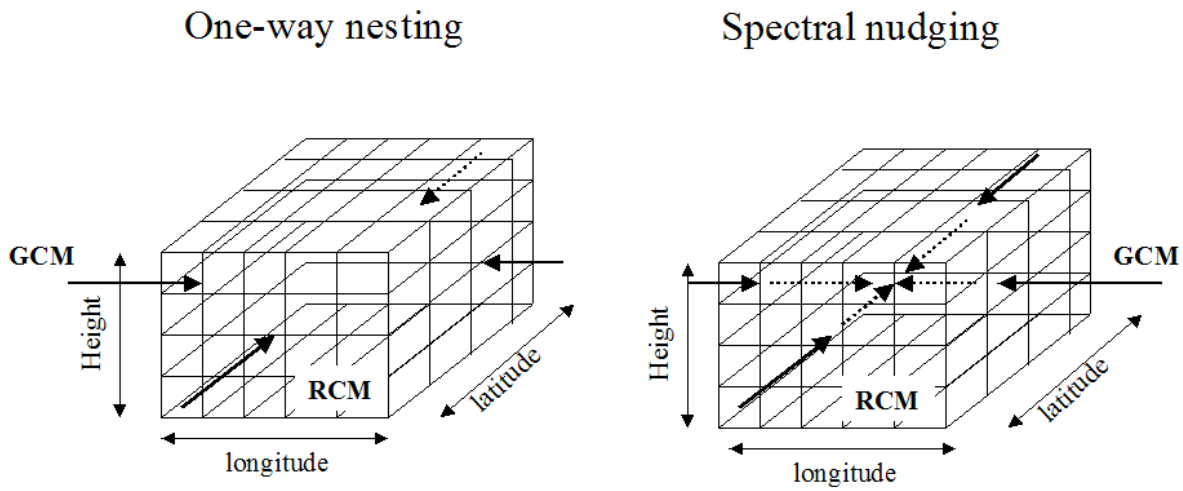

Figure 2.1: A schematic overview of a one-way nesting and spectral nudging approach often applied in dynamical downscaling. Full lines present initial and boundary conditions from the GCM to the RCM. The dotted lines present the replacement of the large-scale RCM fields by the GCM fields. More details on the spectral nudging technique can be found in Von Storch et al. (2000).

Over the past decade, numerous reports described current and future climate simulations based on regional climate models. This chapter doesn’t provide a complete overview of all literature tackling these topics. In the following sections, some examples provide insight in the current and future climate downscaling applications and air-quality-specific applications using regional climate models. For a more complete description of other applications, the reader is referred to chapter 10 of the Third IPCC Assessment Report,

"Regional Climate Information – Evaluation and Projections" in Giorgi et al. (2001) and chapter 11 of the Fourth IPCC Assessment Report – "Regional Climate Projections" in Christensen et al. (2007).

2.3.1 Current climate applications

The importance of regional climate impacts prompts a need to understand the capabilities of regional climate models. Analysis and interpretation the results of regional climate model will help pave the way for interpreting the results of global climate models at higher resolutions. In this framework, the Project to Intercompare Regional Climate Simulations (PIRCS - http://www.pircs.iastate.edu) was developed to provide a common framework for mesoscale models driven by initial and boundary conditions of global climate models (here from the National Center for Environmental Prediction and the National Center for Atmospheric Research – NCEP/NCAR) (Takle et al., 1999). Eight regional models (Takle et al. (1999) – their Table 2) are intercompared and tested against observations of precipitation, minimum and maximum temperature and surface energy fluxes. In general, PIRCS concludes that no single model stands out as best in all comparisons; rather, each model has its individual strengths and deficiencies. This feature illustrates the importance of archiving a variety of output fields that can be compared with observations.

Furthermore, besides large joint efforts, numerous other control (current climate) simulations of RCMs driven by boundary conditions of GCMs are performed by the climate modelling community. From these, it is understood that errors introduced by the GCM large-scale representation are transmitted to the RCM (e.g., Noguer et al., 1998). While the regional biases of the RCM are not necessarily lower than those of the driving GCM, the spatial patterns of climate produced by the RCMs are usually in better agreement with observations compared to those of the GCMs, due to a better representation of topography and high-resolution forcings. E.g., Giorgi et al. (1994) showed that mountain ranges strongly affect the regional pattern of precipitation due to the shadowing effect they cast. Moreover, there is also evidence that RCMs do reproduce prominent mesoscale features of precipitation extremes at scales not accessible to GCMs (e.g. Frei et al., 2003; Huntingford et al., 2003; Christensen and Christensen, 2003) and better than GCMs on their gridscale (Durman et al., 2001). An example of heavy rainfall during autumn simulated by a global and regional climate models is given in Figure 2.2.

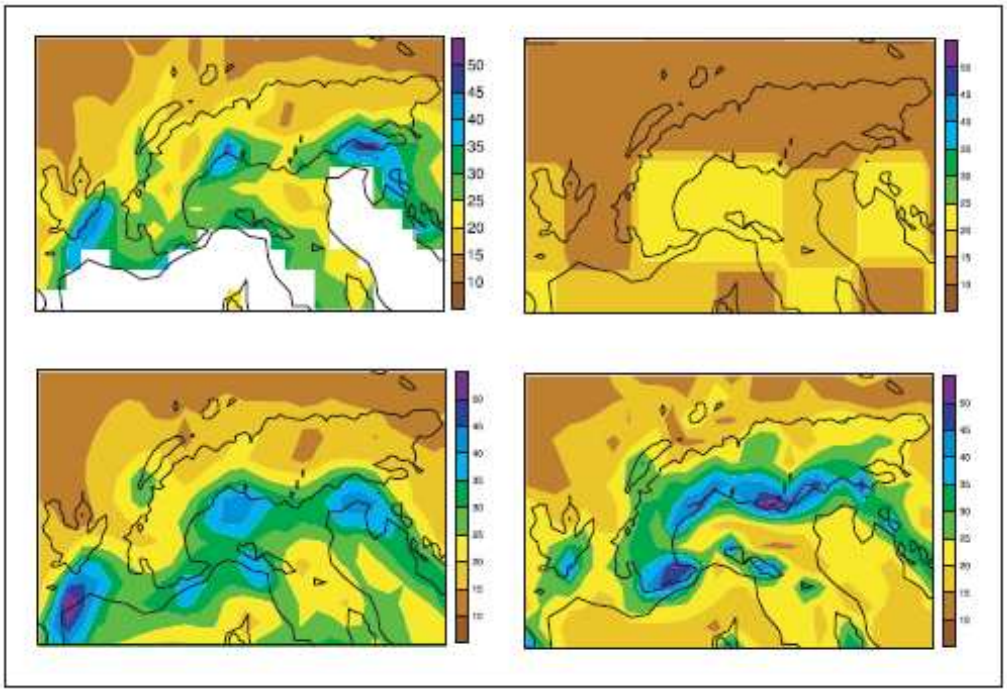

Figure 2.2: The autumn heavy rainfall threshold (mm per day) simulated by the HadAM3P global climate model (top right), the Swiss CHRM (lower left) and UK HadRM3H (lower right) regional climate models, compared with observed gridded data (top left) (Schmidli et al., 2006; compiled from STARDEX final report).

2.3.2 Future climate applications

Similar to present-day RCMs, climate change experiments indicate that, even though the magnitude of surface climate change in the nested (RCM) and driving (GCM) models are usually similar, the mesoscale details of the simulated changes can sometimes be different between different RCMs (Machenhauer et al., 1998; Pan et al., 2001). For example, Whetton et al. (2001) show significant different patterns of changes in temperature and rainfall in a regional climate change simulation for Victoria, Australia. While winter rainfall decreased in the driving GCM, it increased in the RCM. Due to this better spatial representation and capability in providing prominent mesoscale features, RCMs are largely adopted for hydrological studies, in order to assess the impact of climate change on the hydrology, water resources in river basins and extreme flood events (e.g. Wilby et al., 2000; Hay et al., 2002; Hay and Clark, 2003; Huntingford et al., 2003; Christensen et al., 2004; Wood et al., 2004).

Although the impacts of climate change in the Mediterranean region are expected to be large in the Mediterranean region, only few impact assessments studies have been reported. In general, most GCMs have projected an increase in temperature and a decrease in annual precipitation. For example, Alpert et al. (2008) have shown tendencies towards decreasing precipitation, counteracted

by an increase in extreme precipitation events in combination with an increase in temperature for the eastern Mediterranean. Moreover, Fujihara et al. (2008) predicted an annual precipitation decrease for the Seyhan river basin area (Turkey) between 157 - 182 mm (25 to 29%) in future GCMs, with an annual evapotranspiration decrease around 36 mm; the annual runoff decreased by 118-139 mm in GCM scenarios.

Recently, a large European effort was implemented to develop regional climate scenarios in the framework of the Prediction of Regional scenario and Uncertainties for Defining EuropeaN Climate change risks and Effects project (PRUDENCE, e.g. Christensen, et al., 2002; Schär et al., 2004; Deque et al., 2005). This project was initiated because the uncertainties of current climate change scenarios are poorly characterized and their resolution is insufficient for regional modelling. To date, the assessment of potential impacts of climate change has generally relied on projections from simple climate models or coarse resolution AOGCMs, neither of them capable of resolving spatial scales of less than ~300 km. This coarse resolution precludes the simulation of realistic extreme events and the detailed spatial structure of variables like temperature and precipitation over heterogeneous surfaces e.g. the Alps, the Mediterranean or Scandinavia. PRUDENCE, a European-scale investigation, has the following objectives: (1) to address and reduce the above-mentioned deficiencies in projections, (2) to quantify our confidence and the uncertainties in predictions of future climate and its impacts, using an array of climate models and impact models and expert judgment on their performance and (3) to interpret these results in relation to European policies for adapting to or mitigating climate change (Christensen, 2001). More information on the GCM and RCM models used, the applications and the results of this project can be found on http://prudence.dmi.dk/ and a summary of the PRUDENCE model projections of changes in European climate by the end of this century is given in Christensen and Christensen (2007).

A continuation of this large joint effort is the ENSEMBLES project (http://www.ensembles-eu.org/). The project aims to develop an ensemble prediction system for climate change based on the principal state-of-the-art, high resolution, global and regional climate models, validated against quality-controlled, high-resolution gridded datasets for Europe; to produce an objective probabilistic estimate of uncertainty in future climate at the seasonal to decadal and longer timescales; to quantify and reduce the uncertainty in the representation of physical, chemical, biological and human-related feedbacks in the Earth System (including water resource, land use, and air quality issues, and carbon cycle feedbacks) and finally to maximize the exploitation of the results by linking the outputs of the ensemble prediction system to a range of

applications, including agriculture, health, food security, energy, water resources, insurance and weather risk management (Hewitt and Griggs, 2004).

In addition, two more projects are focusing on climate change impacts on Central/Eastern Europe. The CECILIA (Central and Eastern Europe Climate Change Impact and Vulnerability Assessment) project includes applications of RCMs at a resolution of 10 km in hydrology, water quality and management, air quality, agriculture and forestry. The CLAVIER (Climate Change and Variability: Impact on Central and Eastern Europe) project analyses climate change impacts on weather patterns and extremes, human health, natural ecosystems and water resources, and evaluates the economic impacts on agriculture, tourism, energy and public sector industry and services (Christensen et al., 2007a).

2.3.3 Air quality applications

The use of dynamical downscaling of GCMs in terms of air quality modelling has only begun to develop recently. Nevertheless, a number of studies employed regional climate models in combination with chemical transport models (CTMs) to downscale GCMs in order to gain further insight in the effect of a changing climate on future air quality levels. Here, the RCM provides the meteorological information to the CTM, in an on- or offline mode. An offline mode means that the RCM is run first to produce the three dimensional meteorological fields, which are afterwards used to drive the CTM. In contrast, the online mode passes the meteorological information directly (at the same time step) from the RCM to the CTM.

In air quality modelling of the future, a whole range of GCM-RCM-CTM coupled model chains are employed for a variety of climate change scenarios, future periods, chemical species (especially O_3 and PM_{10}) and geographical areas. In general, most studies agree that the formation and availability of chemical species is influenced by changes in temperature, water vapor (Racherla and Adams, 2008), cloud cover and natural/anthropogenic emission changes (Hogrefe et al., 2004a, b; Murazaki and Hess, 2006). Hereby, an increase in global and regional temperatures could accelerate the chemical reactions that lead to the formation of pollutants and increase the volatility of aerosols (Racherla and Adams, 2008), although this response will likely depend on the non-linearity's in the atmospheric chemistry mechanisms (Giorgi and Meleux, 2007). In addition, higher temperatures should increase the biogenic emission of pollutant precursors, which is likely to increase atmospheric aerosol and O_3 levels. An increase in precipitation can play a role in terms of greater atmospheric cleansing, while a decrease favors an increased photolysis rate associated with reduced cloudiness, increased temperatures and reduced wet

removal (Giorgi and Meleux, 2007). The overall effect of these climate change factors simulated by RCM-CTM model chains are summarized by Jacob and Winter (2009) in their Table 2. For the U.S., a change in maximum 8 hourly mean O_3 is expected ranging from –6% to +25% depending on the region and the future SRES scenario. Thereby, O_3 concentrations are expected to decrease or change insignificant in the Midwest U.S., West and Southeast (Murazaki and Hess, 2006; Nolte et al., 2008; Avise et al. 2008; Tagaris et al., 2007), while a large increase is expected in the Northeast and East U.S. (Hogrefe et al., 2004a, b; Kunkel et al., 2007; Lin et al., 2008; Murazaki and Hess, 2006; Nolte et al., 2008; Racherla and Adams, 2008). This increase is accompagnied by a lengthening of the ozone season in spring and autumn (Chen et al., 2008; Mahmud et al., 2008) and a higher frequency of longer high ozone concentration pollution episodes (Chen et al., 2008).

For PM, most studies emphasize the importance of changing precipitation in modulating the PM sink. In this respect, the differences between GCM/RCMs in the regional precipitation response to climate change are a major cause of discrepancy in the PM response (Racherla and Adams, 2006). Factors other than precipitation are also important in driving the sensitivity of PM to climate change, as for e.g. wildfires from droughts, higher water vapor leading to higher concentrations of H_2O_2, the principal SO_2 oxidant (Liao et al., 2006) and a positive response to rising temperature (Heald et al., 2008). This, in combination with the diversity of the PM components and the general uncertainty in GCM projections of the hydrological cycle, points out that the effect of climate change on PM is more complicated compared to O_3. The studies dealing with the climatological effect on PM species are summarized in Jacob and Winter (2009), in their Table 3.

Until now, all examples have shown a significant impact of meteorological climate changes on future air quality levels. Another explaining factor hereby are the (precursor) emission themselves. For example, Tagaris et al. (2007) state that climate change has a rather small impact on pollutant concentrations, in comparison to the importance of the emission changes. Others also stress the importance of high spatial resolution in order to assess climate change – air quality interactions as they are determined by fine-scale structures in emissions and climatic/chemical factors (Giorgi and Meleux, 2007). This shows that there is still no consensus on the course of future air pollutant levels under a possible changing climate. The global and regional diversity, combined with the numerous available models (GCMs, RCMs, CTMs) and various modelling frameworks (e.g. with/without including changes in anthropogenic/biogenic emissions, geographical areas, future time slices…) makes a uniform and clear conclusion difficult. Furthermore, Gustafson and Leung (2007) concluded in their research on the possible use of dynamical downscaling in air quality

studies that, once the downscaling has been done by the RCM, a comparison with observations must be done based on the quantities that are important for air quality assessment. Thereby, the boundary layer height, besides other variables, has been shown to play a role in the dilution of pollutant concentrations (Pielke et al., 1991; Rao et al., 2003).

Dabbert et al. (2004) states that meteorology is critical for air quality predictions and that boundary layer dynamics and wind direction are perhaps the two most poorly determined meteorological variables for regional air quality prediction. Therefore, Chapter 7 of this dissertation provides an effort to indirectly improve the representation of the boundary layer for urban environments in a mesoscale model. A sensitivity experiment is performed to more realistically improve the effect of the thermal roughness length parameterization and heat capacity, important for a correct representation of the urban energy balance and consequently important for the boundary layer dynamics. Due to computational constraints, the dynamical downscaling method is not pursued further, but will be used in the future during the CLIMAQS (see Chapter 8) project.

2.4 Dynamical and statistical downscaling: intercomparison studies

Although the sections above provide enough evidence for a large application of both dynamical and statistical downscaling techniques in current and future climate and air-quality applications, studies comparing both downscaling methods remain relatively limited. Unfortunately, to the author's best knowledge, no intercomparison studies on air-quality applications are available, and therefore, the section below provides insight in studies related to other climatological applications and summarizes the most important features that can be drawn from them.

From a more general perspective, dynamical downscaling tools show to have good physically based grounds to estimate the effect on climate change on the regional scale (Kidson and Thompson, 1998). One drawback here is that one needs to reduce the systematic simulation errors, both introduced from the driving AOGCM (Chapter 5 - Demuzere et al., 2008a) and as a direct result of the nested RCM (Noguer et al., 1998; Murphy et al., 1999). For example, Hay and Clarck (2003) show that only after a bias correction to the RCM model output, the accuracy of the daily runoff simulations improved dramatically. This need for a bias correction may be somewhat troubling, as it is unknown if bias corrections to downscaled model output will be valid in a future climate. Therefore, it warrants to identify the causes for (and removal of) systematic biases in dynamical downscaling simulations, and to improve these simulations

of daily variability in the local climate. They argue that, until then, a statistical downscaling approach in simulating runoff appears to be the safer downscaling choice. Moreover, another advantage of the statistical methods is the smaller computational effort. Often, a drawback here is the limited availability of continuous and long time series of observations. Assuming that the necessary observations are available, the statistical methods could be improved by using longer calibration time series or a wider range of predictors (Murphy et al., 1999).

Some authors found that dynamical and statistical methods have comparable capabilities in determining daily and monthly station anomalies for temperature and precipitation (Kidson and Thompson, 1998; Mearns et al., 1999). Others show that the ensemble means from a statistical downscaling approach shows better capability in simulating minimum and maximum temperature, although worse results were obtained for precipitation compared to the RCM, probably due to the large stochasticity of precipitation in the statistical model (Wilby et al., 2000). In contrast, a study shown by Hanssen-Bauer et al. (2003) shows that differences between statistical and dynamical downscaled changes in annual mean future temperatures in Norway are insignificant, while for precipitation, only the dynamical downscaling showed a significant increase in the southwest of Norway compared to an insignificant change from the statistical method.

Moreover, as was seen from the intercomparison studies between different statistical and dynamical downscaling studies, Mearns et al. (1999) states that it is not possible to bring forward one method that returns more “correct” responses to external forcings of climate compared to the other. They urge to have more comparative studies, and encourage research programs that lead to rigorous intercomparisons of statistical downscaling methods and nested regional climate modelling methods. Leung et al. (2003) endorses the above-mentioned opinion and state that intercomparison of downscaling techniques may help focus efforts on subsets of techniques and evaluate how much downscaling contributes to the total uncertainty in climate change scenarios. The few studies performed so far show that statistical downscaling and regional climate models have similar skill in simulating the mean and variability of present climate conditions. However, significant differences exist between statistical and dynamical downscaled future climate conditions. This is partly explained by the fact that statistical downscaling experiments typically employ only a subset of the boundary information used by RCMs. Therefore, future statistical downscaling techniques versus RCM intercomparison studies need more carefully designed experiments to ensure greater parity of forcing conditions.

To further illustrate the previously-mentioned uncertainties in the use of both methods, Planton et al. (2008) suggest that, although both dynamical or statistical downscaling approaches have their known strengths and weaknesses, neither their validation on present climate conditions, nor their potential ability to project the impact of climate change on extreme event statistics (e.g. high percentiles) allows one to give a specific advantage to one of the two types. They state that the uncertainties associated to the global climate models and to the scenarios dominate the uncertainty of climate change. Therefore, a complete evaluation of the relative importance of these causes of uncertainties on the projection of climate extremes implies the construction and use of multi-model ensembles of simulations including different downscaling approaches, as was suggested before by Mearns et al. (1999), Leung et al. (2003) and Hay and Clarck (2003). Similarly, although Spak et al. (2008) have found similar skills for a dynamical and statistical downscaling approach for summer mean temperatures over Eastern USA, they state that regional assessment of various variables can be improved by assessing multiple downscaling methods for the same AOGCM, ranging from state-of-the-art dynamical models to relatively simple statistical predictions. Using multiple downscaling methods with an ensemble of AOGCMs will yield the most plausible projections and will develop a comprehensive understanding of the physical and mathematical reasons behind apparent (dis)agreement among distinct regional downscaling techniques.

Previous examples often tackled mean distribution of certain variables, while impact studies often require information on the (extreme) quantities of climate variables. In the framework of the STARDEX project, this has been tested for various statistical and dynamical downscaling techniques. Haylock et al. (2006) applied six statistical and two dynamical downscaling models (see paper for more details) with regard to their ability to downscale indices of extreme precipitation in northwest and southeast England. In general, they conclude that the performance among the eight downscaling models was high for those indices and seasons that had greater spatial coherence. The models based on non-linear ANNs were found to be the best at modelling the inter-annual variability of the indices; however, their strong negative biases implied a tendency to underestimate extremes. Also, six of the models were applied to the Hadley Centre global circulation model HadAM3P forced by emissions according to two SRES scenarios. This revealed that the inter-model differences between the future changes in the downscaled precipitation indices were at least as large as the differences between the emission scenarios for a single model.

This result implies caution when interpreting the output from a single model or a single type of model (e.g., a regional climate models) and shows the advantage of including as many different types of downscaling models, global

models and emission scenarios as possible when developing climate-change projections at the local scale. Schmidli et al. (2007) compared six statistical downscaling models and three regional climate models in their ability to downscale daily precipitation statistics in the European Alps (Figure 2.3). The six statistical methods used here include, amongst others, regression methods and a circulation pattern classification method. The comparison is carried out over the European Alps for current and future (2071–2100) climate. The evaluation of simulated precipitation for the current climate showed that the statistical and dynamical approaches tend to have similar biases but that they differ with respect to interannual variations. The statistical models strongly underestimate the magnitude of the year-to-year variations. Clear differences emerge also with respect to the year-to-year anomaly correlation skill: in winter, the RCMs achieve significantly higher skills than the statistical downscaling approaches. In summer, there is still good qualitative agreement between the RCMs but large differences between the statistical and between the statistical and dynamical techniques.

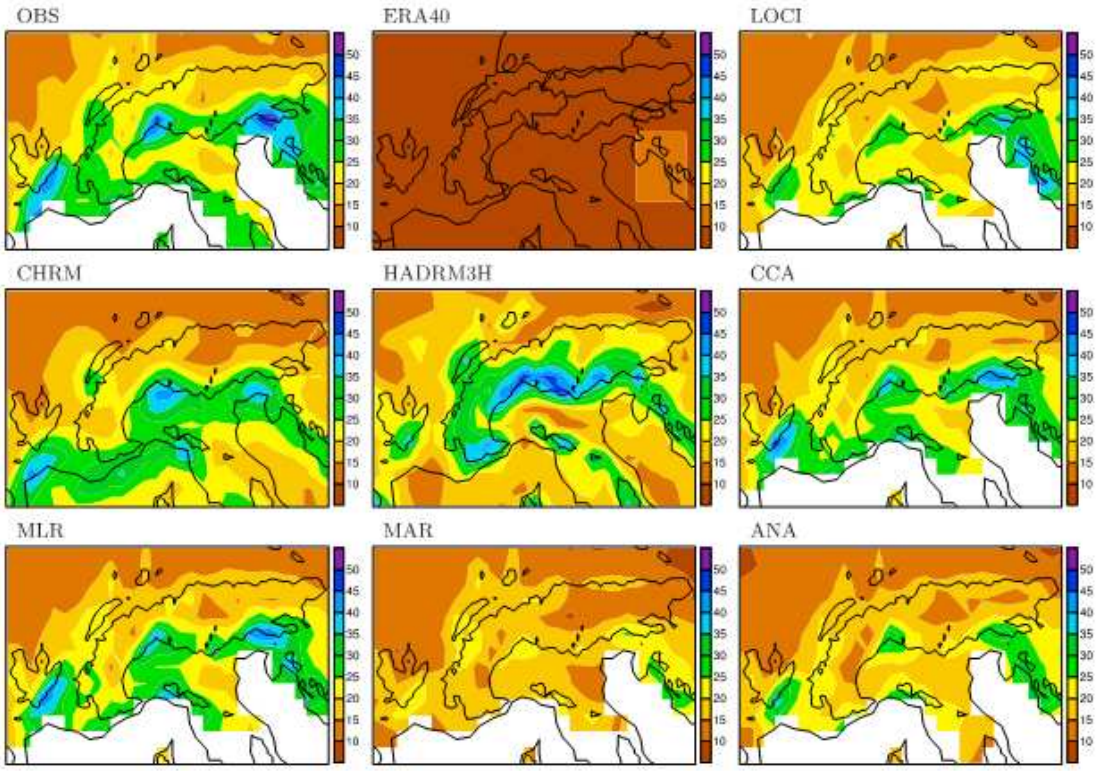

Figure 2.3: 90% quantile of daily precipitation (mm/d) in autumn (SON) for OBS (top left plot) and the models for the ERA15 validation period 1979–1993, for the European Alps. The models are denoted by LOCI (= Local intensity scaling), CHRM (= climate version of NWP model from ETH Zurich), HADRM3H (= the regional climate model of the Hadley Centre of the UK Meteorological Office), CCA (= canonical correlation analysis), MLR (= multiple linear regression), MAR (= multivariate autoregressive model) and ANA (= 2-step analogue method). More information on the methods and a discussion of the figure can be found in Schmidli et al. (2007).

2.5 General conclusions

Since many impact studies require climate change information on a spatial scale much finer than that provided by atmospheric ocean coupled global climate models (AOGCMs), downscaling approaches are an appropriate method to bridge the gap between what AOGCMs produce and what impact assessors require. The idea to use regional climate models for regional climate studies was originally proposed by Dickinson et al. (1989), whereas the statistical downscaling is developed analogously to the "perfect prog" and "model output statistics" approaches used for short-range numerical weather prediction. Whereas the former follows the idea of using global model simulations or (re)-analysis products to provide the initial conditions and time-dependent lateral meteorological boundary conditions to drive high-resolution RCM simulations, the latter seeks to derive quantitative relations between large-scale circulation indices and local climate or environmental variables.

This literature review shows the existence of numerous studies on both dynamical and statistical downscaling applications, covering large parts of the globe and especially with respect to (extremes in) temperature and precipitation. The adaptation of these strategies in air quality applications has only begun to develop more recently, whereby a great deal of this research focuses on the United States. Within this framework, this dissertation is developed and tackles O_3 and PM_{10} levels under current and future climate conditions with a focus on the Benelux area, and more specifically Cabauw (The Netherlands), as this rural measurement site has sufficient data available. This points to another important feature: the choice of methods is largely dependent on data availability and furthermore, on computer efficiency, practical feasibility within the foreseen time frame and strengths and weaknesses of the downscaling methodologies as described in the current literature. Thereby, comparison studies of dynamical and statistical methods in simulating contemporary climate by Kidson and Thompson (1998), Mearns et al. (1999), Murphy (1999) and Oshima et al. (2002) are limited to temperature and precipitation fields and confined to North America, Europe, and Japan. Similar levels of performance for present-day climate for the dynamical and statistical methods are a common finding, independent of region, RCM, AOGCM, statistical technique, temporal scale, and even performance metric. Other studies (Mearns et al., 1999; Murphy, 2000; Oshima et al., 2002; Hanssen-Bauer et al., 2003; Schmidli et al., 2007; Spak et al., 2008) compared RCM and statistical downscaling methods under projected climate change. These comparative studies all found divergence between the downscaling methods for temperature/precipitation projections under climate change forcings, but without systematic explanations for the magnitude of divergence. For example, Murphy (1999) noted a change in the strength of predictor/predictand relationships, and Mearns et al. (2000) found

that the statistical approach produced an amplified seasonal cycle, while the RCM generated greater variability in the spatial patterns of regional temperature change. Here, it is generally suggested that a regional assessment of a specific variable can be improved by assessing multiple downscaling methods for the same AOGCM combined with using multiple downscaling methods driven by an ensemble of AOGCMs. This approach yields the most plausible projections and develops a comprehensive understanding of the physical and mathematical reasons behind apparent agreement and disagreement among distinct regional downscaling techniques.

This dissertation aims to identify elements from a range of methods that are valuable for this kind of research. In first instance, two statistical downscaling methods are applied and evaluated on their ability to simulate present-day levels of O_3 and PM_{10}: a circulation classification technique and a multiple-regression approach. The review on the former demonstrates that the field of circulation classifications is evolving rapidly and their applications in climatology and meteorology are increasing. There is presently as to the circulation classification method preferable for downscaling of future climate scenarios with respect to, among others, air-quality assessment. We opt to use the objectified version of the Lamb catalogue as performed by Jenkinson and Collison (1977) and refined by Jones et al. (1993). Its smaller-scale and fairly easy definition makes this catalogue transferable to other regions; moreover, its simplicity in terms of input data (sea level pressure) and indices describing large-scale patterns based on the locations of high and low pressure systems, provide an easy physically-interpretable framework for further air quality studies under a future changing climate. From the review on the regression-based techniques, we have seen that differences between linear (e.g. multiple-regression techniques) and non-linear (e.g. neural- network techniques) are shown to be limited (Comrie, 1997; Wilby et al., 1998; Gardner and Dorling, 2000a) and that the use of multiple-regression analysis is preferable in order to describe the physical mechanisms. Therefore, we opt to use a stepwise multiple-linear regression model. This approach will guarantee simplicity by the linear structure of the model and practical feasibility by the possibility to include a diverse range of variables that are provided/forecasted by AOGCMs/operational models (Table 2.1). As this method has, to the author's best knowledge, not yet been applied directly in downscaling AOGCM predictor variables in terms of air quality products, this approach will contribute to the debate whether a regression tool only is able to reproduce the observed variability of air quality variables. In a second step, a dynamical approach, based on the mesoscale models ARPS (Advanced Regional Prediction System), is tested in terms of the urban energy balance; one of the meteorological actors important for air quality modelling.

Chapter 3

The impact of weather and atmospheric circulation on O3 and PM10 levels at a rural mid-latitude site*

3.1 Introduction

Ground-level ozone (O_3) and particulate matter (PM_{10}) have been identified as two of the most important air pollutants for Europe in general (Jol and Kielland, 1997; Brunekreef and Holgate, 2002) and over the Benelux region in particular (Tulet et al., 2000). Since their adverse health effects have been observed for decades, the supervising European institutions have produced appropriate legislation and several emission reduction measures have been taken to reduce ambient air pollution (European Community, 1999; WHO, 2000, 2005). Nevertheless, levels of O_3 and PM_{10} continue to exceed frequently the target values and the long-term objectives established in EU legislation. Moreover, international literature shows that air pollution continues to be detrimental to human health despite these emission standards (van der Wal and Janssens, 2000; Medina et al., 2004; Schlink et al., 2006).

* Demuzere, M., Trigo, R. M., Vila-Guerau de Arellano, J. and van Lipzig, N. P. M., 2008. The impact of weather and atmospheric circulation on O3 and PM10 levels at a mid-latitude site. Atmos. Chem. Phys. Discuss. 8, 21037-21088.

In recent decades, typical causes of high ozone and PM_{10} pollution received ample treatment in the scientific literature. Relatively high levels of these pollutants are usually associated to the close proximity of high precursor emissions and as a result of industrial and societal developments. Moreover, ambient air pollution is also strongly influenced by meteorological factors, due to a complex combination of processes and influences, namely; emission, transport, chemical transformations, and removal via wet and dry processes (Seinfeld and Pandis, 1998). Thus, weather/climate elements play a significant role in all these processes' components. On a local scale, emission (e.g., biogenic or dust emissions) may depend on climate variables such as temperature and surface wetness; (photo) chemical processes depend on temperature, humidity, solar radiation fluxes and cloudiness; the precipitation process influences wet removal. From a regional point of view, short and long-term transport depends on the magnitude of surface turbulence and on the atmospheric circulation (at the synoptic scale). This means that the distribution of pollutants is not only dependent on the spread of its emissions, but is also affected by various weather/climatic drivers (Giorgi and Meleux, 2007).

Over the last few decades, the effects of chemical tracers on climate change have been investigated extensively (Intergovernmental Panel on Climate Change, 2007). Conversely, comparatively less attention has been devoted to the issue of climate-change effects on air quality (Andersson and Langner, 2007a; Jacobson, 2008). However, we believe that, in order to understand the full range of atmospheric processes that govern the evolution of air quality under a changing climate, one has to understand and quantify the processes that impact on the atmospheric pollutants on a present time scale. Air quality is affected by both local (in situ) and regional scale processes on a few tens and hundreds kilometers. As current AOGCMs (Atmospheric-Ocean Coupled Global Climate Models) are only capable of resolving phenomena at the resolution of a few hundreds of kilometers, the climate change-air quality interactions are hampered. Furthermore, many chemical atmospheric elements, and particularly those with adverse impacts on human health, such as tropospheric O_3 and PM_{10}, have a lifetime of the order of some hours to days (Seinfeld and Pandis, 1998). As a result, their distribution is highly variable in space and time and is often tied to the distribution of sources (Giorgi and Meleux, 2007).

The main aim of this paper is to study the above-mentioned weather climatology-air quality relation at both the regional and local spatial scales. On the one hand, weather-air quality interactions on the local-scale are quantified based on techniques often used in short-term air quality forecasts. Here, the

selection of an appropriate method depends on its simplicity, practical feasibility, sufficient accuracy and should be computationally inexpensive, so that it can easily be applied to output of different climate models (Semazzi, 2003). The latter rules out the use of a complex climate-air quality modelling system (in off-or online mode), a field of research that has been reviewed comprehensively recently by Giorgi and Meleux (2007).

Many empirical prediction models have been developed to investigate the relationships between meteorological and air quality data. Numerous reports describe model results on different air quality variables and different locations from multiple linear regression (MLR) analysis (Hubbard and Cobourn, 1998; Barrero et al., 2006; Stadlober et al., 2008), nonlinear multiple regressions (Cobourn, 2007), artificial neural networks (ANN) (Gardner and Dorling, 1998; Nunnari et al., 1998; Reich et al., 1999; Benvenuto and Marani, 2000; Perez et al., 2000; Perez, 2001; Kukkonen et al., 2003; Hooyberghs et al., 2005; Papanastasiou et al., 2007), generalized additive models and fuzzy-logic-based models (Cobourn et al., 2000). Other authors compared several methods on a single dataset (from the same measurement site) or combined various approaches in order to improve the specific air pollutant forecast (Agirre-Basurko et al., 2006; Goyal et al., 2006; Al-Alawi et al., 2008). Comrie (1997) compared the potential of traditional regression and neural networks to forecast ozone pollution under different climate and ozone regimes. Model comparison statistics indicate that neural network techniques are only slightly better than regression models for daily ozone prediction. Cobourn et al. (2000) compared nonlinear regression and neural network models for ground-level ozone forecasting in Louisville (U.S.A). They conclude that both models performed essentially the same, as measured by various errors statistics. In contrast, Gardner and Dorling (2000), concluded that significant increase in performance is possible when using MLP models, whereas the use of regression models are more readily interpretable in terms of the physical mechanisms between meteorological and air quality variables.

Taking into account results obtained in previous research showing a similar performance between linear regression and neural network techniques, we decided to employ here a stepwise multiple linear regression model which guarantees, simultaneously, robustness and simplicity. Practical feasibility is obtained by including these parameters that are provided/forecasted individually by AOGCMs/operational models. On the other hand, the discriminative power of a circulation classification method is tested as an air quality assessment tool, keeping in mind its potential future use in downscaling future climate scenarios for air quality purposes (Huth et al., 2008). Prior to the

selection of variables for the model, a comprehensive correlation study is conducted between the meteorological and air quality variables. Afterwards, levels of O_3 and PM_{10} are reconstructed using a stepwise multiple linear regression technique and a circulation pattern approach. Finally, both methodologies results are objectively compared, with the aim of stressing their corresponding strengths and weaknesses for long-term air quality assessment studies.

To the best of our knowledge, this approach has never before been conducted for the Benelux area. In fact, this integrated approach connects both atmospheric chemistry on the local scale using observations from rural sites in The Netherlands and synoptic climatology based on ECMWF (European Centre for Medium-range Weather Forecasting) operational analysis data. Although the different aspects of the methodology are widely used in their specific field of application, they are seldom compared against each other. Many authors solely used the first step in forecasting future levels of air quality variables (e.g. Oanh et al., 2005; Wise and Comrie, 2005), while many studies investigated air quality in relation to the latter (Comrie, 1992; Davies et al., 1992a, b; Cannon et al., 2002; Kassomenos et al., 2003; Bridgeman and O'Connor , 2007). An objective combination of both methodologies results in a further insight in weather-air quality related issues, and presents their corresponding (dis)advantages for long-term air quality assessment studies.

3.2 Data

In order to get insight in the weather-air quality interactions on the local and regional scale, different sets of meteorological and air quality data are used and described in the following sections.

3.2.1 ECMWF operational data

We have extracted large-scale operational data from on a 2.5° x 2.5° grid for the larger European Atlantic Region (20 °W – 35 °E, 75 °N – 35 °N). This dataset is used to determine prevailing circulation patterns at the regional scale. The data covers the 2001- 2004 period, identical to the period selected to construct the linear model from the measurements described in section 3.2.2. For the circulation pattern approach, 12h UTC mean sea level pressure (MSLP) is used, while mean temperature (K) and relative humidity (%) are daily averaged from the four provided time steps for the period 2001-2004. In order to compute the

long-term climatological normal, we have extracted 12h UTC MSLP and daily mean temperature and relative humidity for the period 1971-2000.

3.2.2 Local meteorological measurements

Previous efforts to relate air quality variable concentration data to surface meteorological variables have shown that temperature (Smith et al., 2000), wind speed, relative humidity, and cloud cover are relevant variables (NRC, 1991). Other meteorological-air quality studies have found wind direction, dew point temperature, sea level pressure and precipitation useful in the modelling and forecasting of air quality variables (Gardner and Dorling, 1999; Delcloo and De Backer, 2005; Hooyberghs et al., 2005; Grivas and Chaloulakou, 2006; Andersson et al., 2007a, b; Papanastasiou et al., 2007). Furthermore, Comrie (1997) states that the use of several types of models for ozone prediction can be particularly sensitive to different weather-ozone regimes and urban measurement locations. In order to by-pass this complexity, this study solely uses measured high-temporal resolution data from rural sites. This is done in order to get insight into the meteorological – air quality interactions with a limited interference from local emission sources, implying a limitation of this approach to sites where the variability of emissions is of minor importance. In this respect, we have only considered measurements from rural observation sites, with a daily (or higher) temporal resolution meteorological measurements for the period 2001-2006 and with the availability of air quality measurements (see section 3.2.3). This results in a selection of four rural stations located in central and southern sections of The Netherlands (Table 3.1 and Figure 3.1).

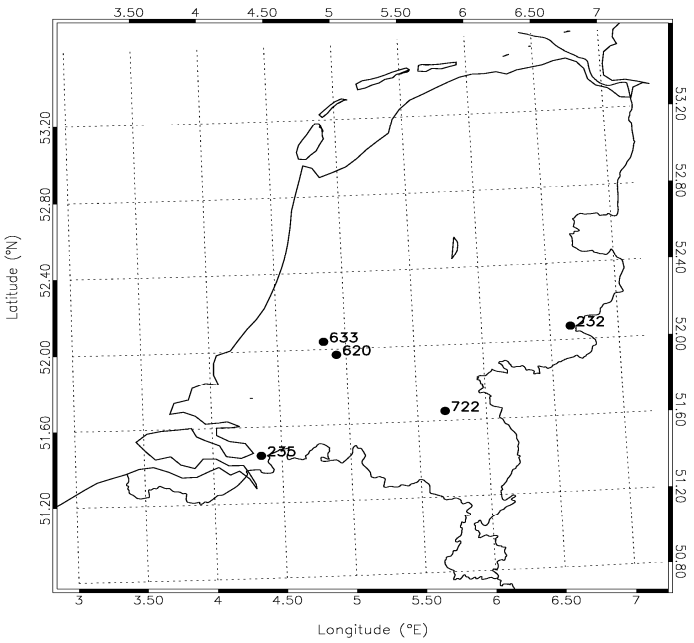

Figure 3.1: Location of the rural meteorological and air quality measurement sites in The Netherlands.

For all stations, wind speed (FF) and direction (DD), daily mean (Tmean), minimum (Tmin) and maximum (Tmax) temperature and relative humidity (RH) are available. For Cabauw and Volkel, additional information is available on daily mean precipitation (Rain). Furthermore, all stations (except Hupsel) measure sea level pressure (P0). Cabauw has additional information on shortwave downward radiation (SWD) and cloud cover (CC). As Cabauw has no direct measurements of relative humidity, shown by Barrero et al. (2006) to correlate significantly ($p < 0.01$) with suspended particles, NO_2, SO_2 and O_3, the relation between 2m air and 2m dew point temperature is used to derive the relative humidity. A quality control was performed at the KNMI (Royal Dutch Meteorological Institute) whereby quality numbers for each measured parameter are defined in the same way as in the former continuous Cabauw programme (Beljaars and Bosveld, 1997). After removal of spurious data, the measurements are averaged to daily values, in order to be able to make a connection with coarsely spatial and temporal gridded data from ECMWF operational analysis or AOGCMs. As for the air quality variables (see section 3.2.3), the first 4 years are used to built the regression model, while the period 2005-2006 is used to validate the model.

Table 3.1: Characteristics of the meteorological and air quality measurement sites in The Netherlands for the period 2001-2006.

Code	Location	Latitude	Longitude	Height (m)	Start measurements	End measurements	Available variables
Meteorological stations (KNMI)*							
375	Volkel	52,07°N	6,65°E	20.1	1/03/1951	Present	DD, FF, Tmean, Tmin, Tmax, Rain, P0, RH
340	Woensdrecht	51,45°N	4,35°E	14.9	2/05/1995	Present	DD, FF, Tmean, Tmin, Tmax, P0, RH
283	Hupsel	51,65°N	5,7°E	29	1/01/1990	Present	DD, FF, Tmean, Tmin, Tmax, RH
348	Cabauw	51.97°N	4.296°E	-0.7	1/01/1997	Present	DD, FF, Tmean, Tmin, Tmax, SWD, RH, P0,CC, Td, Rain
Air quality stations (RIVM -AIRBASE)							
232	Volkel	52,07°N	6,65°E	20.1	Depends on the variable		O_3, NO, NO_2, SO_2
235	Woensdrecht	51,45°N	4,35°E	14.9	Depends on the variable		O_3, NO, NO_2, SO_2, PM_{10}
722	Hupsel	51,65°N	5,7°E	29	Depends on the variable		O_3, NO, NO_2
620	Cabauw	51.97°N	4.296°E	-0.7	Depends on the variable		O_3, NO, NO_2, SO_2
633	Zegveld	52.139°N	4.838°E	3	Depends on the variable		PM_{10}

* A more detailed description of these measurement stations is available at http://www.knmi.nl/klimatologie/daggegevens/download.html

3.2.3 Air quality data

In addition to the meteorological variables, NO, NO_2 and SO_2 concentrations are added as independent variables explaining the variation of O_3 and PM_{10}. The air quality data was obtained from the AIRBASE database (http://air-climate.eionet.europa.eu/databases/EuroAirnet/). Hourly measurements of O_3, NO, NO_2 and SO_2 are selected from the rural stations where available, for the period 2001-2006. Again, these locations are chosen with the expectation that, by selecting a rural background station, non-local correlations would be more clearly revealed and that the confounding effect of local urban vehicular NO_x emissions will be limited (Gardner and Dorling, 2000). Taking into account the use of meteorological variables on a daily scale, a representative daily value is considered for each pollutant. For SO_2 and PM_{10} daily means are considered, while for O_3 the daily 8-hourly maximum mean and for NO and NO_2 the daily maximum value is used (European Community, 1999).

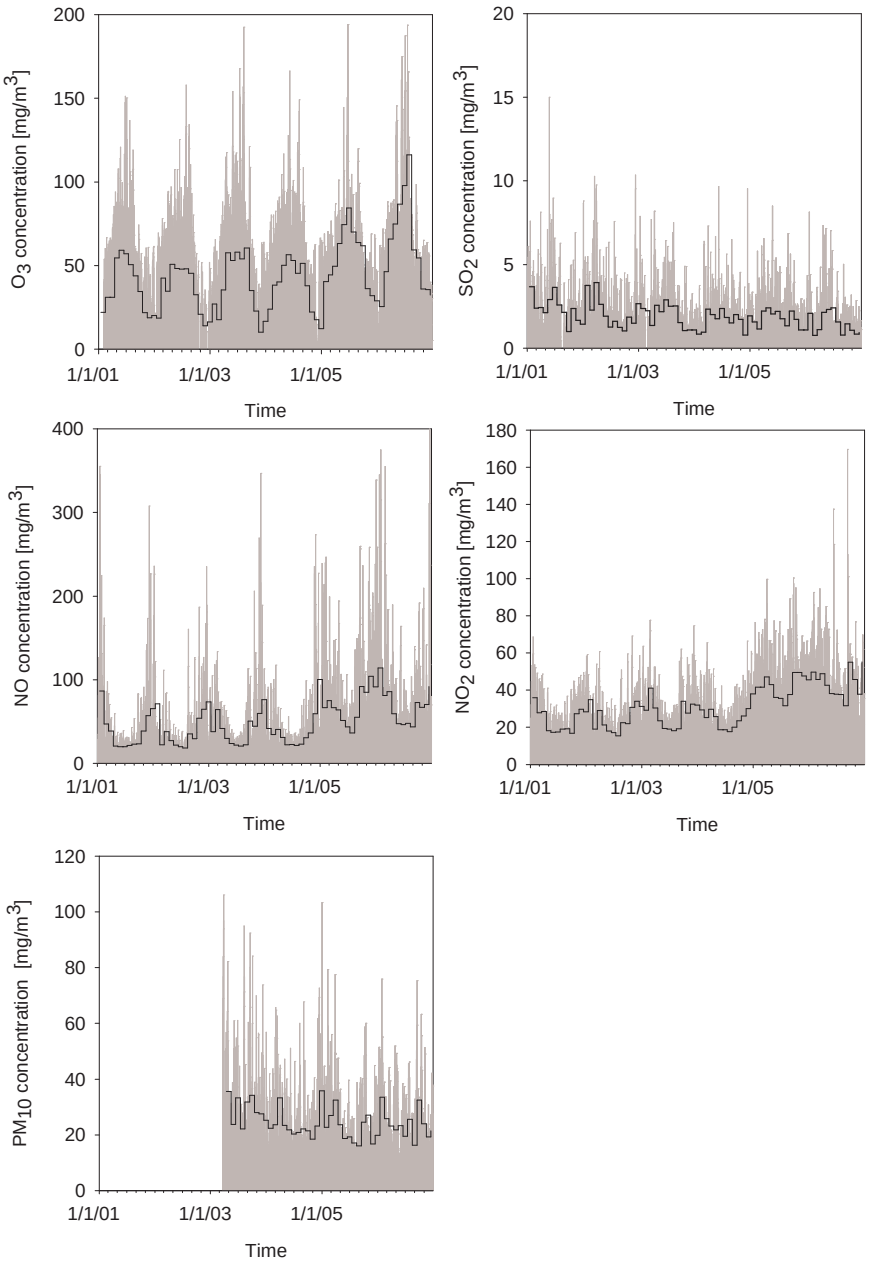

Figure 3.2: Time series of daily (grey bars) and monthly mean (black line) values for surface O_3, NO, NO_2, SO_2 and PM_{10} measured at Cabauw/Zegveld between the period 2001-2006 (03/2003-2006 for PM_{10}).

Monthly and annual cycles are clearly revealed for O_3, NO and NO_2 (Fig. 3.2). The yearly cycles of O_3 reveal the highest peak concentrations in summer, whereas for NO and NO_2, the annual cycle is characterized by a summer minimum and a maximum in winter. This can be understood from the mutual

relation between O_3, NO and NO_2 in which the oxides of nitrogen (next to CO and volatile organic compounds (VOC) react with the hydroxyl radical OH) as precursors in the nonlinear chemical process forming O_3 (NRC, 1991; Sillman, 1999; Satsangi et al., 2004; Lasry et al., 2005). In this respect, scientists have attempted to characterize local regions as 'NO_x-limited' and 'VOC-limited' with respect to the reduction of photo-oxidant formation. The regime in a particular region will depend principally on the concentration of NO_x and the VOC/NO_x ratio. Thereby, urban areas are often denoted as 'VOC-limited' (lower VOC concentrations), whereas rural and suburban areas are denoted as 'NO_x -limited' (lower NO_x concentrations) (Reis et al., 2000). Here, NO_x acts as a catalyst and produces O_3 until its removal as NO_3 by deposition processes or its conversion into other forms of nitrogen. More detailed information on the photochemical reactions forming ozone under varying NO_x and volatile organic compounds emissions can be found in Sillman and He (2002). For SO_2 and PM_{10}, concentration levels are rather constant throughout the year. The highest monthly SO_2 concentrations are reached in January and June, while the maximum daily concentration is reached in March. Additionally, differences among the seasons can be considered relatively small (< 1 standard deviation).

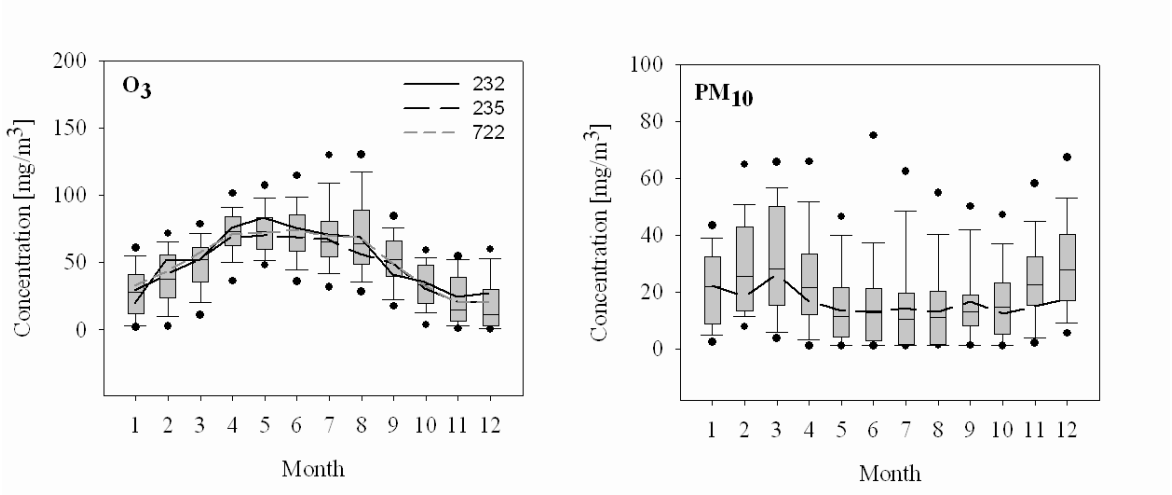

Figure 3.3: Monthly distribution of O_3 and PM_{10} concentrations for Cabauw/Zegveld (as Box-Whiskers), Volkel (232), Woensdrecht (235) and Hupsel (722). The boxes present the median, the first and third quartiles, while the whiskers and dots present the minimum and maximum value and possible outliers respectively.

In order to know whether different rural sites in the Netherlands have similar characteristics in terms of O_3 and PM_{10} concentrations, the annual cycle for all selected sites is depicted in Fig. 3.3. Concerning O_3 it is found that the highest median concentrations are observed in spring months (MAM) for all stations, whereas peak concentrations occur in summer (JJA). This refers to the presence

of a spring and summertime maximum often seen in midlatitudes (Delcloo and De Backer, 2008). As it is also shown by Fig. 3.2, the lowest daily medians of surface ozone concentrations are found in November, December and January. For PM_{10}, maximum daily mean concentrations are found in June and December, while in Cabauw and Woensdrecht a less distinct peak can be observed in February and March. Furthermore, it is clear that for both O_3 and PM_{10}, all sites are characterized by similar annual cycles in terms of their median concentrations. Furthermore, the Directive 1999/30/EC and following up Directive 2008/50/EC of the European Parliament (EU, 1999, 2008) suggest a threshold concentration of 120 µg/m³ and 50 µg/m³ for a maximum eight-hourly mean O_3 and daily mean PM_{10} concentration respectively for Europe. The number of days exceeding these thresholds for the different rural sites range between 3 - 4.5 % yr^{-1} for O_3 and 6.2 - 8 % yr^{-1} for PM_{10}. This shows that there are only minor differences in O_3 and PM_{10} concentrations for different rural measurement sites in The Netherlands, as was also suggested by Flemming et al. (2005) for other rural areas.

3.3 Methods

It is now widely accepted that there are two main approaches in synoptic climatology to investigate the links between local-scale environmental features and large-scale circulation patterns (Yarnal, 1993): the environment-to-circulation approach and the circulation-to-environment approach. The former structures the circulation data based on criteria defined by the environmental variable and lacks any capability in a predictive mode, but can be of use in a descriptive way to get more insight in those patterns that are regulating the magnitude of surface environmental variables. Conversely, the latter classifies the circulation data based on standard pressure fields (e.g. SLP or 500 hPa geopotential height), prior to seeking links with the local-scale environment. In this study, we adopt the latter, which has the capability to calculate expected air quality conditions related to each circulation pattern, and to compare this forecast with the observed air quality values to evaluate the strength of the circulation-to-environmental approach (Cannon et al., 2002).

3.3.1 Stepwise regression analysis

Our goal is to model the maximum 8-hourly mean O_3 and mean daily PM_{10} levels by a linear model that will form the basis for our understanding and reconstruction of the air quality variables based on local-scale meteorological

and air quality observations. For this purpose, we use a robust approach based on stepwise multiple linear regression models for both the dependent variables O_3 and PM_{10}.

Prior to the regression analysis we assess the linear nature of the relationship between the dependent and independent datasets. In case these relations are non-linear, an appropriate variable transformation is applied in order to assure linearity. Secondly, the data is checked for the existence of multicollinearity. If the tolerance (a measure for the strength of a linear relationship among the independent variables) between two variables is below a threshold value of 0.1 (Norusis, 2002), then these variables are highly related and their simultaneous use can be misleading and interfere with a correct interpretation of the regression results. In such a situation, the variables that suffer from multicollinearity should be identified and some of them removed from the rest of the analysis. Only then we apply the multiple linear regression with a stepwise method for variable selection to reconstruct time series for O_3 and PM_{10} with F probability <0.05 to enter and F probability <0.10 to exit. The model was developed with the data subset covering the whole period, from January 1, 2001 to December 31, 2004. Missing data was treated following a listwise deletion (Norusis, 2002), which means that for PM_{10}, only the period from 20th of March 2003 until 31st of December 2004 is considered.

3.3.2 Circulation-to-environmental approach

As our aim is to test the circulation patterns as a future air quality assessment tool, the circulation-to-environmental approach will be followed using the automated Lamb Weather Types (hereafter called WTs) adapted from Jenkinson and Collison (1977) and Jones et al. (1993) to the Low Countries. The rationale for using this approach is that the identification of a clear link between circulation patterns and air quality variables could be used as a downscaling tool for air quality assessment, using operational analysis or AOGCM data as input.

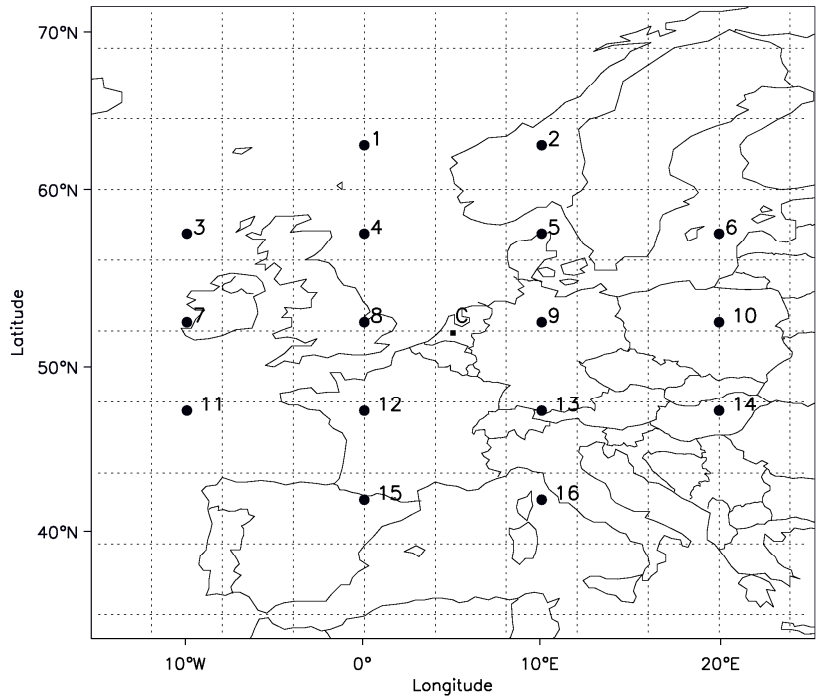

Figure 3.4: Location of Lamb weather type grid on a 5° x 10° resolution, with 16 point centered over the Benelux. "C" denotes the location of the Cabauw measurement station and the grid center.

The WTs are developed using ECMWF MSLP data and for a given day they describe the location of the high- and low-pressure centers that determine the direction of the geostrophic flow. A grid with 16 points is assigned over the larger Western and Central Europe, with a central point over the Benelux, in 52.5°N and 5°E (Fig. 3.4). We computed a set of simple atmospheric circulation indices using mean sea level pressure (MSLP) at 12UTC in these 16 grid points, namely the direction and vorticity of geostrophic flow: southerly flow (SF), westerly flow (WF), total flow (F), southerly shear vorticity (ZS), westerly shear vorticity (ZW) and total shear vorticity (Z). A small number of empirical rules devised previously (Jones et al., 1993; Trigo and DaCamara., 2000) are then used to classify each day as one of the 27 circulation types recently developed in Demuzere et al. (2008).

3.3.3 Model evaluation measures

Statistical model performances are evaluated using appropriate scalar measures and skill scores (Wilks, 1995), namely: the Pearson correlation coefficient (R), mean square error (MSE), root mean square error (RMSE) and explained variance in % (R^2). According to Murphy (1988), the skill of any given model

is a measure of the relative accuracy of a model with respect to a standard reference model. Hence, the skill of any model should be interpreted as the percentage improvement over a reference or benchmark model (Wilks, 1995). The two most commonly applied reference models used in atmospheric sciences are climatology and persistence. Therefore, two skill scores based on the MSE will be used in this paper with the climatological mean (MSE_{clim}) and the persistence (MSE_{pers}) as a reference:

$$SS_c\,(MSE) = \frac{MSE - MSE_{\text{clim}}}{0 - MSE_{\text{clim}}}\ x\ 100\%$$

$$SS_p\,(MSE) = \frac{MSE - MSE_{\text{pers}}}{0 - MSE_{\text{pers}}}\ x\ 100\%$$

with the "0" corresponding to the accuracy level that would be achieved by a perfect model.

Furthermore, the Kruskal-Wallis one-way analysis of variance is used as a non-parametric method to test the difference of O_3 and PM_{10} population medians among the weather type groups (Kruskal and Wallis, 1952). A 1% significance level is used and hereafter denoted as α_{KW} in section 3.4.3.

3.4 Results and discussion

3.4.1 Diurnal, seasonal and annual cycles

Prior to the selection of the weather and air quality variables for the regression analysis, their mutual relations are investigated as a function of time. Therefore, Pearson correlation coefficients are calculated between each of the selected air quality and meteorological variables for each month separately in (Fig. 3.5 and 6). We have used anomalies of each variable in order to remove the annual cycle. Furthermore, we have taken into account autocorrelation effects when computing the Pearson correlation values. Hence, the sample size n is replaced by an effective (smaller) sample size n_{eff} that returns the Pearson correlation coefficient with its respective "adjusted" level of significance (Santer et al., 2000). Previous works have stressed the existence of temporal lags on the relations between air quality and meteorological variables (Kalkstein and Corrigan, 1986; Styer et al., 1995; Ziomas et al., 1995; Cheng and Lam, 2000). In order to investigate such hypothesis we have included in the analysis all

meteorological values registered with 6, 12, 18, 24 and 48-hour lag period (not shown). Below, results obtained for O_3 and PM_{10} are described separately.

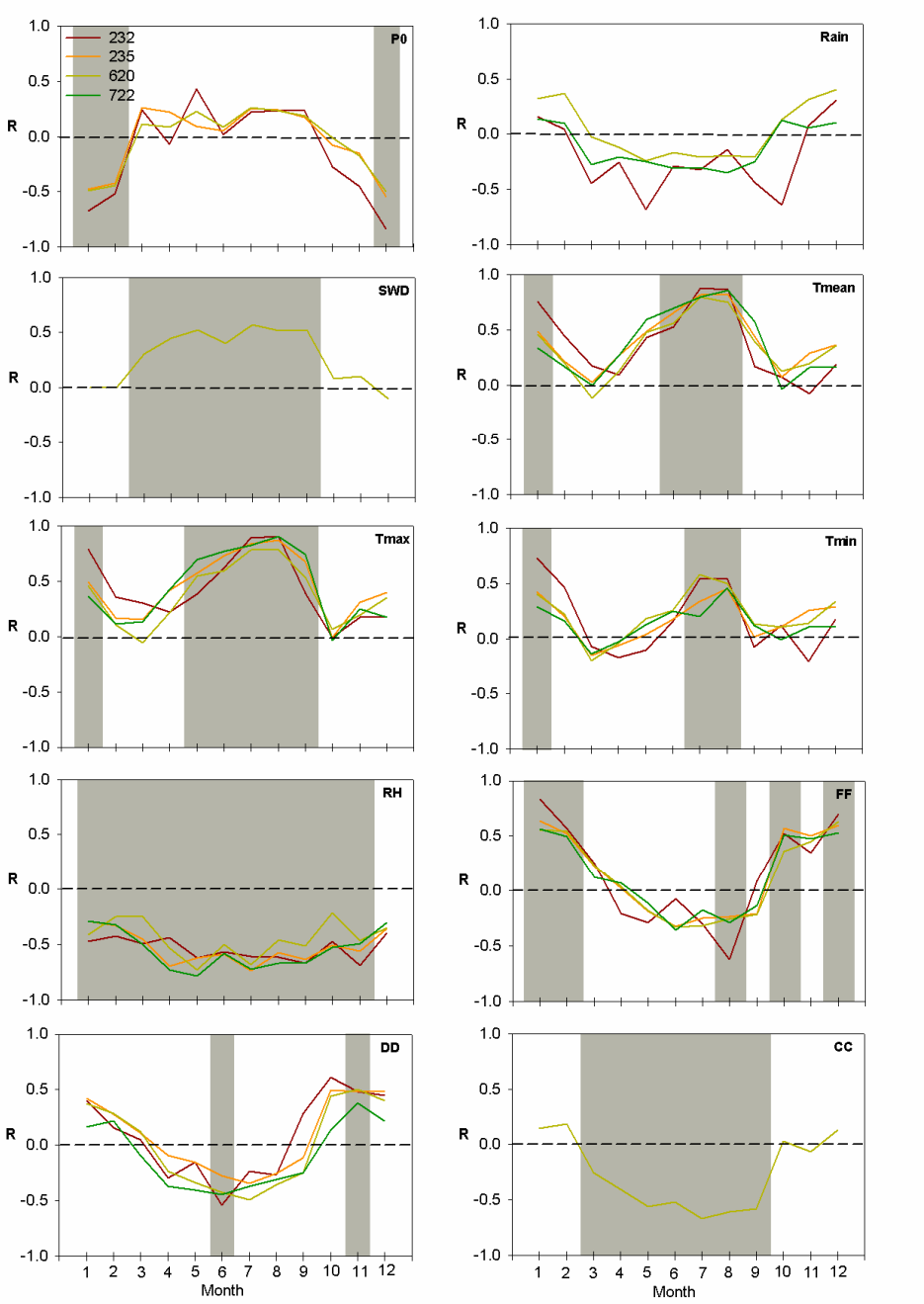

Figure 3.5: Monthly mean Pearson correlation coefficients between daily maximum 8-hourly mean O_3 and all available meteorological variable anomalies for Volkel (232), Woensdrecht (235), Cabauw/Zegveld (620) and Hupsel (722). Correlation coefficients significant on the 99% level are depicted by the grey shaded area. Meteorological variables abbreviations are denoted in Section 3.2.1.

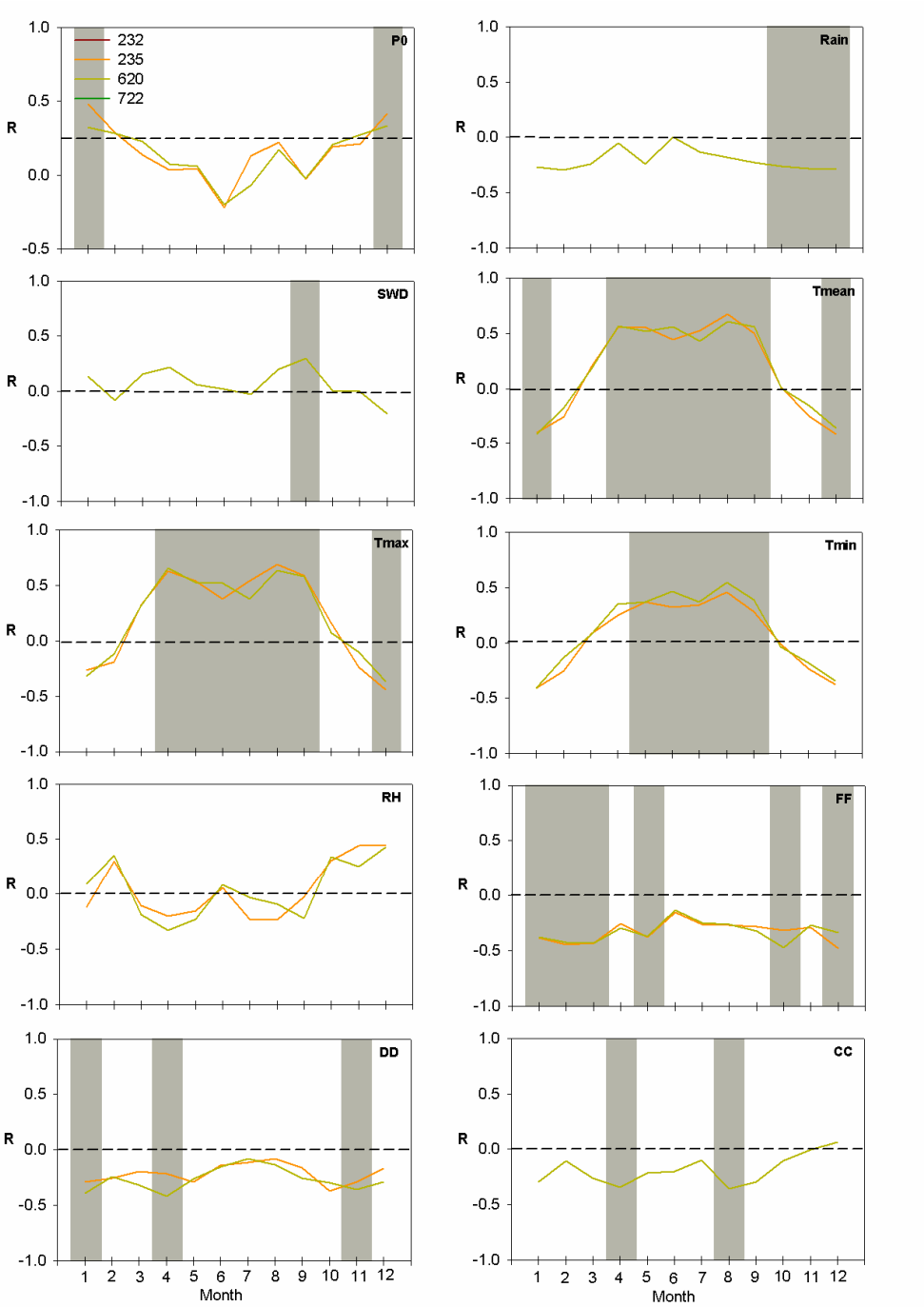

Figure 3.6: As in Figure 3.5, but for PM_{10} and the stations of Woensdrecht (235) and Cabauw/Zegveld (620) only.

O_3 – In general, O_3 correlations are not responding differently on the different time lags. Only for the 12 and 18-hour time lag, correlations coefficients between O_3 and SWD changes from positive to negative values. This is due to daily cycle of the radiation terms at mid-latitudes, which changes from a positive sign during daytime to a negative sign at night. The annual cycle of the

correlations coefficients for temperature show a similar response as for SWD (Fig. 3.5), with a strong positive correlation between O_3 and Tmean /Tmax (with R= 0.89/0.91 respectively) in summer. This response is the opposite of that found for cloud cover, with strong negative correlations in summer. Over the whole year, O_3 is significantly negatively correlated with relative humidity. During summer (JJA), O_3 concentrations are negatively correlated to wind speed, with a minimum of –0.61, whereas this signal reaches a maximum of 0.83 in winter (DJF). This dichotomy is in good agreement to the results of Davies et al. (1992), who found similar correlations between a wind speed index and O_3 concentrations measured in Cabauw for the period 1978-1988 (see their Fig. 3.4). Another striking effect is the significant negative correlation between sea level pressure and O_3 in winter. Together with the significant positive correlations of wind speed for this season, this could point to a transport of ozone from the lower troposphere due to troposheric folding, as described by Davies et al. (1992) and Delcloo and De Backer (2008).

PM_{10} – In general, correlations between PM_{10} and meteorological variables on different time lags weaken as a function of an increasing time lag. Only the correlation coefficients for both the radiation variables swap sign in the course of the year, with a peak difference in summer, when solar radiation is the highest at these mid-latitude locations. The response of air temperature on PM_{10} varies seasonally (Fig. 3.6), with the highest positive correlation coefficients during the JJA (0.69), and negative during DJF (-0.44). This is consistent with the results of van der Wal and Janssen (2000), who found that higher PM_{10} concentrations in winter (summer) coincide with lower (higher) temperature for PM_{10} levels in The Netherlands. For relative humidity, there is an insignificant correlation throughout the year, whereas this correlation is systematic negative for daily precipitation, although the correlation coefficients are only significant for the months October, November and December. Similar to O_3, wind speed is significant negative correlated to PM_{10} for large parts of the year.

Previous research introduced a weekly cycle index as an additional variable in forecasting a) pollutant levels for the Athens area (Ziomas et al., 1995; Grivas and Chaloulakou, 2006), b) PM_{10} levels in the Volos (Greece) area (Papanastasiou et al., 2007) or c) PM_{10} values for Belgium (Hooybergs et al., 2005). However, in our case a weekly cycle is not well established for most pollutants with the exception of NO_x, that shows a decrease during weekends (Saturday and Sunday) (Fig. 3.7). The fact that all measurement stations are denominated as rural, can explain why the day-of-the-week influence on the short-term variability is small. Flemming et al. (2005) confirms this limited weekly variation in O_3, NO, SO_2 and PM_{10} concentrations for German rural

measurement stations. Furthermore, a weekly cycle characterised by the decreasing of NO_x and corresponding increasing of O_3 during the weekend suggests that this is a NO_x limited system (Reis et al., 2000).

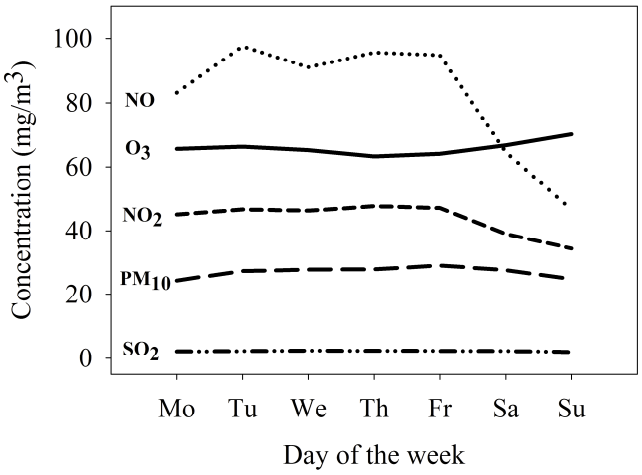

Figure 3.7: Weekly cycles for O_3, NO, NO_2 and SO_2 and PM_{10} concentrations derived from the measurement station of Cabauw.

In general, this analysis between the meteorological and air quality relationships shows only minor differences among the four different rural measurement sites considered within The Netherlands. These results appear to confirm those obtained by previous authors showing that rural areas can be considered as spatially homogeneous in terms of air quality concentrations (e.g. Flemming et al., 2005). Taking these facts into account we opt to carry on our analysis with Cabauw data only. Nevertheless, as correlation coefficients between meteorological and air quality variables do not provide any information on the slope of the linear relation, a simple test is performed for these meteorological variables available for more than one station (not shown). The linear relations between meteorological and air quality variables reveal similar slopes in terms of sign and in terms of the slope an overall deviation in magnitude lower than 0.05. Hence, we consider the Cabauw station to be representative for rural areas in The Netherlands, a decision that is further supported by the fact that, unlike the others, this station has a comprehensive set of both meteorological and air quality variables.

Furthermore, the lag analysis also points out that the addition of time lags shorter than 1 day does not provide sufficiently additional information. Therefore, only the 1 and 2 day time lags for both meteorological and air

quality variables are taken into account in the subsequent regression analysis. Finally, as mentioned before and shown in Fig. 3.7, a weekly cycle in air quality measurements from Cabauw is not well established; therefore, this variable is also dismissed.

3.4.2 Stepwise multiple regression

A large amount of research has been conducted in the last decade to test the capacity of (linear) multiple regression (MLR) analysis and (non-linear) neural networks for air quality prediction purposes based on both air quality and meteorological input. It has been shown that model errors decrease by including persistency (lag effect) of the air quality variables (Perez et al., 2000; Smith et al., 2000; Perez, 2001; Barrero et al., 2006; Grivas and Chaloulakou, 2006). The aim of this research is to develop an approach that is also useful for downscaling operational low-resolution or AOGCM output data in terms of air quality assessment on the longer time scales. In this context, there is no information on the (future) air quality data and emissions as a dependent input variable. Therefore, the regression analysis is performed for two sets of predictors, both using measurements from Cabauw only: 1) without any air quality data, hereafter called MET, and 2) with the 24- and 48-hour time lag values of air quality variables included as independent variables, hereafter called METCHE.

Table 3.2 shows the resulting model coefficients for both O_3 and PM_{10}. All the variables introduced in the model are associated to a coefficient that is statistically significant. For both MLR_{MET} and MLR_{METCHE}, relative humidity is the most significant variable. This is in accordance with similar results using MLR for the prediction of ozone in four locations in Taiwan (Lu et al., 2006) and based on PCA for the region of Oporto in Portugal (Sousa et al., 2007). Furthermore, Tmax plays an important role, both on the present and previous day in both analyses for O_3. Including air quality variables as predictors explains 15% more of the observed O_3 variance, whereby O_3 and NO_2 concentrations from the previous day provide additional relevant information in agreement with results obtained in previous studies by Davis and Speckman (1999) and Barrero et al. (2006). Both MLR_{MET} and MLR_{METCHE} also reflect the importance of shortwave downward radiation and wind speed, and for MLR_{METCHE}, the concentrations of nitrogen oxides on the previous day.

Table 3.2: Summary of the model coefficients b, the standardized coefficients β, t-statistic and partial explained variance R^2 for the stepwise multiple regressions MLR_{MET} and MLR_{METCHE} for O_3 and PM_{10}.

O_3	MLR_{MET}					MLR_{METCHE}			
Variable	b	β	t	Partial R^2	Variable	b	β	t	Partial R^2
(Constant)	-0.60		-1.51		(Constant)	-0.59		-1.60	
RH	-0.80	-0.30	-9.59	0.23	RH	-0.68	-0.26	-8.56	0.24
TA002max	1.52	0.26	6.79	0.071	O3 (lag24)	0.36	0.36	14.73	0.16
P0 (lag24)	-0.32	-0.14	-5.89	0.023	TA002max (lag24)	1.39	0.23	7.38	0.033
SWD	0.06	0.16	5.07	0.01	NO2 (lag24)	-0.17	-0.14	-4.62	0.022
TA002max (lag24)	0.82	0.14	4.36	0.01	SWD	0.054	0.15	4.97	0.015
F010	1.37	0.13	4.79	0.01	O3 (lag48)	-0.12	-0.12	-5.12	0.012
DO10 (lag24)	0.19	0.066	2.60	0.006	P0 (lag24)	-0.30	-0.13	-5.60	0.008
TA002min	-0.65	-0.10	-2.65	0.005	TA002max	1.05	0.18	4.91	0.006
SWD (lag24)	0.021	0.058	2.20	0.002	TA002min (lag24)	-0.56	-0.081	-2.60	0.005
D010	0.012	0.056	2.05	0.002	F010	1.26	0.12	4.54	0.005
					F010 (lag 24)	-1.18	-0.11	-3.85	0.003
					D010	0.022	0.076	3.29	0.004
					TA002min	-0.58	-0.089	-2.48	0.003
					NO (lag24)	-0.023	-0.072	-2.42	0.002
Calibration [a]									
R^2	0.37					0.52			
RMSE	14.3					12.8			

PM_{10}	MLR_{MET}					MLR_{METCHE}			
Variable	B	β	t	Partial R^2	Variable	b	β	t	Partial R^2
(Constant)	1.08		2.49		(Constant)	0.91		2.06	
F010	-1.48	-0.18	-4.54	0.088	PM10 (lag24)	0.34	0.34	9.57	0.18
TA002max	1.34	0.29	7.55	0.037	NO (lag24)	0.037	0.16	3.85	0.07
F010 (lag24)	-1.27	-0.17	-4.18	0.039	RH	0.44	0.23	4.84	0.047
SWD	-0.048	-0.19	-3.91	0.027	TA002max	1.10	0.23	6.02	0.046
CC (lag48)	-0.81	-0.12	-3.36	0.018	F010 (lag24)	-1.28	-0.16	-3.83	0.015
Rain	-75.2	-0.15	-3.94	0.013	RH (lag24)	-0.19	-0.097	-2.42	0.013
RH	0.32	0.17	3.62	0.011	Rain	-65.45	-0.12	-3.23	0.008
D010 (lag24)	-0.24	-0.11	-3.01	0.012	SWD	-0.032	-0.12	-2.71	0.009
Rain (lag24)	-40.8	-0.084	-2.27	0.006	NO (lag48)	0.018	0.081	2.23	0.006
					D010 (lag24)	-0.016	-0.075	-2.01	0.005
Calibration [b]									
R^2	0.25					0.42			
RMSE	11.1					10.1			

a Calculated over the period 2001-2004

b Calculated over the period 20-3-2003 to 31-12-2004

For PM_{10}, wind speed is most significant when no air quality predictors are included while Tmax is important in both models, results that agree with those obtained by Stadtlober et al. (2008) for Bolzano (South Tirol - Italy). The model results improve from $R^2 = 25.0$ for MLR_{MET} to $R^2 = 42.0$ when the air quality variables are included (MLR_{METCHE}). Here, the previous day PM_{10} concentration is shown to be an important parameter for the prediction of PM_{10} levels, as was shown in previous works (e.g. Hooyberghs et al., 2005; Stadtlober et al., 2008). Furthermore, also previous day NO is in important indicator for high PM_{10} concentrations. This strong correlation indicates road traffic as a local source (Harrison et al., 1997). Although Cabauw/Zegveld is classified as a background rural station, the different behavior of NO depending on the day of the week (Fig. 3.4) points to a possible influence of road traffic on the PM_{10} measurements. This tendency is confirmed by the recent results of Schaap et al. (2008), who have found higher $PM_{2.5}$ concentration in Cabauw compared to other European rural background areas. A comparison of the quality of the two models for PM_{10} shows that our results are of similar magnitude of those by Slini et al. (2006) and van der Wal and Janssen (2000), that have obtained a correlation coefficient of respectively 29.7 and 25.0 % without any further information on air quality predictors. In the following section 3.5, a more thorough validation of the MLR approach and a comparison with the circulation approach will be performed.

3.4.3 Circulation-to-environment approach

The interannual variability of the eleven resulting Weather Types (WTs) is depicted in Fig. 3.8, showing the relative frequency of each WT averaged for each month over the period 2001-2004. The anticyclonic type is the most frequent circulation pattern throughout the year, except for the month of October, which is dominated by the southwest (SW) and west (W) circulation types. Throughout the year, the relative frequency of cyclonic situations is almost constant, reaching a peak in August. The meridional circulation types north (N) and south (S) are rather constant throughout the year, except for a decrease of N observable from October to December. All WTs with a westerly component and thus originating in the Atlantic Ocean (SW [southwest], W [west], NW [northwest]) present stable relative frequencies through most of the year, although the NW regimes decline during winter and early spring. This phenomenon is counteracted by an increase of anticyclonic types between March and May, which is in agreement with the well known maximum of blocking frequencies over the Euro-Atlantic region (d'Andrea et al., 1998; Trigo et al., 2004). The remaining types with an eastern component (NE, E [east] and SE [southeast]) are the least frequent of all weather types throughout

the year with the relative frequencies of E being virtually zero between May and August.

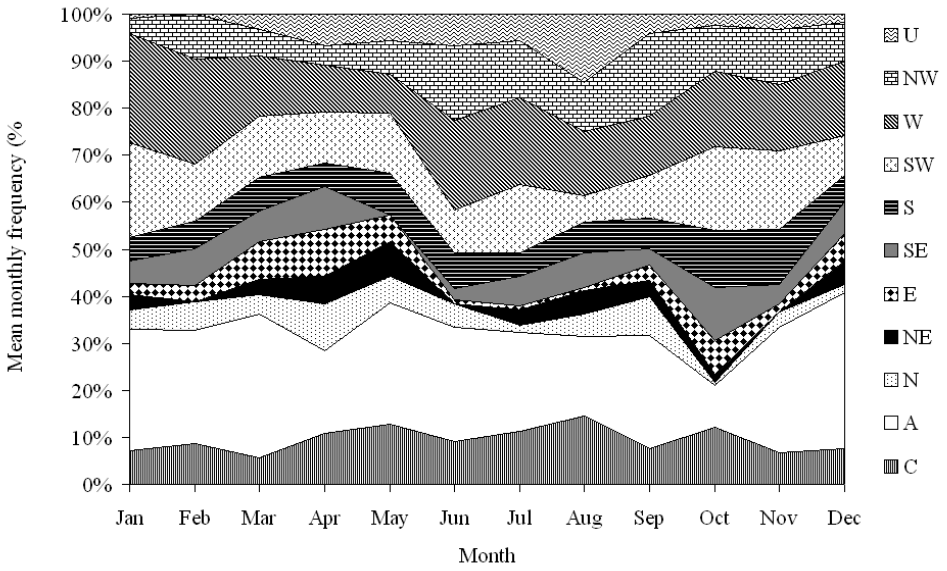

Figure 3.8: Monthly mean frequencies of Lamb Weather Types over the period 2001-2004. The acronyms of circulation patterns are as follows: U = unclassified, NW = northwest, W = West, SW = southwest, S = south, SE = southeast, E = east, NE = Northeast, N = North, C = Cyclonic and A = Anticyclonic.

The analysis in section 3.2.3 (Fig. 3.3) has shown that the annual distribution of O_3 and PM_{10} is similar over the various rural sites in The Netherlands. Therefore, the circulation type-specific O_3 and PM_{10} concentrations are analysed for the Cabauw measurement site only. Figures 3.9 and 3.10 depict the statistical distribution of O_3 and PM_{10} according to their respective WT class. Because some weather type clusters have insufficient data, a few percentile bars/outliers are absent from Fig. 3.10. For O_3, an insignificant explained variance (0.03) and α_{KW} >1% show a limited discriminative power over the whole year (Fig. 3.9).

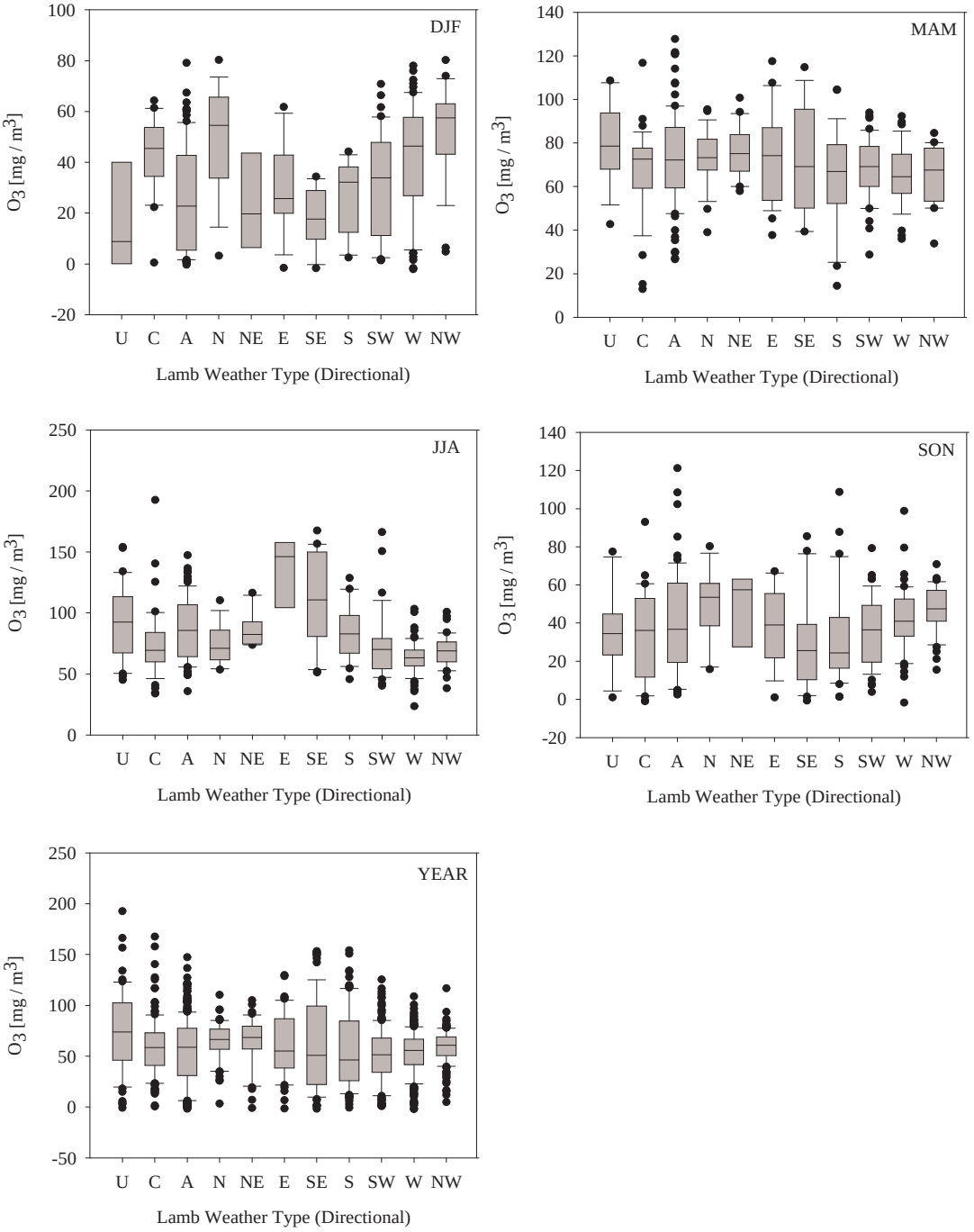

Figure 3.9: Box – Whiskers plots with the concentrations of O_3 according to the Lamb weather type classes per season and year, averaged over the period 2001-2004. The box and whiskers present the median, the first and third quartiles, the minimum and maximum value and possible outliers. The circulation types are the same as in Figure 3.8.

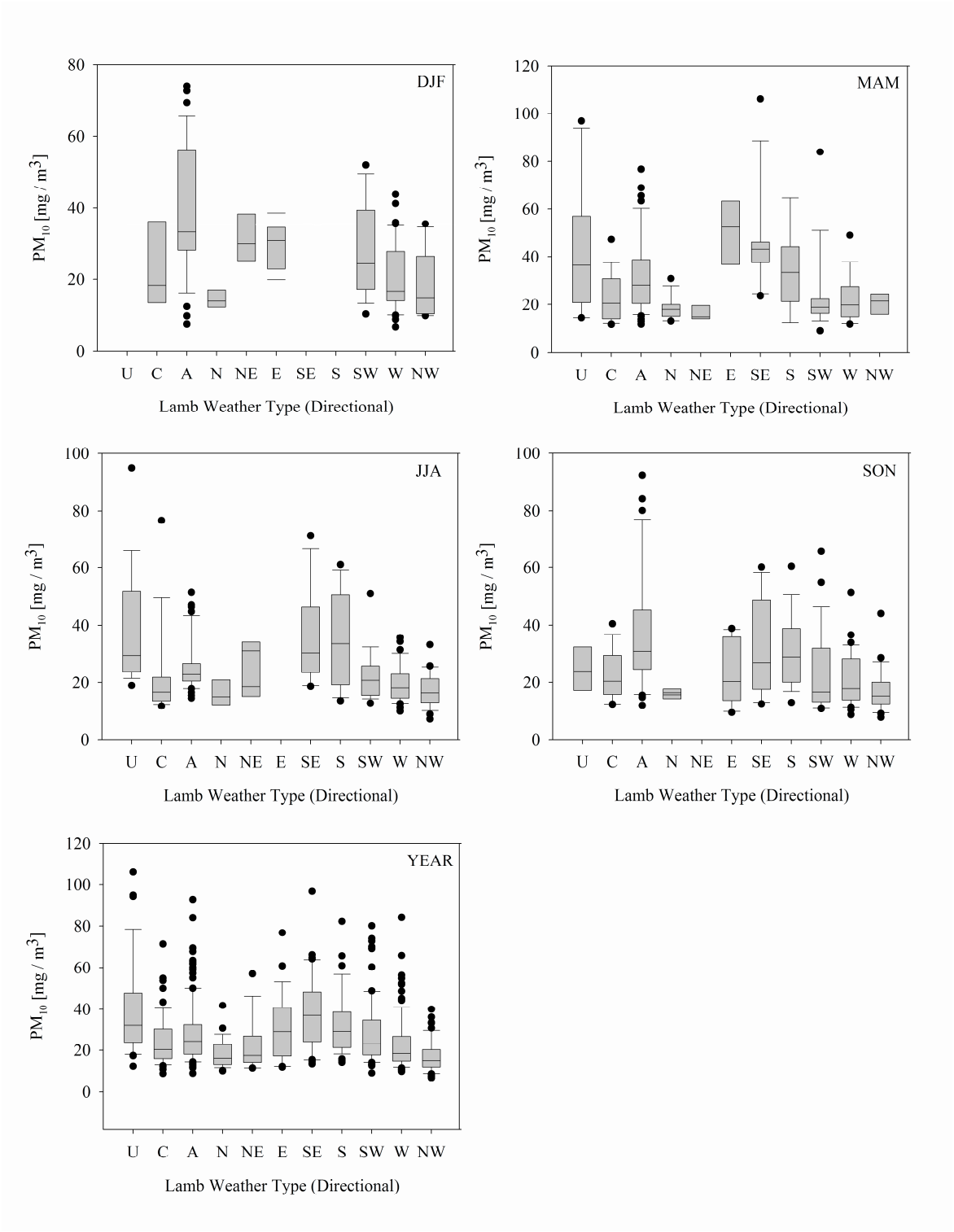

Figure 3.10: As in Figure 3.9, but for PM_{10}.

Nevertheless, the results based on seasons show some significant results. For DJF, highest concentrations can be observed in the C (Cyclonic), N, W and NW WTs. Davies et al. (1992b) obtained similar dependence for ozone with N, NW and W weather patterns in Cabauw. It is noticed that some of the latter are related to strong winds and tropopause folding mechanisms whereby ozone can be transported from the lower troposphere (Delcloo and De Backer, 2008). The lowest DJF concentrations can be found in E, SE and S directional circulation patterns. This discriminative power of the WT technique for O_3 assessment is supported by an explained variance of 26.0% and $\alpha_{KW} < 1\%$. Lamb weather types do not succeed in explaining a great deal of the observed variance in MAM, which is also supported by an insignificant R^2 factor (5.0%) and $\alpha_{KW} > 1\%$. The relation between the WTs and concentration of O_3 in JJA is opposite compared to the DJF situation. Whereas in DJF the highest concentrations are found in West to North directions, in JJA these can be found in opposite East – Southeast directions. This coincides with the highest median concentrations of NO and NO_2 for the SE circulation pattern (not shown). This increased transport of NO_x in summer from the densely populated Ruhr area (located south-easterly) makes the atmosphere more abundant of O_3 precursors, which can lead, in combination with positive temperature anomalies/increased solar radiation, to higher O_3 formation and concentrations. The SON patterns are typical of a transitional period characterised by changing conditions from JJA to DJF, namely with a shift in highest concentrations from North to Easterly directions, and lower concentrations from Southeast to Southerly directions. For both JJA and SON, $\alpha_{KW} < 1\%$, so that the medians of the O_3 and PM_{10} clustered per weather type group are significantly different.

In general, the Kruskal-Wallis test shows that the Lamb weather types are able to distinguish between high and low episodes of PM_{10}, with $\alpha_{KW} < 1\%$ in all seasons and over the whole year averaged. For DJF, the Box-Whisker plot shows the lowest concentrations of PM_{10} originating from Western to Northern circulation patterns, and the highest median concentrations during A and SE WTs. This is supported by the findings of van der Wal and Janssen (2000) who has obtained the highest PM_{10} levels in DJF in The Netherlands with winds prevailing from east to southeast. The explained variance is the highest (30.0%) when compared to the other seasons. In MAM, the highest PM_{10} concentrations are grouped with the WTs ranging from East to South directions, which could be associated to the transport of PM_{10} from the high industrial Ruhr area. As for DJF and MAM, the highest PM_{10} levels can be found for the SE and S classes, and the lowest levels for types originating from West to Northwest. Again, this confirms the results of van der Wal and Janssen (2000) who reported higher levels of PM_{10} in JJA during dry weather condition with positive temperature

anomalies, which is the case for the SE and S Lamb weather types (not shown). In autumn, the explained variance is the lowest (21.0%), although the highest levels of PM_{10} can again be associated with southeast to southern flow patterns.

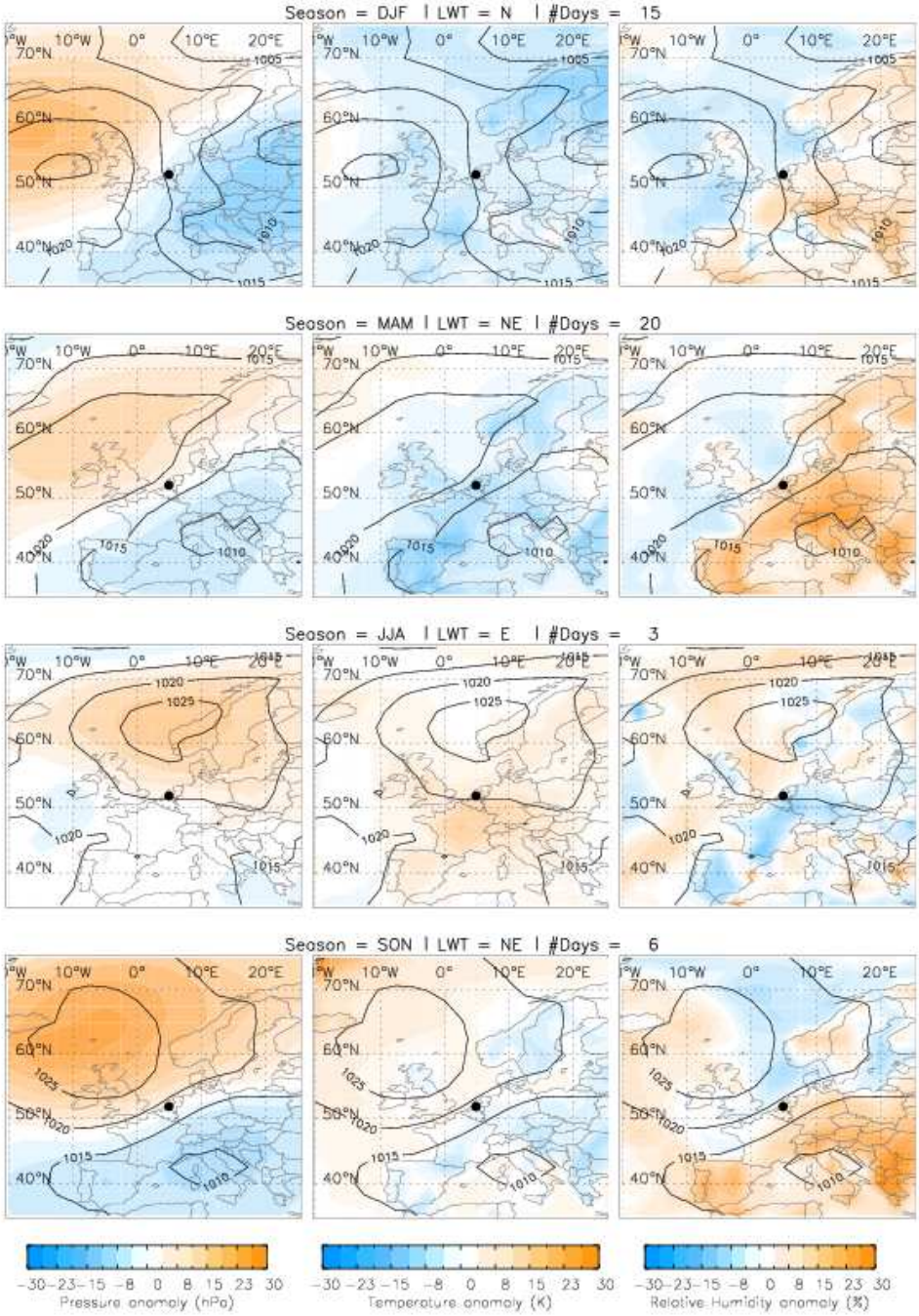

Figure 3.11: Mean surface pressure fields (in hPa) for the circulation type in each season characterized by the highest median O_3 concentration for the period 2001-2004. Shaded colors show the pressure anomalies (left panels), 2m temperature anomalies (middle panels) and relative humidity anomalies (right panels) from the long-term mean (1971-2000). The full dot refers to the Cabauw measurement location.

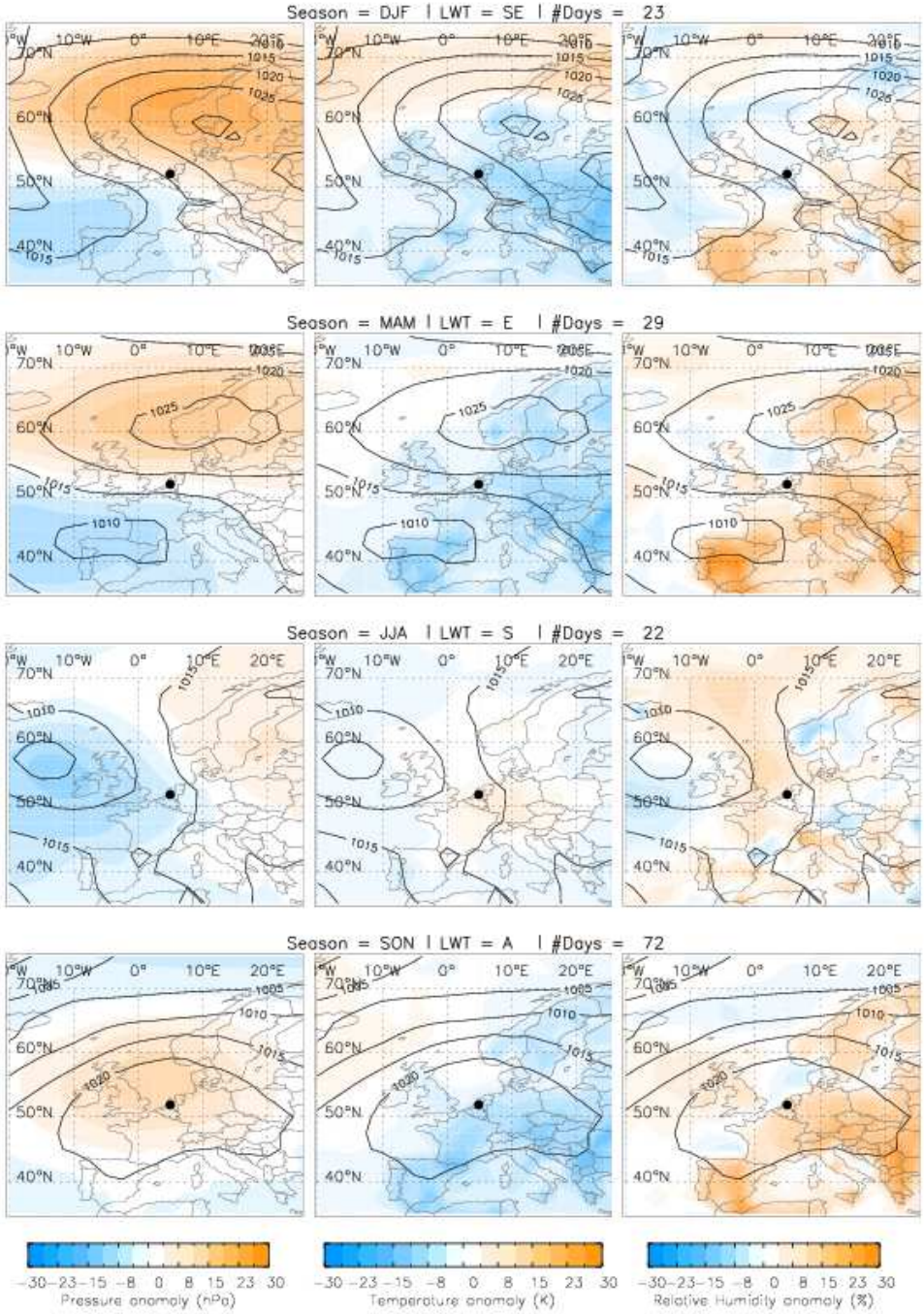

Figure 3.12: Same as Figure 3.11, but for PM_{10}.

In order to gain further insight into the physical conditions behind the WT-air quality relationships, we derive the seasonal composite pressure maps for each circulation pattern that is associated with the highest median of O_3 and PM_{10} (Fig. 3.11 and 3.12). For each season, the circulation type with the highest median of the air quality variable is identified, and the corresponding mean

circulation pattern is depicted for the period 2001-2004 together with the MSLP, temperature and relative humidity anomalies (computed with the normal period from 1971-2000). For O_3, the winter surface MSLP composite map shows a meridional pressure gradient, with high pressure located just west of Ireland, and a low-pressure system positioned over north-eastern Europe. This implies a strong northerly circulation that is consistent with previous results of a strong correlation between high O_3 levels and strong winds in winter (Davies et al., 1992b). The anomaly maps show an enhanced positive pressure anomaly south of Iceland, and a negative anomaly east of Cabauw. These patterns also suggest strong winds and high frequencies of troughs or even cut-off lows in the vicinity of the observation station, which suggests transport of air mass from the upper troposphere (low troposphere) to the surface (Delcloo and De Backer, 2008). This could explain the higher concentrations associated with these patterns, as in non-summer months there is less opportunity for photochemical production of ozone in the boundary layer (Davies et al. 1992b).

The spring MSLP maps show the Azores high pressure system extending far towards the northeast and a low located over Italy. This pattern results in a weak northwest-southeast pressure gradients and resulting winds from the northeast and a negative (positive) temperature (relative humidity) anomaly over continental Europe. The spring MSLP anomalies indicate that the pressure gradient is slightly stronger than normal, a fact that is consistent with the positive (albeit insignificant) relation with wind speeds in spring.

The JJA composite MSLP maps show a strong anticyclonic system located north of Cabauw, resulting in a weak meridional flow. This situation transports warm and dry air from east and central Europe to large parts of Western Europe promoting the appearance of a positive (negative) temperature (relative humidity) anomaly fields. This is consistent with the strong positive (negative) relation between temperature (relative humidity) that characterises high O_3 levels in summer. Pressure gradients and corresponding anomalies are generally weak, which is also consistent with the negative relationship between high O_3 levels and wind speed. These findings confirm the results of Delcloo and De backer (2008), who have shown that high summer ozone events in Uccle (Belgium) - which has generally similar synoptic characteristics as Cabauw – are often generated by slow moving air masses, residing over the continent. Furthermore, our results agree with those of Guicherit and Van Dop (1977), who found a similar relation in the 1970s between high ozone levels and the synoptic situation above The Netherlands. The Grosswetterlagen patterns (Baur et al., 1944; Hess and Brezowsky, 1952) associated with their high ozone levels events describe a closed high over Middle Europe (HM), high over Scandinavia

(Hfa) or high over the North Sea – Iceland (Hna), comparable to our results using Lamb weather types.

The autumn composite MSLP map exhibits a strong northwest-southeast pressure gradient, with an enhanced flow from the northeast. A positive pressure anomaly located northeast of the British Isles presents the highest magnitude when compared to those obtained in other seasons. Anomalies for temperature and relative humidity are generally characterised by negligible values which consistent with our explorative correlation analysis in section 3.4.1.

For PM_{10}, high levels occur during those occasions where air masses are advected from the south or east. In DJF, a large anticyclonic system covers large parts of north and Eastern Europe, associated with a high positive pressure anomaly centred west of the Norwegian coast. Such pattern results in a south-eastern flow (over the highly industrialized Ruhr area), and advection of cold continental air. This is consistent with the negative correlation of PM_{10} levels with temperature and mean sea level pressure (section 3.4.1) and the results obtained by van der Wal and Janssens (2000), who have used PM_{10} data of nineteen monitoring sites in The Netherlands (for the period 1993-1994). In MAM, this pattern is similar, although weaker, with a positive anticyclonic system placed over Scandinavia, and a low pressure placed over the Bay of Biscay, again advecting cold air from central Europe. In summer, pressure gradients are generally weaker, with a small negative (positive) pressure anomaly located west of Ireland (Baltic Sea) promoting the advection of warm air from the south. A result that is consistent with the positive correlation of PM_{10} levels and wind speed in JJA, confirming the results obtained by van der Wal and Janssen (2000) who stated that concentrations of PM_{10} are higher than normal during summer under conditions of high temperatures and dry weather. Autumn is characterised by a blocking high-pressure system over the northern sea, which results in calm, colder than normal weather over the area.

3.5 Validation of MLR and LWT

In the previous sections 3.4.2 and 3.4.3 we have derived results for the MLR and WT approaches highlighting the resemblance with similar research done for Benelux and in other regions. Here we provide an objective comparison between the results obtained with the MLR and the WT air quality assessment models, using the period 2001-2004 for calibration and the remaining years 2005-2006 for validation purposes. For MLR, the regressions obtained in

section 3.4.2 are used on the validation dataset while for the WT methodology, O_3 and PM_{10} means are computed for each of the circulation patterns for 2005-2006. The average value of the air quality variable associated with each circulation pattern is used to reconstruct the time series.

Table 3.3: Validation of the multiple linear regression in 2 modes (MLR – MET and MLR – METCHE) and the Lamb weather type approach in 2 modes (LWT-year and LWT-seas) using the explained variance (R^2), root mean square error (RMSE) and two skill scores (SS_c and SS_p) for O_3 and PM_{10} over the whole measurement period and the validation period 2005-2006.

Calibration (2001-2004)	R^2 (%)					RMSE	SSc	SSp
O3	Year	DJF	MAM	JJA	SON			
MLR - MET	37.2	29.2	36.0	50.4	33.6	15.1	94.6	36.3
MLR - METCHE	51.8	50.4	43.6	60.8	44.9	13.3	95.8	50.4
LWT - year	1.2	3.24	3.61	8.41	0.00*	19.0	91.4	-0.95
LWT - seasonal	12.3	5.29	5.76	22.1	4.84	17.9	92.4	10.7
PM10								
MLR - MET	25.0	23.0	26.0	28.1	24.0	12.1	72.8	16.9
MLR - METCHE	42.3	31.4	50.4	36.0	46.2	10.7	86.3	34.5
LWT - year	13.0	12.3	17.6	16.0	9.61	12.9	80.1	4.59
LWT - seasonal	17.6	17.6	22.1	18.5	16.8	12.6	81.1	9.63
Validation (2005-2006)								
O3								
MLR - MET	51.8	64.0	38.4	68.9	26.0	11.3	96.8	9.90
MLR - METCHE	62.4	65.6	51.8	77.4	28.1	10.1	97.4	28.0
LWT - year	4.0	0.09*	1.69	13.0	0.49*	15.7	93.7	-73.8
LWT - seasonal	20.9	23.0	6.25	29.2	0.16*	14.2	94.8	-43.3
PM10								
MLR - MET	34.8	21.2	51.8	44.9	32.5	6.06	78.3	1.18
MLR - METCHE	36.0	27.0	46.2	51.8	30.3	6.24	93.4	-4.58
LWT - year	15.8	16.8	24.0	21.2	7.84	6.74	92.2	-22.2
LWT - seasonal	23.3	22.1	27.0	24.0	20.3	6.44	92.9	-11.3

Results achieved with all the developed models, for both the calibration and validation periods, are shown in Table 3.3. In general, MLR techniques are known to underestimate peak levels of ozone (Barrero et al., 2006). Interestingly, although the MLR model is built using the calibration dataset only, we can observe an increase in accuracy for O_3 (>10% in explained variance) when the model is applied to the validation dataset for both MLR_{MET} and MLR_{METCHE}. Thus, errors between observed and modelled O_3 levels from

the validation period decrease (while R^2 increases), especially in JJA and DJF with 15% and 30% respectively. In terms of seasonal differences, the regression model explains more of the observed variance in DJF and JJA and less in the transition seasons. The skill score against the climatological mean is higher than 90% for both MLR_{MET} and MLR_{METCHE}, which points out that a forecast based on climatology is easily outperformed by a linear model (or an analysis based on circulation patterns). As expected, persistence corresponds to a benchmark model considerably more difficult to beat, therefore any positive values of SSp are particularly relevant. The better quality of the MLR_{METCHE} model when compared with the MLR_{MET} can be observed in this assessment against persistence, with an improved skill score from 36 to 50% (validation period) and from 9.9 to 27% (validation period) for MLR_{MET} and MLR_{METCHE} respectively.

Table 3.3 also reveals an improvement for the WT approach applied on the validation dataset compared to the calibration dataset. In general, the circulation patterns explain less than 21% of the observed O_3 variance, again with the highest scores being observed in DJF and JJA. Explained variance improves significantly (between 10 to 16%) for the WT based on seasonal means compared to yearly averages. However, overall scores are considerably lower when compared to those obtained with MLR while the RMSE values are about 5 $\mu g/m^3$ higher compared to those from the regression analysis. Although WT presents a good skill score against the climatological mean, it fails to show any significant improvement against persistence, revealing sometimes even a lower quality than the persistence model. These results implies that, although circulation patterns are able to discriminate between high (low) concentrations for different seasons and WTs, day-to-day variability and the complex sequence of physic-chemical ozone formation/destruction mechanisms play a large role that can not be fully captured by the circulation pattern classification.

For PM_{10}, the performance of the model improved significantly for MLR_{MET} model, with a R^2 increase of 25 and 35% for the calibration and the validation periods respectively. However, the MLR_{METCHE} reveals a slight decrease in performance from 42% to 36% between these two datasets. In general, the overall best performance (based on R^2) is obtained in MAM, JJA and SON, depending if the air quality variables are included as predictors or not. Results are worse for DJF, which could be due to possible high PM_{10} events related to an increased surface stability (surface inversion) that is not captured by MLR trained with surface meteorological data. The skill score for the calibration and validation dataset against climatology improves 15% for both periods, between the MLR_{MET} and MLR_{METCHE}. The skill score against persistence improves

similarly for the calibration dataset, although this is not the case for the validation dataset.

The analysis for the PM_{10}-LWT approach shows low coefficients for R^2, although somewhat higher compared to the R^2 obtained for the O_3-LWT model, with a maximum explained variance for the validation period using LWT based on seasonal averages (R^2 = 23.29). Identical to MLR, the observed variance for PM_{10} is explained the most in MAM, and JJA. The skill score against climatology is higher for both the calibration and validation dataset compared to the MLR_{MET}, with overall high scores (>80%). For the calibration dataset, the LWT approach is performing slightly better than the persistence model, while for the validation dataset, results are worse.

Concerning the WT classification method, it is fair to state that our results partially contradict previous studies that discussed the strength of synoptic categories in relation with air pollution concentrations (e.g. Comrie and Yarnal, 1992; Davies et al., 1992b; Kalkstein et al., 1996; Cheng and Lam, 2000; Ainslie and Styen, 2007). This discrepancy could be due to multiple reasons. However, we firmly believe that the most important reason is associated with the lack of validation measures used in those studies. In fact these studies described synoptic situations associated with characteristic levels of an air quality variable without objectively quantifying this result, an approach that can lead to misleading results. Nevertheless other issues may also intervene, as for e.g. levels of air pollutants associated with typical circulation patterns are solely compared to other classification approaches (Cannon et al., 2002). Furthermore, there are many different classifications techniques of atmospheric circulation types (PCA, clustering, etc) taking into account a different number of variables on various pressure levels (Huth et al., 2008) and their use could alter our findings to a certain degree.

In summary, our statistical analysis reveals that the single use of a weather type approach is limited in terms of short-term day-to-day air quality forecasts. Nevertheless, our analysis also shows that a circulation type approach brings forward some interesting physical relations between large-scale circulation patterns and associated air quality concentrations. This supports the use of this approach with respect to future long-term air quality projections and low temporal air quality fluctuations, as was recently successfully tested for PM_{10} at several Bavarian sites in Germany (personal communication, C. Beck, 2008).

3.6 Summary and conclusion

We investigate the relationships of climatology and air quality by statistically analyzing meteorological and air quality variables calculated and observed at 4 rural sites in The Netherlands. On the one hand, interactions between meteorology and O_3 and PM_{10} on the local-scale are quantified based on a multiple linear regression analysis, a technique often used in short-term air quality forecasts. On the other hand, the Lamb weather type circulation classification method is applied as an alternative air quality prediction tool. This technique is potentially useful as downscaling tool of future climate scenarios for local air quality purposes.

By selecting these methods, we seek simplicity, linearity and practical feasibility of the models in order to make this approach appropriate for downscaling forecasted meteorological fields or AOGCMs scenarios for air quality purposes. The multiple linear regression model guarantees simplicity, and applying the regression without (MLR_{MET}) or with air quality variables (MLR_{METCHE}) as predictors, provides a comprehensive summary on the capabilities of these 2 modes. Comparing the results of this local-meteorology based approach with results from a circulation point-of-view based on mean sea level pressure, which takes into account the large-scale circulation above our area of interest, provides further insight in the controlling processes forming and resulting in representative O_3 and PM_{10} levels for rural midlatitude sites.

Prior to the construction of the multiple regression models, a comprehensive correlation study is conducted between all meteorological and air quality variables for all stations. The dataset is extended including all meteorological variables on a 6, 12, 18, 24 and 48-hour time lag, in order to investigate any lagged effect on the meteorological-air quality relations. In general, this analysis shows a limited response of the air quality variables on the < 1-day lag meteorological variables, apart from the inverse relations with downward solar radiation, explaining the day and night cycle. Furthermore, a clear relation is found between O_3 and (maximum) temperature in JJA, combined with a low relative humidity. Rain amount is significant negatively correlated with PM_{10} in winter, which could point out atmospheric removal due to wet deposition. Wind speed is strongly negative correlated with PM_{10} over the whole year and with O_3 in winter, while this relation is positive during summer for the latter. Furthermore, this analysis shows that different rural sites for a similar mid-latitude area have similar characteristics, both in terms of the annual cycle of O_3 and PM_{10} as in their relation with the suite of selected meteorological variables. This provides confidence in the spatial homogeneous character of rural sites for

a mid-latitude area in the Netherlands and justifies the use of a single rural station (with abundant air quality and meteorological measurements) for the remaining of this analysis.

Secondly, both multiple linear regression modes reveal promising results in forecasting especially O_3 for rural sites in The Netherlands, outperforming both climatology and persistence models. The input variables are selected in the way that they are available from operational forecast or AOGCM output (for the MET mode) and the simple and transparent character of the model provides clear insight in the importance of the specific variables that govern the evolution of O_3 and PM_{10}. The statistical performance is good in comparison to similar statistical studies for both the calibration and the validation period, testing the 2 modes MLR_{MET} and MLR_{METCHE}. In general, including information on the previous-day air quality variables improves the explained variance with 10 to 18% for ozone and PM_{10} respectively, with the best results for MLR_{METCHE} for PM_{10} in the calibration period (42.0%), and for ozone using MLR_{METCHE} in the validation period (62.0%). Moreover, this performance is promising when considering the skill scores against persistence, with an improvement of almost 20% for some model situations.

In order to acquire a deeper understanding of the linear relations obtained, levels of O_3 and PM_{10} are connected to large-scale circulation patterns using the objective Lamb weather type approach. Based on 12h UTC operational analysis of MSLP extracted from ECMWF, eleven circulation types are obtained, being associated with levels of O_3 and PM_{10} at the seasonal and annual scales. As shown by other authors in previous research, some clear physical links can be seen between the large-scale patterns and high (low) pollution events. As a general rule, most relations between pressure, wind speed, temperature and relative humidity and levels of O_3 and PM_{10} found in our correlation analysis (using observations from all rural sites) can be retrieved independently using the seasonal composite circulation patterns and their associated anomalies. For O_3, the surface pressure composite maps generally show an anomalous strong high located north or west from the measurement station, depending on the season. This results in cold and humid (DJF and MAM) and warm and dry (JJA) air advected from north to east wind directions, contributing to higher than normal ozone concentrations. Using the circulation patterns for ozone in winter reveals the highest average concentration in wind direction from W to N, under high wind speed circumstances. This feature suggests the influence of ozone transported from the free troposphere towards the surface, which was also suggested by Davies et al. (1992b) and Delcloo and De Backer (2008). For PM_{10}, high levels are largely controlled by air advected from the south to east.

Hereby, pressure gradients are often low, with a positive pressure anomaly north- to eastwards from the measurement station, again depending on the season.

Finally, reconstructing the time series of O_3 and PM_{10} for the calibration and validation period objectively compares the multiple stepwise regressions and the objective Lamb weather type approach. Although the explained variance and the skill score against climatology is high (>80%), the results against persistence can be rather poor, often revealing important structural weakness of the models. In this regard, the stepwise regression for O_3 performs satisfactory for all indices. Contrarily, although seasonal composite maps have shown a distinct pattern for typical episodes of high average O_3 and PM_{10} concentrations, the Lamb weather type as an air quality forecast model performs poor for both O_3 and PM_{10}, with the skill score against persistence being, in some situations, even worse than persistence itself. On the one hand, this result could be due to the short time availability of the air quality data, which restrains the possibility to obtain a robust dataset with significant within-season and type-associated differences in concentrations of O_3 and PM_{10}. On the other hand, this result points out the limitation of the circulation-based approach in terms of day-to-day air quality forecasts. And although circulation patterns are not able to capture the short- term fluctuations of the pollutants, which is to be expected from the intrinsic nature of the circulation, this approach can provide a clear insight in typical large-scale atmospheric structures and associated anomalies in meteorological variables during high (or low) pollution events. We are confident that the multi model approach presented here can be used in other rural settings, particularly those located in mid-latitudes where several different weather type classifications have been developed and validated. Moreover, as this tool can easily be transferred to other geographical areas, it is a promising tool in discriminating atmospheric conditions leading to relatively low or high concentrations of O_3 and PM_{10} (and probably other polluters as well). In this respect, further research could provide more insight in the possible adaptation of the multiple regression results on AOGCM output, the use of circulation pattern in providing possible long-term trends of a specific air quality variable, and on the use of a combination of a combined multiple regression and circulation-type approach. Thereby, O_3 and PM_{10} levels could be explained using the multiple regression technique for the local-scale photochemical formation and the circulation-based approach for the large-scale transport of (secondary) pollutants from other source areas.

Chapter 4

A new method to assess air quality levels using a synoptic-regression approach. Part I: Present-day O_3 and PM_{10} analysis*

4.1 Introduction

Since high concentrations of O_3 and PM_{10} affect public health, much attention is paid to the improvement of the accuracy of short-term deterministic and statistical prediction models and the development of robust long-term air quality prediction systems. Complex models, including a full description of atmospheric chemistry and meteorological processes, are often used with respect to the former (Otte et al., 2005; Giorgi and Meleux, 2007). Although these techniques are shown to be powerful for short-term predictions, the complex climate-air quality modelling-systems, together with their computational/technical characteristics, makes them less useful for long-term predictions based on AOGCM outputs (Giorgi and Meleux, 2007).

Therefore, statistical downscaling methods were developed to determine predictive relationships between air pollution concentrations and individual meteorological

* Demuzere, M., van Lipzig, N.P.M., 2008. A new method to assess air quality levels using a synoptic-regression approach. Part I: Present analysis for O_3 and PM_{10}. Atmospheric environment (submitted).

parameters. This was done for different air quality variables and different locations. Different methods can be distinguished namely multiple-linear regression (MLR) analysis (Hubbard and Cobourn, 1998; Barrero et al., 2006; Stadlober et al., 2008), nonlinear multiple regressions (Cobourn, 2007), artificial neural networks (ANN) (Gardner and Dorling, 1998; Nunnari et al., 1998; Reich et al., 1999; Benvenuto and Marani 2000; Perez et al., 2000; Perez, 2001; Kukkonen et al., 2003; Hooyberghs et al., 2005; Papanastasiou et al., 2007), and generalized additive models and fuzzy-logic-based models (Cobourn et al., 2000). Among these approaches, regression methods are well documented because of their ease of implementation and their low computation requirements (Maerns et al., 2003; Wilby and Wigley 1997; Wilby et al., 2004). The technique first detects present-day relationships between local meteorological variables (or "predictors") and e.g. air quality variables (or "predictands"). These relations based on (non) linear multiple regressions have been described in literature numerously, as for e.g. in Chaloulakou et al., 2003a,b; Barrero et al., 2006; Ainslie and Steyn, 2007. The use of another downscaling tool, circulation patterns (Wilby and Wigley, 1997), is widespread, although less common in air quality research. In that respect, this technique is adopted by Comrie et al. (1992a), Davies et al. (1992a, b) and McKendry (1994) to explain observed ozone variability at measuring sites in the Europe, US and Canada.

Some authors have tried to combine the above-mentioned two downscaling techniques. A stratification based on the circulation pattern is adopted to introduce nonlinearity into the model (Huth et al., 2008) under the assumption that the relations between large-scale predictors and predictands may vary depending on the type of the synoptic pattern. This technique is applied for downscaling surface meteorological variables (e.g. temperature, precipitation, etc.) by Cavazos (1999), Enke and Spekat (1997) and Li and Sailor (2000). Nevertheless, this synoptic-regression based approach has not been adopted in terms of air quality assessment yet. To the author's best knowledge, there has been only one study so far that used a within-synoptic-type air pollution model to study future air pollution levels for a variety of pollutants (Cheng et al., 2007a, b).

The aim of our study is to test a set of simple linear regression methods together with a stratification of the dataset by its daily synoptic patterns prior to the regression method in their ability to hindcast levels of O_3 and PM_{10}. To achieve this goal, regression results from previous research based on station measurements from Cabauw (Chapter 3 - Demuzere et al., 2008b) are used to reconstruct the observed maximum eight-hourly mean O_3 [$\mu g/m^3$] and daily mean PM_{10} [$\mu g/m^3$] levels for the period 2001-2004 (calibration) and 2005-2006 (evaluation). Furthermore, the Lamb weather type classification is used as a synoptic circulation-typing tool to enter

nonlinearity of the regression equations into the downscaling model in order to construct a robust method for the improved projections of air quality levels. These methods are calibrated on observed air quality data from the Cabauw measurement tower and the measurement station of Zegveld-Oude Meije (The Netherlands) for the period 2001-2004.

The Intergovernmental Panel on Climate Change pointed out that climate change may increase the concentration of O_3, although the magnitude of the effect is still uncertain (IPCC, 2001). Therefore, assessing a possible impact of a climatic change in meteorological variables and synoptic circulation on air pollution concentrations requires additional attention. Before the above-mentioned downscaling approach is used to bridge the gap between what is produced by AOGCMs and what is needed in climate impact research (Part II of this analysis), the observed local relations between meteorological and air quality variables need to be tested on the larger scale. After all, AOGCM-output is at present only available at typical scales of 300x300 km^2. Therefore, the validity of these station-based synoptic regression configurations as an air quality downscaling tool is tested using low-resolution operational ECMWF data for the period 2005-2006. In this way, a regression-based model forced with meteorological ECMWF data is used as a prototype for a modelling system in which AOGCM-output is downscaled for the purpose of obtaining projections for future air quality levels.

4.2 Data

High temporal resolution meteorological data for the period 2001-2006 from the rural measurement station of Cabauw (The Netherlands), partly operated by the KNMI and located in a rural area (Beljaars and Bosveld, 1997) were used. Ten-minute measurements are averaged to daily values. More details on the measurement site characteristics and quality control are provided by Demuzere et al. (2008b). The calibration of the multiple-linear regression equation is based on local observations of two meter air and dew point temperature (T and Td), daily maximum and minimum temperature (Tmax and Tmin), wind speed and direction (F010 and D010), total cloud cover (TCC), total precipitation (Tprec) and shortwave downward radiation (SDW) from the Cabauw measurement site for the period 2001-2004. Relative humidity (RH) is calculated from T and Td using the Magnus-Tetens approximation. Similar meteorological information is obtained from the operational ECMWF model on a N400 Gaussian grid resolution for the period 2005-2006. As this methodology is developed for providing future air quality projections based on global climate model information, the ECMWF data is aggregated to the spectral

T63 resolution (1.85 ° x 1.85 °), which is identical to the resolution of e.g. the SRESA1B IPCC 4AR ECHAM5-MPI/OM experiment (Marsland et al., 2003; Roeckner et al., 2003, 2004).

There is a continuing debate as to whether AOGCM outputs should be treated as individual grid points or areal aggregates in comparison with individual station data (Skelly and Henderson-Sellers, 1996). Huth et al. (2001) and Gachon and Dibike (2007) have shown that for daily maximum temperatures/heat waves and mean/extreme temperatures respectively, there is virtually no difference between a single grid point use and neighboring grid point averages. As Cabauw is situated in the centre of four surrounding grid points, the average of the neighbouring four ECMWF grid points is used in the further analysis. This means that an area of ≈ 350 x 350 km² is taken into account.

The air quality data for ozone is taken from Cabauw, for the period 2001-2006, while PM_{10} is taken from the neighbouring station Zegveld-Oude Meije. The Directive 1999/30/EC and following up Directive 2008/50/EC of the European Parliament (EU, 1999, 2008) describe a threshold concentration of 120 µg/m³ and 50 µg/m³ for a maximum eight-hourly mean O_3 and daily mean PM_{10} concentration respectively for Europe. These threshold values are important for possible regional air quality mitigation strategies and therefore, the remaining of this study focuses on these thresholds as the framework to validate the downscaling methodologies provided in section 4.3.

4.3 Methods

Multiple-linear regression models have widely been adopted to reconstruct observed time series of O_3 and PM_{10} for various heterogeneous regions based on measurements (Hubbard and Cobourn, 1998; Barrero et al., 2006; Stadlober et al., 2008). Moreover, Huth et al. (2008) point out the power of a pointwise linear regression method (using grid point values instead of principal components as predictors) in comparison with non-linear methods such as neural networks. And although Huth et al. (2008) does not find clear evidence in the improvement of downscaling temperatures when stratifying the dataset by classification patterns prior to the regression analysis, Cheng et al. (2007a) have shown this approach to be promising in terms of air pollution variables. Therefore, in order to clarify the potential of each method in air-quality applications, three regression-based approaches are examined and compared: (1) a multiple-linear regression model as developed in Demuzere et al. (2008b), hereafter named MLR, (2) a multiple

regression model with the Lamb weather types (Jones et al., 1993; Trigo and DaCamara, 2000) included as predictors (MLR_{LWT}) and (3) a stratification of the data by the Lamb weather type technique prior to the multiple linear regression (LWT_{MLR}). As seasonality could be an important factor in terms of O_3 and PM_{10} reconstruction (Tarasova et al., 2007), model approaches (2) and (3) are also run in a seasonal mode, whereby the regression analysis is done for each season separately. These techniques are hereafter referred to as MLR_{SEAS} and $LWT_{SEAS+MLR}$ for (2) and (3) respectively. The latter results in a set of N_{LWT} times N_{SEAS} regression equations and describes the seasonal within-weather-type air pollution characteristics, where N_{LWT} is the number of weather type classes and N_{SEAS} is the number of seasons. Moreover, it is important to underline that air quality variables are not taken into account as predictor variables. Previous research pointed out that model errors decrease by including persistency (lag effect) of the air quality variables (Perez et al., 2000; Smith et al., 2000; Perez, 2001; Barrero et al., 2006; Grivas and Chaloulakou, 2006). However, as there is no information on future air quality data as input variables, they cannot be included in the regression analysis as predictors. For future use, this approach has two important assumptions: 1) applying this method on future AOGCM scenarios assumes that the present-day relations between meteorology and air-quality variables stay constant through time and 2) when applying these techniques for future air quality projections, the impact of meteorological changes on future O_3 and PM_{10} levels is isolated, and possible changes in future (precursor) emissions are not assessed.

A preliminary analysis has shown that there are only small differences between observed and downscaled O_3 and PM_{10} time series obtained using various predictors (raw data, anomalies and normalized anomalies). Therefore, for simplicity, the linear, pointwise, regression-based downscaling models are developed using raw observed meteorological input data from Cabauw for the period 2001-2004. For all variables, daily mean values are used, except for Tmax and Tmin, which represent maximum and minimum daily temperature.

The Lamb weather types (WTs) are developed using operational ECMWF sea-level pressure (SLP) data for the calibration period 2001-2004 and for the validation period 2005-2006. For a given day, the WTs describe the location of the high and low-pressure centers that determine the direction of the geostrophic flow. A grid with 16 points is assigned over the larger Western and Central Europe, with a central point over the Benelux, in 52.5°N and 5°E. We computed a set of simple atmospheric circulation indices using 12h sea level pressure (SLP) in these 16 grid points, namely the direction and vorticity of geostrophic flow: southerly flow (SF), westerly flow (WF), total flow (F), southerly shear vorticity (ZS), westerly shear

vorticity (ZW) and total shear vorticity (Z). A small number of empirical rules devised previously (Jones et al., 1993; Trigo and DaCamara, 2000) are then used to classify each day as one of the 10+1 undetermined circulation types developed in Chapter 5 (Demuzere et al., 2008a). The composite maps of sea level pressure for each Lamb weather type derived from ECMWF SLP fields, averaged over the whole period 2001-2006 are depicted in Figure 4.1.

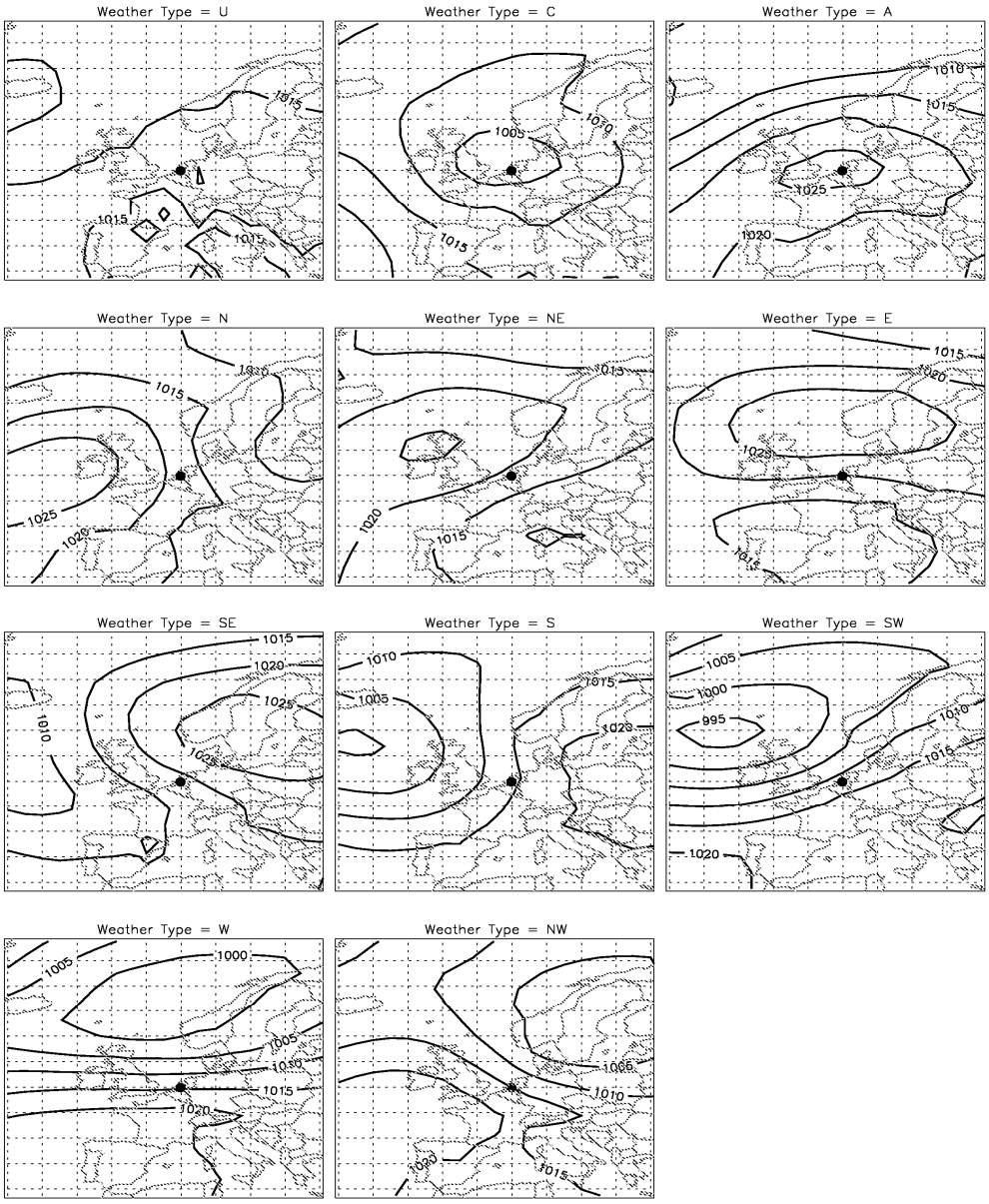

Figure 4.1: Composite maps of sea level pressure for each Lamb weather type derived from ECMWF SLP fields, averaged over the whole period 2001-2006. The Cabauw measurement site is marked with a black dot.

A wide range of possible criteria can be used to evaluate statistical downscaling methods. However, the majority of downscaling studies rely on a more simple measure of accuracy such as the explained variance or root-mean-square error only. Here, the quality and reliability of the downscaled values are examined using several statistical indices proposed by Willmott (1981, 1982) and Willmott and Matsuura (2005). These indices include the mean, the standard deviation (σ) and variance (σ^2) and the mean absolute error (MAE), which averages the absolute error magnitudes. Furthermore, we used the root mean square error (RMSE), measuring the total deviation of downscaled values from observed values, and the explained variance (R^2). The student t-test and the F-statistics are used to test whether observed and downscaled time series have significant different means and variances respectively, on a 95% confidence level. Additionally, Wilks (1995) suggested that the skill of any model should be interpreted as the terms of improvement over a reference or benchmark model. According to Murphy (1988), the (temporal) skill of any given model is a measure of the relative accuracy of a model with respect to a standard reference model. Therefore, the skill scores based on the mean square error (MSE) will be used in this paper with persistence (MSE_{pers}) as a reference:

$$SS_p\,(MSE) = \frac{MSE - MSE_{pers}}{0 - MSE_{pers}}\ x\ 100\%$$

with the "0" corresponding to the accuracy level that would be achieved by a perfect model (Wilks, 1995). Furthermore, as suggested by Huth et al. (2008), the degree of asymmetry and peakedness of the statistical distributions are evaluated in terms of the third and fourth moments, viz. the skewness and kurtosis.

4.4 Results

First, the various multiple-linear regression equations described in section 4.3 are calibrated for the period 2001-2004, using observational data (section 4.4.1). Secondly, it is tested which of the methods is most suitable for hindcasting maximum eight-hourly O_3 and daily mean PM_{10} concentrations for the independent evaluation time period 2005-2006, using observed meteorological data as input to the regression-based model. Thirdly, it is tested whether the MLR equations derived from observed meteorological data still hold when using gridded low-resolution meteorological data as input to the regression-based model. For this purpose operational ECMWF meteorological data for the period 2005-2006 are used (section

4.4.2). Finally, section 4.4.3 describes the within-type variability of the meteorogical predictors provided by Cabauw observations and ECMWF forecast data.

4.4.1 Comparison and evaluation of various downscaling tools

In order to justify the implementation of a circulation approach prior to the linear regression technique, it is important to know whether the introduction of this stratification leads to an improvement in performance of the downscaling procedure. Therefore, the comparisons are carried out not only in terms of correlation coefficients, but also for temporal correlations (persistence) and higher-order statistical moments (skewness and kurtosis). These performance statistics for the calibration and evaluation period are summarized in Table 4.1 and Tables 4.2 and 4.3 for skewness and kurtosis respectively. For the calibration period in general, the combination of synoptic classification using Lamb weather types prior to a seasonal linear multiple regression analysis ($LWT_{SEAS+MLR}$) performs best for both O_3 and PM_{10}. This is shown in terms of explained variance and SS_p for both O_3 and PM_{10} (0.80/75 and 0.60/66 respectively). Furthermore, MAE and RMSE show a similar tendency, with the lowest values for O_3 of 8.3 and 10.9 µg/m³ and for PM_{10} of 5.8 and 8.6 µg/m³ compared to the other approaches. Differences between observed and modelled means are insignificant for all model configurations based on the t-test. In terms of variance, the F-test shows that all models are unable to reproduce the observed variance, except for O_3 using MLR_{SEAS}, LWT_{MLR} and $LWT_{SEAS+MLR}$. As all statistics for PM_{10} are lower than for O_3, these results based on the available meteorological observations suggest that O_3 has more predictability based on meteorology solely compared to PM_{10}.

To further illustrate this, scatter plots of modelled versus observed O_3 (upper panels) and PM_{10} (lower panels) concentrations following the pure MLR (left panels) and synoptic regression (right panels) approach are shown (Figure 4.2). For ozone, the best results are obtained for $LWT_{SEAS+MLR}$, with the regression line closer to the 1:1 (perfect model) line. For PM_{10}, there is a large difference between the various models, with again the best performance for the $LWT_{SEAS+MLR}$ model.

Table 4.1: Statistics describing the performance of the calibration time series (2001-2004) and evaluation series (2005-2006). The measures include the mean ($\overline{x}$), standard deviation (σ), variance (σ^2), mean average error (MAE), root mean square error (RMSE), explained variance (R^2 in %) and skill score against persistence (SSp). Values significant different on the 95% confidence interval based on t-test and chi-square test for mean and variance respectively are denoted in bold.

	Species	Model		$\overline{x}$	σ	σ^2	MAE	RMSE	R^2 (%)	SSp
Calibration 2001-2004	O_3		Reference	57.0	29.8	887.2				
		MLR		54.9	25.9	671.4	14.3	19.0	61	38
		MLR_{SEAS}		55.1	27.5	758.7	10.4	13.2	65	69
		MLR_{LWT}		56.6	26.0	676.3	12.6	15.9	71	56
		LWT_{MLR}		55.2	27.4	751.5	10.2	13.9	78	67
		$LWT_{SEAS + MLR}$		56.5	28.0	783.1	8.3	10.9	80	75
	PM_{10}									
			Reference	27.2	15.6	244.6				
		MLR		27.7	9.1	83.4	11.1	15.1	12	22
		MLR_{SEAS}		27.1	10.5	110.5	8.6	11.8	41	50
		MLR_{LWT}		27.0	9.9	97.8	8.6	11.8	40	52
		LWT_{MLR}		27.0	12.5	155.3	3.4	10.8	52	62
		$LWT_{SEAS + MLR}$		27.1	13.4	180.6	5.8	8.6	60	66
Evaluation 2005-2006	O_3		Reference	57.59	30.82	955.90				
		MLR	Observations	56.60	25.28	639.29	13.70	17.70	68	50
			ECMWF	58.05	21.52	463.13	16.98	22.42	60	37
		MLR_{SEAS}	Observations	57.13	27.87	776.57	11.77	15.11	58	59
			ECMWF	58.24	22.03	485.32	13.97	17.92	44	43
		MLR_{LWT}	Observations	56.48	26.55	704.85	13.46	17.65	68	51
			ECMWF	63.35	26.62	708.37	16.00	20.22	61	34
		LWT_{MLR}	Observations	57.34	26.81	718.59	13.13	17.35	69	52
			ECMWF	59.42	27.98	782.89	19.68	25.76	61	31
		$LWT_{SEAS + MLR}$	Observations	57.87	29.37	862.85	12.76	16.71	72	56
			ECMWF	57.6	27.14	736.58	16.24	20.42	63	33
	PM_{10}		Reference	23.13	12.05	145.20				
		MLR	Observations	26.64	8.17	66.71	7.16	10.29	32	35
			ECMWF	21.45	8.31	69.04	8.59	10.72	28	43
		MLR_{SEAS}	Observations	25.56	10.20	104.09	8.39	10.62	34	30
			ECMWF	20.72	9.76	95.27	8.35	11.20	27	27
		MLR_{LWT}	Observations	25.18	10.54	111.17	8.47	10.73	31	35
			ECMWF	19.16	10.80	116.57	8.45	10.73	32	31
		LWT_{MLR}	Observations	26.16	12.66	160.15	8.32	10.54	34	34
			ECMWF	23.03	13.78	189.88	8.40	10.62	32	28
		$LWT_{SEAS + MLR}$	Observations	26.75	15.98	255.30	10.55	15.22	34	33
			ECMWF	24.34	15.74	247.75	10.17	15.22	32	28

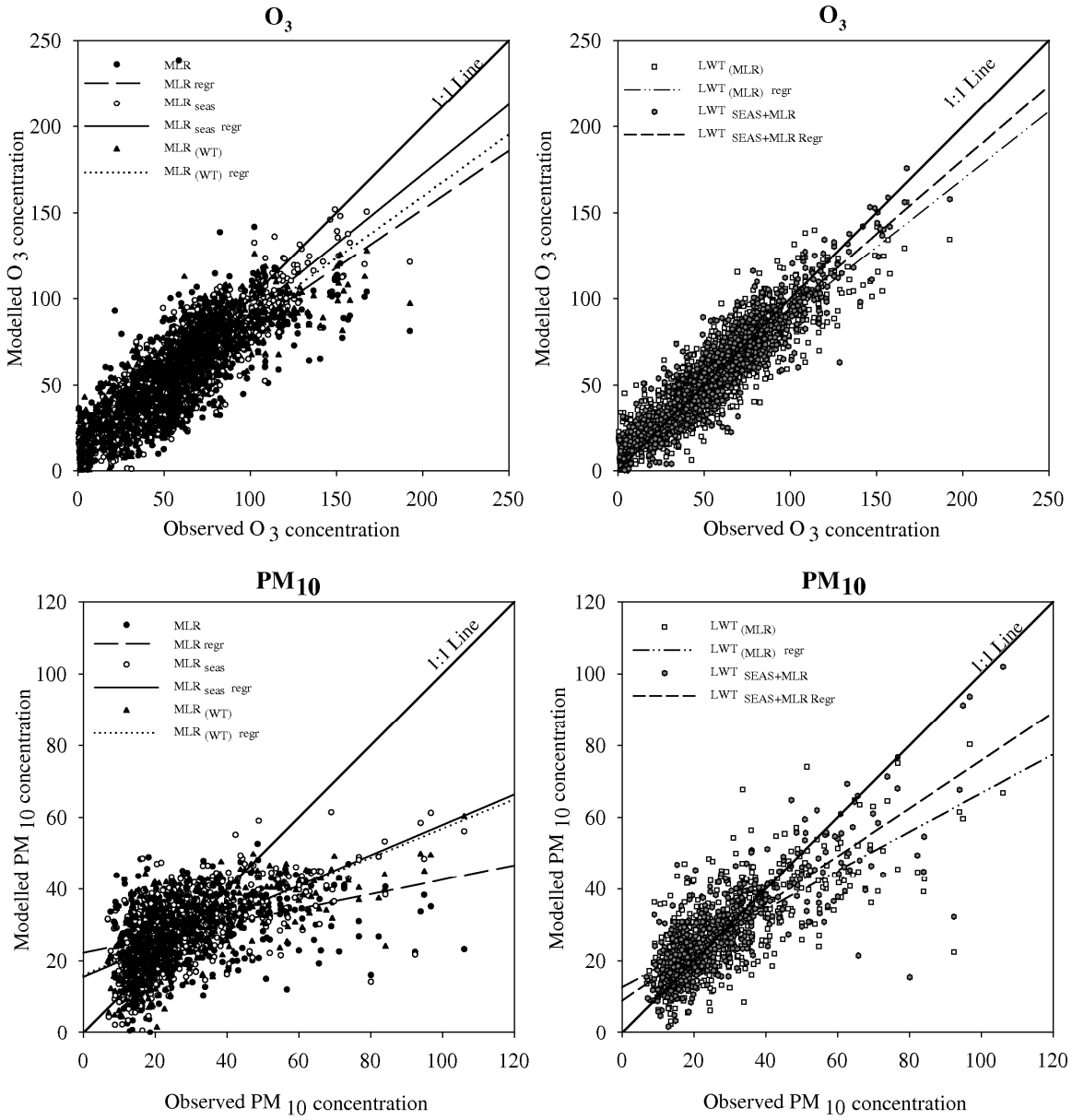

Figure 4.2: Scatter plot of modelled versus observed eight-hourly maximum O_3 (upper panels) and daily mean PM_{10} (lower panels) concentrations [µg/m³] for the calibration period 2001-2004.

Lu et al. (2006) tested a similar approach using traditional MLR regression against different MLR equations for different weather regimes for ozone episodes at 4 measurement sites in Taiwan. The authors found an improvement in R^2 of 50% between their MLR model derived for different weather types and the traditional MLR model. Our results confirm this, with an improvement from 61% for the traditional MLR to 80% for the $LWT_{SEAS+MLR}$ model. Although the improvement here is less strong, the absolute explained variance is much higher than the results obtained by Lu et al. (2006).

Furthermore, Tables 4.1 to 4.3 show the models performance for hindcasting maximum 8 hourly mean O_3 and daily mean PM_{10} levels for the independent evaluation time period 2005-2006, using observed meteorological variables. For O_3, all models perform similar in terms of R^2 and SS_p, with the best results obtained for R^2 for $LWT_{SEAS+MLR}$ (72%) and for SS_p with MLR_{SEAS} (59%). Both model approaches are also able to reproduce the observed variances, whereas all other model configurations have variances significantly different at the 95% confidence interval compared to the observed explained variance. In terms of skewness and kurtosis, the best results are obtained with the $LWT_{SEAS+MLR}$ model, with values of 0.91 and 3.27 respectively, compared to an observed skewness and kurtosis of 1 and 2.28 respectively (Tables 4.2 and 4.3). For PM_{10} in general, lower values of the statistical indices are obtained compared to the results for O_3. Again here, models perform similarly in terms of R^2 and SS_p for all methods, with the best results obtained with MLR_{SEAS}, MLR_{LWT} and $LWT_{SEAS+MLR}$ for the former (34%) and for MLR and MLR_{LWT} for the latter (35%). The large observed skewness and kurtosis values are best reproduced by LWT_{MLR} with respective values of 1.02 and 4.29 compared to an observed skewness and kurtosis of 1.73 and 4.78 respectively. These results are also depicted in Figure 4.3 (upper panels), showing the best representation of observed maximum 8 hourly mean O_3 and daily mean PM_{10} levels based on observed meteorological variables for the independent period 2005-2006 using $LWT_{SEAS+MLR}$ and LWT_{MLR} respectively.

Table 4.2: Skewness coefficients for O_3 (left) and PM_{10} (right) for the various methods and the reference and observed and ECMWF downscaled datasets, for the period 2005-2006.

	O_3			PM_{10}		
	Reference	Obs	ECMWF	Reference	Obs	ECMWF
	1.00			1.73		
MLR		0.26	-0.002		-0.085	0.043
MLR_{SEAS}		0.78	0.42		-0.19	-0.11
MLR_{LWT}		0.28	0.15		-0.27	-0.056
LWT_{MLR}		0.62	0.31		1.02	0.70
$LWT_{SEAS+MLR}$		0.91	0.80		3.08	0.82

Table 4.3: Kurtosis coefficients for O_3 (left) and PM_{10} (right) for the various methods and the reference and observed and ECMWF downscaled datasets, for the period 2005-2006.

	O_3			PM_{10}		
	Reference	Obs	ECMWF	Reference	Obs	ECMWF
	2.28			4.78		
MLR		-0.40	-0.71		-0.083	-0.50
MLR_{SEAS}		0.86	0.43		0.12	-0.20
MLR_{LWT}		-0.27	-0.63		-0.26	-0.49
LWT_{MLR}		0.51	0.028		4.29	6.54
$LWT_{SEAS+MLR}$		3.27	2.31		6.14	6.92

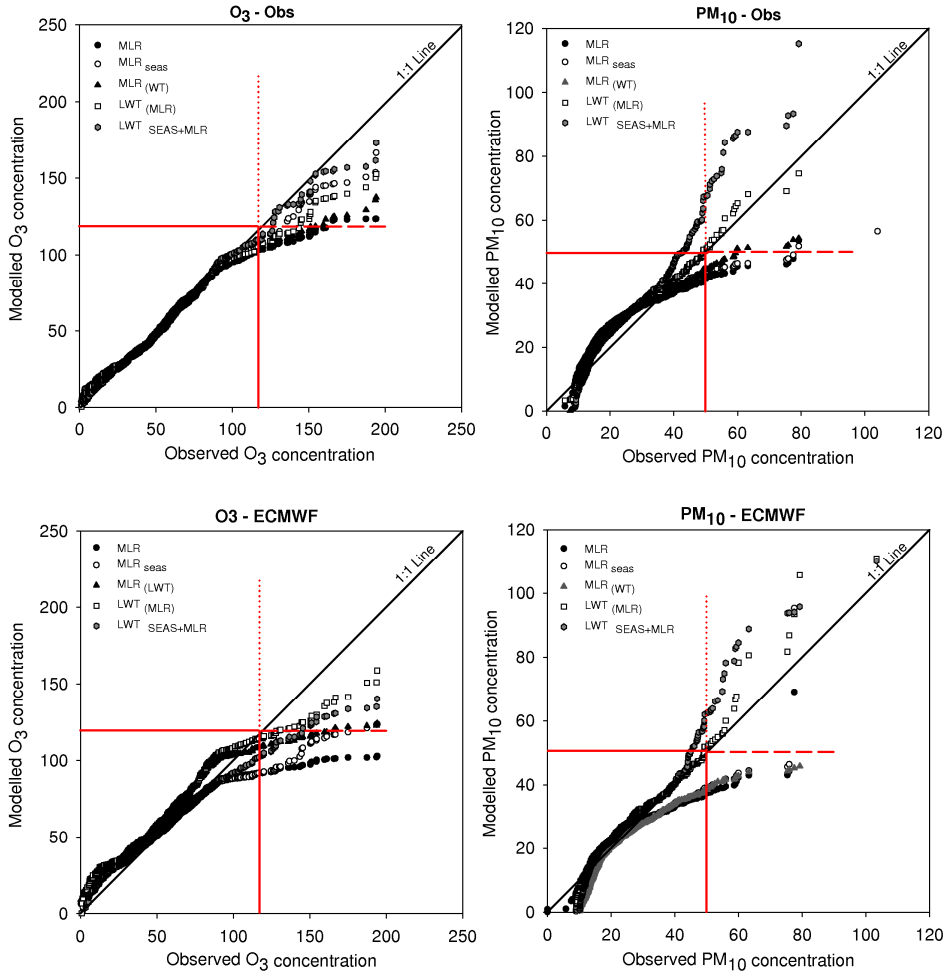

Figure 4.3: Quantile-Quantile(QQ)-plots of modelled versus observed eight-hourly maximum O_3 and daily mean PM_{10} concentrations [µg/m³] for the evaluation period 2005-2006, using observed (upper panels) and operational ECMWF (lower panels) data as predictors for the regression-based models. The 1:1 line presents the perfect model hindcast and the red lines (dotted – observation, dashed – modelled) show the threshold of 120 and 50 µg/m³ for O_3 and PM_{10} respectively.

4.4.2 Evaluation of various downscaling tools for low-resolution data

In order to know whether regression-based models developed from measured predictors are still valid using lower resolution data, such as operational ECMWF data, this approach is tested on the latter for the independent evaluation period 2005-2006.

In general the lower variability of the low-resolution meteorological ECMWF predictors results in a smaller explained variance of operational ECMWF

downscaled O_3 and PM_{10} time series compared to the observed downscaled series (Table 4.1). The explained variance for O_3 is, in accordance to the calibration period, the highest for the $LWT_{SEAS+MLR}$ method for both observed and ECMWF downscaled series (72 and 63%). In terms of SS_p, the pure seasonal regression model MLR_{SEAS} is slightly better than the $LWT_{SEAS+MLR}$ method, with a performance of 59/43% and 56/33% (Observations/ECMWF) respectively against persistence (Table 4.1).

In order to compare the distribution of the observed and modelled maximum eight-hourly O_3 and daily mean PM_{10} throughout the evaluation period, the quantile distribution of the modelled air quality data is plotted against the quantile distribution of the observed air quality data in QQ-plots (Figure 4.3). When using the observed meteorological data as predictors, the best results are obtained for $LWT_{SEAS+MLR}$. When using the ECMWF data as predictors, also the $LWT_{SEAS+MLR}$ gives the best results. Although one could argue that for high O_3 concentrations the best correspondence between modelled and measured quantiles is found for LWT_{MLR}, it is clear that around ozone concentrations of 100 $\mu g/m^3$, O_3 quantiles are overestimated in the LWT_{MLR} model compared to the observations.

As different properties of the downscaled air quality series may be relevant in climate change impact studies in different sectors, the degree of asymmetry and peakedness of statistical distributions are also evaluated in terms of the standardized third and fourth moments, i.e. skewness and kurtosis (Tables 4.2 and 4.3). Following the supposition of Huth et al. (2008) that the number of independent realizations in the time series is 300, than the skewness test for normality (Thode, 2002) indicates that the hypothesis of zero skewness is rejected at the 95% significance level if the skewness coefficient exceeds a value of 0.275 (in the absolute sense). The reference O_3 distribution shows a positive skewness of 1.00 (significant skewed) and a kurtosis of 2.28. When using observed meteorological data as predictors, the methods applying stratification of the O_3 distribution by the Lamb classification method prior to the regression analysis ($LWT_{SEAS+MLR}$) are able to catch the third and fourth order statistical measures much better than methods where such stratification is not taken into account. Similarly, the same conclusions can be drawn when using the ECMWF data as predictors, although the distribution is slightly less positive skewed in that case (Table 4.3).

For PM_{10}, a regression-based approach based on the meteorological variables suggested in Chapter 4 is insufficient to explain a great deal of the observed PM_{10} variability (Table 4.1). The results of the regression-based models are similar in terms of R^2, whereby the best approximation of the observed time series is obtained

by both LWT_{MLR} and $LWT_{SEAS+MLR}$ (both 34% respectively). Contrarily, better results for SS_p are obtained for the standard regression model MLR, with a 35% and 43% improvement for both observed and ECMWF downscaled PM_{10} series compared to the persistence model. For all models except LWT_{MLR} the variance (σ^2) differs significantly from the observed variance in PM_{10}. The reference PM_{10} distribution is highly positively skewed (significant on the 95% level), which is well reproduced by the LWT_{MLR} approach and overestimated by $LWT_{SEAS+MLR}$ when observed meteorological data are used as predictors (Tables 4.2 and 4.3). Moreover, the LWT_{MLR} model more realistically generates the strong reference peakedness of 4.775 compared to the $LWT_{SEAS+MLR}$ approach (Table 4.3). For the ECMWF downscaled PM_{10} time series, the distribution is in general more normal compared to the reference distribution, although the kurtosis is overestimated for the LWT_{MLR} and $LWT_{SEAS+MLR}$ approach (Tables 4.2 and 4.3).

In general, the analysis above shows that for O_3, seasonality is an important factor, which confirms the results of Tarasova et al. (2007). Next to its photochemical production, a variable seasonal impact of meteorological variables (e.g. wind speed and total precipitation) on ozone (Demuzere et al., 2008b) can alter its concentration, which should be taken into account in the downscaling process. For PM_{10}, this effect is less distinct, which is also clear from a less pronounced seasonal cycle in observed PM_{10} concentrations (Flemming et al., 2005; Demuzere et al., 2008b). Moreover, the results in Table 4.1 show that a regression-based approach using only meteorology data is able to explain a great deal of the observed O_3 variability, which is not the case for PM_{10}. This research shows that the meteorological variables available for this regression approach are unable to explain a great deal of the observed PM_{10} variability. One the one hand, PM_{10} levels are influenced by the local emission sources and the long-range transport. This was shown in Chapter 3 (Table 3.3), with a R^2 improvement of 17% when including previous-day PM_{10} concentrations compared to the use of meteorological predictor variables only. Nevertheless, as these concentrations are at present not yet available from AOGCMs, we can not include the PM_{10} emissions themselves as predictor variables into the synoptic regression-based statistical approach. On the other hand, the low explained variability could be due to the absence of the boundary layer height as a predictor variable. Previous research (Hooybergs et al., 2004, 2005) has shown that by far the boundary layer height is the most important parameter in their neural network approach. Unfortunately, boundary layer height measurements are not available at present, and therefore, we did not take into account this variable. Nevertheless, an attempt should be done to take this into account for (short-term) PM_{10} predictions.

Furthermore, the results in Tables 4.1, 4.2 and 4.3 show an additional value of stratifying all days according to their circulation characteristics prior to the regression analysis. Although Huth et al. (2008) states that the effect of introducing non-normality by mixing several normally distributed meteorological parameters using a classification method for temperature downscaling is rather weak and insufficient to produce significant deviations from normality, our result show that this is not the case for air quality distributions. Hereby, large skewness and kurtosis values can only be reproduced by stratifying the dataset and by developing within-weather-type group regression models shown in Tables 4.2 and 4.3. Moreover, the skill score against persistence (SS_p), which tests the temporal structure of the downscaled time series against a 1-day lag benchmark model, shows a better performance for the LWT methods than compared to the more simple linear regression model approaches (Table 4.1). Therefore we opt to use the $LWT_{MLR+SEAS}$ and LWT_{MLR} for O_3 and PM_{10} respectively in the remaining of this study.

Finally, the hypothesis that an observation-based regression still holds when applied on low-resolution gridded (ECMWF) data is validated shown in Tables 4.1, 4.2 and 4.3. Although part of the explained variance is lost due to a lower variability of the meteorological predictors (Figure 4.3), this regression-circulation pattern approach is able to detect the high observed O_3 and PM_{10} concentrations that are important in terms of European air quality Directives and air quality mitigation strategies. This will be discussed in more detail in the following section 4.4.3.

4.4.3 Meteorological predictor variability

In the previous paragraph, regression-based models were used to hindcast air quality levels by calculating O_3 and PM_{10} concentrations from meteorological conditions on a larger scale, as available from ECMWF. However, when the ECMWF output differs from the observed conditions, this will negatively influence the model performance. A similar effect was described by Zhang et al. (2007) who showed that a reduced uncertainty in meteorological conditions results in a much smaller spread in the ensembles distribution of O_3 predictions for the Houston area (USA). Therefore, it is important to provide more insight in the effect of forecasted meteorological ECMWF variable deficiencies on the performance of the regression-based models for each weather type separately. As the regression-based method profits from introducing non-linearity by the objective Lamb classification method prior to the regression analysis, modelled versus observed O_3 and PM_{10} concentrations are analyzed for each weather type class separately (Figures 4.4, 4.5, 4.6 and 4.7).

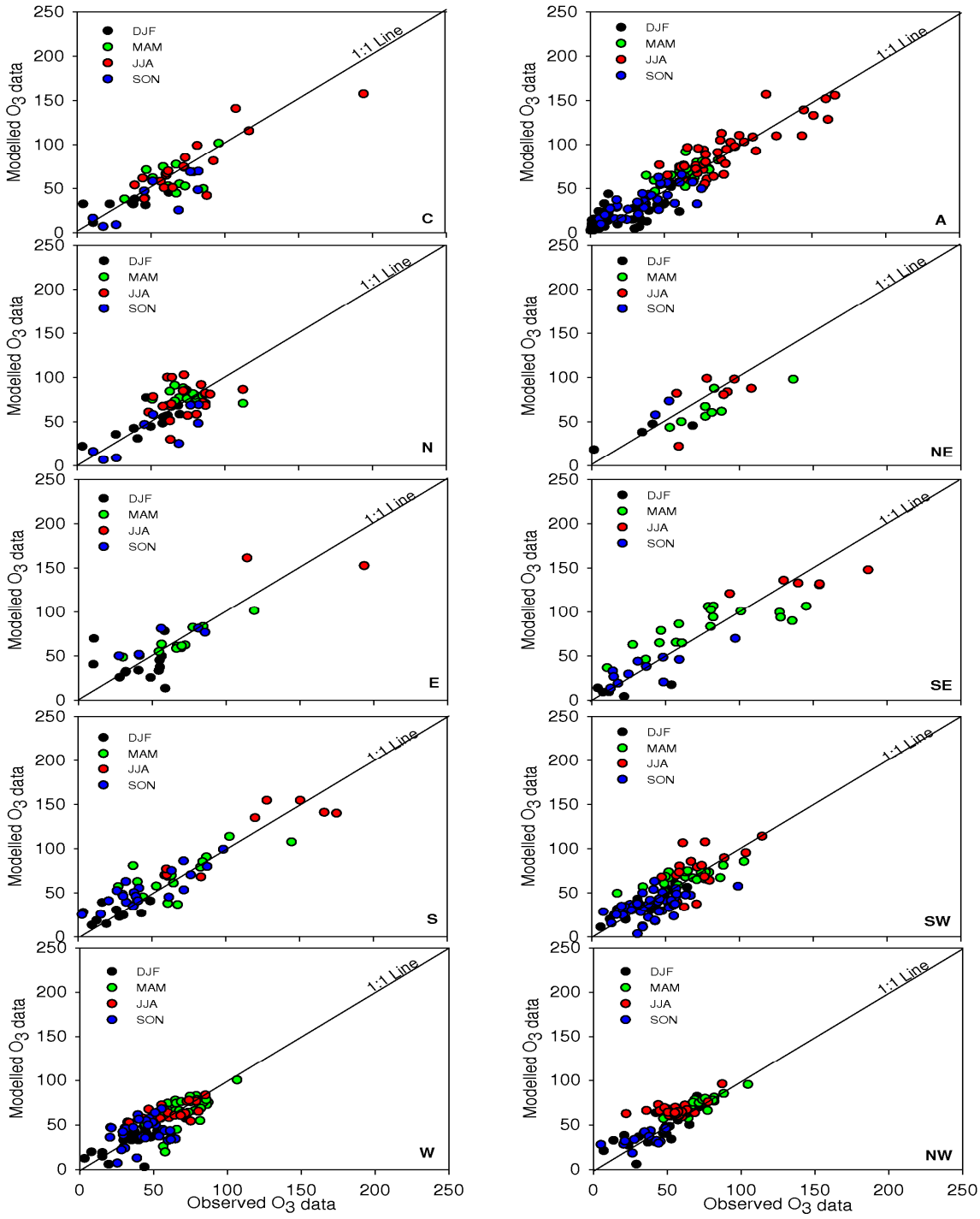

Figure 4.4: Scatter plots showing observed versus modelled O_3 concentrations using observed meteorological data as input to the $LWT_{SEAS+MLR}$ model for each Lamb weather type and for each season separately.

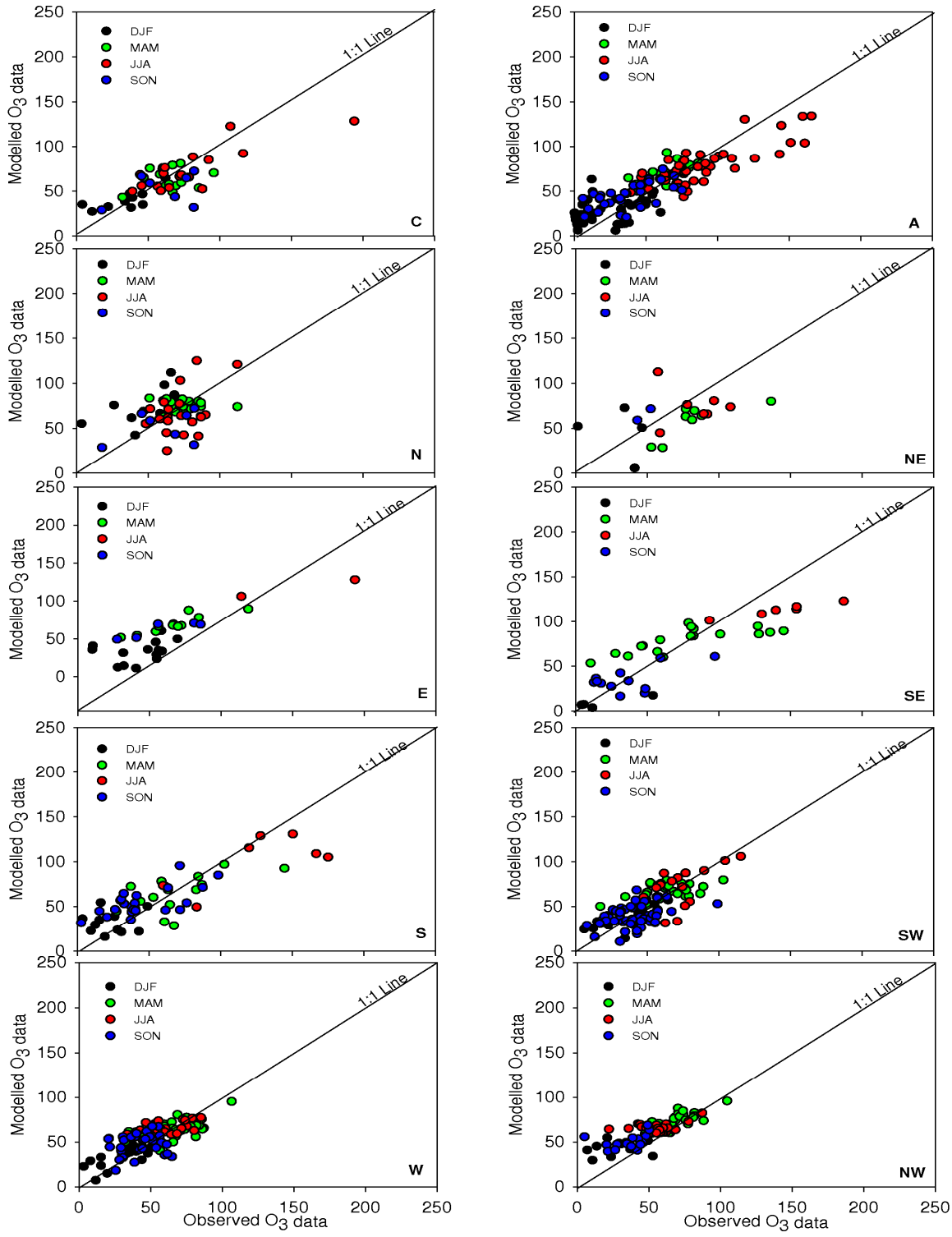

Figure 4.5: Same as Figure 4.4, but now using ECMWF meteorological data as input to the $LWT_{SEAS+MLR}$ model.

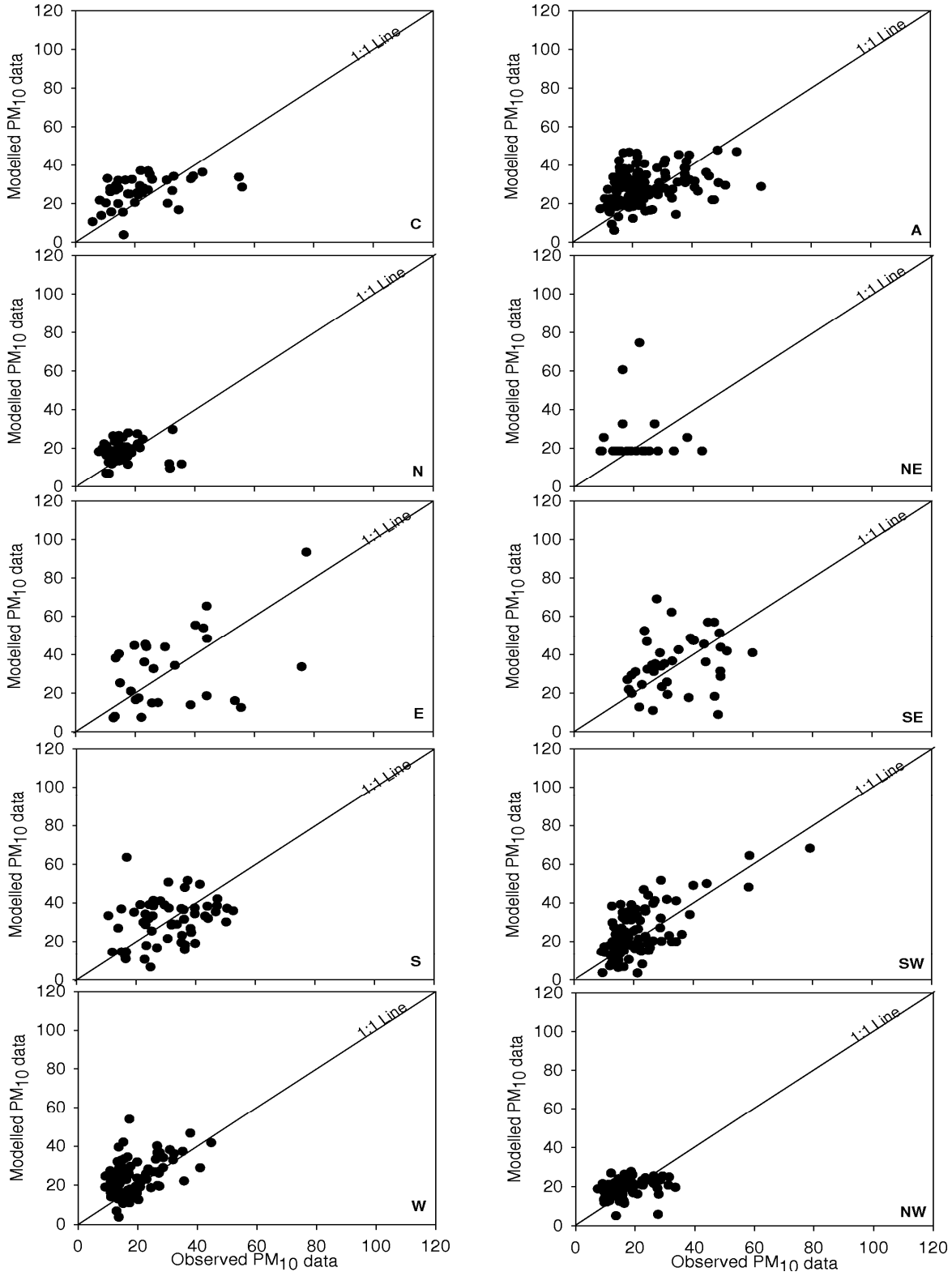

Figure 4.6: Scatter plots showing observed versus modelled PM_{10} concentrations using observed meteorological data as input to the LWT_{MLR} model for each Lamb weather type for the whole year.

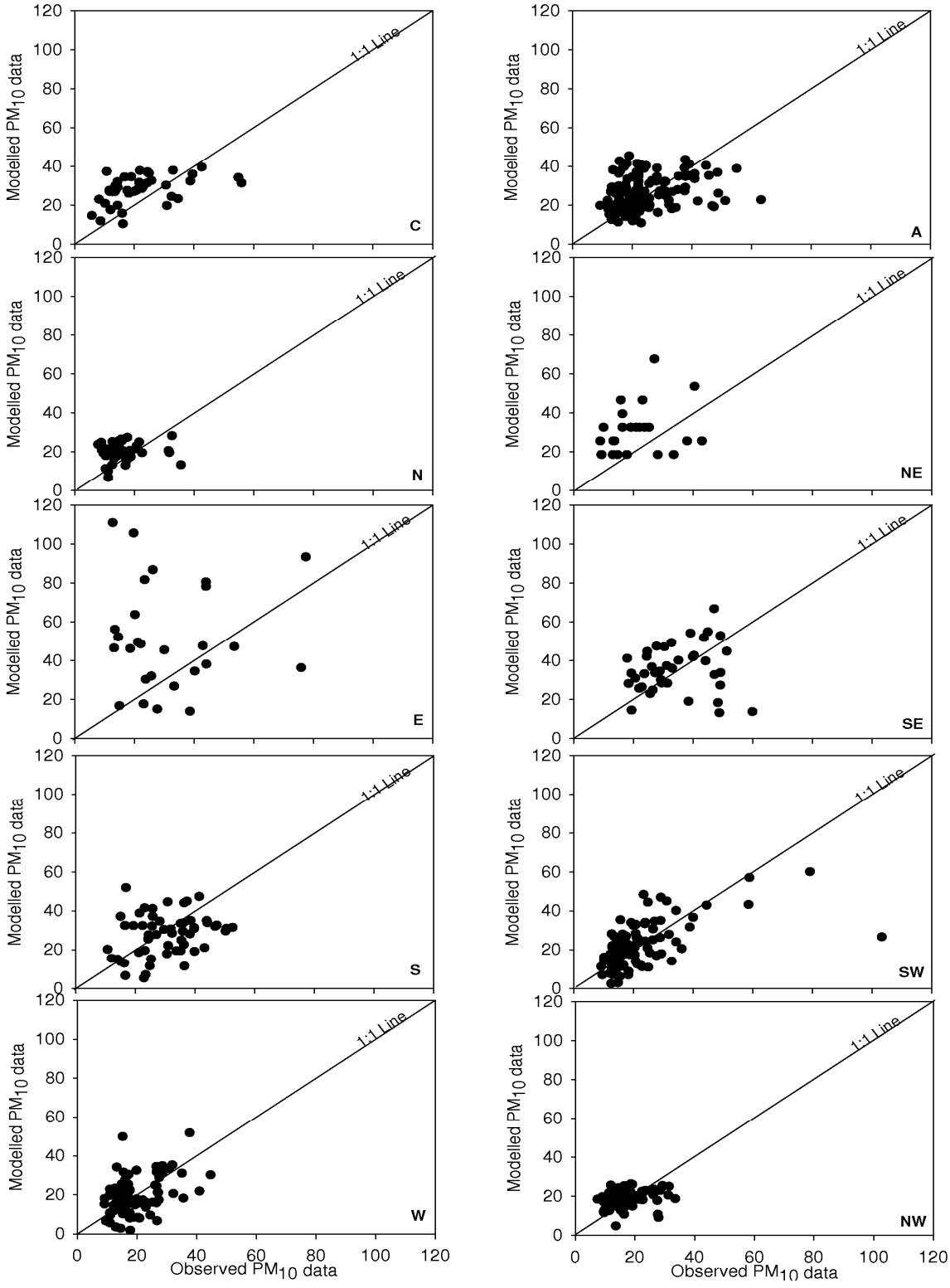

Figure 4.7: Same as Figure 4.6, but now using ECMWF meteorological data as input to the LWT_{MLR} model.

High O_3 concentrations are restricted to the summer season (JJA), and more specific to the Lamb weather types A, E, SE and S. The modelled O_3 time series are in good agreement with the observed O_3 concentrations for the period 2005-2006 (Figure 4.4). All distributions are thereby closely scattered around the perfect 1:1 line. When ECMWF data are used as predictors for the regression-based model, the highest concentrations are found for the same weather type classes (A, E, SE and S). However, the distributions are characterized by a larger scatter and a lower explained variability, in the higher quantiles of the distribution (Figure 4.5).

The modelled versus observed PM_{10} values show a large scatter around the optimal 1:1 line, especially for those types characterized by the highest concentrations (all types except N, NE, W and NW) both when observations and when ECMWF data are used as predictors (Figure 4.6 and Figure 4.7 respectively). Again, these results show that for PM_{10}, a regression-based approach using the available range of meteorological data is insufficient to explain the observed PM_{10} variability. Therefore, the remaining of this sensitivity study of downscaled air quality levels to its meteorological predictor values is restricted to O_3.

In order to understand the deficiencies of the regression-based model, the differences between ECMWF data and observations are studied only for these meteorological predictor variables that are included in the circulation pattern dependent regression equations (Figure 4.8). Data are shown for the JJA months only, as this season is characterized by the highest O_3 concentrations.

Modelled O_3 values for the weather types A, SE and S are positively related to Tmax (Demuzere et al., 2008b), which is underestimated in its median value by up to 3 K in the ECMWF model. TCC, RH and P0 are negatively related to ozone concentrations for the southern circulation pattern. These variables are overestimated by the ECMWF model (Figure 4.8) and dampen high ozone concentrations. The underestimation of modelled O_3 concentrations under high-pressure conditions (type A) are favored by an overestimation of the relative humidity in ECMWF compared to the observations, which is again a predictor in the regression model for O_3 formation.

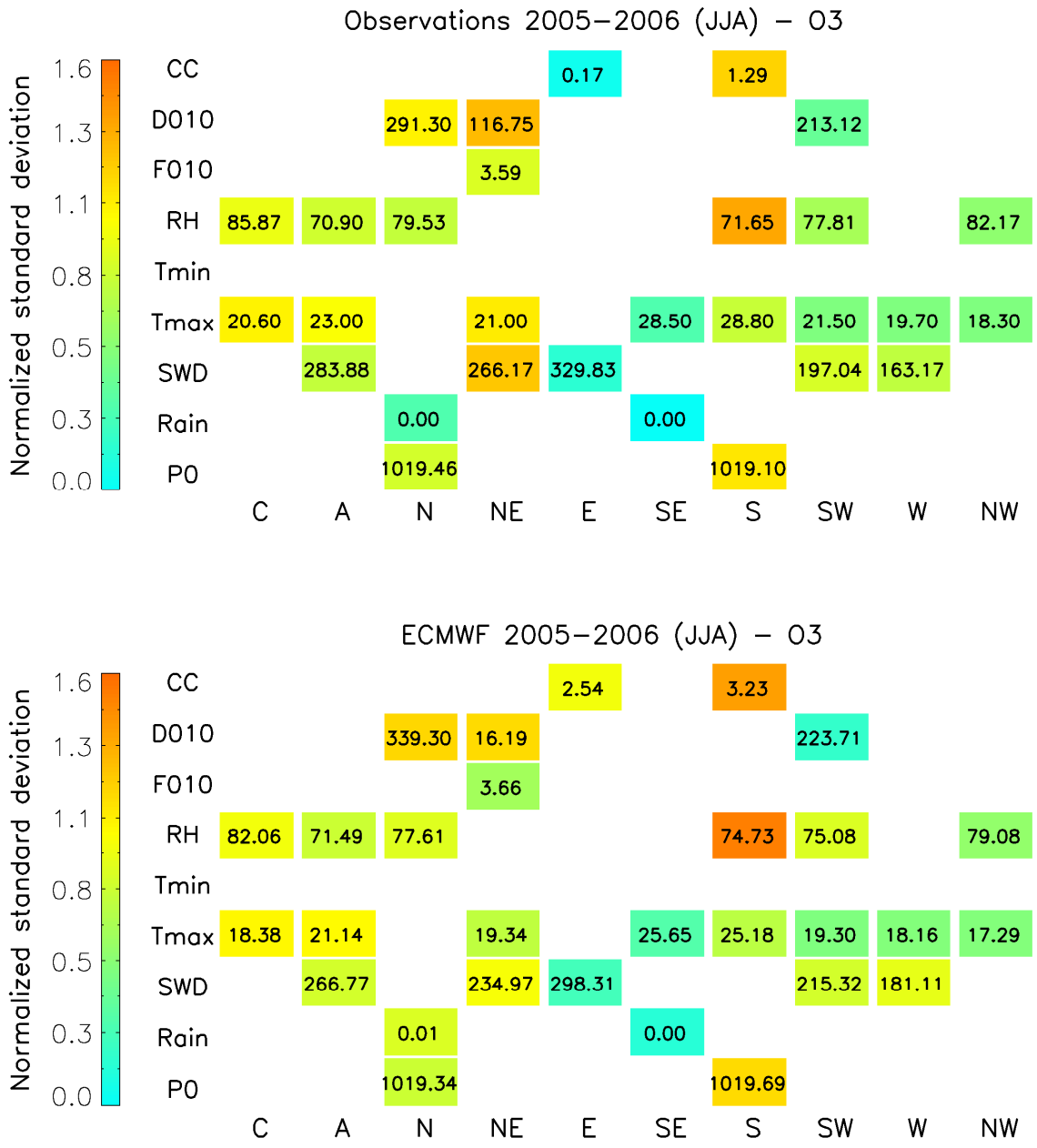

Figure 4.8: Median and normalized standard deviation (colors) for each of the meteorological predictor variables that are used in the circulation-specific regression equations, averaged over the summer (JJA) period 2005-2006. The upper panel presents observations, while the lower panel present the results based on ECMWF data.

4.5 Discussion

Deficiencies in the regression-based models can be due to 1) an inadequate representation of the predictor variables and 2) the fact that most downscaling methods tend to resolve only part of the total variance (Mearns et al., 2003; Barrero et al., 2006). In the previous section we found substantial differences between ECMWF data and observed meteorological variables. This difference can be due to 1) deficiencies in the ECMWF model or 2) the low spatial resolution used in our analysis. After all, in order to test our method for possible future downscaling purposes using AOGCM output as an input for the regression-based models, we averaged four surrounding grid points from the spectral T63 horizontal grid. Therefore the ECMWF predictors are representative for an area of about 350x350 km². By using such a coarse resolution predictor variability is possibly dampened. In order to test this, a comparison is made with ECMWF operational forecast data from a single grid point (52.505 °N / 4.95 °E) extracted from the original N400 Gaussian grid resolution (hereafter referred to as ECMWF1). The ECMWF1 data are representative for a much smaller area of about 25 x 25 km².

The quantile distribution of the ECMWF data is compared to the observed quantile distribution for the relevant meteorological variables (Figure 4.9). The largest differences between ECMWF1 and ECMWF are found for Tmax, RH and cloud cover. Tmax shows a large decrease in RMSE in ECMWF1 caused by a better representation of the higher percentile values. Although the RMSE for RH and cloud cover derived from ECMWF1 is slightly higher than from ECMWF, the quantile distribution of ECMWF1 corresponds more closely to the observations. The impact of these differences in ECMWF predictor values on downscaled O_3 levels is plotted in terms of RMSE for $LWT_{SEAS+MLR}$ (Figure 4.10). Furthermore, a qq-plot is used to present the distribution for both ECMWF and ECMWF1 downscaled O_3 concentrations using the $LWT_{SEAS+MLR}$ approach (Figure 4.11). This comparison shows that in term of RMSE, there is a negligible difference for the downscaled O_3 time series using both spatial average or a single grid point predictor data (Huth et al., 2001; Gachon and Dibike, 2007). Hereby, the RMSE scores are systematically lower for the latter for the circulation patterns characterized by high O_3 concentrations (A, E, SE and S). Nevertheless, the qq-plot (Figure 4.11) shows that higher quantiles of observed O_3 concentrations (>120 µg/m³) are better reproduced by the single grid point predictor data compared to the 4-grid point spatial average. This suggests that the differences between observed and ECMWF downscaled O_3 time series are both due to the usage of the 4-grid point average ECMWF data, dampening some of the predictors variability, as well as deficiencies in the ECMWF, resulting in a insufficient representation of the meteorological variables used as

predictors in the regression-based model. Consequently, this result implies that downscaling techniques using low-resolution gridded data from e.g. AOGCMs suffer from the low-resolution itself although improvement can already be obtained by addressing and carefully taking into account model errors, as was suggested by Cheng et al. (2007b).

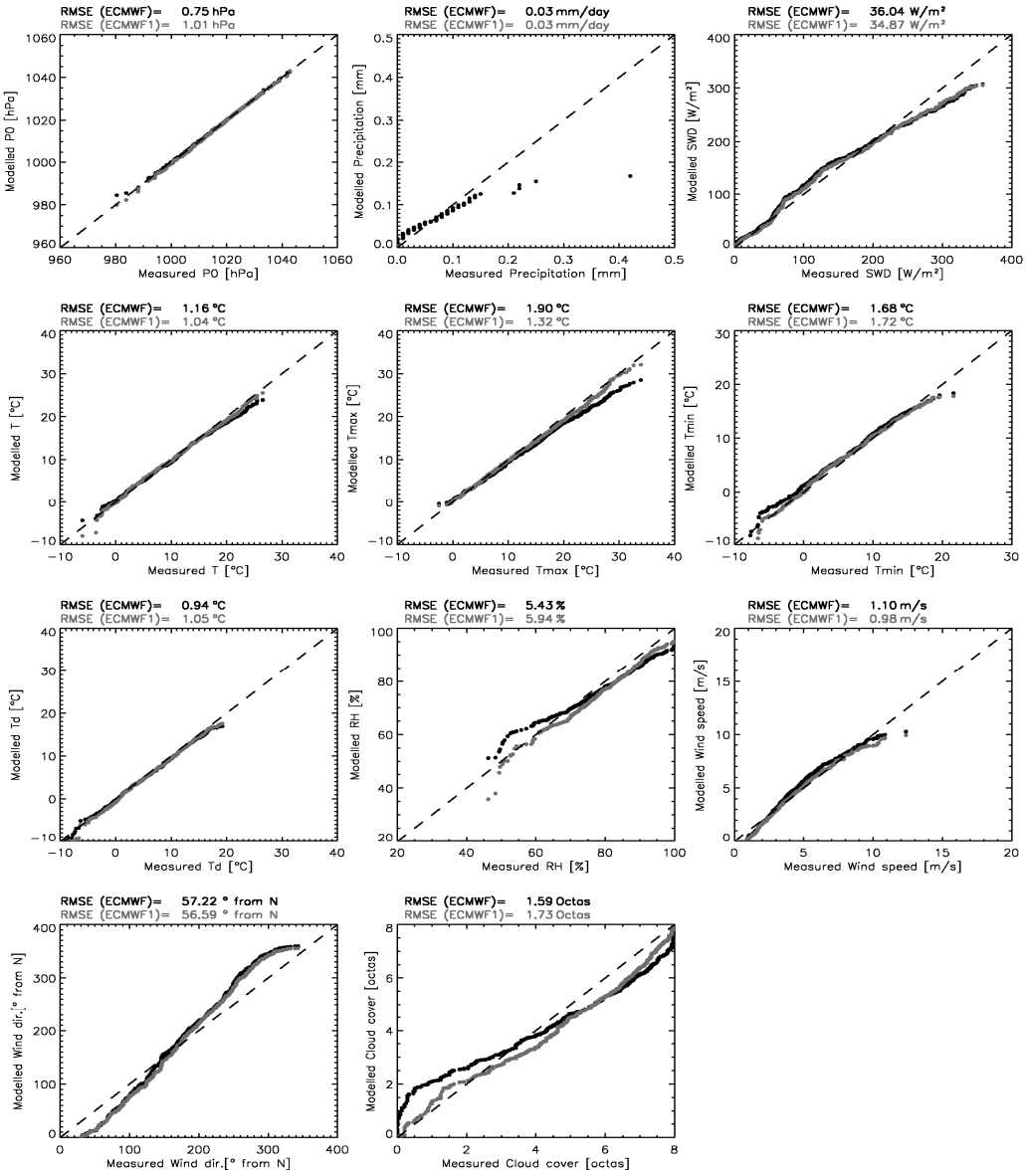

Figure 4.9: Quantile-Quantile(QQ)-plots of ECMWF versus observed meteorological predictor variables for the evaluation period 2005-2006. The 1:1 line presents perfect ECMWF data and the RMSE present the error for both ECMWF spatial averaged on over an area of 350 km^2 (ECMWF) and ECMWF for one grid point (25 km^2) (ECMWF1) compared to reference observed meteorological values from Cabauw.

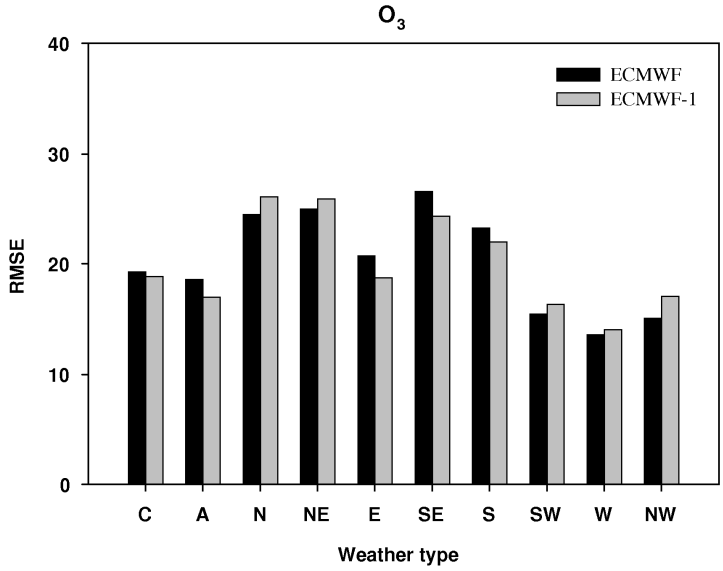

Figure 4.10: Root mean square error (RMSE) values for O_3 for each weather type class derived from 4 grid point averaged ECMWF and single grid point ECMWF (ECMWF - 1) data using $LWT_{SEAS+MLR}$.

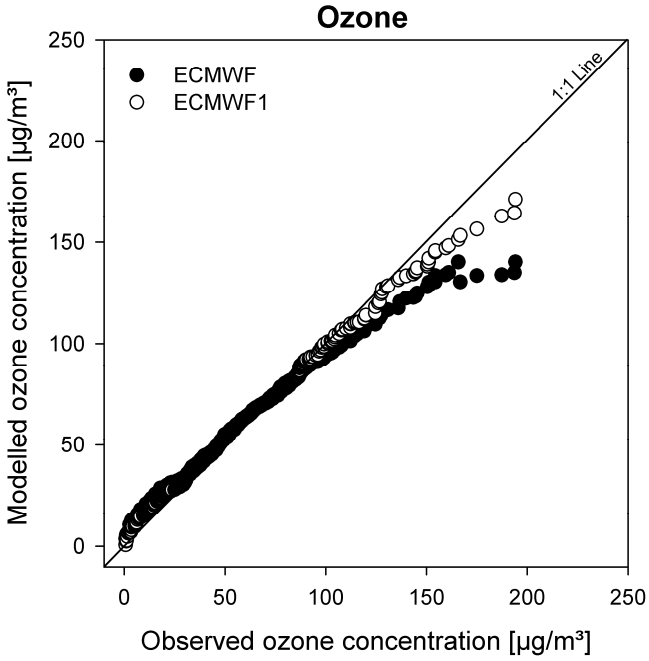

Figure 4.11: QQ-plots of ECMWF and ECMWF1 downscaled versus observed O_3 concentrations for the evaluation period 2005-2006. The 1:1 line presents perfect model line.

4.6 Conclusion

The primary aim of this paper is to evaluate a variety of regression-based methodologies to hindcast levels of O_3 and PM_{10} from meteorological predictors. In order to quantify the performance of the regression-based methods, several criteria are employed, next to general methods proposed by Willmott (1981, 1982) namely: fit between modelled and observed series using the explained variance, shape of the distribution in terms of skewness and kurtosis and persistence using the skill score against a persistence benchmark model. The analysis based on the calibration period 2001-2004 and an independent evaluation period 2005-2006 reveals that a stratification of the dataset using the automated Lamb weather type scheme, prior to the regression analysis improves the downscaling results for O_3 and PM_{10} in terms of explained variances and skill score against the persistence model (1 day lag). Furthermore, simple model regressions have shown not to be able to capture the deviation from normality, e.g. with a non-zero skewness and kurtosis for the observed O_3 and PM_{10} distributions. The introduction of a classification approach can reproduce these non-linearity characteristics. Moreover, as O_3 is highly dependent on seasonal changes in its relations with meteorological predictors, the O_3 regression model is run in a seasonal mode, which is not necessary for PM_{10}.

Before the regression-based methods can be used for downscaling air quality levels from coarse AOGCM-output (with a typical resolution of 300 x 300 km^2), it needs to be tested whether the observed local relations between meteorological and air quality variables hold on a larger scale. Therefore all regression-based models are evaluated using low-resolution ECMWF data interpolated on the spectral T63 horizontal grid for the period 2005-2006. Using these data as an input of the regression-based models leads to a slight decrease of the explained variance due to a lower variability of the meteorological predictors. Nevertheless, this approach can compete with other dynamical and statistical downscaling methods, which are often employed using observed time series, without being tested on low-resolution gridded data.

The somewhat deteriorated model performance is closely related to both ECMWF model deficiencies as well as to the coarse resolution of the data by averaging four surrounding grid points from the spectral T63 horizontal grid. The results from the regression-based model are similar in terms of RMSE, but better for the higher O_3 percentiles when using original ECMWF data on a Gaussian N400 resolution (corresponding to about 25 km^2) from the single grid point nearest to Cabauw as input to the regression-based model. Furthermore, comparing ECMWF meteorological data with observed data has shown some circulation-specific biases

for these variables that play an important role in the ozone formation process. Therefore, we can conclude that apart from the dampening of variance due to the coarse resolution, ECMWF model deficiencies also control the lower performance compared to modelled O_3 and PM_{10} time series when observational meteorological data are used as predictors. It is clear that the errors in the predictor variables need to be reduced or quantified in order to produce realistic air quality projections as a downscaling product of AOGCMs.

At present, chemical transport models are able to make short-term air quality prediction in real-time and should be preferred over statistical methods as they take into account the whole range of meteorological and chemical processes. However, in case this approach suffers from computational constraints, the synoptic-regression based model presented in this paper shows potential, especially for O_3, to be used in short-term air pollution prediction using meteorological output from numerical prediction models. This was also suggested by Cheng et al. (2007a) and further research could provide more insight using this approach.

Chapter 5

An analysis of present and future ECHAM5 pressure fields using a classification of circulation patterns*

5.1 Introduction

Over the past decade, scientific interest in the use of circulation patterns to describe and analyze a wide array of climatologically different situations has been steadily increasing. For example, several studies have been exerted correlating near surface meteorological variables to large-scale circulation pattern changes (Buishand and Brandsma, 1996, Trigo and Dacamara, 2000, Buchanan et al., 2002, Fowler and Kilsby, 2002, Post et al., 2002). For Western Europe and the North Atlantic sector, a major part of the formation and variability in circulation patterns is strongly influenced by the passage of high and low-pressure systems in the midlatitudes. On the contrary, spatial and temporal changes in these patterns will lead to changes in Western European climatic conditions. Thus, it is of great interest to analyze and compare the main circulation patterns and their variability over Western Europe with other important climate indices and patterns for this region, e. g. the North Atlantic Oscillation (NAO). The NAO has been investigated extensively (Marshall et al. (2001) - and references herein) and it has been shown that, for the midlatitudes, the NAO is the major winter climate mode, accounting for about one third of the inter-annual variability (Schwierz et al., 2006). Furthermore, the NAO has

* Demuzere, M., Werner, M., van Lipzig, N. P. M. and Roeckner, E., 2008. An analysis of present and future ECHAM5 pressure fields using a classification of circulation patterns. International Journal of Climatology 29.

already been examined in relation to extreme intensified cyclones (Rogers, 1997; Serreze et al., 1997; Ulbrich and Christoph, 1999; Raible and Blender, 2004) and mean flow (Raible, 2007) or blocking-like patterns over central to northern Europe (Scherrer et al., 2006; Schwierz et al., 2006).

Analyses of circulation patterns and their variability over Western Europe can be either performed by using observational data, i. e. reanalysis data sets, or by using data sets from coupled general circulation model (CGCMs) simulations. The latter will not only allow examining past and present situations but also enable the study of potential future changes with respect to different climate scenarios. In addition, a comparison of circulation patterns imprinted in reanalysis and CGCM data sets can be used as a novel, unique method to explore the accuracy of CGCMs. However, until now only few studies have examined the strength of CGCMs in reproducing circulation patterns (Huth, 2000). Several other studies have evaluated the potential to use blocking as a diagnostic tool for climate models (e. g. Tibaldi, 1993; D'Andrea et al., 1998). However, the use of blocking techniques as a diagnostic tool is intrinsically limiting the research of some very specific climate features. A broader approach using a circulation classification method can give a much more detailed insight on a synoptic time-scale, as such a method can identify not only the position of cyclones and anticyclones (cyclone detection and blocking phenomena), but also the strength and frequencies of zonal and meridional mean flow patterns and the transition between different circulation patterns.

The main focus of our study is the use of an automatic version the Lamb weather type classification method (Jenkinson and Collison, 1977; Jones et al., 1993; Trigo and Dacamara, 2000) as a diagnostic tool to evaluate ECHAM5 pressure fields and to study trends in the frequency of occurrence of circulation patterns for the period 1860-2100. This automatic weather type scheme grid (WT-scheme), initially developed for the British Isles, is centred above Belgium. This region is chosen because of planned studies on the use of circulation classifications for air quality studies in Belgium. However, our method encompasses the circulation patterns for the larger Western and Central European Region and therefore, our results are of interest for this larger region.

The method was designed as an automatic version of Lamb's classification. Buishand and Brandsma (1996), Trigo and Dacamara (2000), Buchanan et al. (2002), Fowler and Kilsby (2002) and Post et al. (2002) for example, describe previous studies and applications. Mostly, local meteorological station measurements are used to establish the relations between weather types and local surface characteristics, while daily gridded fields of SLP from NCEP/NCAR or ECMWF reanalysis data provide the pressure input for the WT-scheme. In this study we use the ECMWF ERA40-reanalysis data (Uppala

et al., 2005) to evaluate the sea level pressure fields from the ECHAM5-MPI/OM model.

The 1961-2000 ERA40 period is used to evaluate the ECHAM5 capabilities in generating the sea level pressure fields. Secondly, climatological trends based on the WTs are calculated for the period 1860-2100. Finally, a comparison of changes in WTs between the A1B, B1 and A2 IPCC scenarios of the ECHAM5-MPI/OM model for the period 2000-2100 is conducted.

This paper is organized as follows. In section 5.2 a brief overview is given of the data and models used in this study, thereby describing both ECMWF-ERA40 data and the general circulation model ECHAM5-MPI/OM, and the Lamb weather type method used to construct a daily circulation pattern database. In section 5.3 the result of the sensitivity of the Lamb weather type number of unclassified days on grid size and resolution is presented, followed by a comparison of ECHAM5-MPI/OM pressure fields with ERA40 data. Hereby, also the relation between WT and NAO-index and related cyclone identification and blocking features are investigated. Furthermore, climatic trends are investigated using the IPCC scenarios provided by ECHAM5-MPI/OM. Section 5.4 discusses our results and presents the conclusions.

5.2 Data and methods

5.2.1 Data

In this study we use the ECMWF - ERA40 SLP dataset on a 2.5° x 2.5° grid, for the larger European Atlantic Region (27.5 °W - 27.5 °E, 85 °N – 15 °N), centered above Belgium. The 6 hourly SLP values (00 h, 06 h, 12 h, 18 h) are averaged over a 24 hourly period in order to obtain daily mean sea level pressure fields for the period 1961-2000 (CTL_{ERA40}). The fields are averaged to seasonal and yearly means. The ECHAM5/MPI-OM SLP fields for the 20th century control (CTL) run for the period 1961-2000 (hereafter referred to as CTL_{ECHAM5}) were generated with the coupled atmosphere-ocean model (ECHAM5/MPI-OM) at a T63L31 resolution (≈ 1.85° x 1.85°) in the framework of the 4th IPCC assessment report.

The coupled model used in this study consists of new model versions for both the atmosphere and the ocean. In the atmosphere model (ECHAM5; Roeckner et al., 2003, 2006a) vorticity, divergence, temperature and the logarithm of surface pressure are represented by a truncated series of spherical harmonics (triangular truncation at T63), whereas the advection of water vapor, cloud liquid water and cloud ice is treated by a flux-form semi-Lagrangian scheme. A hybrid

sigma/pressure system is used in the vertical direction (31 layers with the top model level at 10 hPa). The model uses state-of-the-art parameterizations for shortwave and longwave radiation, stratiform clouds, cumulus convection, boundary layer and land surface processes, and gravity wave drag. The ocean model (MPI-OM; Marsland et al., 2003) uses the primitive equations for a hydrostatic Boussinesq fluid with a free surface. The vertical discretisation is on 40 z-levels, and the bottom topography is resolved by means of partial grid cells. The ocean has a nominal resolution of 1.5° and the poles of the curvilinear grid are shifted to land areas over Greenland and Antarctica. Concentration and thickness of sea ice are calculated by means of a dynamic and thermodynamic sea ice model. In the coupled model (Jungclaus et al., 2006), the ocean passes to the atmosphere the sea surface temperature, sea ice concentration, sea ice thickness, snow depth on ice, and the ocean surface velocities. The atmosphere runs with these boundary values for one coupling time step (one day) and accumulates the forcing fluxes. These fluxes are then transferred to the ocean. The model does not employ flux adjustments.

Global ECHAM5/MPI-OM SLP datasets were provided by the Max Planck Institute for Meteorology, Hamburg, for the years 1860 to 2100. The available simulations include 3 IPCC scenarios A1B, B1 and A2 between years 2001 and 2100 (Roeckner et al., 2006b), for which SLP fields are available at a 6-hourly resolution ($SCEN_{A1B\text{-}Coupled}$). Pressure data for an area identical to the selected ECMWF-ERA40 region were extracted from the T63 ECHAM5/MPI-OM SLP grid and re-gridded by conservative remapping (Jones, 1999) to a 2.5° by 2.5° regular lat/lon grid, which can directly be used in the WT-scheme.

5.2.2 Automatic classification method

A method to classify daily circulation patterns was originally developed by Lamb (1972). This subjective classification used surface pressure synoptic charts describing the flow in the 500 hPa level in the atmosphere. To avoid dependency of the daily weather types on experience and consistency of the researcher, this method was objectified by Jenkinson and Collison (1977). Moreover, as shown by Conway and Jones (1998), circulation patterns fundamentally control meteorological characteristics on the surface, whereby the use of sea level pressure has a lot of advantages. Previous studies done by McKendry et al. (2006) show that upper pressure level patterns are less variable than surface pressure patterns and that particular upper level patterns may be associated with a large range of pressure synoptic types. Therefore the WT method uses surface pressure, which is more appropriate for the classification of circulation patterns than upper level pressure patterns. Based on the Lamb method, the WT circulation pattern for a given day is described using the locations of the high and low pressure centers that determine the direction of the geostrophic flow. It

uses coarsely gridded pressure data on a 16-point moveable grid and is therefore easily applicable in any area with available data.

This method allows twenty-seven different classification weather types to be defined, including eight main directional types: north, northeast, east, southeast, south, southwest, west, northwest and three non-directional types: anticyclonic, cyclonic and unclassified types. Sixteen hybrid types (combination of directional and non-directional types) are also recognized (Lamb 1972). These types are characterized through the use of a set of indices associated to the direction and vorticity of geostrophic flow. The indices used are the following: southerly flow component of the geostrophic surface wind (SF), westerly flow component of the geostrophic surface wind (WF), resultant flow (FF), southerly shear vorticity (ZS), westerly shear vorticity (ZW) and total shear vorticity (Z). These indices were computed using sea level pressure (SLP) values obtained for the retained number of grid points, and are both for the flow units as for the geostrophic vorticity expressed in hPa. The weather types are defined by comparing values of FF and Z:

- Direction of flow (in degrees) is given by $\tan^{-1}$ (WF/SF), 180° being added if WF is positive. The appropriate wind direction is computed using an eight-point compass, allowing 45° per sector.
- If $|Z|<FF$, flow is essentially straight and considered to be of a pure directional type (eight different possibilities according to the compass directions).
- If $|Z|>2FF$, the pattern is considered to be of a pure cyclonic type if $Z>0$, or of a pure anticyclonic type if $Z<0$.
- If $FF<|Z|<2FF$, flow is considered to be of a hybrid type and is therefore characterized by both direction and circulation (sixteen different types).
- If Z or FF < 6, than a day is classified as “unclassified”.

The latter point reveals that a threshold value for Z or FF is used to define whether a day is allocated as unclassified or not. For the analyses of the SLP fields, values of Z and FF do not show any specific clustering or grouping around a specific threshold value, which is in line with the findings of Goodess (2000). Therefore, it is not necessary to implement another more useful cut-off point for our central and western European grid area and hence the original threshold value of 6, defined originally for a grid centered on the British Isles, was retained (Jones et al., 1993).

The analysis of the number of occurrences for each weather type shows relatively small numbers for the sixteen hybrid groups. Moreover, differences in occurrence within one direction (including both the cyclonic and anticyclonic type) are small compared to differences between different directions of types.

Therefore the 27 WTs are combined in a smaller number of main groups, this according to their directional characteristics. All types, both from the pure directional and hybrid types, with the same directional component are combined into the same directional group/type. This results in eight directional types (e.g. N(d) [directional North]= N [North], CN [cyclonic North], AN [Anticyclonic North]), two pure vorticity types A [anticyclonic] and C [cyclonic] and the U [unclassified] type, so eleven types in total (Table 5.1). This strategy of reducing the number of classes facilitates the intercomparison between classification types derived from both ECHAM5/MPI-OM and ECMWF-ERA40 SLP fields. Figure 1 depicts the SLP composite maps for the eleven WTs separately for the ECMWF-ERA40 SLP reference dataset.

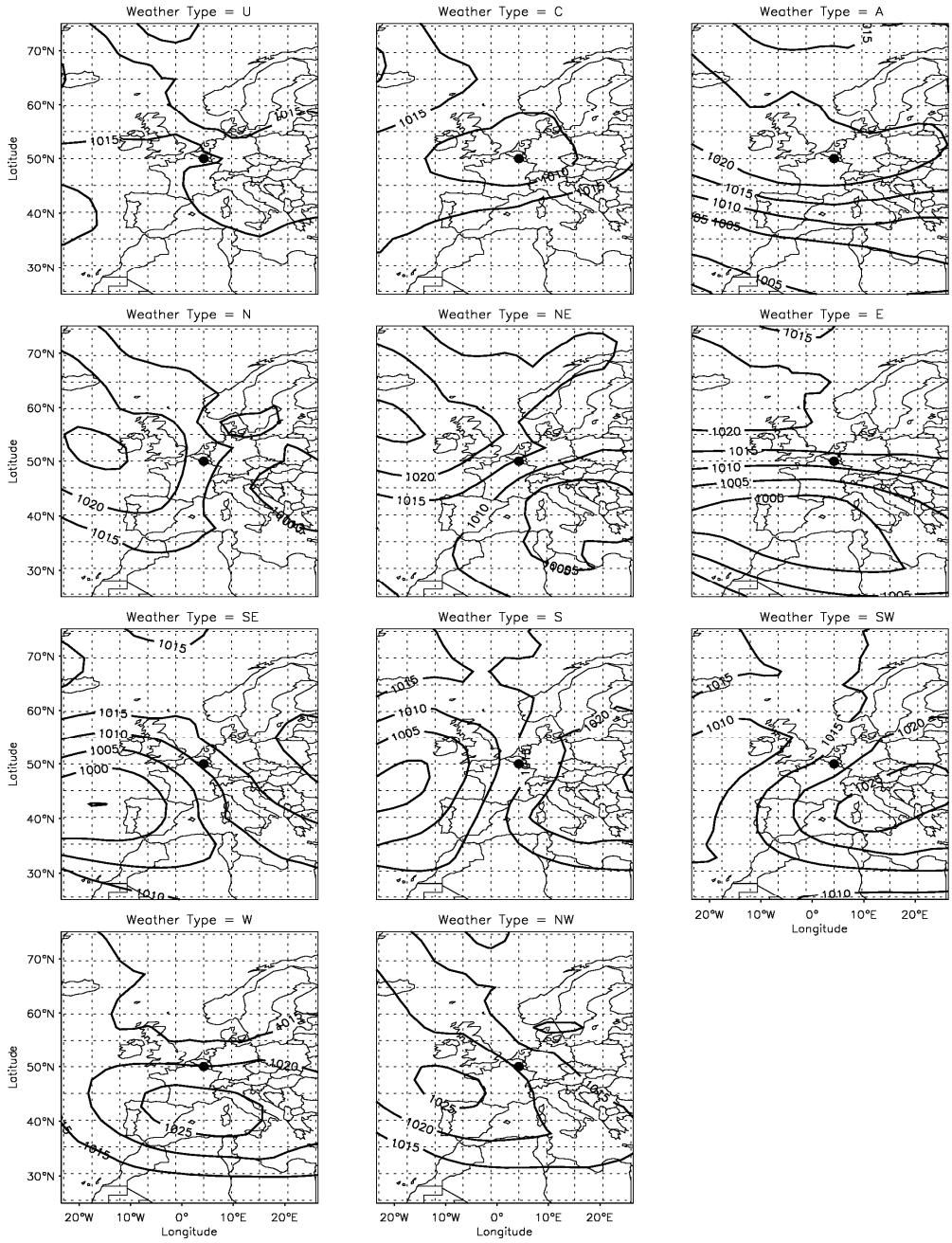

Figure 5.1: SLP composites for all directional Lamb weather types derived from the ECMWF-ERA40 SLP reference dataset, averaged over the period 1961-2000. The black dot represents the center of the Lamb grid configuration, located in Uccle.

First, the number of WTs will be derived based on ECHAM5 – MPI/OM and ECMWF – ERA40 SLP fields for the period 1961 – 2000. To assess whether there are significant differences in observed and modelled frequency distribution averaged over all types and for different periods of time (year, season, month), the χ^2 test is applied using a 0.1 significance level (Chernoff and Lehmann,

1954). In this way, it is possible to get more insight in the overall model performance in terms of weather types over the 40-year period. Interannual variability for each weather type individually is tested with the student t-test on a monthly time scale. To investigate whether differences in trends of weather types based on the three different IPCC scenarios are significant, the Mann-Kendall test (e.g. Verstraeten et al., 2006) was used, using a statistical significance of 10%.

5.3 Results

5.3.1 Grid sensitivity of the WT Scheme

Previous studies using the WT classification scheme used the 16-grid points configuration with a 5° grid resolution (Trigo and Dacamara, 2000; Post et al., 2002; Buishand and Brandsma, 1996; Fowler and Kilsby, 2002 and Buchanan et al., 2002). One would expect that grid size and resolution play an important role in the allocation of weather types and in the number of unclassified days. Therefore, a sensitivity test is done using various numbers of grid points and different grid configurations. Originally, the grid was set up consisting of 16 grid points with a 10° resolution in longitude and a 5° resolution in latitude (Jenkinson and Collison, 1977). Eight sensitivity runs are set up here, differing in number of grid points (9, 16, 32) and grid resolution (2.5°, 5° and 10° in both latitude and longitude) (Figure 5.2). A sensitivity run with a 10° resolution on a 32-point grid is neglected because the area described by such a configuration exceeds our region of interest.

Table 5.1: Overview of the JC Weather Types, representing the 26+1 JC weather types and the reduced 8 directional weather type groups (right column).

Pure Types	Directional Types	Hybrid Types		
U	N	CN	AN	N(d)
C	NE	CNE	ANE	NE(d)
A	E	CE	AE	E(d)
	SE	CSE	ASE	SE(d)
	S	CS	AS	S(d)
	SW	CSW	ASW	SW(d)
	W	CW	AW	W(d)
	NW	CNW	ANW	NW(d)

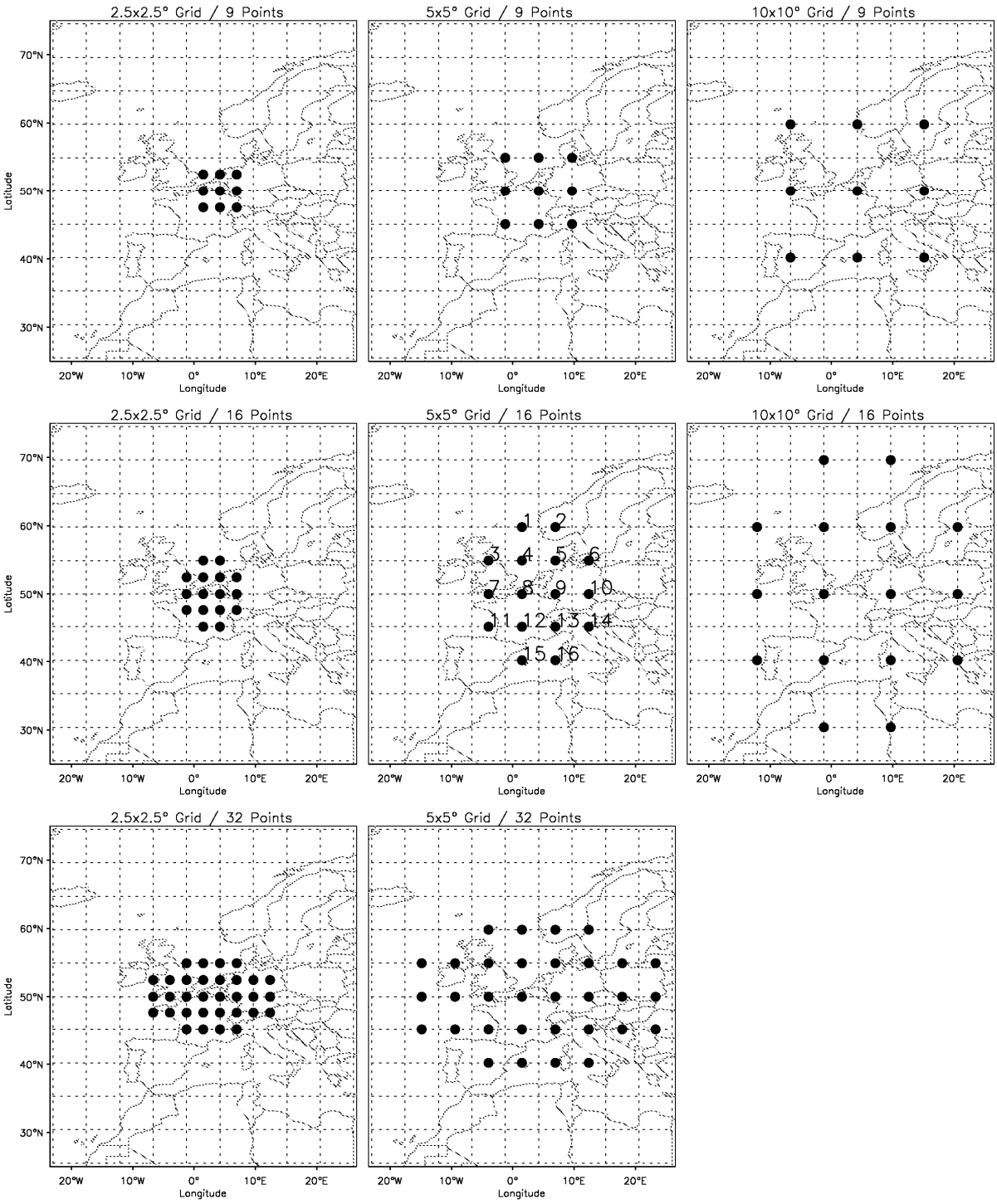

Figure 5.2: Visualization of the grid for the different sensitivity runs. Upper row: 9 grid points 2.5°, 5°, 10°; middle row: 16 grid points on 2.5°, 5°, 10°; lower row: 32 grid points on 2.5 and 10°. Grid points are labeled only for the central plots from 1 to 9, 1 to 16 and 1 to 32 for the 9, 16 and 32 number of points plots respectively.

Overall, we can conclude that the number of unclassified days and the associated standard deviation decreases with a decreasing grid resolution (Table 5.2). For

the configuration with 16 and 32 grid points, a grid spacing of 2.5° is inappropriate leading to a large number of unclassified days, 155 and 136 days per year respectively (Table 5.2). Also, for the configuration with 9 gridpoints, a grid spacing of 2.5° is not appropriate: this grid configuration doesn't capture any circulation pattern (Table 5.2), and classifies each day as pure anticyclonic, which explains the non-existence of unclassified days. From this it is clear that the grid spatial scale needs to be related to the typical scale of synoptic circulation patterns. However, as differences between the 5° and 10° grid resolution using 16 grid points are small (25 and 19 respectively) and previous studies used the 16-grid points and 5° resolution, this study applies the same grid, enabling the opportunity to compare the results to former studies.

Table 5.2: Averaged number and standard deviation per year of unclassified days for the 1961-2000 period, for a grid configuration with 9, 16 or 32 grid points and a resolution of 2.5, 5 or 10°.

Grid Points	9			16			32	
Resolution	2.5°	5°	10°	2.5°	5°	10°	2.5°	5°
Mean	-	62	21	155	25	19	136	35
Stand. Dev.	-	9	6.25	14.64	5.94	4.19	14.25	6.59

5.3.2 Evaluation of ECHAM5 SLP fields using ECMWF - ERA40 data

ECHAM5-MPI/OM SLP fields are evaluated using the reference CTL_{ERA40} dataset, for the December-January-February (DJF), March-April-May (MAM), June-July-August (JJA) and September-October-November (SON) seasons separately. Figure 5.3 shows the seasonal mean SLP of both models together with the absolute bias of the ECHAM5-MPI/OM normalized by the standard deviation of the ECMWF-ERA40 40-year time series for each season separately. The normalized bias is largest during summer and smaller during the winter season. This is due to the small interannual variability (as expressed by the standard deviation of the 40 year time series) during summer, which is related to the weak north-south pressure gradient during this season (van Ulden and van Oldenborg, 2006). Therefore, the discrepancy in WTs between CTL_{ECHAM5} and CTL_{ERA40} is largest during summer, whereas during winter the WT occurrences correspond much better.

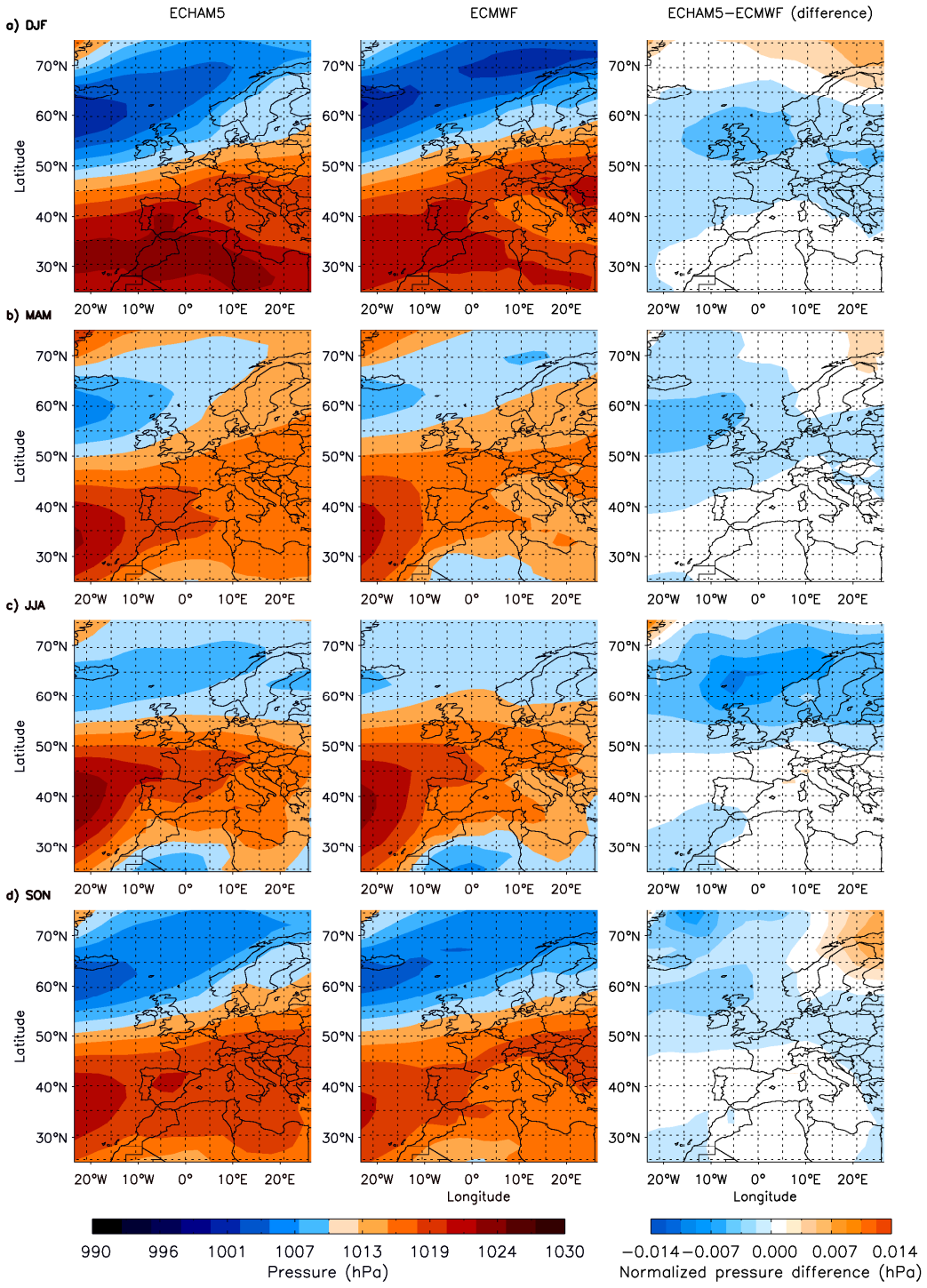

Figure 5.3: Mean Sea Level Pressure during the period 1961-2000, based on ECHAM5/MPI-OM (left column), ECMWF-ERA40 (middle column) and the difference between the two (right column), normalized by the standard deviation. This is done for each season seperately (consecutive a) DJF, b) MAM, c) JJA and d) SON).

The patterns in ECHAM5-MPI/OM are overall similar compared to the ERA40 reference dataset, although differences can be noticed in the strength and location of the anticyclonic belts and low-pressure systems. The differences in

occurrences during the year are largest for circulation type W(d), which is to a large extend caused by a large overestimation in the summer season (Table 5.3). During that season, there is an underestimation of the frequency of occurrence in CTL_{ECHAM5} of 3.5 and 4.3 days for the NE(d) and E(d) directional groups respectively and an overestimation of 3.7 days and 12.8 days for the JJA SW(d) and W(d) respectively. This effect is even enhanced when considering these differences change against the observed absolute occurrences derived from ERA40 (Table 5.3). Here we see that the differences are even larger than the number of absolute occurrences for SW(d), and are high for circulation pattern S(d) too because of its low occurrence in the observations. These findinges can be explained by an underestimation of ECHAM5-MPI/OM MSLP north of the British Isles, and a small overestimation of MSLP around the Mediterranean Sea (Figure 5.3c), associated with an increased North-South pressure gradient in ECHAM5-MPI/OM.

Table 5.3: Mean annual and seasonal frequency differences (in days) of all groups of directional circulation types for ECHAM5 minus ERA40 between 1961-2000. The % provides the differences between ECHAM5 minus ERA40 against the observed occurrence of each circulation type (x100).

	Annual		Winter (DJF)		Spring (MAM)		Summer (JJA)		Autumn (SON)	
	Days	%	Days	%	Days	%	Days	%	Days	%
U	-10.2	-24.8	0.4	12.1	-2.4	-21.6	-6.1	-33.0	-2.2	-26.5
C	2.3	10.1	3.7	84.1	0.2	2.2	-1.7	-35.4	0.2	4.7
A	-16.3	-21.5	-7.6	-39.2	-1.5	-10.4	-0.8	-3.8	-6.3	-29.6
N(d)	-7.3	-58.9	-0.2	-15.4	-0.9	-36.0	-1.3	-44.8	-0.9	-56.3
NE(d)	-9.8	-53.6	-1.0	-34.5	-4.0	-53.3	-3.5	-67.3	-1.4	-50.0
E(d)	-9.7	-27.7	-2.9	-33.7	-2.6	-21.3	-4.3	-55.8	0.0	0.0
SE(d)	0.7	5.8	-0.9	-20.5	0.8	27.6	-0.2	-13.3	0.9	27.3
S(d)	1.3	15.5	0.0	0.0	0.7	38.9	0.6	100.0	0.0	0.0
SW(d)	10.8	36.1	0.9	8.7	5.0	89.3	3.7	115.6	1.3	12.0
W(d)	32.5	35.6	7.4	27.2	5.2	27.1	12.8	64.6	7.0	27.8
NW(d)	1.2	5.3	0.1	1.8	-0.6	-10.5	0.8	11.3	1.0	22.7

For DJF, CTL_{ECHAM5} shows an easterly geostrophic flow anomaly in the northern part and a westerly geostrophic flow anomaly in the southern part of the WT grid (Figure 5.3a). Note hereby that the WT grid is extending from the south of Norway to Sardinia (Figure 5.2). This results in anomalous cyclonic shear vorticity in our region of interest explaining the underestimation in anticyclonic WTs in CTL_{ECHAM5}. In addition, the North-South gradient in the WT grid increases, explaining the overestimation of western WTs in CTL_{ECHAM5} (Figure 5.3a).

For MAM, the location of an anomalous low-pressure system in CTL $_{ECHAM5}$ west of the British Isles, results in a stronger pressure gradient in the Northwest to Southeast axis in our region of interest. This leads to an increase (decrease) of W(d) and SW(d) (E(d) and NE(d)) weather types (Figure 5.3b). As pressure differences are smaller for SON in the LW grid domain (Figure 5.3d), also weather type frequency differences are lowest for this season (Table 5.3).

In general, the more pronounced CTL $_{ECHAM5}$ pressure gradients result in a lower number of unclassified days, both yearly and seasonal, which suggest that CTL $_{ECHAM5}$ pressure patterns have more pronounced (unrealistic) circulation characteristics (Table 5.3). Most significant differences (based on t-test statistics) between CTL $_{ECHAM5}$ and CTL $_{ERA40}$ are found in the late spring, summer and beginning of autumn (from May to September) (Table 5.4; Figure 5.4). During these seasons, weather type occurrences of western types are significantly higher for CTL $_{ECHAM5}$ than for CTL $_{ERA40}$ and the occurrences of eastern types are lower. This corresponds to the results of van Ulden and van Oldenborg (2006), who tested various global coupled climate models with respect to the explained variance in sea level pressure for northern latitudes (their Figure 5.2). They found that ECHAM5-MPI/OM, next to others, has difficulties in correctly simulating circulations from April to September. These discrepancies could arise because ECHAM5-MPI/OM doesn't use flux adjustment (as compared to other models), and therefore, model bias in SST can be expected which will also affect circulation patterns. van Ulden and van Oldenborg (2006) tested various IPCC AR4 models in terms of circulation. ECHAM5-MPI/OM was shown to be one of the best models, although also here summer circulations in northern latitudes (30°-90°N) are shown to be difficult to simulate correctly. Moreover, a comparison to a flux adjusted model (MIROchi – their Figure 18) showed that the latter was better in simulating the explained spatial variance in SLP, compared to the other non-flux adjusted models, including ECHAM5. Also the model resolution should be taken into account. Roeckner et al. (2006a) found that the JJA westerly wind bias around 50°N is still present at T106L31 resolution but clearly smaller than at the resolution used in our study (see their Figure 10).

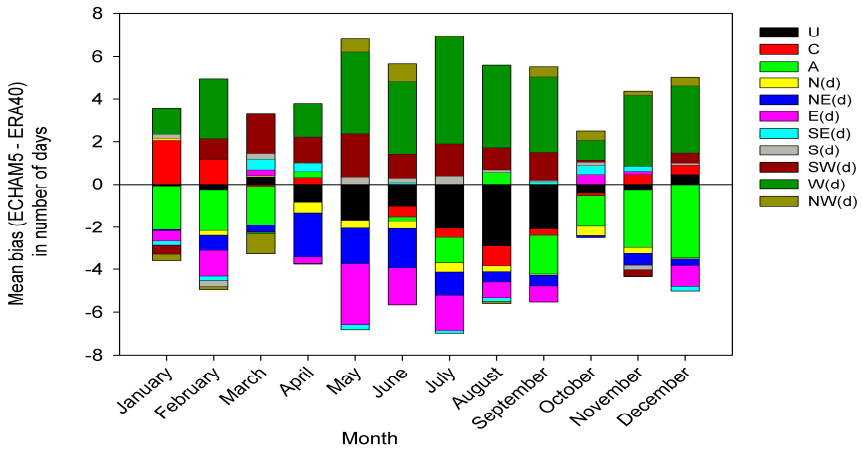

Figure 5.4: Mean monthly bias for each individual directional weather type, for each month between 1961-2000, calculated as the difference between ECHAM5 and ECMWF-ERA40.

Table 5.4: Monthly frequency differences (in days averaged over 40 years) for all groups of WTs for ECHAM5 minus ERA40. Differences significant on the 99% level are denoted in bold. The bias presents the differences in monthly frequencies (days per month) averaged over all years for all types (CTL_{ECHAM5} minus CTL_{ERA40}). Months with a yearly averaged bias > 1 are denoted by *.

	U	C	A	N(d)	NE(d)	E(d)	SE(d)	S(d)	SW(d)	W(d)	NW(d)	Bias (days/month)
January	-0.07	2.07	-2.05	0.09	-0.05	-0.49	-0.19	0.19	-0.42	1.21	-0.3	0.65
February	-0.28	1.14	-1.88	-0.23	-0.7	-1.23	-0.21	-0.28	1	2.79	-0.12	0.9
March	0.37	-0.09	-1.81	0.05	-0.33	0.26	0.49	0.26	1.84	-0.07	-0.95	0.59
April	-0.84	0.33	0.26	-0.49	-2.07	-0.35	0.4	0	1.23	1.56	-0.02	0.68
May	-1.65	0	-0.02	-0.37	-1.72	-2.81	-0.23	0.35	2.02	3.84	0.6	1.24*
June	-1.02	-0.49	-0.19	-0.37	-1.88	-1.72	0.09	0.21	1.09	3.42	0.86	1.03*
July	-2.05	-0.44	-1.23	-0.42	-1.05	-1.65	-0.12	0.4	1.51	5	0.05	1.26*
August	-2.88	-0.98	0.56	-0.26	-0.47	-0.72	-0.21	0.12	1.05	3.88	-0.09	1.02*
September	-2.09	-0.3	-1.84	-0.05	-0.49	-0.77	0.14	0.07	1.26	3.56	0.51	1.01*
October	-0.42	-0.12	-1.42	-0.44	-0.09	0.47	0.4	0.16	0.09	0.95	0.42	0.45
November	-0.28	0.47	-2.67	-0.28	-0.6	0.14	0.23	-0.21	-0.3	3.33	0.19	0.79
December	0.47	0.42	-3.44	-0.05	-0.35	-0.95	-0.21	0.09	0.47	3.16	0.4	0.91

The difference in frequency distribution of weather types between CTL_{ECHAM5} and CTL_{ERA40} is assessed using the χ^2 test. During the summer season CTL_{ECHAM5} distribution of weather types significantly differs from CTL_{ERA40} (Table 5.5). During spring, autumn and winter both populations are not significant different. On a monthly scale, significant differences between CTL_{ECHAM5} and CTL_{ERA40} are revealed in May and July weather type frequencies (Table 5.5).

Additionally, WTs are derived removing the systematic errors in ECHAM5-MPI/OM prior to doing the classification. Firstly, the monthly mean 40-year bias is calculated as the difference between ECHAM5-MPI/OM and ECMWF-ERA40 SLP. Secondly, the weather types are derived after subtracting this bias from the original daily ECHAM5-MPI/OM SLP. There is a significant impact of eliminating the biases on the WT classification (Table 5.6). The variability in WTs in Western Europe is very well presented by ECHAM5 once the systematic errors in SLP are removed: There is no significant difference in terms of mean annual, seasonal and monthly weather type frequencies between ECMWF-ERA40 and the bias-corrected ECHAM-MPI/OM SLP (Table 5.6). Therefore it is concluded that the discrepancy in WT occurrences between ECHAM5-MPI/OM and ECMWF-ERA40 can be explained by the monthly mean bias.

Table 5.5: Statistical analysis between observed and expected frequencies of weather types during the 1961 – 2000 period. Values less than 0.1 are contrary to the hypothesis that CTL_{ECHAM5} is a good approximation of CTL_{ERA40} (both populations are significantly different) (marked in bold).

	Year	Season	Month
Dec	$0.55\ 10^{-3}$	0.20	0.33
Jan			0.98
Feb			0.60
Mar		0.25	0.82
Apr			0.62
May			$4.6\ 10^{-2}$
Jun		$4\ 10^{-3}$	0.11
Jul			$5.5\ 10^{-2}$
Aug			0.28
Sep		0.42	0.19
Oct			0.77
Nov			0.49

For each month, the mean bias for all weather types over the 40-year period is calculated. This bias presents the mean difference in number of occurrences (days) between CTL_{ECHAM5} and CTL_{ERA40} calculated for each month separately over all directional weather types (Table 5.4, right column). Biases are largest for May and July (1.24 and 1.26 days respectively). For all months from May to September, biases are exceeding a value greater than 1 day (Table 5.4). For the remaining months, values are less than 1 (day). Based on the significant differences on a monthly and seasonal time scale from Table 5.4, and taking into account this value of 1 day as a threshold, we conclude that ECHAM5-MPI/OM generally reproduces the observed weather types quantities for the October-November-December-January-February-March-April (ONDJFMA) months for

the period 1961-2000. Non-negligible differences for the May-June-July-August-September (MJJAS) period are found, where CTL_{ECHAM5} overestimates (underestimates) the number of westerlies (easterlies). Therefore, in order to avoid the model uncertainties concerning MJJAS circulation patterns in the ensuing analysis, our further analyses are restricted to the ONDJFMA period.

Table 5.6: Same as Table 5.3, but using ECHAM5 SLP with a monthly bias-correction.

	Annual		Winter (DJF)		Spring (MAM)		Summer (JJA)		Autumn (SON)	
	Days	%	Days	%	Days	%	Days	%	Days	%
U	-4.59	-1.3	-0.28	-0.1	-0.43	-0.1	-1.64	-0.4	-2.24	-0.6
C	-0.98	-0.3	1.29	0.4	-0.74	-0.2	-1.23	-0.3	-0.30	-0.1
A	0.93	0.3	-0.24	-0.1	1.42	0.4	1.30	0.4	-1.56	-0.4
N(d)	0.73	0.2	0.12	0.0	0.53	0.1	0.63	0.2	-0.56	-0.2
NE(d)	-2.63	-0.7	-0.18	0.0	-1.72	-0.5	-0.09	0.0	-0.64	-0.2
E(d)	1.11	0.3	-0.82	-0.2	-0.34	-0.1	0.64	0.2	1.64	0.4
SE(d)	0.67	0.2	-0.64	-0.2	-0.20	-0.1	0.39	0.1	1.12	0.3
S(d)	-0.19	-0.1	0.22	0.1	-0.26	-0.1	0.34	0.1	-0.48	-0.1
SW(d)	-1.94	-0.5	-1.12	-0.3	0.24	0.1	-0.13	0.0	-0.93	-0.3
W(d)	3.81	1.0	1.71	0.5	1.02	0.3	-1.52	-0.4	2.60	0.7
NW(d)	3.0	0.8	-0.1	0.0	0.5	0.1	1.3	0.4	1.4	0.4

In Figure 5.5, mean sea-level pressures composites are plotted for the years 1961-2000, for the ONDJFMA period. Generally, the SLP shows similar patterns for CTL_{ECHAM5} and CTL_{ERA40}, although values differ regionally. The CTL_{ECHAM5} run overestimates pressure over the Sahara region and northern parts of Scandinavia, with pressure differences up to respectively 2.5 and 3.0 hPa, whereas pressure patterns are slightly underestimated from Central Europe to the Northwest region of Ireland, with differences up to 3 hPa. Generally, the pressure differences between CTL_{ECHAM5} and CTL_{ERA40} are small over the WT grid, and therefore differences in WTs are small for these months. Note that there are no significant trends in weather type occurrence over the 40-period in ERA40.

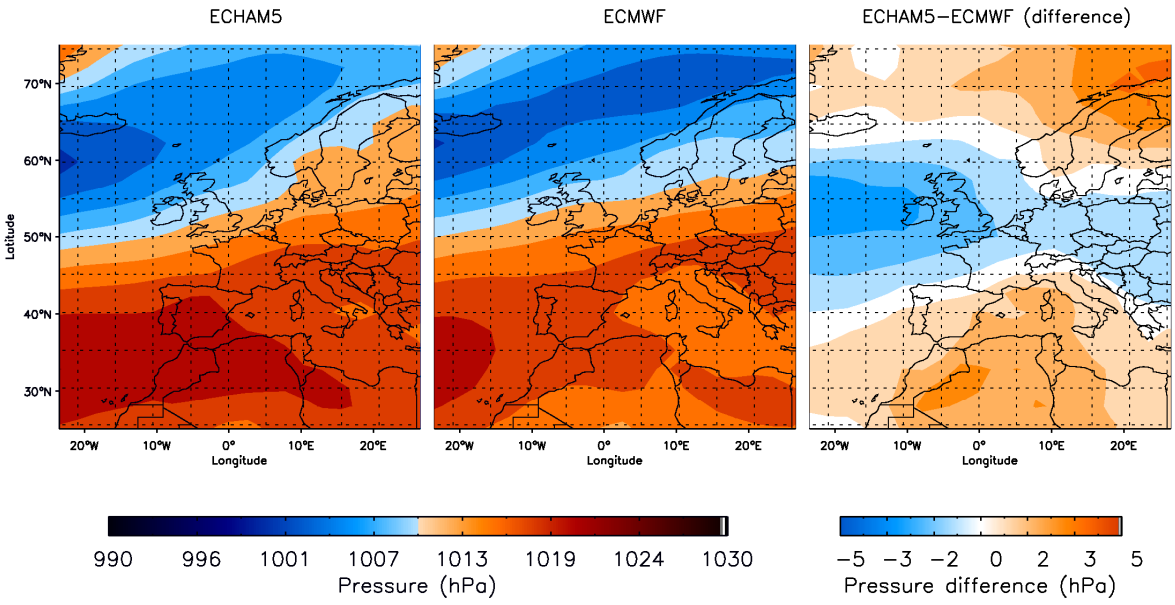

Figure 5.5: Mean Sea Level Pressure averaged over the period 1961-2000, for the ONDJFMA period only. The ECHAM5-MPI/OM SLP pattern is shown in the left panel, ECMWF-ERA40 in the middle and the difference between the two in the right panel.

5.3.3 The relation between weather types and other indices of large-scale flow

Since the NAO index, cyclone identification and blocking indices are often used to characterize atmospheric flow conditions in Western and Central Europe, this section compares some of these measures with the WT method in order to evaluate climate models. Many authors have proposed methods to calculate NAO indices, based on (normalized) pressure differences between stations pairs, area-weighted pressure extremes or principal component time series corresponding to a pressure field principal component pattern (Osborn et al., 1999 – references therein). Some authors (Ulbrich and Christoph, 1999; Hu and Wu, 2004) show that the largest values in teleconnectivity do not coincide with the reference locations used in the NAO index definition provided by Hurrell (1995). In addition, they point out a shift in the NAO action centers in global warming climate simulations. Latif et al. (2000) confirm this with a canonical correlation analysis applied on ECHAM4. Their analysis reveals a northeastward shift in the NAO centers of action. As pointed out by Campbell et al. (1995) and Huth (1997) there is a lack of consensus on the spatial NAO characteristics. This is especially relevant for studying changes in the NAO, as the shift in the NAO action centers depends on the methods used to characterize the NAO. It is, however, of lesser importance here as the aim of our analysis is to relate the present-day NAO with present-day SLP circulation patterns. For such an analysis, the precise definition of an index is of less importance provided that the comparison is performed on an identical basis (Osborn et al., 1999). Indices derived for longer timescales show that the NAO is best discerned when time-

averaged (monthly or, preferably, seasonal) atmospheric fields are analyzed (Marshall, 2001; Loptien and Rubrecht, 2005). Therefore, the seasonal DJF NAO index is derived from both ECMWF-ERA40 and ECHAM5-MPI/OM by calculating the difference of normalized sea level pressure from the nearest grid boxes to the Ponta Delgada (Azores) and the Stykkisholmur (Iceland) measurement sites (Figure 5.6). In addition, the NAO index based on measurements from Hurrell (1995) is added as the reference NAO index (Figure 5.6).

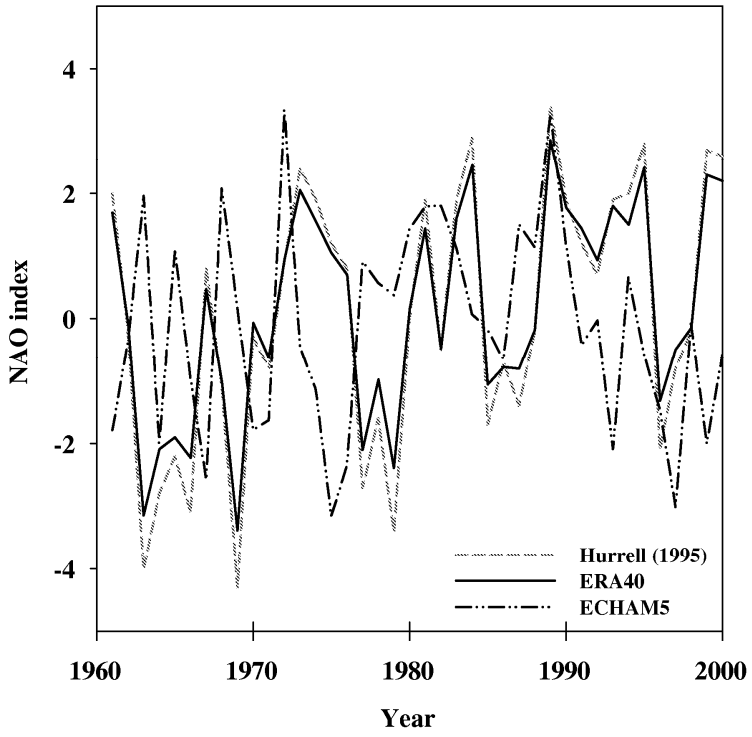

Figure 5.6: The station-based NAO-index from Hurrell (1995) and derived from ERA40 and ECHAM5-MPI/OM as the difference of normalized sea level pressure from the nearest grid boxes to the Ponta Delgada (Azores) and Stykkisholmur (Iceland) between DJF 1961-2000.

Pearson correlation coefficients are calculated between the DJF frequencies of weather types and the DJF NAO index, both for CTL_{ERA40} and ECHAM5-MPI/OM (Table 5.7). There is a strong significant negative correlation between the DJF NAO index and both CTL_{ERA40} and CTL_{ECHAM5} cyclonic weather types. This can be explained by a northward shift of cyclones (above 60°N) during winters with a positive winter NAO index (Raible, 2004; Raible, 2005; Sickmöller et al., 2000). Since the northern boundary of the WT grid is located at 60°N, our WT classification method is not capturing the increase in cyclones north of 60°N during a positive NAO phase. Our results confirm the findings of Sickmöller et al. (2000) who states that cyclone clustered based on their occupation (northeastward (NE), zonal (ZO) and stationary (ST)) show clear

negative correlations with NAO for their NE and ZO cyclone clusters over central Europe.

Table 5.7: Correlation between the NAO index and the CLT_{ERA40} & CTL_{ECHAM5} directional WTs frequencies using ERA40 NAO and ECHAM5-MPI/OM NAO, this for DJF. Values on a 90% significance level are denoted in bold.

	U	C	A	N(d)	NE(d)	E(d)	SE(d)	S(d)	SW(d)	W(d)	NW(d)
DJF											
ERA40	-0.031	-0.37	0.19	-0.04	-0.24	-0.28	-0.37	-0.17	0.006	0.45	-0.01
ECHAM5	0.11	-0.27	0.29	0.02	-0.07	-0.15	0.11	-0.21	-0.21	0.17	-0.05

Scherrer et al. (2006) have shown, next to others, that there is a positive correlation between three blocking indices and a positive NAO-phase. This is consistent with the significant positive correlation between NAO and anticyclonic weather types for both CTL_{ERA40} and CTL_{ECHAM5} (Table 5.7). The underestimation of the correlation coefficient in CTL_{ECHAM5} is due to an underestimation of anticyclonic weather types frequencies in CTL_{ECHAM5} compared to CTL_{ERA40} (Table 5.3). The slope of the regression curve between anticyclonic weather type frequency and NAO index is similar in CTL_{ECHAM5} compared to CTL_{ERA40} (Figure 5.7a).

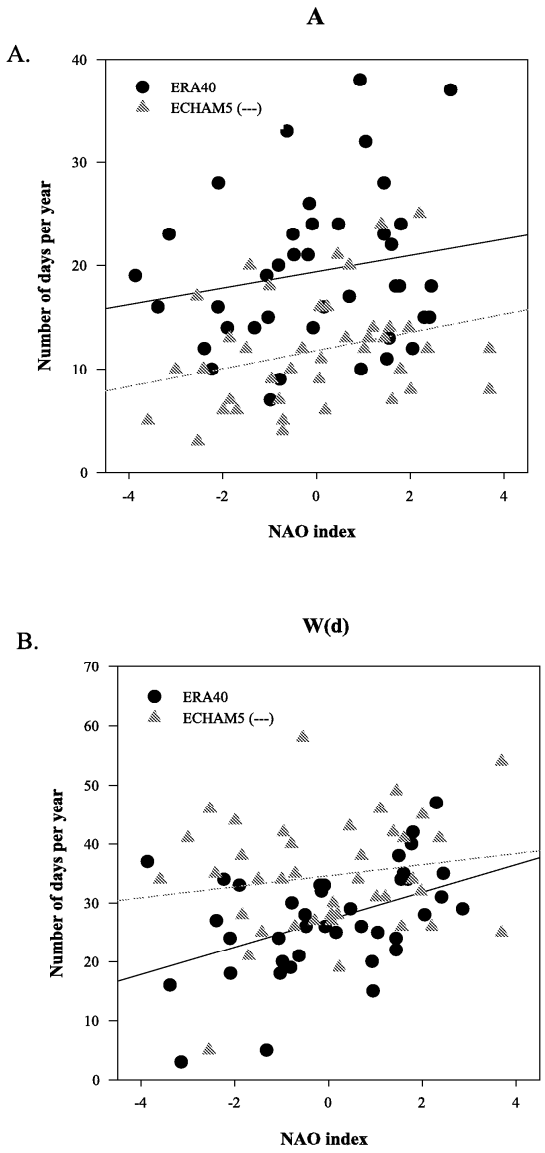

Figure 5.7: Mean frequencies of the a) A and b) W(d) weather types (in mean number of days per year) against the NAO index, plotted with an ascending NAO index.

The directional western weather type correlates positively with the winter NAO index (Table 5.7), but the correlation is only significant at the 90% level for CTL_{ERA40} and not for CTL_{ECHAM5}. Figure 5.7b shows that not only the correlation coefficient, but also the slope of the regression between western directional type W(d) and NAO index differs, even though the mean pressure pattern anomalies during the positive NAO years (NAO+) and negative NAO years (NAO-) (Figure 5.8) are almost identical. To analyse this in more detail, the regression between the mean yearly indices SF, WF, FF and Z of the WT method (see 5.2.2) and the NAO-index for CTL_{ECHAM5} and CTL_{ERA40} were calculated (not shown). There is no difference in the slope of the regression

between geostrophic flow indices SF, WF and FF and NAO index between ECHAM5-MPI/OM and ECMWF-ERA40. Contrarily the vorticity index Z shows a less negative slope in CTL_{ECHAM5} compared to CLT_{ERA40}. Note that such a difference between CTL_{ECHAM5} and CLT_{ERA40} in the sensitivity of the shear vorticity to the NAO index can also be identified from Figure 5.8. Since the sensitivity of Z to the NAO index is underestimated in CTL_{ECHAM5}, the sensitivity of C to the NAO index is slightly underestimated as well. This is compensated by a slight underestimation of the sensitivity to NAO index of W(d), SE(d) and E(d) (Table 5.7; Figure 5.7b).

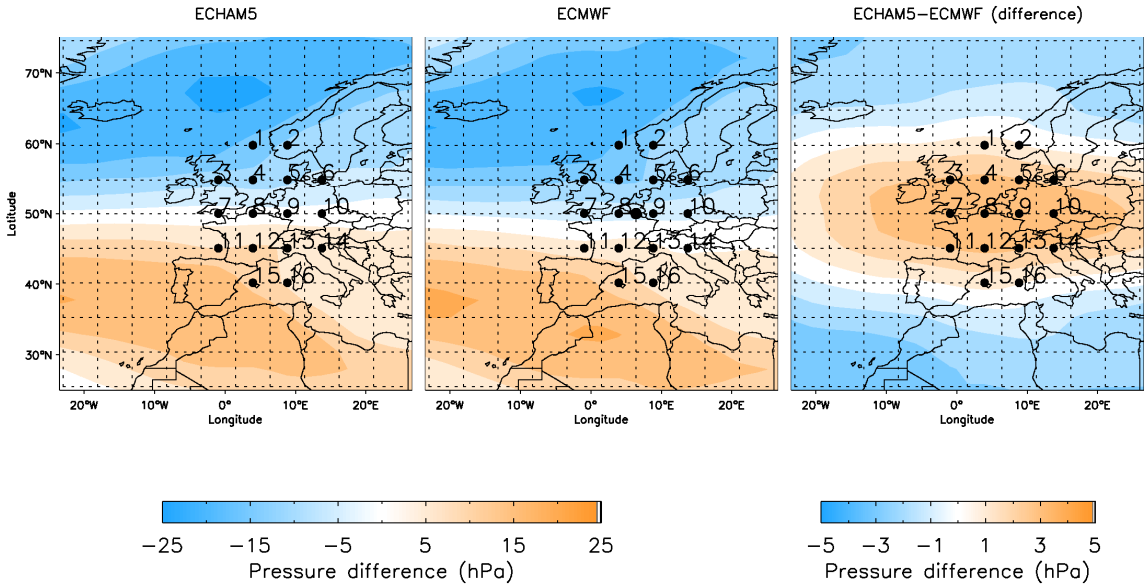

Figure 5.8: Mean SLP differences between NAO+ and NAO- years (for DJF), for CTL_{ECHAM5} (left panel) and CLT_{ERA40} (middle panel) and $CTL_{ECHAM5} - CLT_{ERA40}$ (right panel).

On the one hand, our approach confirms the results of many authors who have already shown that a positive NAO corresponds to an enhanced zonal flow over central Europe with an anomalously low (high) pressure over the subpolar (subtropical) North Atlantic (Hoerling et al., 2001) (Figure 5.8). On the other hand, it clearly points out the additional value of using this weather type approach as a diagnostic evaluation tool for CGCMs. Not only does it capture large-scale features found by other authors combining a multiple set of methods (NAO index, cyclone algorithms, blocking indices), it also shows that although pressure pattern differences between NAO+ and NAO- are similar for CTL_{ERA40} and CTL_{ECHAM5} (Figure 5.8), one should also check the frequency of occurrence of the large-scale circulation patterns, which can be easily done using the WT method.

5.3.4 Climatic trends in Weather Types

In this section, ECHAM5-MPI/OM climate change experiments with observed atmospheric greenhouse and aerosol concentrations since 1860 and different assumptions on future greenhouse gas and aerosol concentrations are discussed, namely the IPCC scenarios A1B, B1, and A2 until the year 2100. Following the IPCC report 2001, scenario A1B describes the future with a fast economic growth, a world population that peaks in the mid-century and declines afterwards and new and more efficient technologies. The scenario B1 is described by a similar population curve as A1B, but with an emphasis on global solutions to economic, social and environmental sustainability, including improved equity. The last scenario A2 differs herein that population continues growing through the century with a regionally developing economic growth and fragmented technological changes (IPCC 2001).

For each weather type group and scenario, the yearly mean number of occurrences is calculated for the 2001-2100 ONDJFMA period ($SCEN_{A1B\text{-}Coupled}$, $SCEN_{B1\text{-}Coupled}$ and $SCEN_{A2\text{-}Coupled}$). Trends are calculated for the eight directional and two pure (anti) cyclonic weather type groups between 2001-2100 and for the various scenarios A1B, B1 and A2. The trend analysis based on the Mann-Kendall test for the directional groups N(d), NE(d), SE(d), S(d), SW(d) and NW(d) shows no significant trends over the whole time period (not shown). The (anti) cyclonic and W(d) and E(d) series of occurrences and their linear trends are shown in Figure 5.9. Within each directional weather type group, trends for scenarios A1B, B1 and A2 are similar over the whole period, as well in amplitude as in overall trend. Year-to-year variability is large, as one could expect. Because long-term differences between the various scenario trends based on weather types are small, this study will continue its focus on the scenario A1B, only. Trends have been re-calculated for the A1B scenario over the whole 240-year period, expanding from 1860 till 2100, selecting ONDJFMA months, only (Figure 5.10).

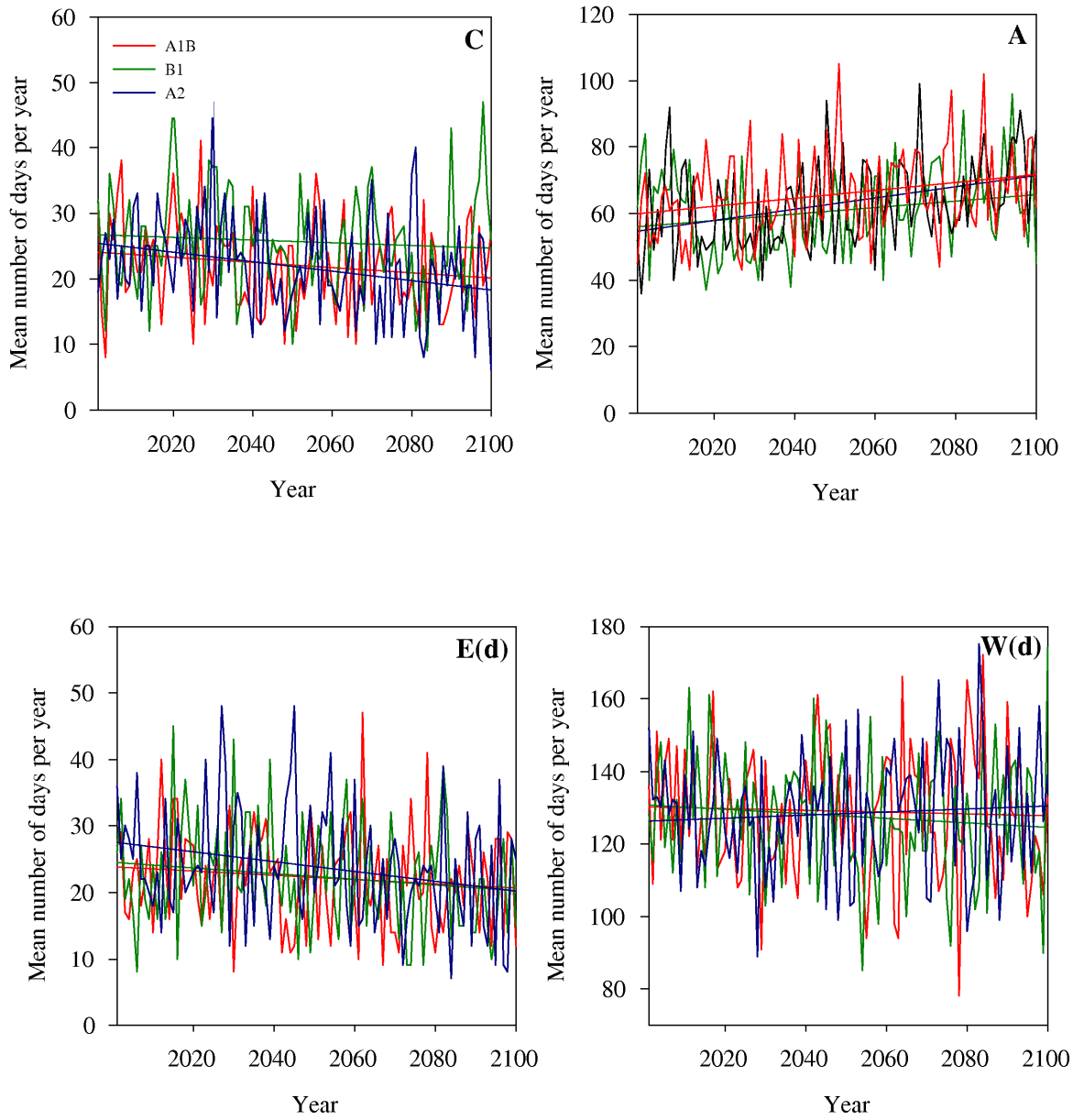

Figure 5.9: Mean number of days per year with weather types C, A, W(d) and E(d) for the $SCEN_{A1B\text{-}Coupled}$ (red), $SCEN_{B1\text{-}Coupled}$ (green) and $SCEN_{A2\text{-}Coupled}$ (blue) simulations with ECHAM5 – MPI/OM from 2000 – 2100, for the ONDJFMA period only. The bold line in its respective color denotes the trends for the different scenarios.

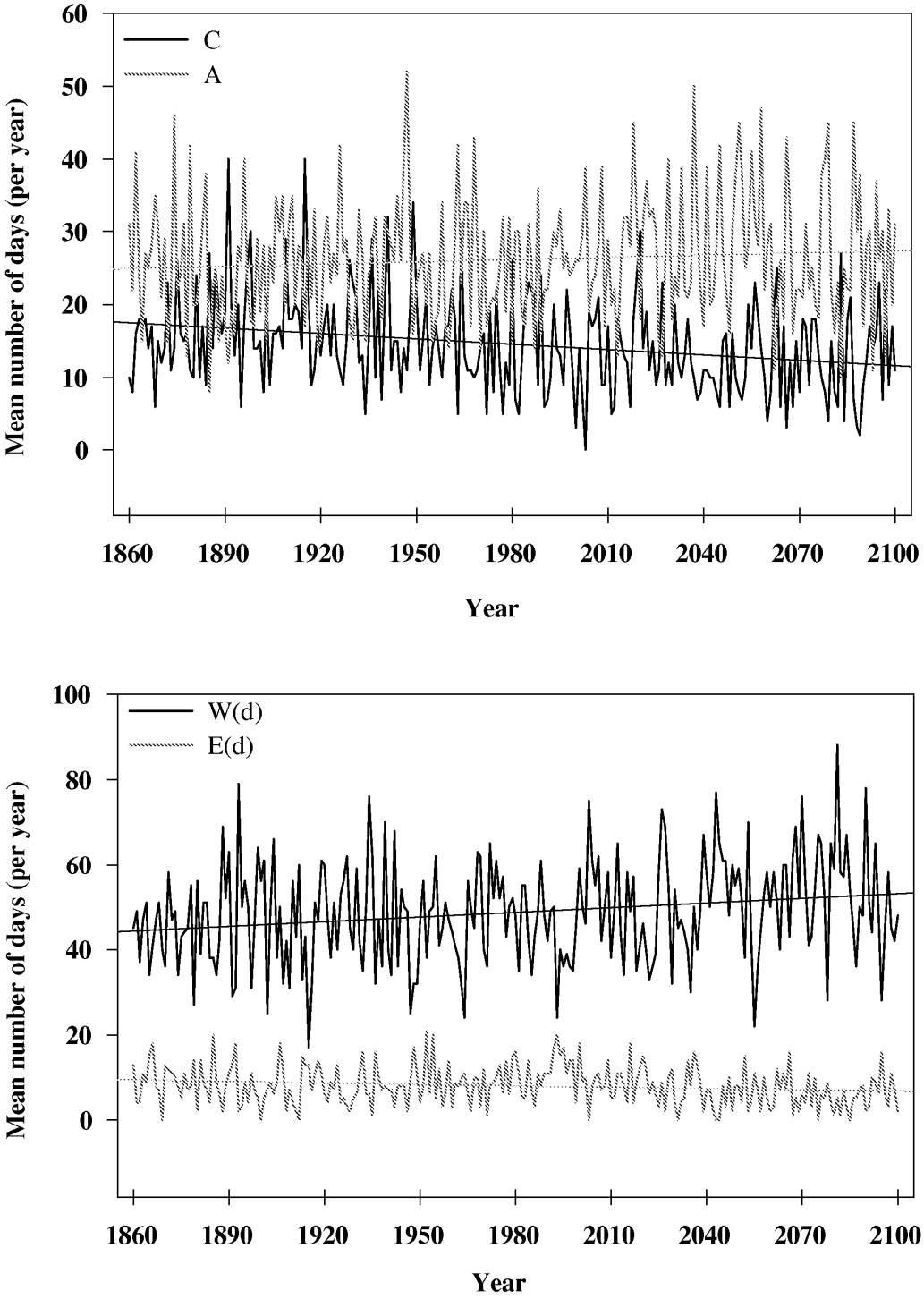

Figure 5.10: Same as Figure 5.9, but for the $SCEN_{A1B\text{-}Coupled}$ run and the 1860 – 2100 ONDJFMA period only.

Thereby, we can see an increase in number of the western directional type, balanced by a smaller decrease of pure cyclonic and all eastern directional weather types. The Mann-Kendall test is applied to test the trends' significance. For the representative directional and the two pure cyclonic WTs, the Mann-Kendall trend test P-values and linear trends are given (Table 5.8).

Table 5.8: The Mann-Kendall rank test is used to calculate significance of the $SCEN_{A1B\text{-}Coupled}$ circulation trends between the 1860 – 2100 period (ONDJFMA). 90% level of significance is indicated in bold, 95% level by *.

Type	C	A	N(d)	NE(d)	E(d)	SE(d)
Linear trend	-5.807	2.489	-0.11	-1.11	-4.3	-1.6
Mkprob	0.000106*	0.252208	0.284108	0.025138	0.002343*	0.127748
Type	S(d)	SW(d)	W(d)	NW(d)	All West	All East
Linear trend	0.201	1.512	11.91	-1.2	12.22	-7.011
Mkprob	0.878028	0.3939	0.00034*	0.066631	0.001055*	0.001689*

The statistical analyses shows that the increasing (decreasing) trend in all-West (all-East) is determined to a large extent by a significant increase in pure West directional types (by a decrease in pure East directional types) (Table 5.8). The increase of W(d) results in an absolute mean increase of almost 73 extra days over 240 years of westerly flow W(d) over central Europe during the months ONDJFMA. Again, a large year-to-year variability is found for all directional groups.

5.4 Conclusions

Until now, only few studies have tackled the strength of CGCMs in reproducing circulation patterns. In this respect, the automated WT classification method is tested as a diagnostic tool to evaluate CGCMs for the Western and Central European region. The WTs for a 40-year control run (1961-2000) of the ECHAM5-MPI/OM ACGCM for Western and Central Europe are evaluated using the ECMWF-ERA40 database. In general, ECHAM5-MPI/OM appears to be able to reproduce the frequencies in directional circulation types, especially for the late autumn, winter and early spring period ONDJFMA. For late spring, summer and early autumn (MJJAS), significant differences are found for most of the directional types. In particular western types are significantly overestimated by ECHAM5-MPI/OM, while eastern types are underestimated.

As the North Atlantic Oscillation climate variability is of large interest for the Western and Central European climate, this large-scale teleconnection pattern is compared to the WTs for the DJF winter period. The NAO index is positively correlated with the frequency of occurrence of westerly weather types whereby our approach confirms the results obtained by earlier research that a positive NAO phase is characterized by a stronger zonal flow, due to positive (negative) pressure anomalies over the subtropical (subpolar) ocean (Hoerling et al., 2001). Furthermore, a positive relation between the NAO+ phase and blocking over Central Europe, as shown by Scherrer et al. (2006), is recognized by our

classification approach: the relation between the frequency of occurrence of the anticyclonic weather type and the NAO index is positive. The negative correlations between cyclones and the NAO index as found by Sickmöller et al. (2000) are confirmed by a negative correlation between the frequency of occurrence of the cyclonic weather type C and the NAO index.

In order to avoid model deficiencies in the analyses of potential future changes of circulation patterns, ECHAM5-MPI/OM climate scenarios are tested for the ONDFJMA period, only. Although interannual variability between the A1B, B1 and A2 IPCC scenario schemes is large, the trends for the circulation types between 2000 and 2100 using the three IPCC scenarios are similar. The Mann-Kendall test is used to calculate the $SCEN_{A1B\text{-}Coupled}$ circulation trends between 1860 and 2100. While in general the trends for the directional groups are insignificant, there is a significant increase (decrease) in western (eastern) directional groups. This suggests that one can expect a larger influence of western circulation over Central Europe during future autumn and winter seasons. However, one should keep in mind that the used ECHAM5-MPI/OM model showed the largest deviations from the ECMWF-ERA40 data for exactly the same circulation patterns, W(d) and E(d), during the summer months. Thus, further analyses and GCM inter-comparison studies are certainly needed to test the robustness of the detected future circulation changes.

In order to increase the reliability of coupled general circulation models in future projections, down-scaling, air quality monitoring, boundary conditions for regional climate models and other applications, one has to make sure that overall circulation patterns are projected with confidence in all seasons. Thus, the approach suggested here could provide a rather simple methodology to detect changes and differences in circulation patterns on a synoptic time-scale, which makes this weather type scheme an appropriate tool for CGCM evaluation. Much research has been done on the NAO-related climatic impacts (see Marshall et al., 2001 and references therein), as well as on cyclone activity and blocking. Based on an automated classification method, as presented in this paper, climate impacts for various regions and on a synoptic timescale could easily be investigated for present day climate and future CGCM scenarios. Thereby, further work is underway to extend the present analysis on its implications on regional surface climate variables (Trigo et al., 2002, 2004) as precipitation (Hurrell et al., 2004) and temperature (Schär et al., 2004).

Chapter 6

A new method to assess air quality levels using a synoptic-regression approach. Part II: Future O_3 projections*

6.1 Introduction

Over the past 20 years, levels of ozone have been a concern to policymakers in Europe, as observed O_3 levels continue to exceed internationally accepted guidelines for the protection healthiness and vegetation in the spring and summer months (EU, 1999, 2008). Since the NO_x and VOC protocols of the United Nations Economic Commission for Europe (UN ECE) Convention on Long-range Transboundary Air Pollution (CLRTAP) almost 20 years ago, downward trends in VOC and NO_x have been observed. As a consequence, also episodic peak ozone levels decreased over parts of north-west Europe (Derwent et al., 2003). Despite these reductions in episodic peak levels, ozone levels are still a cause for concern during in the 21st century and air quality guidelines are still exceeded in most years in some EU countries. In this respect, the question is whether further regional pollution control strategies (e.g. CAFÉ thematic strategy for Air Pollution – EU 2005) will be stringent enough to reduce the overall ozone levels in Europe to its postulated levels.

Future air quality levels will be affected by several factors including changing biogenic and anthropogenic emissions, (intercontinental) long-range transport and possible changes in the regional climate (Metcalfe et al., 2002; Derwent et

* Demuzere, M., van Lipzig, N.P.M., 2008. A new method to assess air quality levels using a synoptic-regression approach. Part II: Future O_3 projections. Atmospheric environment (submitted).

al., 2003, 2004; Delcloo and De Backer, 2008). As an example, Derwent et al. (2008) suggests an increase in regional-scale ozone due to a drying out of soils and vegetated surfaces and Lee et al. (2006) suggest that increasing temperatures may lead to increased biogenic isoprene emissions, strengthening the regional-scale ozone formation. In this respect, projections from AOGCMs are commonly used as scenarios of future climate in the twenty-first century. Unfortunately, the resolution of these global climate models exceeds the impact assessors' needs, which often requires information equivalent to point observations. Therefore, a downscaling approach is used to bridge the gap between what AOGCMs produce and what impact assessors require (Wilby and Wigley, 1997). Some authors have attempted to classify the different approaches for climate modelling (e.g. Giorgi and Mearns, 1991; Wilby and Wigley, 1997), with Hewitson and Crane (1996) and Hewitson and Crane (2002) suggesting two categories of downscaling methods: process-based (dynamical) techniques, involving the explicit solving of the physical dynamics of the system and empirical (statistical) techniques that use the identified relationships derived from observational data. Often, dynamical downscaling is done in first instance for the present-day climate. Afterwards, the evaluated model setup is being used to investigate the influences of a possible future climate change on various (atmospheric) properties (e.g. Hogrefe et al. 2004; Andreani-Aksoyoglu et al., 2008).

Dynamic and statistical downscaling techniques are complementary and both methods should be used to evaluate future ozone levels (Mahmud et al., 2008). Giorgi and Meleux (2007) have shown that the complex climate-air quality modelling-systems, together with their computational/technical characteristics, make dynamical downscaling methods less useful for long-term predictions based on AOGCM outputs. These limitations are particularly due to spatial and temporal constraints in terms of computational power. Gillani and Pleim (1996), afterwards refined by Cohan et al. (2006), set an upper limit for the horizontal grid resolution for air quality modelling to less than 12 km. With such a high resolution, it is hardly possible to simulate 10 years or more, which is necessary to obtain reliable results (Forkel and Knoche, 2007). Therefore, statistical downscaling methods are useful in terms of temporal and spatial computational requirements.

This study uses the synoptic-regression based approach, presented in Chapters 3 and 4 of this dissertation (Demuzere et al., 2008b, c). The approach has successfully been applied to downscale maximum eight-hourly mean ozone levels from observed and coarse resolution ECMWF (European Center for Medium-Range Weather Forecasts) meteorological variables for the rural background station of Cabauw (The Netherlands). The synoptic-regression based relationships between meteorology and observed maximum eight-hourly

mean ozone concentrations are built on present-day data (see Chapter 4) and therefore intrinsically include present-day precursor emission information. As the evolution of biogenic and anthropogenic emissions and their feedbacks onto the physic-chemical formation processes of ozone under future climate conditions is uncertain, the same relations are kept for downscaling possible future climate scenarios. In doing so, we assume that the present-day relations between meteorology and air-quality variables stay constant through time. Moreover, when applying these techniques for future air quality projections, we aim to identify the impact of meteorological changes on future maximum eight-hourly mean ozone levels solely, without taking into account possible changes in future (precursor) emissions.

6.2. Datasets

6.2.1 Air quality data

In order to evaluate the downscaled maximum eight-hourly mean ozone time series using AOGCM present-day meteorological variables, one needs a long enough homogeneous maximum eight-hourly mean ozone record (which is calculated as the daily maximum of the 8-hourly running mean). As the Air Quality Monitoring Network of RIVM (National Institute of Public Health and Environment) is measuring ozone in The Netherlands since the 70s (Beck et al., 1996), this dataset is available. However, in order to test the performance of the downscaling approach itself, it is important to check any inconsistencies in the dataset due to a change in for e.g. monitoring aspects, anthropogenic emissions and quality control.

Except for the year 1986, the amount of missing data is limited to less than 5% over the period 1981-2000. In contrast to the second half of the period, values of maximum eight-hourly mean ozone exceed 200 $\mu g/m^3$ during the period 1981-1990, with a maximum in 1982 (252 $\mu g/m^3$). First, a standard normal homogeneity test (SNHT) of the form of Alexandersson and Moberg (1997) is performed to check for change-points in the ozone record. A critical value of the SNHT statistic T of 14.94 is used on the 99% significance interval, as suggested by Khaliq and Ouarda (2007) for a sample size of 7500 elements. According to this analysis, a change point is detected in 1984 and 1990. Furthermore, the Mann-Kendall test is used to see whether there are significant trends over the whole observation period 1981-2000 and the sub-period 1991-2000. Figure 6.1 shows there is a significant (on the 99% level) linear decrease of –12.76 $\mu g/m^3$ in maximum eight-hourly mean ozone concentration over the whole period. Similar, Beck et al. (1996) found a significant decrease in ozone concentration (on the 95% level) in Cabauw over the period 1980-1992. When only the

second half of the observation period (1991-2000) is considered, there is no significant trend in the observations (P>0.01). According to Roemer (2001), the significant negative trends over the period 1981-2000 do not match with observed trends of maximum eight-hourly mean ozone concentration in the neighboring monitoring stations of for e.g. Germany and Belgium. This artificial trend is probably due to a change in ozone monitors in the beginning of 1990 from a Philips PW 9771 based on the chemiluminescent reaction of ozone and rhodamine B to a Thermo Environmental Instrument (TEI) model 49W based on UV absorption at 254 nm (Uiterwijk et al., 1990). Furthermore, a change in on site calibration instrument, calibration method and practice occurred in the same time span. Therefore, in order to encompass this inconsistency in the dataset, we opt to work with a present-day 1991-2000 reference period.

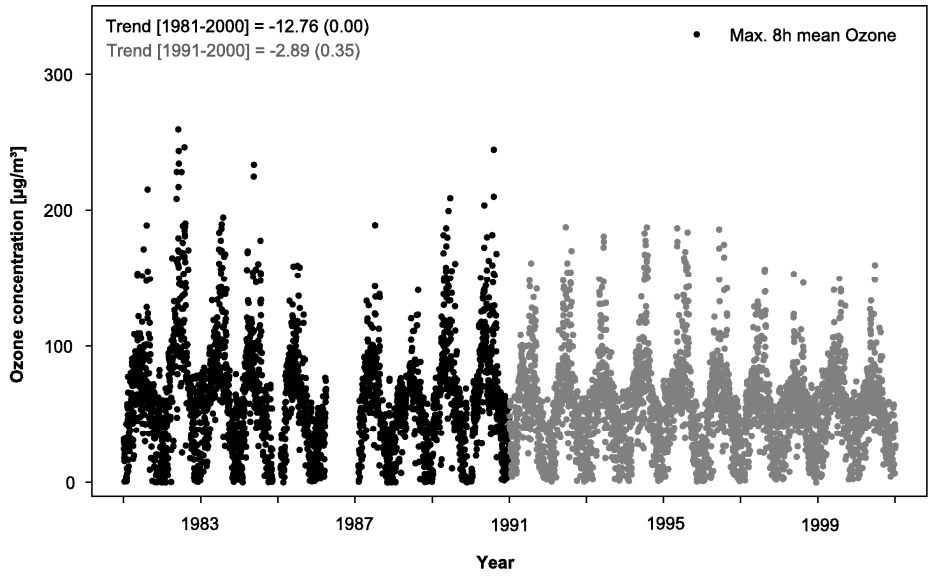

Figure 6.1: Observed maximum 8-hourly mean O_3 concentration for Cabauw for the period 1981-2000. The linear trend value (Mann-Kendall P-value) is given for the periods 1981-2000 and 1991-2000.

6.2.2 Meteorological data

The AOGCM used in this study consists of the model versions ECHAM5 and MPI/OM for both the atmosphere and the ocean respectively, which are used in the framework of the 4th IPCC assessment report. In the atmosphere model ECHAM5, vorticity, divergence, temperature and the logarithm of surface pressure are represented by a truncated series of spherical harmonics (triangular truncation at T63), whereas the advection of water vapor, cloud liquid water and cloud ice is treated by a flux-form semi-Lagrangian scheme (Roeckner et al., 2003, 2006). The ocean model (MPI/OM; Marsland et al., 2003) has a nominal resolution of 1.5° and the poles of the curvilinear grid are shifted to land areas over Greenland and Antarctica. The vertical discretisation is on 40 z-levels, and

the bottom topography is resolved by means of partial grid cells. In the coupled model (Jungclaus et al., 2006), the ocean passes the sea surface temperature, sea ice concentration, sea ice thickness, snow depth on ice, and the ocean surface velocities to the atmosphere. The atmosphere runs with these boundary values for one coupling time step (one day) and accumulates the (non-adjusted) forcing fluxes.

In order to evaluate the synoptic-regression based downscaling tool as developed in Chapter 4, observed present-day (1991-2000) maximum eight-hourly mean ozone levels are reconstructed based on present-day meteorology from the ECHAM5 SRES 20C control run with greenhouse gasses increasing as observed through the 20th century. The meteorological variables include 2 meter air and dew point temperature (T and Td), daily maximum and minimum temperature (Tmax and Tmin), wind speed and direction (F010 and D010), total cloud cover (TCC), total precipitation (Tprec) and shortwave downward radiation (SDW) four times daily (0, 6, 12, 18 hour UTC) at a T63L31 resolution for four neighboring grid points (3.75 - 5.62 °E, 51.29 - 53.15 °N) around the Cabauw measurement station (cf. Demuzere et al. 2008b). Except the minimum and maximum daily temperature, all variables are averaged to daily mean values whereby the relative humidity (RH) is calculated from T and Td using the Magnus-Tetens approximation. The ECHAM5 12UTC sea level pressure data (SLP) used to derive the objective Lamb circulation patterns as described in section 3 is selected on the larger European-Atlantic Region (27.5°W - 27.5°E, 15°N - 85°N) on a T63L31 resolution and re-gridded by conservative remapping to a 2.5° by 2.5° regular lat/lon grid, which can directly be used in the circulation type scheme.

The available future simulations from ECHAM5 in the framework of the 4th IPCC assessment report include the SRES scenarios A1B, B1 and A2 between the years 2001 and 2100 (Roeckner et al., 2006), for which all meteorological fields are available at a 6-hourly resolution. The three SRES scenarios describe the relationships between the forces driving greenhouse gas and aerosol emissions and their evolution in the future, whereby each scenario represents different social, demographical, economic, technological and environmental developments. A more detailed description of the scenarios is given in Nakicenovic et al. (2000), while the effect of the scenarios on surface meteorological variables is presented in Chapter 10 of the 4th IPCC assessment report (Meehl et al., 2007).

Unfortunately, measurements of the predictor variables are not available from the Cabauw measurement site for the period 1991-2000. However, in order to evaluate the downscaled ECHAM5 maximum eight-hourly mean ozone concentration time series for the present-day climate, the ECMWF - ERA40

reanalysis data (hereafter referred to as ERA40) (Uppala et al., 2005) can be used as a reference dataset, although it has to be taken into account that this dataset also has uncertainties in its surface meteorological variables (e.g. Chapter 4). The ERA40 SLP is selected for the same European Atlantic region on a 2.5°x2.5° grid using the 12 UTC time step. Similar, all meteorological variables are obtained from ERA40 for the period 1991-2000 on a 6 hourly resolution, for 4 neighboring grid points on a 1x1° resolution (4-5°E, 51-52°N). All variables are reduced to their daily means, except for the daily maximum and minimum temperature. To study the effect of the horizontal resolution, ECMWF - ERA40 reanalysis data is also extracted from the original ERA40 N80 reduced Gaussian resolution for the single nearest neighboring grid point to the Cabauw measurement station (hereafter referred to as ERA40-1).

6.3 Methods

The synoptic-regression tool applies a circulation pattern classification prior to the multiple regression analysis in order to introduce a non-linearity, thus meaning a stratification of the data in terms of a set of circulation patterns. The classification is based on the automated Lamb Weather Type classifications adapted from Jenkinson and Collison (1977) and Jones et al. (1993) to the Low Countries. The circulation patterns are developed using gridded SLP data and for a given day they describe the location of the high and low-pressure centers that determine the direction of the geostrophic flow. A grid with 16 points is assigned over the larger Western and Central Europe, with a central point over the Benelux, in 52.5 °N and 5 °E (Cabauw) (Fig. 6.2). Indices referring to the direction of vorticity and geostrophic flow are calculated daily from the sea level pressure values at 12UTC in these 16 grid points: southerly flow (SF), westerly flow (WF), total flow (F), southerly shear vorticity (ZS), westerly shear vorticity (ZW) and total shear vorticity (Z). A small number of empirical rules devised previously (Jones et al., 1993; Trigo and DaCamara., 2000) are then used to classify each day as one of the 27 circulation types. Afterwards, all daily types are clustered according to their preferential geostrophic wind direction, as was done in Chapter 5 (Demuzere et al., 2008a).

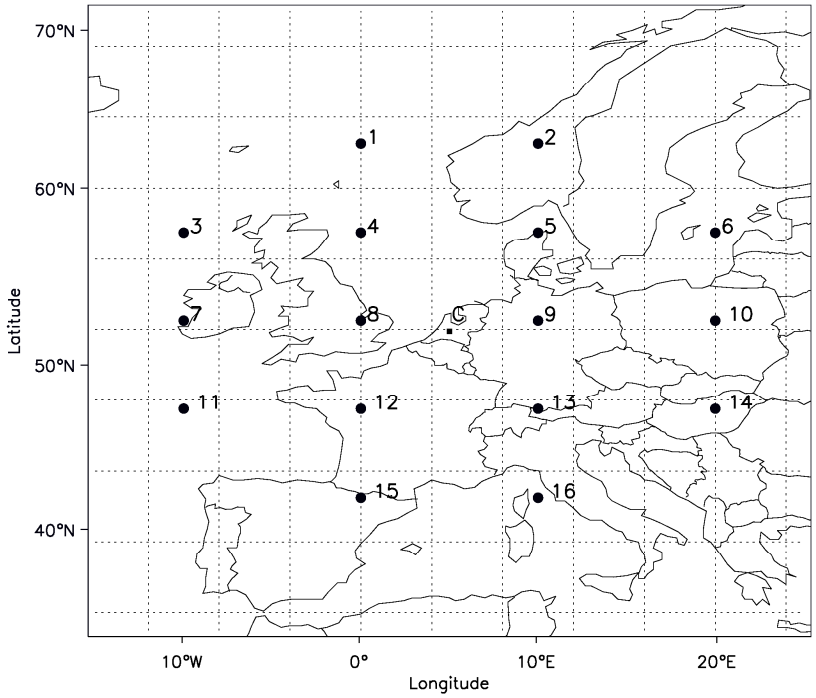

Figure 6.2: Location of the 5° x 10° SLP grid used, with 16 point centered over the Benelux. "C" denotes the location of the Cabauw measurement station and the grid center.

The analysis in Chapter 4 reveals that a stratification of the dataset using the automated Lamb weather type scheme, prior to a multiple linear regression analysis improves the downscaling results for maximum eight-hourly mean ozone concentration in terms of explained variances and skill score against the persistence model (1 day lag). Thereby, the observed non-linear characteristics (e.g., skewness and kurtosis) of the observed maximum eight-hourly mean ozone concentration distributions are well reproduced. After the classification, all members of each circulation-type class are ascribed to a linear regression equation, this for each season separately. Table 6.1 enlists for each season the frequency of occurrence of all predictor variables in the set of linear equations. Over all seasons, shortwave downward radiation (SWD), relative humidity (RH) and maximum temperature (Tmax) are the most frequently occurring predictor variables, with the largest individual frequency for the latter in JJA (72.7%). In winter, wind speed (F010) is equally important as Tmax in summer, while in the transition seasons MAM and SON, the relative frequencies of occurrence are similar for each predictor variable.

Table 6.1: The number of predictor occurrences in the synoptic-regression approach over all circulation types and for each season (DJF – winter, MAM – spring, JJA – summer, SON – autumn).

	DJF	MAM	JJA	SON
Sea Level Pressure (P0)	7	1	2	1
Total Precipitation (Tprec)	2	1	3	2
Shortwave Downward Radiation (SWD)	7	7	6	4
Maximum Temperature (Tmax)	3	3	8	4
Minimum Temperature (Tmin)	1	1	0	2
Relative Humidity (RH)	3	6	6	6
10m Wind Speed (F010)	8	3	2	3
Wind Direction (D010)	5	1	4	4
Total Cloud Cover (TCC)	4	2	2	2

The linear relationships between the three most important JJA predictor variables and observed maximum eight-hourly mean ozone concentration within each circulation-type class are shown in Figure 6.3. The predictor variables are grouped for the E (east), SE (southeast) and S (southern) circulation patterns (characteristic for high maximum eight-hourly mean ozone concentrations) and only shown for JJA as an example. The maximum temperature has the strongest linear relation with maximum eight-hourly mean ozone concentrations (R^2=0.68), followed by a negative correlation for relative humidity (R^2=0.49). In the synoptic-regression approach, RH is negatively correlated to ozone formation (Chapter 4 - Demuzere et al., 2008c). From a chemical point-of-view, this relation is not straightforward. A decrease of RH together with an increase of the photolysis rate, due to a decrease in cloud cover (Meleux et al., 2007), could lead to a lower production of OH radicals. Thereby OH does not just oxidize VOCs (volatile organic compounds) but also allows the conversion of NO to NO_2. This cycle suggests a decrease of ozone formation with a decrease of OH, while on the other hand, the O_3 removal by the process of NO_x titration will decrease (Sillman, 1999). OH radicals also react with NO_2 leading to HNO_3, a sink for the ozone production. These features cannot be explained using a statistical downscaling tool, but should be further investigated with state-of-the-art chemical transport models. Furthermore, an increase in shortwave radiation positively influences the photochemical production of ozone with a positive linear correlation of R^2 = 0.34 (Fig. 6.3). For more details on the calibration and evaluation of this synoptic-regression downscaling approach, the reader is referred to Chapters 3 and 4 of this dissertation.

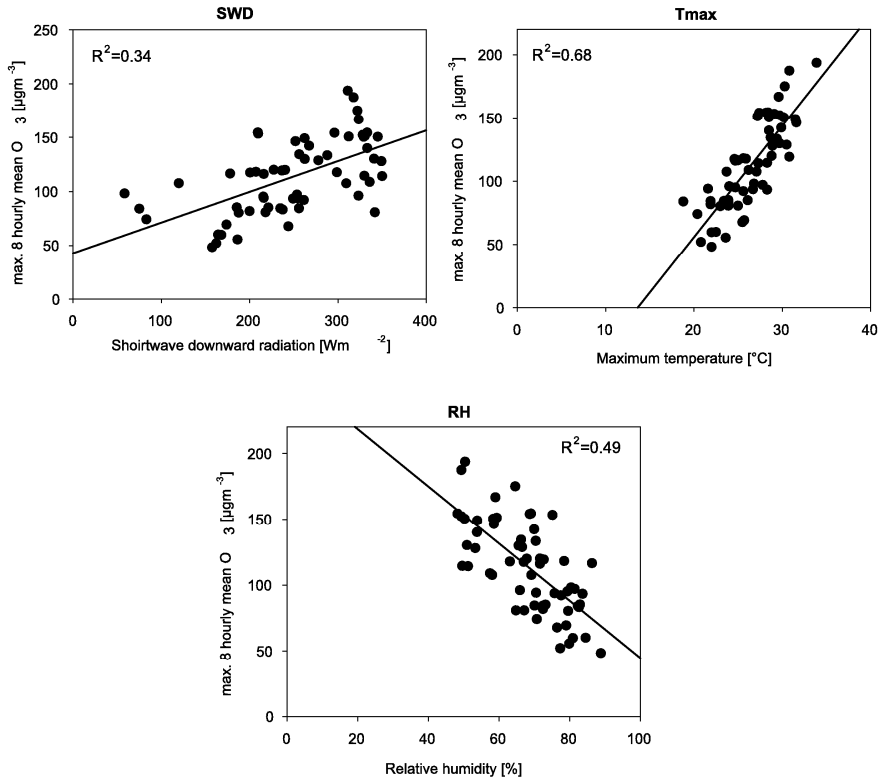

Figure 6.3: Linear relationship between daily observed shortwave downward radiation (SWD), maximum temperature (Tmax), relative humidity (RH) and observed maximum eight-hourly mean ozone concentrations, with measurement taken from the period 2001-2006 (Chapter 4 – Demuzere et al., 2008c). The circulation patterns E, SE and S are grouped together and are shown for JJA only.

In first instance, the synoptic-regression based downscaling tool is used to downscale maximum eight-hourly mean ozone concentrations for present-day conditions based on daily mean ECHAM5 meteorological data. Afterwards, the same approach is followed to downscale future levels of maximum eight-hourly mean ozone concentrations based on the ECHAM5 SRES A2, A1B and B1 scenarios for two selected future periods 2051-2060 and 2091-2100. Thereby, the relationships derived from the present period 2001-2006 (Chapter 4) are assumed to remain constant in the future and future changes in biogenic and anthropogenic (precursor) emissions are not taken into account.

6.4 Results

In this section, results of the statistical downscaling of present-day and future AOGCM data in terms of maximum eight-hourly mean ozone concentrations is discussed. As the circulation patterns are an important factor in the statistical downscaling approach (Chapter 5 - Demuzere et al. 2008a), present-day circulation patterns derived from ECHAM5 SLP are evaluated with the

circulation patterns derived from ERA40 SLP fields (section 6.4.1). Secondly, the synoptic-regression based statistical downscaling tool is applied on the present-day meteorological variables from ECHAM5 and compared to the observed maximum eight-hourly mean ozone concentration time series at the Cabauw monitoring station for the period 1991-2000 (section 6.4.2). Finally, a set future maximum eight-hourly mean ozone concentration estimates are done based on ECHAM5 future A2, A1B and B1 scenarios for the periods 2051-2060 and 2091-2100 (section 6.4.3).

6.4.1 Objective Lamb circulation patterns (1991-2000)

First, the objective Lamb circulation patterns (Jones et al., 1993, Trigo and Dacamara, 2001, Demuzere et al., 2008a) are derived for both ERA40 and ECHAM5 sea level pressure fields for the period 1991-2000 (Fig. 6.4). The spatial agreement of the circulation patterns derived from ERA40 and ECHAM5 is good, with a similar location of the high and low-pressure systems for each circulation type.

Nevertheless, there are some differences in the strength of the pressure systems, which also returns in differences in frequencies of occurrence for some circulation patterns (Fig. 6.5). To assess whether these differences are significant over all types per month and for each type over the whole year, the χ^2 test is applied using a 0.1 significance level (Chernoff and Lehmann, 1954). If the goodness-of-fit is low (with $P < 0.1$), the hypothesis that the given modelled frequencies are an accurate approximation to the observed frequency distribution has to be rejected. The difference in overall frequency distribution of the ECHAM5 circulation types per month is insignificantly different compared to the ERA40 observed frequency distribution, except for February ($P = 0.09$). This can be seen in Figure 6.5, with a highest number of misclassified days by ECHAM5 ($\approx$ 10 days). The frequency distribution per type over the whole year only shows a significant difference in the Western circulation pattern ($P = 0.04$) between the modelled (ECHAM5) frequencies and the observed (ERA40) frequencies. Thereby, this bias in westerlies is positive (negative) in the months July, August, September (January, February, March and December) (Fig. 6.5). This result is in contrast with the findings in Chapter 6 of this dissertation, which has shown that there are significant differences between ECHAM5 and ECMWF circulation patterns for the months April to September for the period 1961-2000. This discrepancy is further elaborated in Appendix B.

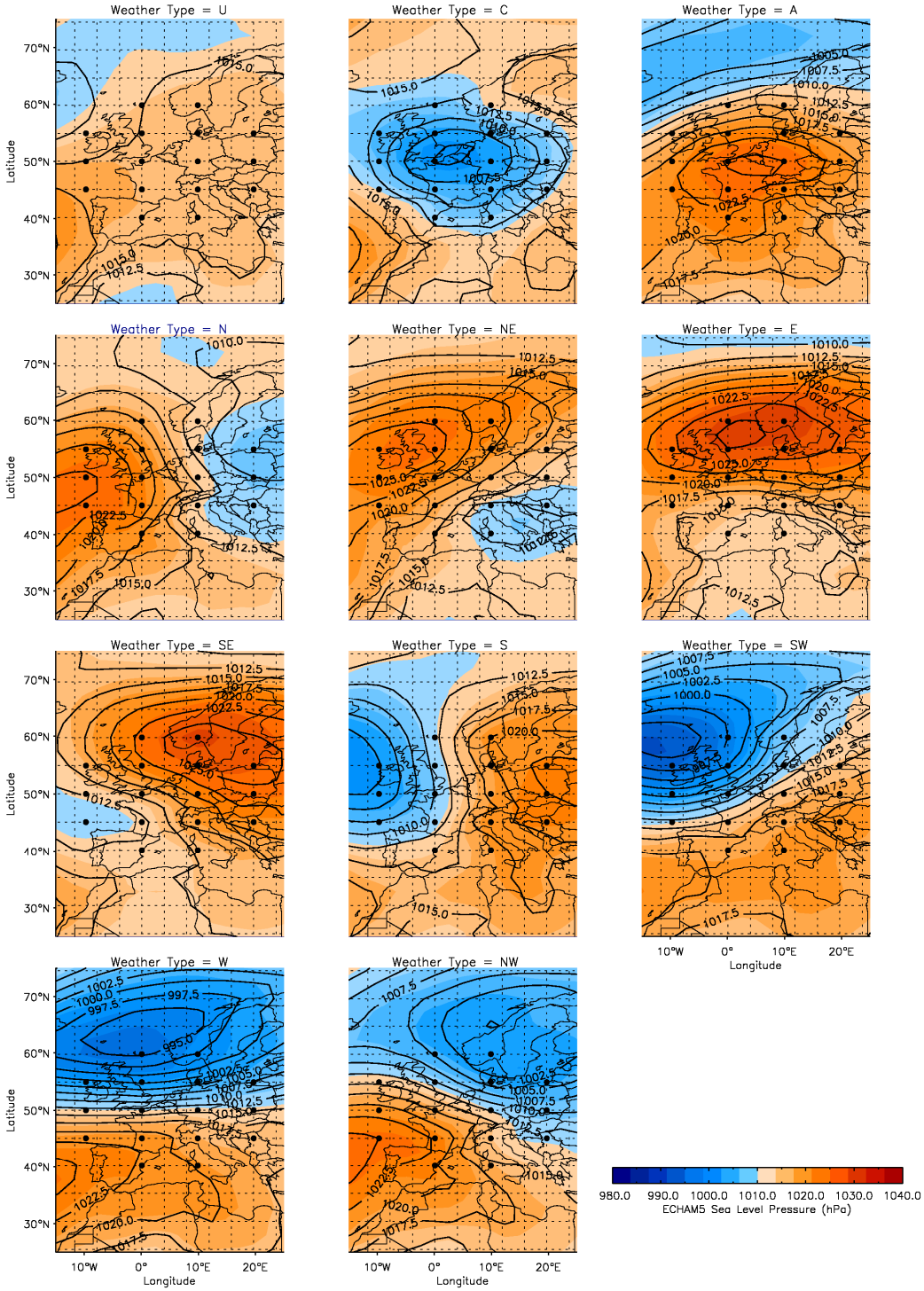

Figure 6.4: Composite maps for the circulation patterns derived from ERA40 SLP (black lines) and ECHAM5 20C control run (shaded colors) for the period 1991-2000.

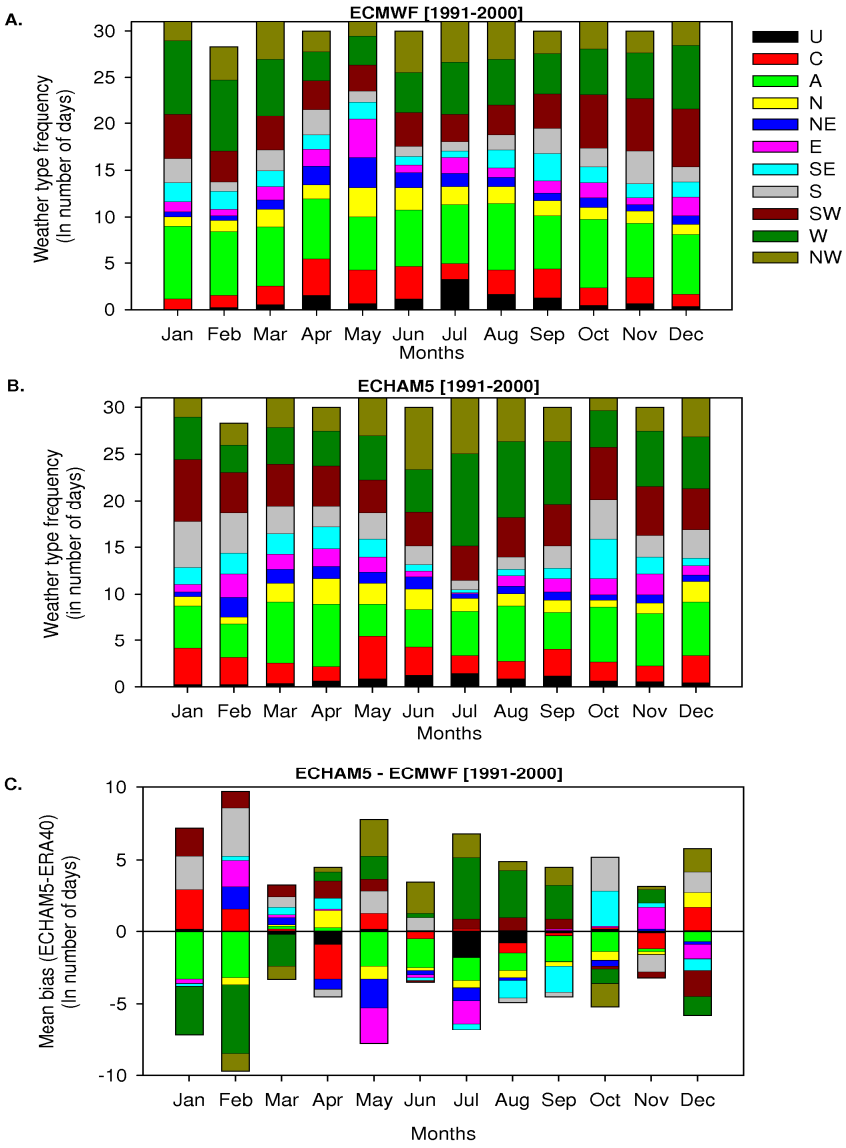

Figure 6.5: Bar chart showing the frequencies (in mean number of days per month) for each circulation pattern for ECMWF (a), ECHAM5 (b) and the ECHAM5-ECMWF difference (c) for the period 1991-2000.

As the circulation patterns dominating high ozone concentrations (in summer) are controlled by east to south directions (Chapter 4), this significant bias in westerlies has only a minor impact on the results of this downscaling approach.

6.4.2 Downscaled O_3 for the present-day climate (1991-2000)

In Chapter 4 of this dissertation, the synoptic-regression based statistical downscaling method is thoroughly tested using both observed and coarse resolution ECMWF operational data. Thereby, the model was shown to have an acceptable skill in terms of explained variance, RMSE and skill score against persistence using the coarse resolution ECMWF data, although the higher percentiles were underestimated in comparison to the use of single grid-point

higher-resolution ECMWF predictor variables. The unexplained part of the variance is due to a combination of the intrinsic limitation of a regression method to capture the higher percentiles (Wilby et al., 2004), the scale-dependency of the predictor variables and ECMWF model deficiencies. In Figure 6.6, these error trends are confirmed for the period 1991-2000 using both the coarse resolution ERA40 and ERA40-1 predictor variables. The explained variances for both datasets are respectively 60 and 61%, similar to the explained variance obtained using the 2005-2006 validation period (63%) in Chapter 4 of this research. In contrast to the explained variance, larger differences can be found in the higher percentiles of the downscaled maximum eight-hourly mean ozone concentration distribution (see Fig. 4.11 in Chapter 4). This can be seen from the number of days with a concentration higher than or equal to the 120 $\mu g/m^3$ set by the European Union as a guidelines on Air Quality for human health protection (EU, 1999, 2008); 62 and 79 days respectively compared to an observed 141 days over the whole period.

This effect of underestimating the higher maximum eight-hourly mean ozone concentration percentiles is enhanced using ECHAM5 meteorological variables as predictors for the present-day period of 1991-2000 (Fig. 6.6). Although the overall mean from the prediction model using ECHAM5 1991-2000 predictor data is similar compared to the observations (54.6 vs 55.2 $\mu g/m^2$), the standard deviation is significant smaller (of 24.0 vs. 31.6 $\mu g/m^2$). This difference is due to an overestimation of the lower maximum eight-hourly mean ozone concentration percentiles in the ECHAM5 model, which in general have a higher frequency of occurrence compared to the higher percentiles. In contrast, the higher percentiles are largely underestimated, which can be seen from, for example, the number of days that are exceeding the 120 $\mu g/m^3$ threshold (21 days).

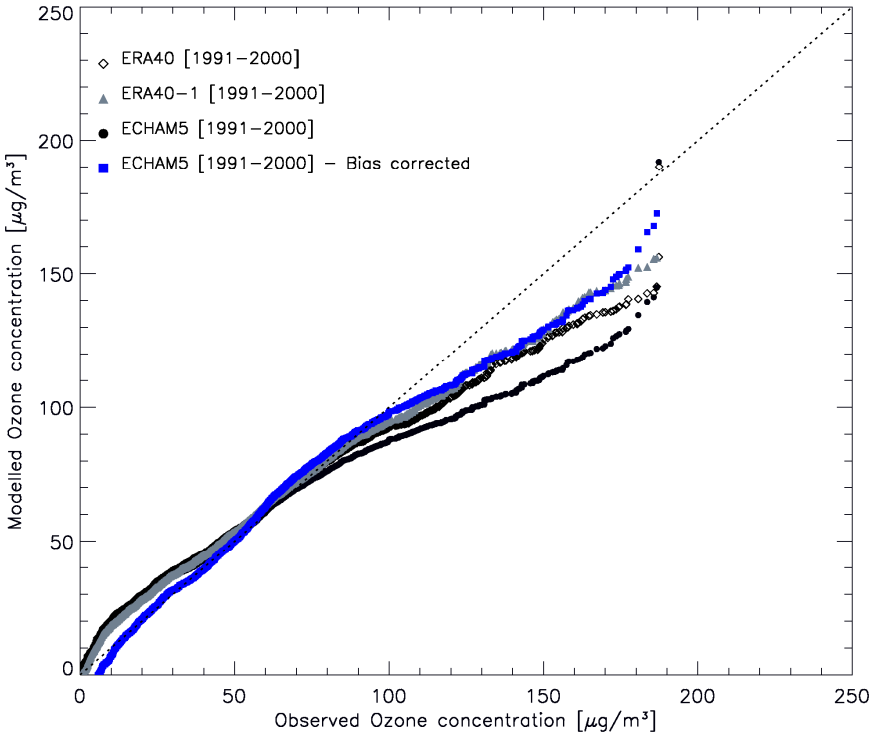

Figure 6.6: Quantile-quantile plot showing observed versus downscaled maximum eight-hourly mean ozone concentration concentrations using ERA40 (diamonds), ERA40 - 1 (gray triangles) and ECHAM5 (black circles) predictor data for the period 1991-2000. The bias-corrected ECHAM5 downscaled O_3 concentrations are shown in blue squares.

Section 6.4.1 has shown that there are no significant differences between modelled and observed Lamb circulation patterns for the period 1991-2000, except for February. As this month is characterized by a relatively low concentration of maximum eight-hourly mean ozone (Fig. 6.7), this difference in circulation pattern frequencies cannot explain the large underestimation of the higher O_3 percentiles by ECHAM5. Consequently, the reason for the difference in observed and downscaled maximum eight-hourly mean ozone concentration must lie in the representation of the meteorological variables that are used in the statistical downscaling process (Table 6.2). Hence, ECHAM5 summer (JJA) predictor values are compared with the ERA40-1 JJA predictors. This is done for the patterns E, SE and S only, as they are associated with the highest concentrations in summer.

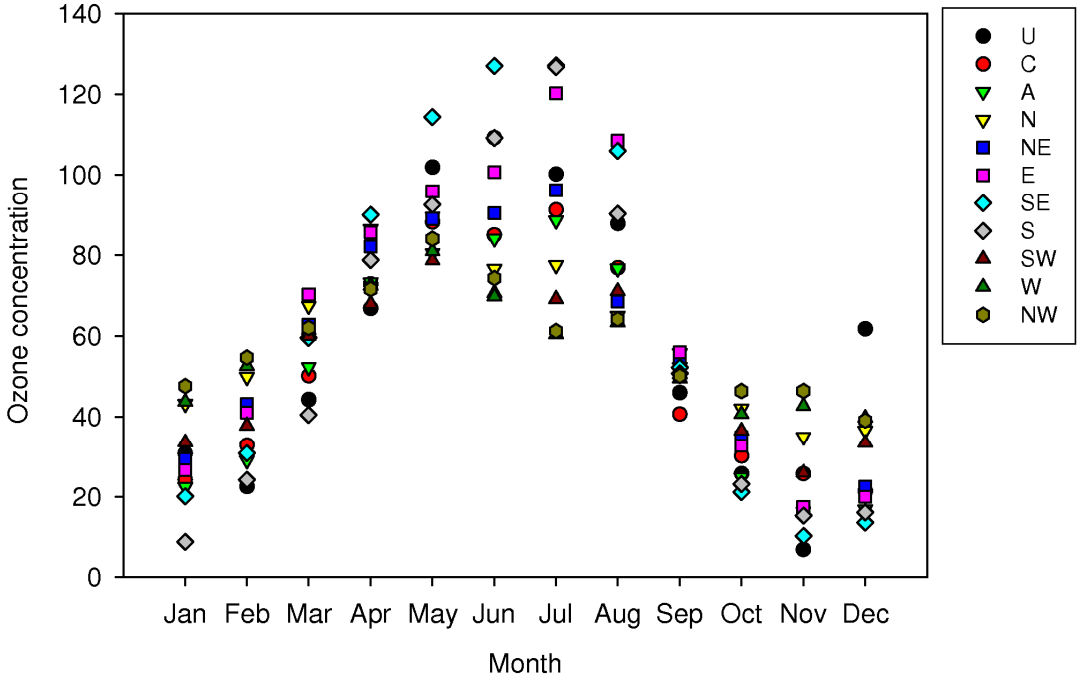

Figure 6.7: Mean ozone concentration for each month and specific circulation pattern separately, averaged over the period 1991-2000.

Table 6.2: ECHAM5 – ERA40-1 differences in predictor variables statistics used in the synoptic-regression downscaling approach the 1991-2000 summers, for the circulation types E, SE and S only. Values are shown for the minimum (Min.), 5th and 95th percentile and maximum (Max.).

	E		SE		S			
	SWD	CC	Tprec	Tmax	P0	Tmax	RH	CC
Min.	-44.24	-0.04	0	-0.81	-5.52	0.72	16.47	-0.22
5th percentile	-48.28	-0.08	0	-1.5	-2.15	-2.6	13.69	-0.31
95th percentile	-8.92	0.4	0.05	-3.87	0.08	-1.99	8.74	0.04
Max.	-10.87	0	0.05	-3.87	2.2	-1.34	14.75	0.05

For the eastern circulation patterns, ECHAM5 (under) overestimates the mean amount of cloud cover in the (lower) higher percentiles, associated with an overall underestimation of the shortwave radiation in ECHAM5. This results in a reduced ozone formation for this pattern, as CC (SWD) reduces (stimulates) the photochemical ozone production. The southeastern pattern SE is associated with a small overestimation in the precipitation distribution statistics and too low maximum temperatures in ECHAM5 compared to the observed ERA40-1 values, especially in the 95th percentile (-3.87 °C) and maximum (-3.87 °C). Again, both features contribute to an underestimation of downscaled maximum eight-hourly mean ozone. Also for the southern pattern, ECHAM5 is characterized by lower Tmax and a general overestimation of P0, RH and CC in

the higher percentiles (Table 6.2). As the latter are negatively correlated to maximum eight-hourly mean ozone concentrations, the net effect of the biases in meteorological variables dampens the production of maximum eight-hourly mean ozone. Together with the effect of the horizontal resolution (Fig. 6.6), we can conclude that a large part of the differences between observed and downscaled ECHAM5 maximum eight-hourly mean ozone concentrations are resulting from the differences between ECHAM5 and ERA40-1 predictor values.

The differences between observed and modelled present-day maximum eight-hourly mean ozone concentrations should be addressed, in order to estimate future maximum eight-hourly mean ozone levels. Therefore, we perform a bias correction method proposed by Cheng et al., (2007) which takes into account the differences between the ECHAM5 downscaled and observed maximum eight-hourly mean ozone concentrations. In a first step (1), this is done for the present-day climate, and afterwards, the same bias correction is applied to future air pollution concentrations (2) described in section 6.4.3. By doing so, we assume that the model bias in a future climate is the same as in the present-day climate. The first step in this bias correction procedure uses the following expression:

$$(1) \qquad O_{3\,pres-new} = (O_{3\,pres-old} - \bar{O}_{3\,pres-old}) \frac{\sigma_{pres-Obs}}{\sigma_{pres-old}} + \bar{O}_{3\,Obs}$$

where $O_{3\,pres-old}$ and $O_{3\,pres-new}$ are daily model predictions using present-day ECHAM5 data before and after the bias correction. $\sigma_{pres-Obs}$ and $\sigma_{pres-old}$ are standard deviations of the observations and model predictions for the present-day run respectively. $\bar{O}_{3\,pres-old}$ and $\bar{O}_{3\,Obs}$ are respectively the means of the present-day downscaled and observed O_3 time series. In this way, the mean and standard deviation of $O_{3\,pres-new}$ is identical to the observed time series.

In order to know whether the model bias is spread randomly over different circulation patterns or if the maximum eight-hourly mean ozone bias is circulation type-specific, the significance test suggested by Räisänen et al. (2001) is used which tests the significance of the circulation-type dependent bias in maximum eight-hourly mean ozone concentration (modelled versus observed) against the type-specific internal variability. The estimate of the statistical significance is inferred from the t-statistics:

$$(2) \qquad t_i = \frac{M_i - O_i}{\sqrt{(\sigma^2{}_{Mi} + \sigma^2{}_{Oi})/(n_i - 1)}}$$

Hereby, M_i and O_i denote the means of the modelled and observed maximum eight-hourly mean ozone concentration respectively, for each circulation pattern *i*. σ^2_{Mi} and σ^2_{Oi} refer to the internal variances for both modelled and observed time series, and *n* refers to the number of days in each circulation cluster *i*.

In general, there is an inhomogeneous distribution of the bias over the different circulation patterns (Table 6.3). All patterns have a positive type-specific bias $M_i - O_i$, except for the cyclonic, east and southeastern patterns. Nevertheless, all t-values are low, which indicates that the type-specific bias is insignificant compared to the type-specific internal maximum eight-hourly mean ozone variability. Hereby, a high bias is often associated with a high internal variability (e.g. types E and SE). Therefore, the bias correction method (1) is applied for the whole year, without taking into account the type-specific biases.

Table 6.3: Modelled minus observed maximum eight-hourly mean ozone biases for the period 1991-2000 for each circulation pattern and its significance against the pattern-dependent internal variability. M-O refers to the bias between modelled (M) and observed (O) maximum eight-hourly mean ozone concentrations, $\sigma^2_M - \sigma^2_O$ to the difference in modelled and observed variance, n the number of days in each circulation pattern cluster and t the t-statistic from the Räisänen et al. (2001) significance test.

	C	A	N	NE	E	SE	S	SW	W	NW
M - O	-3.54	3.14	8.11	4.22	-28.40	-12.79	9.83	3.86	0.71	6.86
$\sigma^2_M - \sigma^2_O$	2598.04	3557.10	1555.01	3669.46	4314.43	7132.35	4495.38	2077.56	1090.15	870.47
n	232.00	745.00	262.00	220.00	217.00	164.00	241.00	423.00	454.00	310.00
t	0.00	0.00	0.01	0.00	-0.03	-0.01	0.01	0.00	0.00	0.01

Applying the bias correction results in a significant improvement, especially for the higher percentiles (Fig. 6.6). This can be seen again from the number of days that are higher than or equal to the 120 µg/m³ threshold: from 21 days decade^{-1} in the original present-day downscaled maximum eight-hourly mean ozone concentration time series to 79 days decade^{-1} for the bias corrected maximum eight-hourly mean ozone levels, identical to using the ERA40-1 predictor variables. Moreover, the bias corrected ECHAM5 maximum eight-hourly mean ozone series is closer to the perfect model line (1:1 line) in the lower and higher percentiles (Fig. 6.6).

6.4.3 Future O_3 levels (2051-2060 and 2091-2100)

Daily maximum eight-hourly mean ozone concentrations for two future periods – 2051-2060 and 2091-2100 – are estimated using the statistical synoptic-regression based approach with the future SRES A2, A1B and B1 scenarios and associated future circulation patterns. According to the removal of the bias in

the first step (1), the differences in overall means ($\bar{O}_3$) and standard deviations (σ) between the after (*pres-new*) and before (*pres-old*) correction of the present-day downscaled maximum eight-hourly mean ozone are used to adjust future maximum eight-hourly mean ozone concentrations ($O_{3\,fut-old}$) in a second step (3) using the following equation:

$$(3) \qquad O_{3\,fut-new} = (O_{3\,fut-old} - \bar{O}_{3\,pres-old}) \frac{\sigma_{pres-new}}{\sigma_{pres-old}} + \bar{O}_{3\,pres-new}.$$

Hereby, $O_{3\,fut-new}$ present future daily model prediction after the bias correction, assuming that the model bias in the future will be similar the bias in the present-day climate. This results in a downscaled bias-corrected ozone concentration for the three SRES climate change scenarios for the periods 2051-2060 and 2091-2100 (Fig. 6.8).

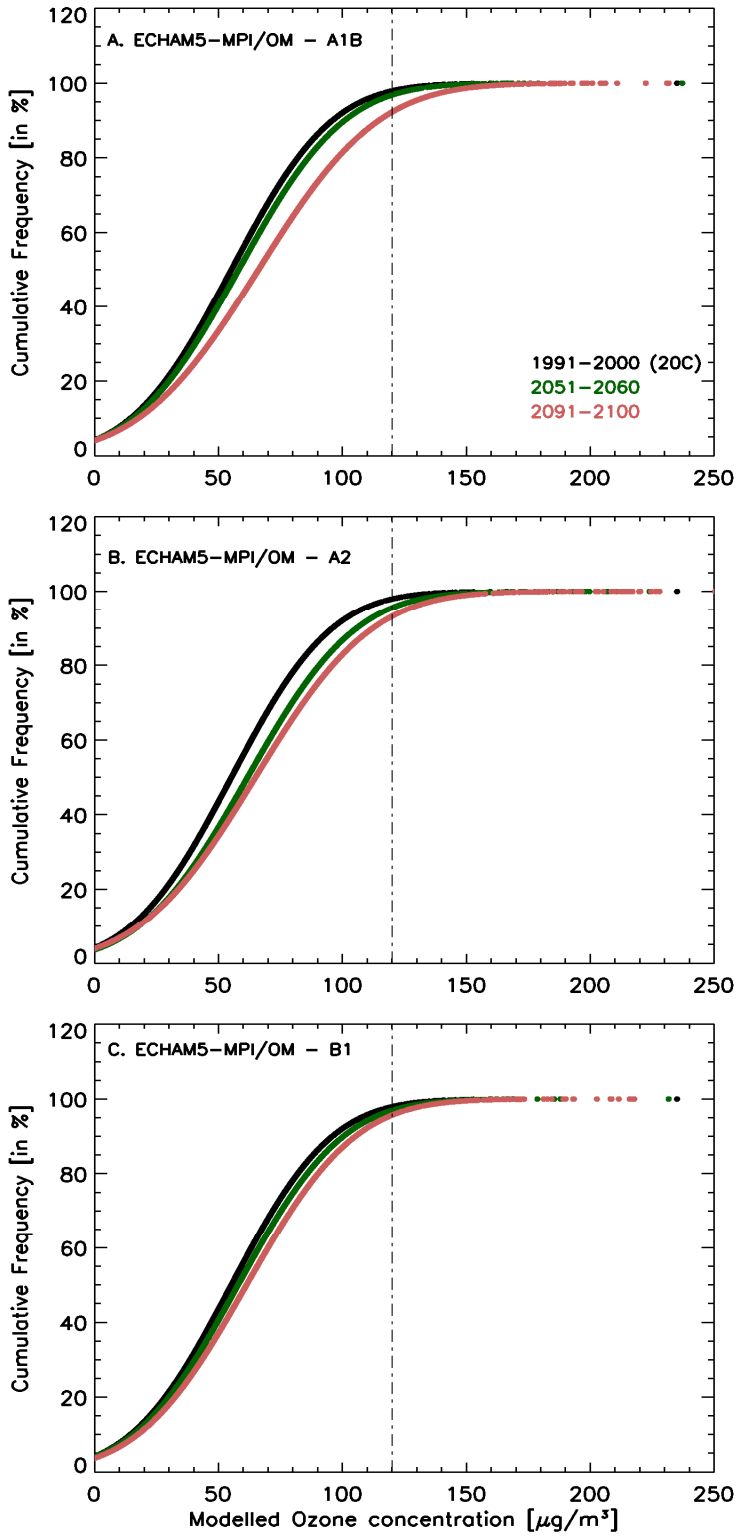

Figure 6.8: Cumulative probability functions (CDF) for the present-day 20th century control run (black) and future (2051-2060: green, 2091-2100: red) bias-corrected downscaled maximum eight-hourly mean ozone concentrations, for the scenarios A1B (plot A.), A2 (plot B.) and B1 (plot C.).

Under the various SRES scenarios, the overall maximum eight-hourly mean ozone concentration increases with 2.5 to 6.5 and 6.1 to 10.9 µg/m³, for the

2051-2060 and 2091-2100 periods respectively, against the present-day 10-year average of 55.2 µg/m³. When considering the summer season only, the range of change over all scenarios increases with 5.4 to 12.5 µg/m³ and 13.4 to 26 µg/m³ (for 2051-2060 and 2091-2100 respectively) against a present-day summer average of 73.5 µg/m³.

In addition to changes in mean concentrations, changes in the number of days within low, moderate and high levels of ozone seen over a whole year are of interest to the public and policy makers (Table 6.4). Days with low air pollution are characterized by a concentration < 80 µg/m³, days with moderate air pollution have an maximum eight-hourly mean O_3 concentration between 80 and 120 µg/m³ and days with high concentrations exceed the threshold of 120 µg/m³. The application of different SRES scenarios has a variable impact on the number of days in each specific maximum eight-hourly mean O_3 concentration category. By the middle and end of this century, the number of days with high levels of O_3 could increase in a range of 5.6 – 12.3 % (4.3 – 9.5 days yr^{-1}) and 9.2 – 27.5 % (7.1 – 21.1 days yr^{-1}) respectively, with the highest increase against the 2050s for the A2 and by the end of this century for the A1B scenario. A similar effect can be seen for the days with a moderate maximum eight-hourly mean O_3 concentration, varying between 2.2 to 11.9 % (1.7 – 9.2 days yr^{-1}) and 11.7 to 19.2 % (9 – 14.8 days yr^{-1}) for the periods 2051-2060 and 2091-2100 respectively. This is counteracted by a strong decrease in the number of days with low concentrations (8.1 – 24.3% and 20.9 – 46.8 % of the days by the 2050s and 2090s respectively). Similar to the results in Figure 6.8, Figure 6.9 again depicts the large scatter when applying the different SRES scenarios. Here, the absolute number of days exceeding the 120 µg/m³ threshold in the present-day climate are given, together with the change in number of days exceeding this threshold by the middle and end of this century. The error bars present the lowest/highest change over the three scenarios, while the average change is calculated as the mean change over the three scenarios. Thus, on average, there is an increase of 2.2, 4.2 and 4.0 days $month^{-1}$ exceeding this threshold for June, July and August 2051-2060 respectively. By the end of this century, the overall effect increases, with 3.2, 6.3 and 8.5 days $month^{-1}$ for June, July and August respectively. The error bars present a large uncertainty depending on the future scenario, with a maximum variability of 4 days $month^{-1}$ by the 2050s almost 7 days $month^{-1}$ by the end of the century.

Table 6.4: Differences in absolute number of days (and expressed in %) between future number of days and present-day number of days exceeding the thresholds for the high, moderate and low O_3 concentration categories. The difference is expressed as the difference between the two future periods from the three SRES A2, A1B and B1 scenarios and the observed number of days in 1991-2000. The scenario with the highest increase and decrease in O_3 concentration for each future period are denoted in italic.

Category [µg/m³]		No. Of days	A2				A1B				B1			
		(observed)	2051-2060		2091-2100		2051-2060		2091-2100		2051-2060		2091-2100	
			days	(%)	days	%	days	%	days	%	days	%	days	%
High	>=120	13.7	9.5	12.3	12.7	16.5	4.3	5.6	21.2	27.5	4.5	5.8	7.1	9.2
Moderate	80-120	39.8	9.2	11.9	12.2	15.8	4.7	6.1	14.8	19.2	1.7	2.2	9.0	11.7
Low	<80	266.3	-18.7	-24.3	-24.9	-32.3	-9.0	-11.7	-36.0	-46.8	-6.2	-8.1	-16.1	-20.9

Although peak ozone months are known to be June, July and August, Figure 6.9 shows that under future climate, a lengthening of the ozone season could occur. In the present-day climate, the highest number of exceedences occur in July (2.9 days month^{-1}), followed by June and August (1.4 and 1.5 days month^{-1}respectively). In the future climate scenarios, this could shift from July to August, the latter characterized by an increase between 6.5 and 14.2 days month^{-1} with high levels of maximum eight-hourly mean ozone concentration by the end of the century (Fig. 6.9). This change in distribution of days exceeding the 120 µg/m³ threshold is caused by a larger increase (decrease) in Tmax (RH) from August to October by the end of this century, in comparison to late spring and early summer (not shown). Moreover, as suggested by Chen et al. (2008) and Mahmud et al. (2008), the ozone season could be lengthened, especially in autumn. Thereby, September and October could be associated with an increase in number of days exceeding the 120 µg/m³ threshold, up to 1 day per month by the end of this century, compared to 0.4 and 0.11 days per month in the present-day climate.

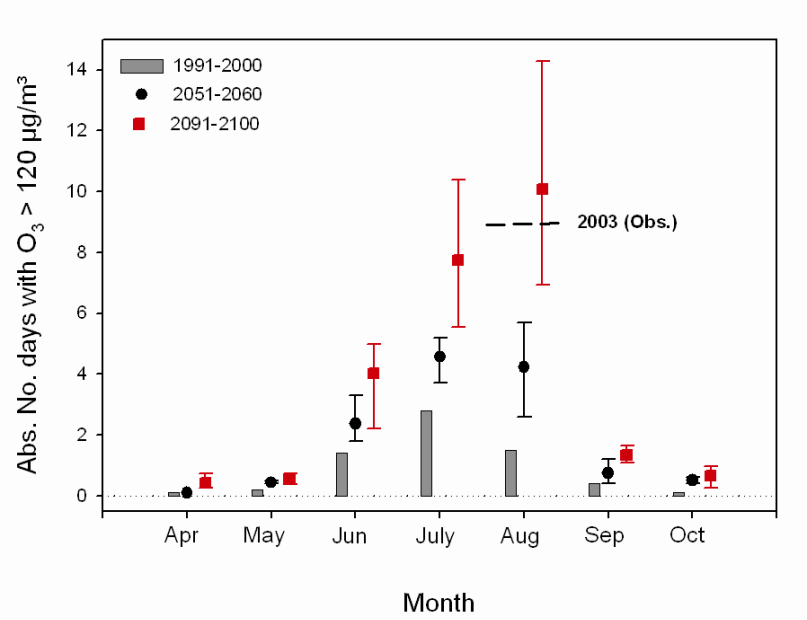

Figure 6.9: The number of days per month exceeding the 120 µg/m³ threshold for the present-day climate and future climate SRES scenarios, for the periods 2051-2060 and 2091-2100. The number of exceedences is denoted as absolute values per month. The short black dashed line indicates the number of observed exceedences in August 2003.

6.5 Discussion

As the synoptic-regression based approach does not take into account emissions as predictor values, the change in number of days with moderate and high downscaled maximum eight-hourly mean ozone concentrations between the future SRES scenarios and the present-day 20C climate run can be caused by two interrelated effects: 1) a change in frequency of those circulation patterns favoring high O_3 concentrations and 2) a change in meteorological predictor values regulating the production of ozone in the type-specific regression analysis (Table 6.1 and 6.5 and Fig. 6.10).

In order to test the sensitivity of future ozone levels to the change in frequency of occurrence of the future Lamb circulation patterns, the Mann-Kendall test is used to calculate the trends in JJA frequencies of E, SE and S circulation patterns for the period 2001-2100. As it is shown in Chapter 5 (Demuzere et al., 2008a), there is a large interannual variability between the three future SRES scenarios without a significant difference in their future trends and frequencies, we opt to test the A1B scenario only. This trend analysis shows an increase of the frequency of these patterns (0.96 number of days yr^{-1}), which is insignificant at the 90% level. As a result, this increase in circulation patterns characterised by high O_3 concentrations has an insignificant impact on the large estimated increases of maximum eight-hourly mean ozone concentrations.

As this trend analysis shows no significant change in the frequency of occurrence of these specific circulation patterns, the change in the individual meteorological variables between the different periods is investigated. Fig. 6.10 depicts the cumulative frequency distribution for the predictor variables that occur most frequently in summer (Table 6.1). Here, the SRES scenarios A1B and A2 show the highest increase in maximum temperature, with an averaged increase of 4.8°C in August by the end of this century (Fig. 6.10). Furthermore, all scenarios show a reduction of cloud cover, as described in Giorgi et al. (2004), Meleux et al. (2007) and Forkel & Knoche (2007), which is associated with an increase in future shortwave downward radiation (Langner et al., 2005; Meleux et al., 2007) (Fig. 6.10). The change in relative humidity is rather small, with generally a decreasing trend, strongest in August and by the end of this century.

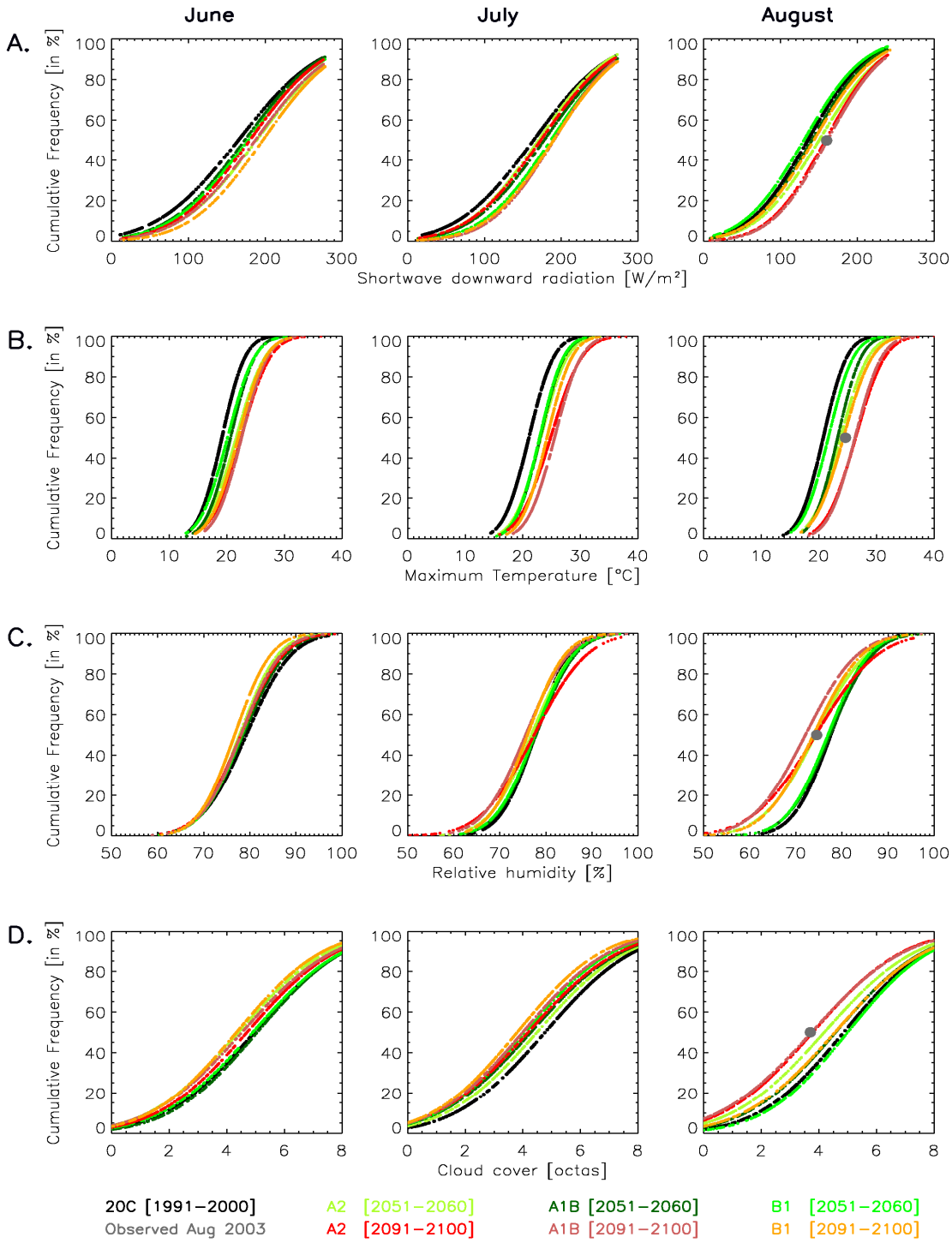

Figure 6.10: Cumulative probability density functions for ECHAM5 present-day (black) and future A1B scenario predictor variables (2051-2060: red – 2091-2100: blue). The rows present the meteorological variables: A. Shortwave downward radiation (W/m²), B. Maximum temperature (°C), C. Relative humidity (%) and D. Wind speed (m/s), while the columns present the summer months June, July and August. The mean conditions in August 2003 (from ECMWF operational data) are depicted by the filled grey square.

To estimate the individual contribution of each predictor variable, a sensitivity experiment is performed for all circulation patterns conducive for high maximum eight-hourly mean ozone concentrations in summer (Table 6.5). For

each predictor variable, the present-day median is replaced by its future value, while keeping the other predictor variables to their present-day levels. Thereby, the predictor variables are perturbed with the difference between future and present-day medians (for the E, SE and E patterns), averaged over the three scenarios, which provides a measure for the individual contribution of each predictor variable to the change in future maximum eight-hourly mean ozone concentration. In general, the maximum temperature has the largest contribution, with an ozone increase of 5.9 and 12.5 µg/m³ by the middle and end of this century respectively (respectively 48 and 44.1% of the change). The highest frequency of occurrence for this predictor in the regression model shown in Table 6.1 denotes the importance of this variable on maximum eight-hourly mean ozone concentrations in a future climate. Furthermore, the strong linear trend of Tmax depicted in Fig. 6.3 gives confidence in the robustness of the statistical downscaling tool, as a future climate tends to show a shift towards higher maximum temperatures (Beniston, 2004), which are linearly related to maximum eight-hourly mean ozone concentrations (under the assumption that present-day relations will be similar in the future). The contribution of the shortwave radiation decreases between the middle and end of this century with 12.5%, to an increase of 6.1 µg/m³ for the period 2091-2100. The decrease in cloud cover results in an average increase of 2.1 and 6.3 µg/m³, which accounts for respectively 17 and 22.5% of the total change. The mean sea level pressure P0, total precipitation and relative humidity only contribute marginally to the total change, with a maximum of 9.5 % for all this variables together by the end of this century.

Table 6.5: The individual influence of each predictor variable in the synoptic-regression based approach on the resulting downscaled maximum eight-hourly mean ozone concentration, averaged for the E, SE and S circulation patterns in summer. The percentage of maximum eight-hourly mean ozone changes between the A1B future climate periods and the downscaled maximum eight-hourly mean ozone concentration for the reference period are given in brackets.

	Predictors	O_3 concentrations			
	Mean (1990-2000)	2051-2060 – 1990-2000		2091-2100 – 1990-2000	
		µg/m³ (%)		µg/m³ (%)	
P0 [hPa]	1018.3	0.1	(1.1)	0.1	(0.3)
Tprec [mm/day]	0.007	0.1	(1.1)	1.8	(6.4)
SWD [W/m²]	200.6	4.1	(34.1)	6.1	(21.6)
Tmax [°C]	23.3	5.9	(48.7)	12.5	(44.1)
RH [%]	77.7	-0.1	(-0.9)	1.6	(5.6)
CC [octas]	3.5	2.1	(17.0)	6.3	(22.5)

In order to verify whether these findings are physically plausible, our results are compared with the observed heat wave in August 2003, characterized by a poor

air quality (especially in terms of O_3) and excess of mortalities in large parts of Western and Central Europe (WHO, 2005), In this respect, Beniston (2004), Schar et al. (2004) and Vautard et al. (2007) suggested the extremely warm summer of 2003 to be representative for the climate at the end of this century. Therefore, we analysed this in terms of measured August 2003 O_3 levels, and first compared the number of exceedences > 120 µg/m³ against present-day and future modelled exceedences (Fig. 6.9). Secondly, the mean of the distribution of the August 2003 observed meteorological variables favouring high ozone concentrations are displayed in Figure 6.10. During this 2003 August, 9 days exceeded the threshold of 120 µg/m³ in Cabauw, which lies in the upper range of the number of exceedences for the 2050s and corresponds closely to the mean number of exceedences by the end of this century (9.7 days month^{-1}). This is confirmed by the exceptional warm and dry weather during August 2003, which characteristics corresponds to ECHAM5 scenarios by the end of this century. For shortwave downward radiation and cloud cover, the August 2003 values correspond to the A2 and A1B scenarios, while for RH and Tmax, the observed values correspond more closely to the B1 scenario. This suggests, that, not only in terms of temperature, as was shown by Beniston (2004) and Schär et al. (2004), but also in terms of O_3, the August 2003 conditions could become representative for future conditions.

6.6. Conclusion

The synoptic-regression based downscaling approach developed in Chapter 4 of this study can be used to estimate future maximum eight-hourly mean ozone concentrations for areas in Western Europe. Explanatory meteorological predictor variables are taken from ECHAM5 for the present-day 1991-2000 period and 2 future periods 2051-2060 and 2091-2100 for the SRES A2, A1B and B1 scenarios. Hereby, any information on biogenic and anthropogenic emissions is not explicitly taken into account. Although the capabilities of the downscaling method were tested thoroughly in Chapter 4 using coarse resolution meteorological ECMWF variables, it appeared that results deteriorated when using ECHAM5 meteorological data. Therefore, it was necessary to apply a bias correction method that takes into account the differences between the ECHAM5 downscaled and observed maximum eight-hourly mean ozone distribution quantities.

In this study, the future estimates of maximum eight-hourly mean ozone concentrations are derived as a statistical downscaling product from only one AOCGM simulation (ECHAM5-MPI/OM), under three SRES scenarios. Nevertheless, the conditions used here are in line with those projected by most other global models (Giorgi and Bi, 2005a, b). It should, however, be noted that

by taking into account only one GCM, the range of uncertainty might be underestimated. Under the various SRES scenarios, the overall mean maximum eight-hourly mean ozone concentration increases by 2.5 to 6.5 and 6.1 to 10.9 µg/m³, for the 2051-2060 and 2091-2100 period respectively, against the present-day 10-year average of 55.2 µg/m³. When considering the summer season only, the impact of climate change increases considerably, with a range between the different future scenarios of 5.4 to 12.5 µg/m³ and 13.4 to 26 µg/m³ (for 2051-2060 and 2091-2100 respectively) against a present-day summer average of 73.5 µg/m³. In terms of number of days exceeding the threshold set by the European Guidelines on Air Quality, the number of days with high levels of maximum eight-hourly mean ozone concentration (> 120 µg/m³) could increase by the middle and end of this century in a range of 5.6 – 12.3 % and 9.2 – 27.5 % respectively.

The changes in maximum eight-hourly mean ozone concentration obtained from our statistical downscaling approach are mainly due to a positive shift in the frequency distribution of the meteorological variables driving the high ozone concentrations. In this respect, an increase in maximum temperature has been shown to be the main driver for an increase in maximum eight-hourly mean ozone concentration, together with an increase of shortwave downward radiation and an overall decrease in cloud cover. And although the different SRES scenarios project a large variability in the various predictors, the overall changes result in a significant increase in ozone concentrations. In order to verify whether these findings are physically plausible, our results are compared with the observed heat wave in August 2003, characterized by a poor air quality and excess of mortalities in large parts of Western and Central Europe. This shows that for the main predictors driving high ozone concentrations, the observed values fit closely to the predictor's future distributions, taking into account the given scenario assumptions. Thus, the 2003 heat wave, with related high maximum eight-hourly mean ozone concentrations, can serve as an analogue to what may occur more regularly in the future, not only in terms of temperature, but also in terms of maximum eight-hourly mean ozone concentrations.

This paper studies the impact of global climate change on future O_3 levels only, without taking into account future changes (reductions) in emissions. We have shown here that, under changing atmospheric conditions, the maximum eight-hourly mean ozone concentration increases significantly by the end of this century, assuming present-day emissions, which are indirectly taken into account in the statistical downscaling tool. Here, the question arises whether current emission control strategies will be sufficient to reduce O_3 precursor levels in order to keep the future O_3 concentrations below the European thresholds. In this respect, future climate changes should be taken into account

in the decision process on the European thresholds of Air Quality, and the thresholds should be set equal or lower in the future to protect the human health and the natural environment. After all, tropospheric ozone is the third most important man-made greenhouse gas after CO_2 and methane. Furthermore, joint efforts should be done first to develop an integrated model setup, as was suggested by Vautard et al. (2007), in order to quantify air quality levels under changing climate conditions. This should be done in order to set-up appropriate emission reduction measures to achieve acceptable ozone levels in the future, both on local, regional and the global scale.

Chapter 7

Modelling the energy balance in Marseille: Sensitivity to roughness length parameterizations and thermal admittance[*]

7.1 Introduction

Cities' surfaces are characterized by various building materials, each with their respective thermal characteristics, and are configured in complex geometric structures such as street canyons. This urbanization process more and more replaces natural surfaces with buildings and paved surfaces. Thereby, together with human activities in these areas, changes in moisture, heat and momentum exchange processes will occur in the boundary layer and distinguish urban areas from their surrounding rural areas. The urban heat island (UHI), characterized by urban warming relative to the rural surroundings, is the most obvious consequence of urbanization (Fan and Sailor, 2005; Sarrat et al., 2005). In order to develop effective mitigation strategies in these urban environments, it is important to understand all processes leading to the formation of an UHI and significant related processes such as air quality, cooling energy demand and human comfort. Recently, there has been a growing interest in quantitative research in urban

[*] This chapter is based on the following research paper: Demuzere, M., De Ridder, K. and Van Lipzig, N. P. M., 2008. Modeling the energy balance in Marseille: Sensitivity to roughness length parameterizations and thermal admittance. Journal of Geophysical Research-Atmospheres 113, 1-19.

boundary layer dynamics and air pollution processes (Davies et al., 2007). Piringer and Joffre (2005) comment that the incorporation of urban-type surface forcing is important for a correct modelling of urban pollution dispersion. The latter is controlled by many meteorological parameters where the mixing height is one of the parameters that determine the volume of air through which the pollution is mixed (Collier et al., 2005). Thereby, a need has grown to simulate meteorological fields for complex situations at finer spatial resolutions. This has partly been stimulated by scientific and technological advances and partly by policies requiring more detailed assessment of air pollution on urban to regional scales. Therefore, dynamical models have increasingly been used worldwide for meteorological and air pollution applications. Models developed for shorter long-range applications are not always appropriate in flow conditions involving intermediate meso-scale features and processes because appropriate approximations and parameterizations need to be different for models of different scales. In addition, at these mesoscales, the simulated phenomena are driven by both local scale influences (e.g. urban areas) as well as synoptic scale processes. Seaman (2000) states that surface fluxes of heat, moisture, momentum and short/long wave radiation are crucial for air-quality applications because they are the primary mechanisms driving the development of the turbulent boundary layer (PBL). As turbulence is critical to vertical transport, horizontal plume dispersion and dry deposition in the PBL (Seaman 2000, 2003), it is worthwhile to investigate specific land surface characteristics and thermal parameterizations. Both parameters, especially over urban surfaces, partly control the magnitude of the sensible heat flux, which is a necessary prerequisite of models to calculate air pollution dispersion, urban mixing depth and mesoscale airflow (Grimmond and Oke, 2002).

Recently, detailed urban models have been developed taking into account the impact of horizontal (canyons, floors, roofs) and vertical (walls) surfaces in the momentum, heat and turbulent kinetic energy equations (Taha, 1999; Martilli et al., 2002; Masson et al., 2000; Kanda et al., 2005). One drawback of this approach is the need for a large number of thermal and geometric parameters, which are often unknown. When one is not interested in the details of the urban canopy climate, simpler schemes can be used (Grimmond and Oke, 2002). Among these is the soil-vegetation-atmosphere transfer scheme developed by De Ridder and Schayes (1997) which was recently upgraded to better represent urban surfaces (De Ridder, 2006) and incorporated in the Advanced Regional Prediction System (ARPS), a non-hydrostatic mesoscale meteorological model. The original thermal roughness length parameterization based on the bulk temperature difference proposed by Anderson (1993) was replaced by adopting the Brutsaert (1982) parameterization

for thermal roughness length, designed specifically for surfaces containing solid obstacles (in contrast to porous obstacles such as vegetation).

The aim of this paper is to investigate the influence of the modelled urban surfaces and characteristics on the atmosphere at the scale of a city. In particular, it is verified whether the above-mentioned roughness parameterization by Brutsaert is the most suitable one, compared to other parameterizations suggested by Zilitinkevich et al. (1992) and Cahill et al. (1997). Furthermore, sensitivity experiments are conducted on the thermal admittance value (μ). This quantity presents the amount of heat that passes in an unit of time through an interfacing area when the opposite sides differ in temperature by one Kelvin (Priestley, 1959), and is calculated as the square root of the product of the volumetric heat capacity (Cp) and thermal conductivity (k). In order to evaluate the validity of these parameterizations and parameter values, ARPS was run in a three-level nested setup over the Marseille Berre-Pond Region (South of France), using data from the experimental campaign ESCOMPTE (Experience sur Site pour COntraindre les Modeles de Pollution atmospherique et de Transport d'Emissions), which took place in the summer of 2001. Finally, our results from the simple model approach are compared with results from the more complex TEB-ISBA (Mestayer et al., 200) and LUMPS (Grimmond and Oke, 2002) schemes, applied for the same period of time in Marseille Centre.

The remainder of this paper is organized as follows. In Section 7.2, the methods are discussed, describing the mesoscale meteorological model ARPS, the land surface scheme, and the different roughness length parameterizations and thermal admittance values. In Section 7.3, the ESCOMPTE measurement sites and data are described, and subsequently the model evaluation is described in Section 7.4. In Section 7.5, an analysis of the sensitivity simulations is performed using the different thermal roughness parameterizations and thermal admittance values, followed by a discussion and formulation of the conclusions in Section 7.6.

7.2 Methods

7.2.1 Model description

A mesoscale non-hydrostatic model, the Advanced Regional Prediction System (ARPS) (Xue et al., 2000; Xue et al., 2001) was run for the period 20 to 23 June 2001, covering the Marseille Berre-Pond Region. ARPS employs a finite-difference approximation of the fully compressible Navier-Stokes equations, which

are solved on a terrain-following grid. The model contains advanced parameterizations for moist processes and radiation transfer. The 1.5-order turbulent kinetic energy-based closure scheme is used for the turbulent mixing terms. The land surface scheme provided in ARPS was replaced by the scheme developed by (De Ridder and Schayes, 1997). It contains one vegetation layer, a soil skin layer and four subsurface soil layers. The shortwave and longwave radiation in the vegetation is calculated using the two-stream theory. Turbulent transfer at the surface is treated in a very simple manner, considering canopy-air and ground-air exchanges separately. Plant water flow is governed by differences in water potential between the soil and the leaves. The stomatal resistance formulation uses the effective leaf area index and the leaf water potential as key variables. The transpiration scheme implicitly accounts for the influence of photosynthetically active radiation (PAR) (De Ridder and Schayes, 1997), soil moisture, atmospheric saturation deficit and leaf temperature. The land surface scheme employs the mosaic approach, in which different land use types are allowed to co-exist within a surface grid cell. The surface heat fluxes are calculated for each land use type separately, and subsequently, the total flux within one cell is calculated using the fraction of each type as a weight.

Recently the land surface scheme by De Ridder and Schayes (1997) was modified to better represent urban surfaces (De Ridder, 2006). Using a simple approach, all urban surfaces are represented as a bare soil, with appropriate values for the momentum roughness length, the albedo, the emissivity, with a thermal conductivity of $k = 2\ \mathrm{W\,m^{-1}\,K^{-1}}$ and a volumetric heat capacity of $Cp = 2 \times 10^6\ \mathrm{J\,m^{-3}\,K^{-1}}$ (Garratt, 1992). Also, urban surfaces are considered impermeable, so that rainfall – apart from a small surface storage component – is mostly lost as runoff. The model was extended with a parameterization of the roughness length for heat (z_{0h}) specifically designed for urban surfaces. This roughness length is crucial in the calculation of the surface sensible heat flux over cities, and accounts for the obstacle-rough types of surfaces that are characteristic for cities, in contrast to the common parameterizations that are solely applicable to the so-called 'porous-rough' surfaces such as vegetation. Although the thermal roughness schemes tested in this study (section 7.2.3) are only valid for bluff-rough surfaces, many urban land uses can be a mix. For each land cover type within the grid cell (mosaic approach), an appropriate roughness length for both heat and momentum is used whereby the resulting fluxes are subsequently obtained as a weighted average. Hereby, the weights are calculated as the percentage of occurrence of each land use type within one grid cell. As will be seen below, the main purpose of the present paper is to evaluate the validity of the various parameterization schemes of z_{0h} and

of the values used for thermal conductivity and heat capacity, using detailed experimental data.

7.2.2 Description of the simulations

The ARPS simulations were performed using three-level grid nesting. The Operational Reanalysis Data from the European Centre for Medium Range Weather Forecasting (ECMWF) with a resolution of approximately 50 km provided 6-hourly initial and boundary conditions for a model run with 16 km resolution and 75 grid points in each horizontal direction. An intermediate grid was nested in the output fields of the latter, covering a domain consisting of 83 horizontal grid points at a resolution of 4 km. A fine grid was nested in the 4-km domain, using a 1-km horizontal resolution and 103 grid points (Figure 7.1). In all these simulations, in the vertical, 35 levels were used with a 25 m spacing near the surface increasing to 1 km near the model top, which was located at 15 km altitude. The model was integrated using a leap-frog discretisation with time steps of 40 s, 15 s and 6 s for the three nesting levels respectively.

Land cover-dependent parameters such as aerodynamic roughness length and albedo, were specified as a function of land cover type, which were interpolated from the CORINE land cover map (European Commission, 1994). Following land use classes from CORINE land cover map are used: 1) water, 2) urban, 3) pasture, 4) crops, 5) forest, 6) perpetual snow/ice, 7) shrubs & barren land (Table 7.1 and Figure 7.1). The CORINE land cover map has a resolution of 250 m. Using a window equal-sized to the ARPS grid resolution, the percentage of occurrence of each land cover type for each grid cell is derived. Finally, for each grid cell, the dominating land cover type (with the highest percentage of occurrence) is retained.

Table 7.1: Overview of the land cover types derived from the CORINE land cover map and their respective roughness length and albedo (OKE, 1987).

Land Cover Type	Roughness length (z_0)	Albedo
Water	0.0001	0.05
Urban	1.2	0.15
Pasture	0.01	0.2
Crops	0.01	0.2
Forest	1.2	0.15
Perpetual snow/ice	0.001	0.7
Shrubs and barren land	0.1	0.15

Terrain height was interpolated from the Global 30 Arc-Second Elevation Data Set (GTOPO30) completed in late 1996 and distributed by the U.S Geological Survey. Sea surface temperature was derived for June 2001 from NOAA/NASA Pathfinder Advanced Very High Resolution Radiometer (AVHRR) SST imagery. Vegetation abundance was specified as a function of the Normalised Difference Vegetation Index (NDVI) contained in imagery from the VEGETATION instrument onboard the SPOT satellite platform, following relations established by Wittich and Hansing (1995) and Gutman and Ignatov (1998).

7.2.3 Thermal roughness length and thermal admittance

7.2.3.1 Thermal roughness length parameterization

The thermal roughness length is the height above the displacement height defined by the Monin-Obukhov similarity (MOS) theory, which defines the effective source of sensible heat in the canopy, which is at a lower level than the roughness length for momentum due to a greater aerodynamic resistance for the transfer of heat than for momentum (Troufleau et al., 1997). Thereby, this z_{0h} can be interpreted as the surface intercept of the atmospheric surface layer temperature profile in the same way as z_{0m} is the zero velocity intercept for the surface layer velocity profile (Arya, 2001). The roughness length for temperature is necessary to estimate the sensible flux from atmospheric surface layer similarity theory in conjunction with air temperature measurements (Mahrt et al., 1997). Brutsaert (1982) proposed a theoretical relationship for z_{0h} as a function of the interfacial transfer coefficient $St_0^{-0.5} - Cd_0^{-0.5}$ for rough-bluff surfaces, which reads as:

$$z_{0h} = z_{0m} \exp\left[(-k)\left(St_0^{-0.5} - Cd_0^{-0.5}\right)\right] \qquad (1)$$

where z_{0m} is the roughness length for momentum, z_{0h} the thermal roughness length and k (=0.4) the Von Kármán constant. Cd_0 $(=\bar{u}/u_*)$ is the drag coefficient at the top of the interfacial sublayer (with $\bar{u}$ the mean wind speed and u_* the friction velocity), St_0 is the Stanton number, written as a function of the roughness Reynolds number Re_* $(=u_* z_{0m}/\nu)$ (with ν $(=1.461\ 10^{-5}\ [m^2 s^{-1}])$ the kinematic molecular viscosity), Pr the Prandtl number and C_R a geometric coefficient (Garratt, 1992), which results in:

$$z_{0h} = z_{0m} \exp\left[(-k)\left(C_R^{-1}\,\mathrm{Re}_*^{\beta}\,\mathrm{Pr}^{\gamma} - Cd_0^{-0.5}\right)\right] \qquad (2)$$

Numerous sets of values for $C_R^{-1}, \beta, \mathrm{Pr}^{\gamma}$ and $Cd_0^{-0.5}$ have been developed (see also Table 7.1 of Cahill et al. (1997)). Based on laboratory measurements, Brutsaert (1982) derived $C_R^{-1}\ \mathrm{Pr}^{\gamma} = 6.2$ with $\beta = 0.25$ and $Cd_0^{-0.5} = 5$, resulting in:

$$z_{0h} = z_{0m} \exp\left[(-k)\left(6.2\,\mathrm{Re}_*^{0.25} - 5\right)\right] \qquad (3)$$

This difference between z_{0m} and z_{0h} often is described with a dimensionless parameter defined by $\mathrm{kB}^{-1} = \ln(z_{0m}/z_{0h})$, whereby $\mathrm{B}^{-1} = 6.2\,\mathrm{Re}_*^{0.25} - 5$. There are many other formulas to predict B^{-1}, whereby most of them focus on sparse vegetation surfaces (Ma and Daggupaty, 2000 and references therein). For natural homogeneous surfaces it has widely been observed that z_{0m} differs by up to an order of magnitude from z_{0h}, whereby $B^{-1} \cong 5$ (Garratt, 1992; Ma and Daggupaty, 2000). For urban surfaces with their complex geometry, this approximation no longer holds. With this sensitivity study we seek to validate a number of parameterizations for the thermal roughness length over urban grid cells on a mesoscale. Cahill et al. (1997) used meteorogical measurements taken from the Campbell Tract and the dry Owens Lake sites to describe adequately the sensible heat fluxes. Based on the field measurements, they propose changes in the Brutsaert parameters $Cd_0^{-0.5}, C_R^{-1}\ \mathrm{Pr}^{\gamma}$ and β, so that (3) can be written, either

with a value for $Cd_0^{-0.5}$ of 9.5:

$$z_{0h} = z_{0m} \exp\left[(-k)\left(6.2\,\mathrm{Re}_*^{0.25} - 9.5\right)\right] \qquad (4)$$

with values for $C_R^{-1}\ \mathrm{Pr}^{\gamma}$ and β of 4.31 and 0.247 respectively:

$$z_{0h} = z_{0m} \exp\left[(-k)\left(4.31\,\mathrm{Re}_*^{0.247} - 5\right)\right] \qquad (5)$$

Zilitinkevich et al. (1992) and Zeng and Dickinson (1998) suggested the following parameterization for the thermal roughness length, based on dimensional analysis and interpretation of heat transfer experiments:

$\ln\left(\frac{z_{0m}}{z_{0h}}\right) = a\left(\mathrm{Re}_*\right)^{0.45}$, where a = 0.13 (Zilitinkevich, 1970). (6)

7.2.3.2. Thermal admittance

The city centre of Marseille is a dense commercial and residential area, with 4-6 storey buildings characterized by a variety of building materials and surfaces (Grimmond et al., 2004; Lemonsu et al., 2004; Hamdi and Schayes, 2005; Mestayer et al., 2005) and a plan area of vegetated surfaces per total plan area of < 14% (Lemonsu et al., 2004; Hamdi and Schayes, 2005), encompassing, trees, grass terrain and bare soil. Each land cover material has its own thermal properties, and therefore a wide range of volumetric heat capacity (C_p) and thermal conductivity values (k) for urban and natural surfaces has been chosen in order to test the sensitivity of the urban energy balance to the thermal characteristics of these surfaces. Volumetric heat capacity and thermal conductivity are both separately defined in the land surface scheme, whereby the thermal admittance μ, a parameter that combines both properties as $\mu = \sqrt{kC_p}$, is used to refer to the combinations of the former two. In this study, the thermal admittance ranges from approximately 340 J m^{-2} $s^{1/2}$ K^{-1} for dry peat soil and foamed concrete to approximately 2200 J m^{-2} $s^{1/2}$ K^{-1} for wet sandy loam or dense concrete (Welty, 1974; Oke, 1987; Incropera and Dewitt, 1990 and Sabins, 1997). During the sensitivity experiments, only the reference values of the volumetric heat capacity and the thermal conductivity for the urban grid cells are changed (table 7.2). Other land cover types keep their original reference-state values. Furthermore, all parameterizations (3), (4), (5) and (6) are tested by implementing them in the ARPS land surface scheme model. Each parameterization formula is subsequently combined with each of the six combinations of thermal parameter values, resulting in 24 sensitivity runs (Table 7.2).

Table 7.2: Overview of the simulation runs combining the different thermal roughness parameterization schemes (Z_{0h} scheme) with the values of the thermal admittance μ. ρ is the density, Cp is the volumetric heat capacity and k the thermal conductivity (with $\mu=\sqrt{kC_p}$). The thermal roughness lengths are denoted as (3) Brutsaert (1982), (4) Brutsaert – Var1, (5) Brutsaert – Var2, (6) Zilitinkevich (1992).

Run Number	Z_{0h} scheme	ρ ($x10^3$ kg m^{-3})	C_p ($x10^6$ J m^{-3} K^{-1})	k (W m^{-1} K^{-1})	μ (J m^{-2} $s^{1/2}$ K^{-1})
Ref	(3)	Combined in C_p	2	2	2000
1	(3)	2.11	1.94	0.06	341.17
2	(4)	2.11	1.94	0.06	341.17
3	(5)	2.11	1.94	0.06	341.17
4	(6)	2.11	1.94	0.06	341.17
5	(3)	1.6	1.42	0.25	595.82
6	(4)	1.6	1.42	0.25	595.82
7	(5)	1.6	1.42	0.25	595.82
8	(6)	1.6	1.42	0.25	595.82
9	(3)	1.83	1.37	0.83	1066.35
10	(4)	1.83	1.37	0.83	1066.35
11	(5)	1.83	1.37	0.83	1066.35
12	(6)	1.83	1.37	0.83	1066.35
13	(3)	2.11	1.94	0.75	1206.23
14	(4)	2.11	1.94	0.75	1206.23
15	(5)	2.11	1.94	0.75	1206.23
16	(6)	2.11	1.94	0.75	1206.23
17	(3)	2.4	2.11	1.51	1784.96
18	(4)	2.4	2.11	1.51	1784.96
19	(5)	2.4	2.11	1.51	1784.96
20	(6)	2.4	2.11	1.51	1784.96
21	(3)	2	3.1	1.58	2213.1
22	(4)	2	3.1	1.58	2213.1
23	(5)	2	3.1	1.58	2213.1
24	(6)	2	3.1	1.58	2213.1

7.2.4 Model performance evaluation methods

The quality and reliability of the model framework were examined using several statistical indices proposed by Willmott (1981; 1982; 2005). These indices are the following (where P and O denote predicted and observed values respectively):

Mean ($\bar{P}$ and $\bar{O}$), describing the mean of a sample of a random variable.
Standard deviation (S_p and S_o), which is a measure of the dispersion of a data set from its mean. The more spread apart the data is, the higher the deviation.
Variance (S^2_p and S^2_o), which describes the dispersion of a variable around the mean. Variables with little dispersion have realizations tightly clustered around the mean, and vice versa.
Mean absolute error (MAE), which returns the 'total error' divided by the number of samples.
Root mean square error (RMSE), which is a measure of the total deviation of predicted values from observed values.
Correlation coefficient (R), which reflects the extent of a linear relationship between the observed and the predicted values.
Index of agreement (d) in the following form:

$$d = 1 - \left[\sum_{i=1}^{N} (P_i - O_i)^2 / \sum_{i=1}^{N} (|P_i'| - |O_i'|)^2 \right]$$

where $P_i' = P_i - \bar{O}$ and $O_i' = O_i - \bar{O}$. Thereby, P_i and O_i are the modelled and observed variable respectively, and $\bar{P}$ and $\bar{O}$ respectively presents the mean of the modelled and observed variable. It indicates the degree to which the predictions of a model are error free. It is a measure of how well the simulation result distance from the observed mean (Mo) matches, for each individual observation, the observational result distance from the Mo. This dimensionless index has a theoretical range of 1, for perfect agreement, to 0, for no agreement (Papalexiou, S. and Moussiopoulos, N., 2006).

7.3 Data

7.3.1 The ESCOMPTE campaign

The domain of the ESCOMPTE study is characterized by a complex geography, land use and atmospheric circulation. Summer anticyclonic conditions favor an afternoon sea breeze from the southwest, transporting pollution from industrialized and urbanized areas located close to the shore inland. Due to a highly variable terrain elevation, the resulting flows are complex, and therefore form a challenge for mesoscale meteorological modelling. For more detailed information about the ESCOMPTE campaign refer to (Cros et al., 2004). During the summer of 2001, large quantities of instruments were deployed on a large number of fixed sites, airborne devices and mobile instruments. During the whole campaign, fifteen days were characterized as "Intensive Observation Period" (IOP) days. The present study focuses on the first half of the second Intensive Observation Period, hereafter called IOP2a, which took place from 20th to 23rd of June 2001. The first period of IOP2a consists of three days characterized by low to moderate Westerly and Northwesterly winds, followed by a day with decreasing wind speeds and a synoptic pattern favoring the development of a well-established sea breeze from the Southwest (Cros et al., 2004).

7.3.2 The selected fixed measurement sites

The ESCOMPTE database (http://medias.obs-mip.fr/escompte/) includes high resolution meteorological and emission inventories and field experiments in a 120 $\times$ 120 km^2 area centered over Marseille. From this database, three fixed surface stations are used, namely the measurement sites of Marseille Centre, Trets and Meyrargues (Figure 7.1). The fixed measurement stations are selected because of their diversity with respect to location, surface characteristics and measurement heights (Table 7.3). In order to validate simulated sensible heat fluxes, also scintillometer measurements along two pathlenghts over Marseille Centre are used (Figure 7.2 and Table 7.3).

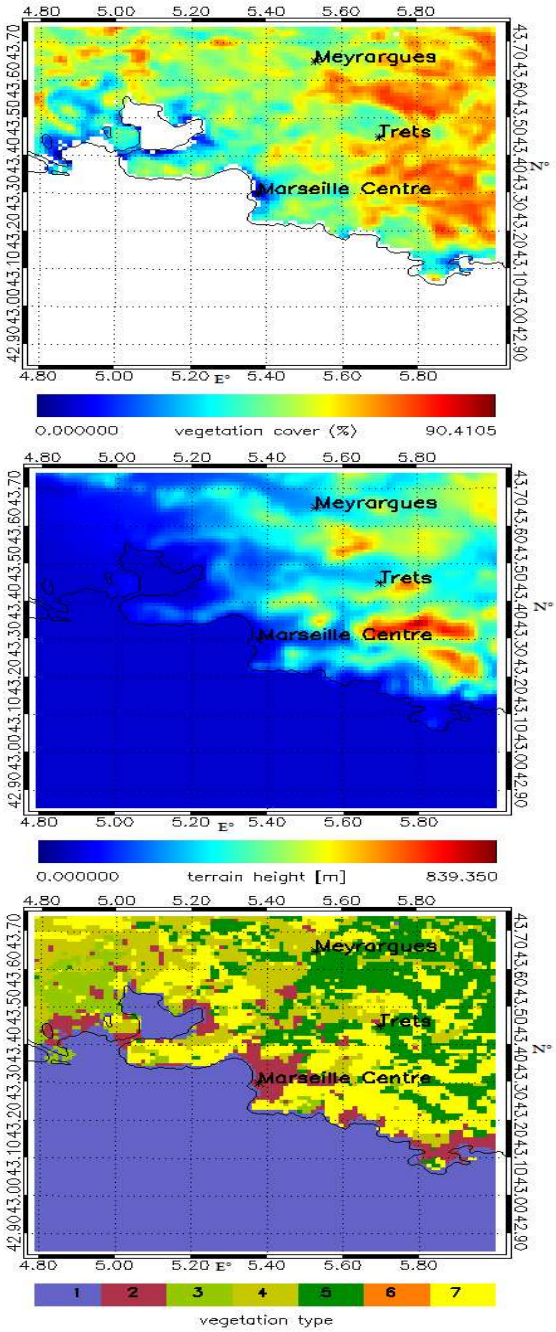

Figure 7.1: Vegetation cover (%), terrain height (m) and vegetation type of the ESCOMPTE campaign measurement area (ARPS domain) with the location of the three selected stationary surface measurement sites Marseille-Centre, Trets and Meyrargues. Vegetation types are derived from the CORINE land cover map and classified as: 1) water, 2) urban, 3) pasture, 4) crops, 5) forest, 6) perpetual snow/ice, 7) shrubs & barren land.

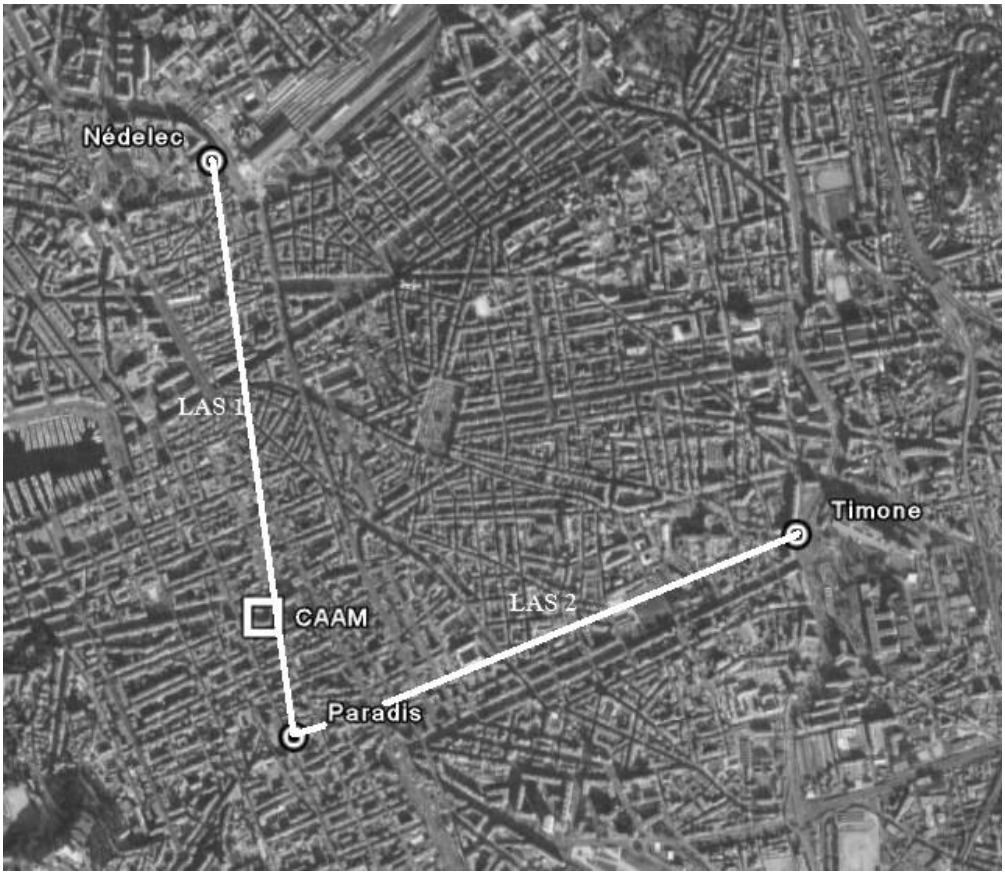

Figure 7.2: Satellite image locating the 3 LAS measurement stations Nédelec, Timone Hopital and Paradis, the LAS measurement pathlenghts, the CAAM measurement tower and the two selected representative measurement points LAS1 and LAS2.

Table 7.3: Characteristics of the 5 measurements sites located in the Marseille Berre-Pond Region (France).

Site	Coordinates		Height asl (m)	Land Cover	Temporal Resolution
Marseille Centre	43.17°N	5.22°E	70	Central Urban Site – Gravel roof of CAAM within a densely built –up area	30 min.
Trets	43.27°N	5.419°E	264	Grass terrain in municipal stadium	hourly
Meyrargues	43.65°N	5.53°N	196	Maize field	15 min.
Nedelec – Paradis (LAS1)	43.295°N	5.379°E	50	Urban – Centre of Marseille	15 min
Nedelec – Timone (LAS2)	43.289°N	5.391°E	74	Urban – Centre of Marseille	15 min

The measurement site of Marseille Centre is centered on the Cour d'Appel Administratif de Marseille (CAAM). It is situated in a dense commercial and residential area of the city. Measurements were taken using a pneumatic tower on the top of the CAAM. More detailed characteristics of this site are fully described in (Grimmond et al., 2004; Lemonsu et al., 2004; Hamdi and Schayes, 2005; Mestayer et al., 2005), which also provides a detailed description of the micrometeorological measurements and instrumentation. The other stations are located in rural areas. Trets is located 30 km northeast of Marseille Centre (Figure 7.1). Measurements were taken on a grass terrain in the municipal stadium, with hourly temperature measurement at a standard height of 2 m and wind speed and direction on a 10 m high pylon. The second rural station Meyrargues is situated in a maize field, located 1.6 km north of the small city of Meyrargues and 41 km north of the CAAM measurement tower and extending over an area of 13 ha. Thereby, the fetch exceeded 100 m or more in all wind directions. During the IOP2a period, there was no irrigation on the field. A standard meteorological station, installed on the site for the experiment, provided measurements of solar radiation, air temperature (3 m height), humidity, pressure, precipitation, and wind speed and direction. In addition, vegetation height and leaf area index (LAI), heat fluxes, soil humidity and temperature were measured. More information describing the measurement site can be found in (Michou et al., 2005).

Next to that, two LAS (Large Aperture Scintillometer) were installed over Marseille city center between 12th of June and 10th of July 2001. Transmitters and receivers were placed on three locations in the city center (Paradis (P), Nedelec (N) and Timone Hospital (T)) (Figure 7.2), whereby pathlenghts are 1785, 1878 and 2308 m for P-N, P-T and N-T respectively. Line averaged Q_H from the LAS are computed using two methods (De Bruin et al., 1995; McAneney et al., 1995). Further information regarding these methods for this specific location can be found in Lagouarde et al. (2002), Hartogensis et al. (2003), Lemonsu et al. (2004) and Mestayer et al. (2005). Mestayer et al. (2005) states that both methods are in good agreement, so therefore only the classic method of McAneney et al. (1995) assuming mixing conditions (hereafter referred to as MXT) will be used. To obtain the footprint of the scintillometer measurements, one has to take into account the weighting of the scintillometer along its pathway, and the footprint of each point along the scintillometer beam. The weighting has a bell-shaped curve (weighting towards the middle of the path whereby first and last 15% of the path only play a minor role (Hartogensis et al., 2003). Moreover, it has been shown that for the Marseille area, the spatial variability of the sensible heat fluxes measured by the LAS is small (Mestayer et al., 2005) and that this surface is rather homogeneous with a dense mixture of old buildings of 4–6 stories high and narrow streets in all

directions (Lagouarde et al., 2002; Hamdi and Schayes, 2005). Therefore, two points in the middle of the path line between Nedelec - Paradis (LAS1) and Timone – Nedelec (LAS2) are selected to be representative measurements sites to validate the modelled sensible heat flux for its respective model grid boxes covering the LAS' path line (Figure 7.2 and Table 7.3).

7.4 Evaluation of the model

7.4.1 Meteorological variables

In this section 7.4, a validation of the ARPS – land surface model set-up in its reference state as described in section 7.2.1 is done. Measurements of temperature are thereby provided at a height of 20 m (above roof top), 3 m and 2 m (above ground level) respectively for the Marseille Centre, Meyrargues and Trets measurement stations. As temperatures from the first ARPS level are simulated at a height of 12.5 m, Monin-Obukhov similarity theory is used to extrapolate simulated temperature values to the measurement level. Applying the Monin-Obukhov similarity theory on the temperature cycle results in a strengthening of diurnal temperature values, with lower and higher temperatures respectively during night and day. In the further analysis for wind speed and direction, a threshold value of 1 m s^{-1} for observations is taken into account, in order not to consider the accuracy of the measurement devices.

As there is a lack of a broader consensus on the magnitude of errors of modelled variables, air quality applications are chosen to set a standard accepted error. In respect to air quality modelling, Bärtsch-Ritter et al. (2003) and Dawson et al. (2007a) have shown that a reasonable 10% error in O_3 concentration prediction for different geographical regions relates to a temperature change of 3.5°C. Also Grell et al. (2005) show that simulating 1-h maximum O_3 concentration are predictable within a 10ppbv O_3 concentration interval. Moreover, Dawson et al. (2007b) have shown that for a reasonable 10% error in $PM_{2.5}$ concentration prediction this corresponds to a 5°C error in temperature. Thereby, for this paper a desired accuracy of ±2 °C (Schlünzen et al., 2003) is set as an acceptable error for temperature, which corresponds well to the lower value of 3.5 °C temperature error limit deduced from ozone applications. As there are no defined accepted errors stated for wind speed and direction, related to air quality applications, an acceptable error range of ± 1 m s^{-1} and ± 30° respectively is set (Schlünzen et al., 2003). For water vapour pressure, a study of Civerolo et al. (2007) on the effects of urbanisation is used to set an upper water vapour pressure limit. Using the coupled

Penn State/NCAR MM5/CMAQ system, they tested the change (increase) of urban land use on surface meteorology and ozone predictions. Thereby they predict more than 0.6 g kg^{-1} decrease of water vapour mixing ratio over the next 50 years, which corresponds to a change of 0.59 hPa in water vapour pressure. The impact of the increased urbanization would thereby result in a 1-5 ppb increase in average O_3 levels. As the direct effect of water vapour on ozone is still ambiguous and this predicted O_3 increase is half of the chosen O_3 error interval, an accepted error estimate of ± 0.6 hPa is set for water vapour.

Figure 7.3 shows model simulations against temperature, wind speed and direction measurements, respectively for Marseille Centre, Meyrargues and Trets. For Marseille Centre, urban conditions generate a weak diurnal cycle in simulated and observed air temperatures (with S^2_o and S^2_p 0.093 and 0.051 respectively), which are captured well by the model. Simulated temperature values for Marseille are slightly high (with a MAE and RMSE of 1.05 °C and 1.39 °C respectively) and a high d and R (0.99 and 0.9 respectively). Modelled wind speeds are in the range of the observation, with a RMSE of 1.42 m s^{-1} (Table 7.4). Wind directions are overall in good agreement with the observations whereby the differences in wind directions for the Marseille Centre measurement station at the end of the second/beginning of the last day, can be attributed to a missing shift to Southeastern wind directions at night and early in the morning by the model, which shows a dominant Northwestern wind direction in the morning (Figure 7.3a). This could point out a missing land breeze during the night, not captured by the model due to a too low surface temperature for the urban grid cells. This bias in wind direction also results in higher modelled wind speeds (compared to observed) at that time, because of the fact that observed Southeasterly winds are blocked by the pronounced hills surrounding Marseille in the south-east, resulting in lower observed speeds over the centre of Marseille.

A

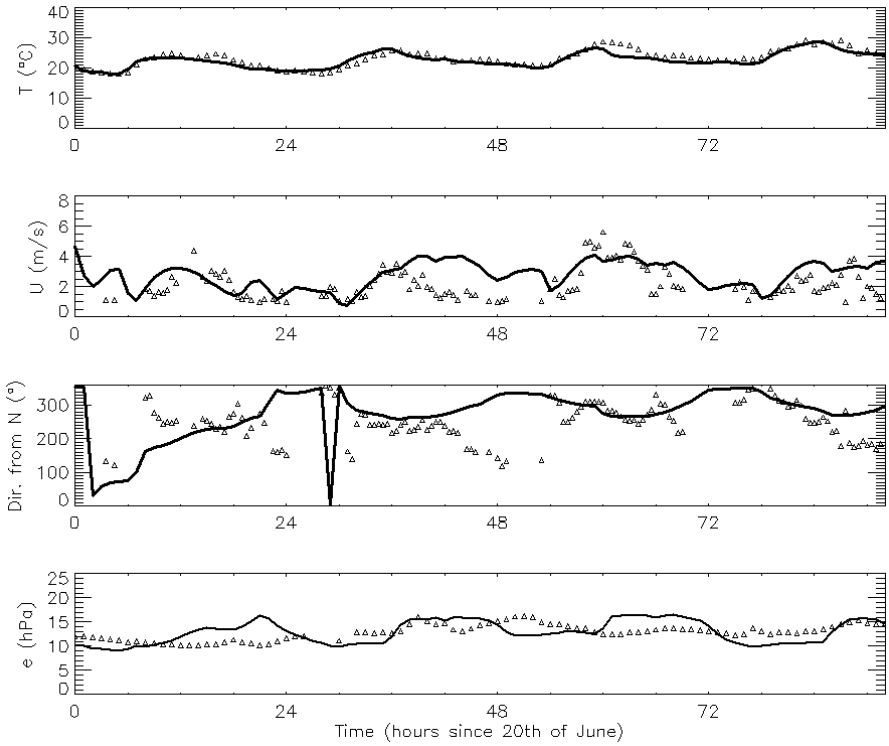

B.

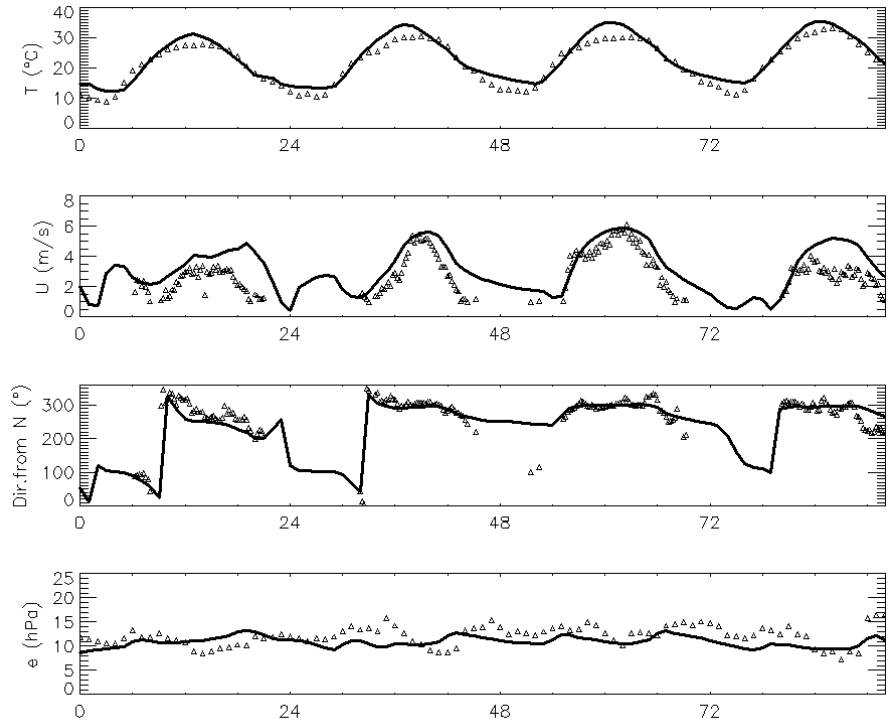

Figure 7.3: Observed (triangles) and simulated (full line) temperature, wind speed and direction and vapour pressure for Marseille Centre (a) and Meyrargues (b) and temperature, wind speed and direction for Trets (c).

C.

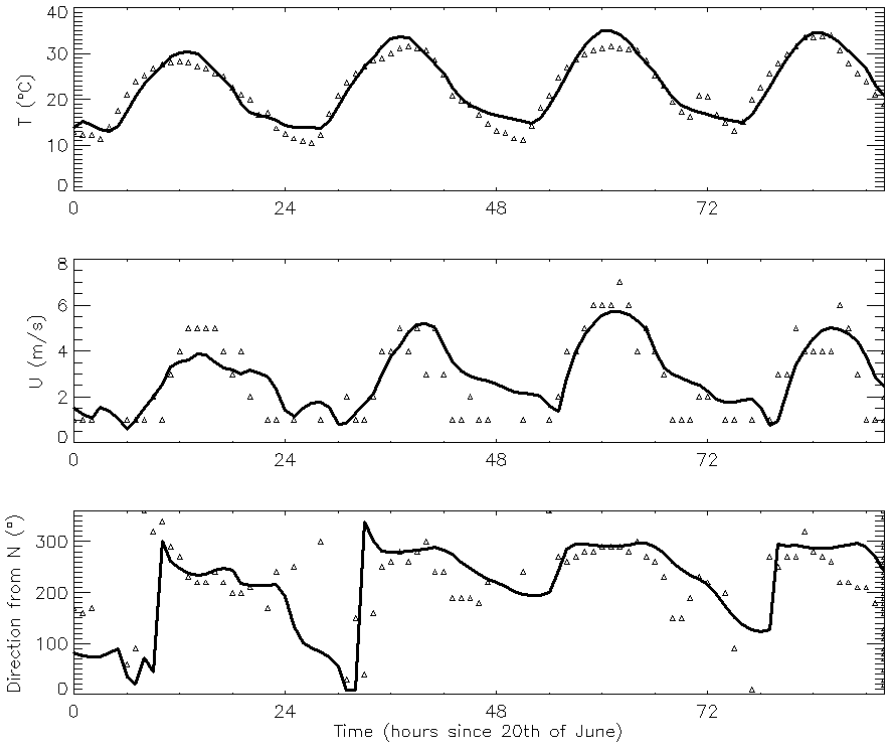

Figure 7.3: Continued.

Simulated temperatures for Meyrargues and Trets are in good agreement with the observations, with a temperature phase shift towards higher maximum values during day and night, resulting in a RMSE/d of 2.88 °C/0.99 and 2.12 °C/0.99 for Meyrargues and Trets respectively (Table 7.4). Also the larger daily amplitude (compared to the urban station) is captured well, explained by the larger S^2_o / S^2_p of 0.56/0.57 and 0.52/0.53 for Meyrargues and Trets respectively. Thereby, all modelled values for temperatures for all the selected locations are within our error limit of ±2 °C.

The model captures diurnal wind speed and direction cycles, characterized by northwesterly wind directions turning to southwest due to a reinforcement of the sea breeze (Figure 7.3). This is confirmed by all statistical indices in Table 7.4, whereby the larger MAE and RMSE values can be attributed to the representation of ° from N, which automatically returns high errors for winds coming from the northerly sector. Also here, wind speed errors are within the accepted range.

For the vapour pressure, root mean square errors for Marseille centre and Meyrargues are respectively 1.82 and 2.38 hPa, whereby the model shows less water vapour in both situations with a difference between $\overline{O}$ - $\overline{P}$ of 0.72 and 1.28

hPa for Marseille Centre and Meyrargues respectively (Table 7.4). This points a small lack of moisture, especially for the rural site (0.38 hPa larger than accepted error) in the model, which also shows a small underestimation of the latent heat fluxes for the Meyrargues measurement site (Figure 7.4b).

Table 7.4: Model performance estimators as described in section 7.2.4 for observed (O) and simulated (P) values of temperatures (T), wind speed (U), water vapour pressure (e), incoming net radiation (Q*), sensible heat flux (QH), latent heat flux (QE) and storage heat flux (ΔQ_s). Values are calculated using hourly values, only in the case where observations are available (denoted by % acc.).

Location	Variable	% acc.	$\overline{P}$	$\overline{O}$	S_p	S_o	S^2_p	S^2_o	MAE	RMSE	D	R
Marseille Centre	T (°C)	99	22.77	23.26	0.23	0.30	0.051	0.093	1.05	1.39	0.92	0.91
	U (m s^{-1})	100	2.506	2.26	0.09	0.12	0.008	0.015	1.08	1.42	0.42	0.042
	D (° from N)	100	272.1	246.47	7.22	5.86	52.11	34.30	72.36	96.32	0.52	-0.01
	E (hPa)	99	12.92	13.64	0.23	1.21	0.051	1.47	1.56	1.83	0.77	0.68
	Q* (W m^{-2})	97	143.3	162.55	26.43	28.98	698.62	840.00	42.38	62.87	0.96	0.98
	Q_H (W m^{-2})	97	78.61	147.59	10.40	14.90	108.019	222.13	75.55	97.05	0.85	0.93
	Q_E (W m^{-2})	85	33.36	25.71	3.26	4.65	10.65	21.60	25.09	38.10	0.66	0.45
	ΔQ_s (W m^{-2})	85	31.33	-38.02	15.15	16.44	229.56	270.20	58.69	71.90	0.93	0.90
Meyrargues	T (°C)	100	23.17	21.68	0.76	0.75	0.57	0.56	2.51	2.88	0.96	0.94
	U (m s^{-1})	100	3.09	2.71	0.16	0.13	0.025	0.016	1.64	2.056	0.36	-0.09
	D (° from N)	100	225.88	264.23	8.89	8.32	78.94	69.16	69.30	102.69	0.74	0.33
	E (hPa)	100	10.93	12.21	1.10	1.00	1.21	1.00	2.071	2.38	0.48	0.25
	Q* (W m^{-2})	100	164.87	184.30	25.57	26.24	653.76	688.35	23.93	40.77	0.99	0.99
	Q_H (W m^{-2})	97	71.38	49.04	12.57	8.65	157.99	74.90	38.80	57.29	0.92	0.94
	Q_E (W m^{-2})	97	85.97	93.80	8.26	11.19	68.15	125.13	24.74	42.69	0.95	0.94
	ΔQ_s (W m^{-2})	97	7.53	37.54	6.71	9.73	44.98	94.6	45.3	68.30	0.80	0.74
Trets	T (°C)	100	23.08	22.611	0.73	0.72	0.53	0.52	1.8	2.13	0.97	0.96
	U (m s^{-1})	100	2.91	2.71	0.15	0.18	0.021	0.032	1.76	2.17	0.40	0.03
	D (° from N)	100	214.54	229.032	8.91	7.75	79.43	60.02	81.72	112.86	0.72	0.01
LAS1	Q_H (W m^{-2})	92	77.55	147.33	9.44	13.12	89.09	172.14	79.72	94.33	0.83	0.93
LAS2	Q_H (W m^{-2})	91	76.53	134.66	9.30	11.89	86.52	141.35	67.48	81.42	0.84	0.92

7.4.2 Heat fluxes

Because heat flux measurements are unavailable for Trets, only the Marseille Centre and Meyrargues station, combined with the scintillometer measurements were used for the evaluation of the simulated heat fluxes. As the storage heat flux (ΔQ_s) is not measured, it is calculated as the residual of the surface energy balance (RES method). This surface energy balance (equation 7) is a statement of the partitioning of radiant energy absorbed at the Earth's surface (Q*) into turbulent fluxes of sensible and latent heat (Q_H and Q_E) and an anthropogenic heat flux from traffic, households and services(Q_F - Appendix A) into the atmosphere and a conductive flux of sensible heat into the substrate (ΔQ_S), which results in:

$$Q^* = Q_H + Q_E + \Delta Q_s + Q_F \quad . \qquad \textbf{(7)}$$

Pleasant temperatures during the simulation period suggest anthropogenic heating from house heating and air-conditioning to be limited. Nevertheless, other sources of anthropogenic heat play a role, so Q_F should be included in these experiments. From the energy release per unit CO_2 emission and the CO_2 flux measurements by Grimmond et al. (2004), the amount of energy released from traffic (Q_{Fv}), taking into account vegetation respiration, is estimated (Appendix A.1). This results in a mean daily value of 12.3 W m^{-2}, a peak value of 18.9 W m^{-2} during daytime, and a minimum value of 5.3 W m^{-2} during the night. These values can be confirmed using the method of Makar et al. (2006) as a validation tool. The diurnal pattern is introduced following the temporal variation of Q_F measured by the CO_2 fluxes (Grimmond et al., 2004) and confirmed by Ichinose et al. (1999) and Sailor and Lu (2004) (Appendix A.1). Next to that, also an estimate of anthropogenic heat of households & services (Q_{Fh}) has been estimated, using the ratio energy use traffic / energy use households and services from Eurostat for France 2001 (Appendix A.2). This results in a daily mean Q_{Fh} of 6.3 W m^{-2}. More details on the calculation of the anthropogenic heat flux can be found in Appendix A.

As mentioned above, the storage heat flux (ΔQ_S) is not measured; it is calculated as the residual of the surface energy balance (RES method). The latter RES method involves an accumulation of the measurement errors of all urban fluxes into the storage heat flux residual term. These estimates also suffer from the inclusion of the almost immeasurable anthropogenic heat flux. Using four different approaches to calculate/model ΔQ_s, Roberts et al. (2006) shows that all methods convergence towards the same results, suggesting that the general form of storage behavior is approximately correct.

A

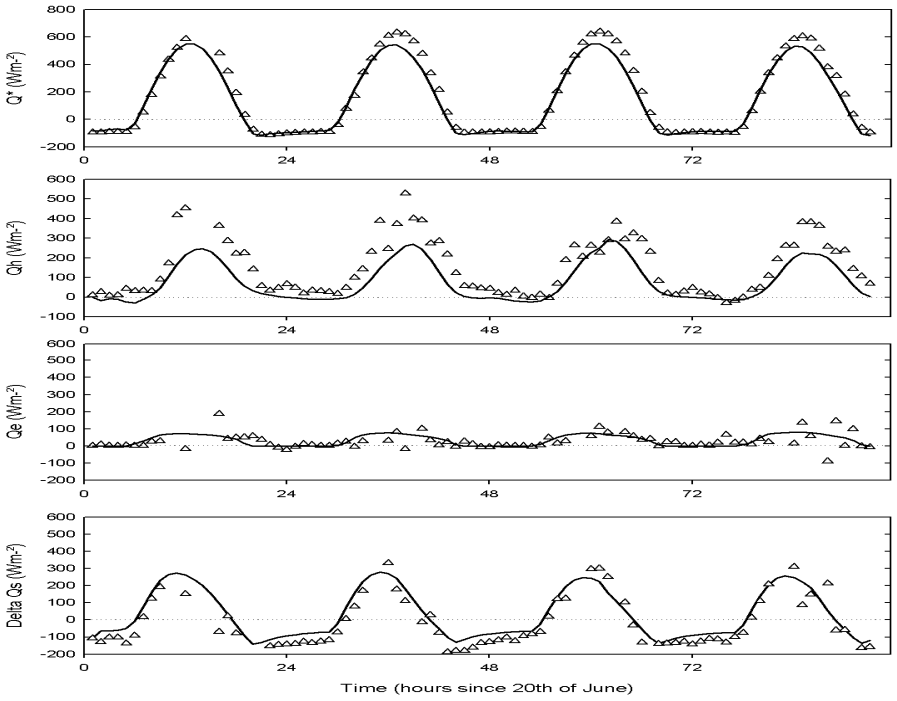

B.

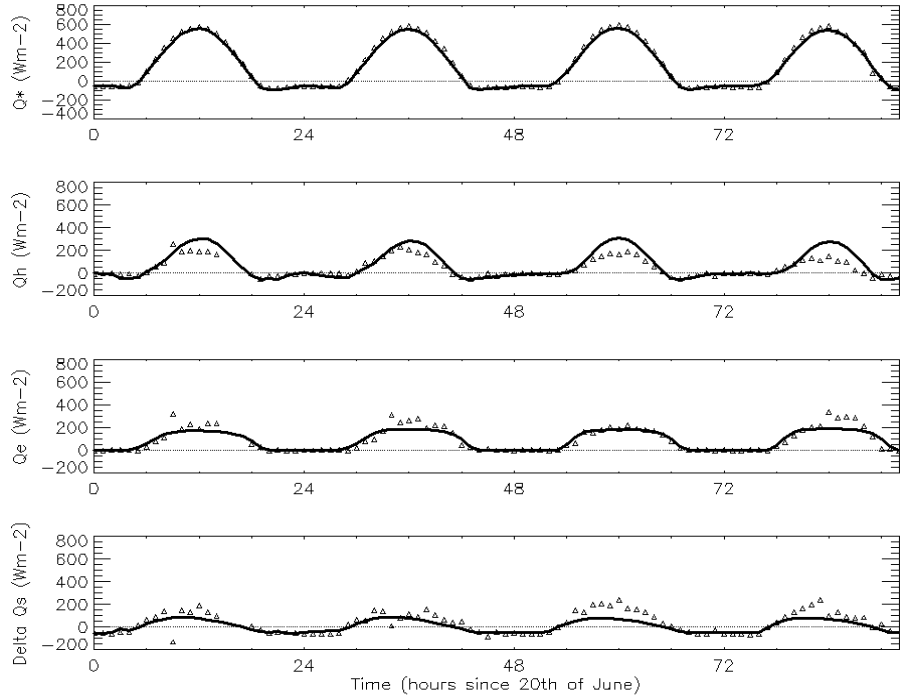

Figure 7.4: Observed (triangles) and simulated (full line) net incoming radiation (Q*), sensible heat flux (Q_H), latent heat flux (Q_E) and storage heat flux (ΔQ_s) for Marseille Centre (a), Meyrargues (b) and the sensible heat flux solely for the 2 selected LAS measurement points (c and d). The storage heat flux is each time calculated as the residual of the 3 other turbulent fluxes.

C.

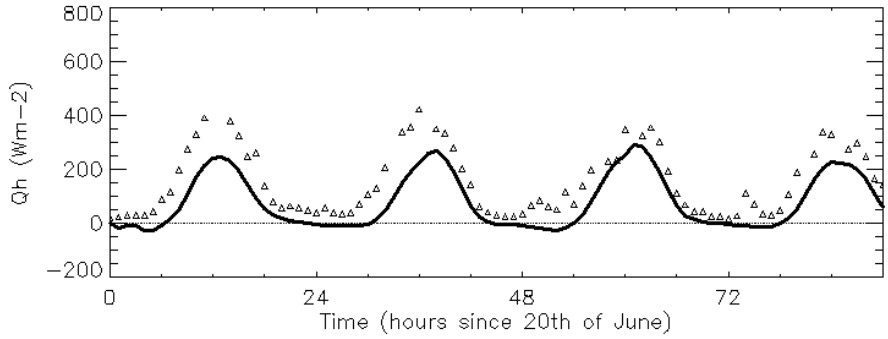

D.

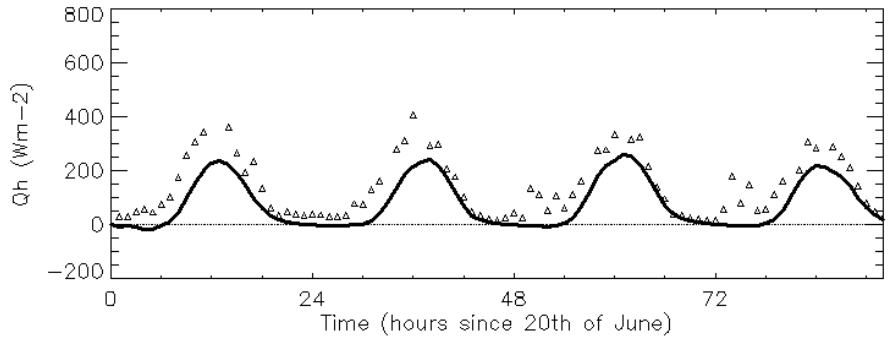

Figure 7.4: Continued.

Figure 7.4a, b, c and d represent simulated heat fluxes for Marseille Centre, Meyrargues, LAS1 and LAS2. The net all-wave radiation is estimated well for Meyrargues, with a MAE / RMSE of respectively 23.9 and 40.77 W m^{-2} averaged over all days (Table 7.4). For Marseille Centre, the RSME increases to 62.9 W m^{-2}, which is probably due to the high value of thermal inertia in the standard run of ARPS. Thereby, the surface temperature T_s doesn't increase fast enough in the morning, resulting in a too low T_s (and too high Q*), while in the afternoon T_s is too high (and Q* too low) by using the extreme low z_{oh} Brutsaert (1982) value (see also table 7.5). The simulated sensible heat flux for Marseille Centre is problematic, as it displays an RMSE of 97.05 W m^{-2} (Table 7.4), with a mean predicted sensible heat flux value, which is half of the observed (78.6 compared to 147.6 W m^{-2} respectively) over the whole period (Figure 7.4b). Also for the 2 LAS measurement points, the MAE / RMSE values show an error, which is of the same order of magnitude as for Marseille Centre. Whereas d has a value of 0.94 in the case of Meyrargues, it has values lower than 0.9 for all other urban measurement sites. Regarding the heat storage flux, we see an underestimation for Marseille Centre as well for Meyrargues with simulated / observed means of respectively 31.3 / -38.02 and 7.5 / 37.5. The difference in MAE and RMSE are of the same order of magnitude, which proof that those errors in heat storage flux by using the

RES method are not responsible for the variances in the sensible heat flux. Comparing these result with the more complex TEB-ISBA model setup, thereby using observed forcing to run in offline mode, results for the heat storage flux are of the same order of error magnitude with a RMSE of 66.2 and 71.1 for the complex TEB/ISBA scheme and our reference run respectively (Lemonsu et al., 2004; Mestayer et al., 2005).

Although these differences for the sensible heat flux can partly be related to the underestimation of the net incoming radiation by the model and uncertainties in the derivation of the heat storage flux, the model still doesn't capture a substantial part of the sensible heat flux. Contrarily, differences between the rural and urban measurement sites are very well captured by the lower sensible and higher latent heat fluxes for the rural station (Figure 7.4b). In general, simulated heat fluxes agree well with observations for Meyrargues, with a RMSE for the net incoming, the sensible and the latent heat flux of 40.8 W m^{-2}, 57.3 W m^{-2} and 42.7 W m^{-2} respectively.

To conclude this section, biases and RMSE values for temperature, wind speed and direction (Table 7.4) are in an acceptable range for the urban and rural stations, and the simulated surface energy balance reproduces well the measurements at the rural sites. In contrast, the simulation of the surface energy balance – and especially the sensible heat flux – of the urban station in the centre of Marseille is poor. As the simulated urban surface energy balance is strongly affected by the thermal roughness length as well as by the values used in the model for thermal conductivity and heat capacity, the following section will attempt to identify combinations of parameter values and z_{0h} parameterizations and thermal admittance as described in Section 7.2.3.1 and 7.2.3.2 respectively that yield better results compared to those obtained with the standard values used in the model and described in Section 7.2.1.

7.5 Sensitivity simulations

Table 7.5 shows the MAE, RMSE and R for the urban station of Marseille Centre and the 2 LAS measurement sites, for each of the different values for the thermal admittance μ and all thermal roughness parameterization schemes. Overall, simulations are in good agreement with observations, with correlation factors higher than 0.9, except for the Marseille Centre run with the lowest value for the thermal admittance (Table 7.5). Furthermore, it is clear that the Zilitinkivich et al. (1992) thermal roughness length parameterization scheme (equation (6)), in

combination with intermediate values for μ, gives the best results compared to the observations. Changing the value of the drag coefficient $Cd_0^{-0.5}$ from 5 to 9.5 (equation (4)) in the original Brutsaert (1982) scheme as suggested by Cahill et al. (1997) has a negligible effect on the sensible heat fluxes (RMSE difference of 2 Wm^{-2}, for all values of thermal admittance μ (Table 7.5). Furthermore, changing the values of $C_R^{-1}\,\mathrm{Pr}^{\lambda}$ and β from 6.2 and 0.25 to 4.31 and 0.247 respectively (equation (5)) in the original Brutsaert (1982) scheme, results in a better representation of the sensible heat flux for intermediate thermal admittance values (592.82 – 2213.1 J m^{-2} $s^{1/2}$ K^{-1}), with a maximum difference in MAE / RMSE of 17 W m^{-2}, for all urban measurement sites and a thermal admittance values of 1784.96 J m^{-2} $s^{1/2}$ K^{-1}.

For all urban measurement sites, the best results are obtained combing the Zilitinkevich et al. (1992) with a thermal admittance value of 1206.23 J m^{-2} $s^{1/2}$ K^{-1}. Sensible heat flux MAE / RMSE values decrease thereby with 8.2 / 12.2, 13.8 / 15.9 and 11 / 10.2 W m^{-2} for Marseille Centre, LAS1 and LAS2 respectively.

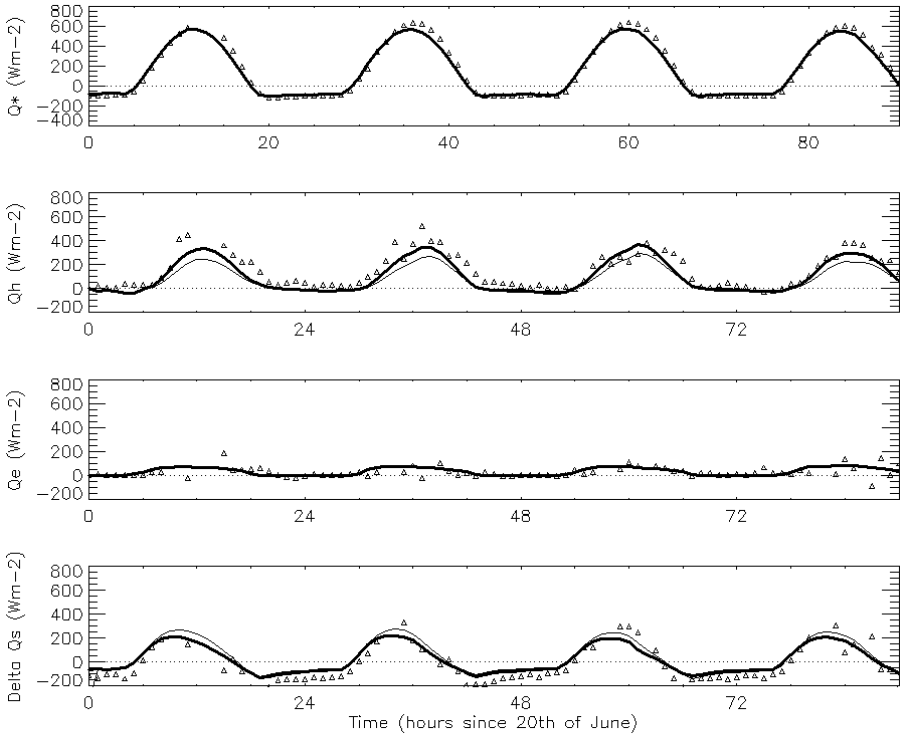

Figure 7.5: Observed (triangles), reference simulated (thin full line) and optimum Zilitinkevich (1992) - μ combination (bold full line) for net incoming radiation (Q*), sensible heat flux (Q_H), latent heat flux (Q_E) and storage heat flux (ΔQ_s) for Marseille Centre.

By using the Zilitinkevich et al. (1992) scheme and the thermal admittance value of 1206.23 J m^{-2} $s^{1/2}$ K^{-1}, not only the sensible heat flux improves, but this also has a positive effect on the modelled net incoming radiation and the air temperature (Table 7.6). The low Q* values in the standard run compared to the Marseille Centre observations (Table 7.4) improve with a decreasing MAE and RMSE of 5.32 and 9.32 W m^{-2}. Furthermore, the modelled air temperature improves with a RMSE and MAE of 0.5 °C for the Zilitinkevich et al. (1992) scheme combined with the thermal admittance of 1206.23 J m^{-2} $s^{1/2}$ K^{-1}. Using this combination of thermal characteristics, less heat is stored in the ground during daytime, resulting in a positive MAE / RMSE values difference between the selected optimum run and the reference run of 5.44 and 5.98 W m^{-2} (Figure 7.5). Although the RMSE heat storage flux in the new run changes to a value of 77.8 W m^{-2}, it is still of the order of magnitude of RMSE that is obtained using the complex TEB-ISBA scheme (Mestayer et al., 2005). This phenomenon is counteracted by an increase of 33.27 W m^{-2} for the sensible heat flux, using the new set of indices for thermal roughness length and thermal admittance. This increase is much larger than the decrease in ΔQ_S, which is also shown by the smaller MAE / RMSE values of 15.82 and –24.22 -W m^{-2} respectively. Although slightly higher, the RMSEs obtained by our simple model approach are comparable to the values obtained by Lemonsu et al. (2004) and Mestayer et al. (2005) using the complex TEB-ISBA model configuration (Table 7.7). Thereby, our configuration results in a more pronounced RMSE, for the net incoming radiation, sensible heat flux and storage heat flux. This is probably due to their more sophisticated TEB-ISBA schemes, thereby including radiation coming from roofs, walls and streets separately. Nevertheless, keeping in mind the simplicity of our approach, the small differences in RMSE for all fluxes supports the use of our configuration for a simple urban meso-scale model approach. Testing the LUMPS model of intermediate complexity (Grimmond and Oke, 2002) on the Marseille city dataset (see Appendix B) shows a lower RMSE for LUMPS for sensible heat, decreasing from 72.8 to 50.5 W m^{-2}. Furthermore, we obtain a similar value for latent heat (38.7 compared to 39.4 W m^{-2}) and an increase of RMSE for the storage heat flux from 77.09 to 97.7 W m^{-2} (Table 7.7), which is similar to the results obtained by Roberts et al. (2006), table 5 therein. A more detailed explanation on the drawbacks of LUMPS to simulate the storage heat flux is given in Roberts et al. (2006). As LUMPS is based on measured net-incoming radiation, and taking into account the fact that the LUMPS approach is more data demanding in terms of surface cover fraction and empirical parameters obtained from measurement campaigns, we remain confident in the usefulness of our method to simply approximate urban energy fluxes in a larger mesoscale setting.

Table 7.5: MAE, RMSE and R of the sensible heat fluxes [W m-2] for the sensitivity runs using different values of thermal admittance [J m-2 s1/2 K-1] and the different thermal roughness lengths parameterizations. Here, the best scores for all three stations are denoted in bold.

	Thermal admittance values																	
	341.17			592.82			1066.35			1206.23			1784.96			2213.1		
	MAE	RMSE	R	MAE	RMSE	R	MAE	RMSE	R	MAE	RMSE	R	MAE	RMSE	R	MAE	RMSE	R
Marseille Centre																		
Brutsaert (1982)	67.97	83.59	0.89	67.74	83.37	0.90	68.04	84.50	0.92	69.3	86.96	0.92	73.71	94.50	0.93	77.75	101.59	0.93
Brutsaert (1982) - Var1	67.31	82.85	0.63	67	82.28	0.90	66.78	82.70	0.92	67.92	85.03	0.92	72.06	92.03	0.93	76.03	99.25	0.93
Brutsaert (1982) - Var2	67.40	84.11	0.88	65.22	80.75	0.89	61.48	75.00	0.92	61.92	76.00	0.92	63.67	79.46	0.93	66.93	85.42	0.93
Zilitinkevich (1992)	70.04	86.92	0.55	66.71	82.37	0.89	60.45	73.24	0.92	59.74	72.83	0.92	60.41	74.04	0.93	62.326	78.40	0.90
Scintillometer - LAS1																		
Brutsaert (1982)	63.40	69.49	0.96	66.03	71.71	0.96	70.35	77.98	0.96	72.28	80.90	0.95	78.22	91.78	0.94	83.21	99.97	0.93
Brutsaert (1982) - Var1	62.42	68.95	0.96	64.63	70.39	0.96	68.77	67.04	0.96	70.64	78.84	0.96	76.46	89.59	0.94	81.46	97.72	0.93
Brutsaert (1982) - Var2	59.96	68.43	0.96	60.06	66.72	0.96	59.23	65.79	0.96	60.85	67.31	0.96	64.95	74.78	0.95	69.55	81.80	0.94
Zilitinkevich (1992)	61.00	71.37	0.96	59.47	67.92	0.96	56.86	62.99	0.96	56.85	62.91	0.96	59.36	67.61	0.95	62.81	73.01	0.95
Scintillometer – LAS2																		
Brutsaert (1982)	51.05	60.57	0.95	52.66	61.85	0.95	56.93	67.34	0.94	59.44	69.82	0.94	65.97	79.01	0.92	71.14	86.10	0.91
Brutsaert (1982) - Var1	50.46	60.25	0.95	51.66	61.03	0.95	55.25	65.85	0.94	57.64	68.20	0.94	64.22	77.18	0.92	69.43	84.21	0.91
Brutsaert (1982) - Var2	52.69	63.61	0.95	50.59	60.90	0.95	48.00	59.22	0.95	49.03	60.01	0.95	52.61	66.00	0.93	58.09	71.66	0.92
Zilitinkevich (1992)	56.54	67.52	0.95	52.85	63.37	0.95	47.35	58.05	0.95	46.58	57.98	0.95	48.31	61.00	0.94	51.23	65.09	0.93

Table 7.6: Resulting changes in $\overline{P}$, S_p; S^2_p, MAE, RMSE and R for [Zilitinkevich et al. (1992), μ = 1206.23] – [Reference run] for Marseille Centre station.

	$\overline{P}$	S_p	S^2_p	MAE	RMSE	R
T (°C)	-0.09	0.03	0.01	-0.05	-0.05	0.01
FF (m s^{-1})	0.24	0.01	0.00	0.04	0.06	0.04
DD (° from N)	1.58	0.22	3.24	2.42	1.84	0.00
E (hPa)	-0.09	0.01	0.01	0.08	0.09	-0.02
Q* (W m^{-2})	16.76	0.29	15.22	-5.32	-9.32	0.01
QH (W m^{-2})	33.27	5.15	133.41	-15.82	-24.22	-0.01
QE (W m^{-2})	0.90	0.09	0.58	0.60	0.61	-0.01
ΔQs (W m^{-2})	-11.10	-2.56	-71.12	5.44	5.98	-0.02

Table 7.7: RMSE comparison between our results, results from the complex TEB-ISBA using a single urban class (Lemonsu et al., 2004), and various urban classes (Mestayer et al., 2005) and results from LUMPS (Grimmond and Oke, 2002 – see appendix B).

	RMSE Our results	RMSE (Lemonsu et al., 2004)	RMSE (Mestayer et al., 2005	RMSE LUMPS
Q* (W m^{-2})	53.6	30	28.8	-
Q_H (W m^{-2})	72.8	63	61.2	50.5
Q_E (W m^{-2})	38.7	42	42.3	39.4
ΔQs (W m^{-2})	77.9	66	66.2	97.7

7.6 Discussion and conclusion

Measurements from the urban station Marseille Centre and the rural stations Meyrargues and Trets, obtained during the ESCOMPTE campaign Intensive Observation Period IOP2a, were used for the evaluation of the mesoscale meteorological ARPS. The model was run for the period 20 to 23 June 2001, for a domain covering the Marseille Berre-Pond Region. The ARPS-LAICa model system was run in a three-nested way, using 6 hourly initial and boundary conditions from the operational ECMWF reanalysis data. Moreover, as suggested by many authors (Taha, 1997, Sailor and Lu, 2004; Kato and Yamaguchi, 2005; Makar et al., 2006; Offerle et al., 2006 and many others), an estimate of anthropogenic heat based on measured CO_2 emissions and energy consumption by households and services, also taking into account CO_2 uptake by plant respiration,

has been included as waste heat in the land-surface scheme. The simulated temperature, wind speed and direction were evaluated using hourly measurements from the urban and rural stations, showing that ARPS is capable of reproducing diurnal cycles of temperature, wind speed and direction and water vapour as well for urban as for rural areas. For all parameters, modelled versus simulation errors are within the defined error limits based on air quality modelling purposes. Subsequently, simulated surface heat fluxes were confronted with measurements from Marseille Centre, Meyrargues and two LAS observation sites. Overall, the simulated fluxes agreed with the measurements fairly well, except for the sensible heat flux over the centre of Marseille and the LAS sites, which were largely underestimated.

In order to address this discrepancy, sensitivity simulations were executed in order to test the impact on the simulated sensible heat flux over urban portions of the domain with respect to different thermal roughness length parameterizations and various thermal surface parameter values. The analysis of these sensitivity simulations showed that the Zilitinkevich et al. (1992) thermal roughness length parameterization scheme, in combination with intermediate values for thermal admittance (μ = 1206.23 J m^{-2} $s^{1/2}$ K^{-1}), gives the best results compared to the observations. This value is confirmed by a study done by Hafner and Kidder (1999), who used thermal channel 4 and 5 to acquire thermal inertia for a model domain covering Atlanta. Thereby, they obtain a thermal admittance value for the inner Atlanta city between 1200 and 1400 J m^{-2} $s^{1/2}$ K^{-1}, which corresponds with our sensitivity results.

These findings are dissimilar to results previously obtained by De Ridder (2006), who found the Brutsaert (1982) parameterization to perform well for the city of Paris. Note though, that in the latter study use was made of instantaneous (at around 14:00 local time) remotely sensed surface temperature for comparison with the simulation. It could well be that the Brutsaert parameterization which yields extremely low values of z_{0h}, in combination with a rather high thermal admittance, correctly generates observed surface temperatures at that particular time of the day. However, also Voogt and Grimmond (2000), using helicopter- and ground-based measurements on an urban quarter in Vancouver, found their analysis to agree well with observations when using Brutsaert's parameterization. Also note, that the findings of this study are representative for the simulation specific characteristics, namely the Marseille Berre-Pond Region and a week in June 2001, governed by a high pressure system without rain. Clearly, more research is required to settle this for other regions or cities and time periods. Nevertheless, a similar study has been performed for the Paris agglomeration,

whereby the same set of parameterizations and a similar set of thermal admittance values have been tested. Surface temperature derived from the SEVIRI instrument on the Meteosat Second Generation platform is compared with modelled surface temperatures. Here, also the Zilitinkevich (1992) parameterization was shown to provide the best results, in combination with a thermal admittance value of similar magnitude (K. De Ridder – personal communication). This results shows that our study is not only valid for Marseille, but also for other dense European cities.

To investigate the main factors controlling urban heat islands and air dispersion on the mesoscale, the difference of the surface energy balance between rural and urban surfaces has to be determined (Hafner and Kidder, 1999). This study has shown that the ARPS-LAICa model setup is able to satisfactory simulate the flux differences between urban and rural areas, especially by using the thermal roughness length parameterization of Zilitinkevich (1992) and a thermal admittance value μ of 1206.23 J m^{-2} $s^{1/2}$ K^{-1}. Moreover, comparisons with more complex models as the TEB/ISBA scheme over the same terrain (Mestayer et al., 2005) shows that using this simple approach, same magnitude of flux errors compared to observations are obtained. Moreover, comparison to a study done by Lemonsu et al. (2004) shows that our simple model set-up generates results for the surface fluxes (in terms of RMSE) similar to that of TEB-ISBA using a single urban class as defined in the CORINE land cover classification (as used in this study) over Marseille. Although LUMPS seems to perform better on the sensible heat flux, one has to keep in mind that this scheme is more complex while additional surface properties are needed to calculate the surface energy fluxes, which is not necessary in our approach. Furthermore, using assumptions for some parameters, as shown in Appendix B, it is still not clear if the empirical parameterizations contained therein can be used in general, and could be used to implement in any NWP model to include urban areas in a simple way over a randomly chosen area.

In the framework of air dispersion modelling, the complex geometry of an urban area makes the modelling within the street canyons difficult, although it is the venting of these street canyons that is important for determining air pollution concentrations. For numerical weather prediction (NWP) models, restrictions on the resolution of the model mean that the cities are often poorly resolved. These restrictions are due to limits on the available computing resources, and the required narrow timeliness of the forecasters providing their data to the community. The resource and timing issues also have implications for the complexity of the model, since more complex models increase the computational cost and hence the time taken to integrate the model (Best, 2005). In this aspect,

some mesoscale modelling studies have been undertaken including urban land cover characteristics. But often, these models have typically a high resolution in which the city is well resolved. In this study, we have followed a simple approach to model the exchange between an urban surface and the atmosphere. For the materials used in the downtown city of Marseille, it appeared that the thermal roughness length parameterization from Zilitinkevic et al. (1992) and a value for the thermal inertia of 1206.23 J m^{-2} $s^{1/2}$ K^{-1} are appropriate. For densely constructed old cities (as is already shown for Paris) we expect similar values to be adequate, for the use in simple mesoscale land surface schemes.

Appendix

A. Estimation of the anthropogenic heat

A.1Traffic

The anthropogenic heat release from traffic (Q_{Fv}), is calculated based on relations between combustion of gasoline/diesel, CO_2 emissions and energy release. Thereby, the resulting CO_2 emission per produced unit of energy from the combustion of gasoline/diesel corresponds to 70g CO_2 per MJ energy (revised 1996 IPCC Guidelines for National Greenhouse Gas Inventories), so that a CO_2 flux of 0.001 g m^{-2} s^{-1} corresponds to 14.3 W m^{-2}. Figure 3.10 (upper panel – calm winds) from Grimmond et al. (2004) shows CO_2 fluxes in µmol m^{-2} s^{-1}; with one mol CO_2 corresponds to a molecular mass of 44 g, so that 1 µmol m^{-2} s^{-1} corresponds to 44 10^{-6} g m^{-2} s^{-1} CO_2. Combining these previous steps results in an energy flux from traffic of 6.3 W m^{-2} per 10 µmol m^{-2} s^{-1} CO_2. Following the CO_2 flux measurements of Grimmond et al. (2004), the diurnal CO_2 flux values range from 10 µmol m^{-2} s^{-1} during the night to 30 µmol m^{-2} s^{-1}, which corresponds to a range of Q_{Fv} between 6.3 (night) to 18.9 W m^{-2} (day). To determine hourly energy flux values from traffic it is then fitted (within its measurement errors) to the diurnal evolution of the measured CO_2 flux, resulting in a traffic induced anthropogenic heat of 5.3 W m^{-2} between 20h – 5h GMT, a linear increase (decrease) between 5h – 8h GMT (18h - 20h GMT) from 5.3 W m^{-2} to 18.9 W m^{-2} and a constant flux between 8h – 18h GMT of 18.9 W m^{-2}, resulting in a daily mean of 12.3 W m^{-2}.

In the above analysis, the CO_2 originating from vegetation is disregarded. The absorption of CO_2 by vegetation during the day results in a negative (downward) CO_2 flux, which should be taken into account while interpreting the CO_2 measurements of Grimmond et al. (2004) to obtain the “pure” traffic signal.

Therefore we use the water use efficiency, which returns the amount of assimilated CO_2 per kg evaporated water. From the observed daytime peak in latent heat flux (70 W m^{-2}) the water mass flux is calculated, yielding a value of 0.028 g m^{-2} s^{-1}. Under a pressure P of 1010 hPa (Grimmond et al., 2004) and a specific humidity q of 8 g kg^{-1} (Mestayer et al., 2005), the vapour pressure e amounts to 13 hPa. This results in a vapour pressure deficit (VPD) of 20 hPa (Oke, 1987). Under such a vapour pressure deficit, water use efficiency is typically of the order of 3 mg CO_2 per g H_20 (Mahrt and Vickers, 2002). This results in a CO_2 flux of 0.084 mg CO_2 m^{-2} s^{-1} for 0.028 g m^{-2} s^{-1} water flux, corresponding to a correction to the anthropogenic heat flux of 1 W m^{-2}, which is negligible. Nighttime respiration should also be taken into account, but as daytime assimilation exceeds nighttime respiration, this term is also negligible (Oke, 1987).

As there are no observations to adopt and validate these values as a formal result, one can look for an entirely different method to check the order of magnitude of these results. Therefore, the method proposed by Makar et al. (2006), also successfully used in Van Weverberg et al. (2007) to estimate anthropogenic heat in Brussels, is used to make an independent approach of the anthropogenic heat flux from traffic in Marseille. Based on satellite-based anthropogenic light irradiance, together with a spatial dissagregation approach as described in Makar et al. (2006), one obtains an annual average anthropogenic heat flux for Marseille amounting to 28.8 W m^{-2} (see www.iiasa.ac.at/Research/TNT/WEB/heat/). Using the ratio of energy from traffic from the Energy Yearly statistics from (http://epp.eurostat.ec.europa.eu/portal/page?_pageid=1073,46587259&_dad=portal&_schema=PORTAL&p_product_code=KS-CN-04-001-3A) Eurostat for France 2001, we can estimate that traffic accounts for 43.3% of the energy released. From that, a daily mean value of Q_{Fv} mounts up to 12.3 W m^{-2}, which confirms our daily mean estimate of 12.3 W m^{-2}.

A.2 Electricity

Next to traffic, also households (heating, air conditioning…) are a source of anthropogenic heat. To estimate the amount of heat released from the households & service sector, we use the ratio energy use traffic / energy use households & services from Eurostat for France 2001, which returns an energy use for traffic of 43600 TOE (tonnes of oil equivalent) and for households & services of 21400 TOE, resulting in a ratio of 0.49. These are annual mean values, so a simplification of this method includes the assumption that this ratio is not

dependent on seasons. From the ratio 0.49, daytime heat release from households results in 6.3 W m^{-2}. Q_{Fh} is kept constant during the daily cycle.

A.3 Conclusion

The total anthropogenic heat flux of 18.6 W m^{-2} is calculated for the CAAM site using the CO_2 fluxes measured by Grimmond et al. (2004). Following Lemonsu et al. (2004) and Hamdi and Schayes (2005) the plan area of vegetated surfaces per total plan area for this urban measurement site adds up to 14%. By multiplying 18.6 W m^{-2} by 0.86, an estimated daily mean of total Q_F of 21.7 W m^{-2} for a 100% total urban area is obtained. The diurnal variation of the anthropogenic heat flux can be seen in figure A.7.1. For our mesoscale modelling purpose, the total amount of Q_F is added to the simulated turbulent sensible heat, in proportion to the percentage vegetated cover fraction for each urban grid cell.

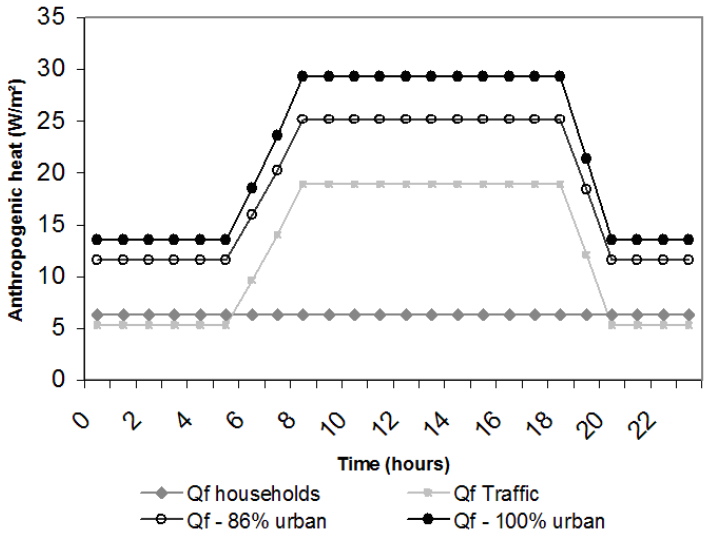

Figure A.7.1: Anthropogenic heat in Marseille for the summer 2001, divided in anthropogenic heat for households & services and anthropogenic heat for traffic.

Although a direct comparison with other estimates is difficult, our approach results in an anthropogenic heat flux value similar to the values obtained by Pigeon et al. (2007) for Toulouse, a French city with comparable characteristics as Marseille (Grimmond et al., 2004). They calculate an anthropogenic heat flux for the local scale and the scale of the agglomeration as the residual of the SEB equation and from the energy consumption inventory respectively, resulting in a value for summer between 15 and 30 W m^{-2} respectively.

Sailer and Lu (2004) proposed a top-down approach for anthropogenic heat based on the energy consumption in the building sector, transportation sector and metabolism. Thereby, each component is a function of the cities' population density. From this point of view, Marseille (density: 3400pers/km²) can be compared to the results from Los Angeles, which has a summer diurnal value of anthropogenic heat between 10 and 30 W/m² (Sailer and Lu, 2004 – figure 6 therein), which is similar Q_F obtained by our approach (Figure A.7.1).

B. Calculation of the Surface Energy Budget using LUMPS (Grimmond and Oke, 2002)

Although mentioned in Mestayer et al. (2005), LUMPS (Local-scale Urban Meteorological Parameterization Scheme) (Grimmond et Oke, 2002) has not yet been tested for Marseille, using the ESCOMPTE dataset. In order to be able to compare our simple approach to the results from LUMPS, we use the observation done by Grimmond et al. (2004) to calculate all fluxes. A full explanation of LUMPS is given in Grimmond and Oke (2002), and hereby, only a short description of its configuration is given.

The heat storage by the urban fabric is parameterized from net all-wave radiation and surface cover information using the objective hysteresis model (OHM) (Grimmond et al., 1991):

$$\Delta Q_s\ [W\ m^{-2}] = \sum_{i=1}^{n}(f_i a_{1i})Q^* + \sum_{i=1}^{n}(f_i a_{2i})\frac{\delta Q^*}{\delta t} + \sum_{i=1}^{n}(f_i a_{3i}) \qquad \textbf{(B.1)}$$

where, i is one of n surface types of varying fraction (f), such as roofs, walls, lawns, or roads. The time derivative of net radiation is approximated as $0.5(Q^*_{t+1} - Q^*_{t-1})$, with t in hours, and the a coefficients empirically derived from independent studies specific on urban surface types. In our approach, four surface types (gravel roof, clay tile roof, impervious ground and vegetation - no water in the city center) for the Marseille city center are taken into account (Roberts et al., 2006), whereby the appropriate source area locations and surface weightings are calculated hourly with a flux footprint model, in combination with an urban geographic information system (S. Grimmond personal communication) (Table B.7.1). The coefficients for $a_{1,2,3}$ are taken from Roberts et al. (2006) (their Table 1).

The turbulent sensible and latent heat fluxes are calculated using the parameterizations proposed by de Bruin and Holtslag (1982) and mentioned in Grimmond and Oke (2002):

$$\Delta Q_H\ [W\,m^{-2}] = \frac{(1-\alpha)+(\gamma/s)}{1+(\gamma/s)}(Q^*-\Delta Q_s)-\beta \qquad \textbf{(B.2)}$$

$$\Delta Q_E\ [W\,m^{-2}] = \frac{\alpha}{1+(\gamma/s)}(Q^*-\Delta Q_s)+\beta \qquad \textbf{(B.3)}$$

where s is the slope of the saturation vapor pressure versus temperature curve, γ is the psychrometric 'constant', $\beta=3$ an empirical parameter taken from Grimmond and Oke (2002) and α is based on the land cover and the land cover characteristics as proposed in Grimmond and Oke (2002). The values for s and γ are calculated based on hourly observations of air temperature (K), vapor pressure (hPa) and pressure (hPa).

Table B.7.1: OHM empirical coefficients for Marseille Centre.

	a1	a2	a3
Gravel roof	0.26	0.89	-24
Tile roof	0.07	0.06	-5
Road (impervious)	0.7	0.41	-0.38
Vegetated	0.32	0.54	-27.4
Water	0.5	0.21	-39.1

Using formulas B1, B2 and B3, based on the observations from the measurement tower on the CAA roof top (Grimmond et al., 2004), some empirical parameters and additional information on the fraction of the land cover, all fluxes are derived from the net radiation on an hourly basis. Anthropogenic heat is not additionally included, but implicitly included since LUMPS is based on measured fluxes, as mentioned in Grimmond and Oke (2002).

Chapter 8

General conclusion and outlook

In this dissertation, three main goals are tackled: 1) to describe the relations between meteorological variables and O_3 and PM_{10} levels in a present-day climate, 2) to use this information in developing a statistical air-quality downscaling tool that considers the combined effect of the large-scale atmospheric circulation and surface meteorology and 3) to calibrate and validate this methodology for the present-day climate using observations. Afterwards, this approach is used to make a first estimate of the impact of a possible future climate change on air quality.

In general, a downscaling approach is followed to bridge the gap between what AOGCMs produce and what impact assessors require. The first four chapters of this dissertation focus on a statistical downscaling approach, which is computationally more efficient and in general more practical compared to a dynamical downscaling approach. Thereby, chapters 3 and 4 describe the role of the individual surface meteorological variables on present-day levels of O_3 and PM_{10} and the development of a synoptic-regression based tool to derive present-day O_3 and PM_{10} levels. Chapter 5 provides more insight in the influence of changing circulation patterns in a future climate and finally, chapter 6 applies the synoptic-regression tool to estimate future trends in surface O_3 concentration. In addition, chapter 7 performs a first step of model improvement relevant for dynamical downscaling used to model air quality concentrations.

8.1 A novel synoptic-regression based tool for downscaling of air quality

Prior to the construction of the statistical downscaling tool, a comprehensive correlation study is conducted between all meteorological and air quality variables using observations from a rural background stations in The Netherlands. In general, a clear relation is found between O_3 and (maximum) temperature in summer, combined with a low relative humidity. Rain amount is negatively correlated with PM_{10} in winter, which could point out atmospheric removal due to wet deposition. Wind speed is strongly negative correlated with O_3 and PM_{10} for large parts of the year, pointing to stable conditions without strong advection and a built-up of species in the boundary layer.

This quantitative information is used to develop two statistical downscaling approaches: 1) a multiple linear regression analysis, often used in short-term air quality forecasts, and 2) the Lamb circulation pattern classification method. The former method is run in 2 modes, viz. with and without air quality variables as predictors, as AOGCMs do not explicitly hold information on future emission (precursor) levels. The latter method provides daily circulation patterns based on geostrophic flow and vorticity indices derived from reanalyzed or operational ECMWF mean sea level pressure in sixteen grid points centered on the Cabauw measurement station. By selecting these methods, we seek simplicity, linearity and practical feasibility of the models in order to make this approach appropriate for downscaling forecasted meteorological fields or AOGCMs scenarios for air quality purposes. Comparing the results of this local-meteorology based approach with results from a circulation point-of-view, which takes into account the large-scale circulation above our area of interest, provides further insight in the controlling processes forming and resulting in representative O_3 and PM_{10} levels for rural background stations at mid-latitude sites.

First, a preliminary analysis has been performed to test whether different rural sites in The Netherlands show similar characteristics in terms of air quality and meteorology. Based on similar annual cycles for both O_3 and PM_{10} and the minor differences between the meteorological and air quality relationships at all sites, the analyses provides solid arguments to consider the Cabauw station as representative for rural areas in The Netherlands. Moreover, this decision is justified because of the fact that Cabauw has the largest data availability, necessary as input for the statistical downscaling approach.

Based on the Cabauw measurements, the multiple linear regression model in two modes provides reliable results, especially for O_3, outperforming both the climatology and persistence models. The statistical performance is good in comparison to similar studies for both the calibration (2001-2004) and the validation (2005-2006) period. In general, including information on the

previous-day air quality predictor variables improves the explained variance with 10 to 18% for ozone and PM_{10} respectively. From the relation between the large-scale circulation patterns and high (low) pollution events, some clear physical links can be seen. Thereby, all relations between pressure, wind speed, temperature and relative humidity and levels of O_3 and PM_{10} found in the comprehensive correlation analysis can be retrieved from the seasonal composite circulation patterns and their anomalies. For O_3, the surface pressure composite maps generally show an anomalous strong high-pressure system north or west of the measurement station, depending on the season. This results in cold and humid (winter and spring) and warm and dry (summer) air advected from north to east wind directions, contributing to higher than normal ozone concentrations. Using the circulation patterns for ozone in winter reveals the highest average concentration in wind direction from west to north, under high wind speed circumstances. This feature suggests the influence of ozone transported from the free troposphere towards the surface in winter, which was also suggested by Davies et al. (1992b) and Delcloo and De Backer (2008). For PM_{10}, high levels are overall controlled by air advected from south to east. Hereby, pressure gradients are often low, with a positive pressure anomaly north- to eastwards from the measurement station, again depending on the season.

Finally, the reconstruction of the O_3 and PM_{10} time series for the calibration and validation period objectively compares the multiple stepwise regressions and the objective Lamb circulation pattern approach. The stepwise regression for O_3 performs satisfactory for all statistical indices. Contrarily, although seasonal composite maps have shown a distinct pattern for typical episodes of high average O_3 and PM_{10} concentrations, the Lamb circulation patterns as a short-term air quality forecast model performs poor for both O_3 and PM_{10}, whereby the skill score against persistence (one-day lag) is, in some situations, even worse than persistence itself. Although circulation patterns can provide a clear insight in typical large-scale atmospheric structures and associated anomalies in meteorological variables during high (or low) pollution events, this approach is not able to capture short-term fluctuations of the pollutants.

In a next step, O_3 and PM_{10} levels are explained using a combination of a linear multiple regression and a circulation-type approach. This analysis, based on the same above-mentioned calibration and evaluation periods, reveals that a stratification of the dataset using the automated Lamb circulation pattern scheme, prior to the regression analysis improves the downscaling results for O_3 and PM_{10} in terms of explained variances and skill score against the persistence model. For O_3, this approach is shown to be beneficial for representing higher-order statistical moments (e.g. skewness and kurtosis). In contrast, the synoptic-regression approach using only meteorology data was found insufficient to explain the observed PM_{10} variability. Thus, this suggests that for PM_{10}, other

meteorological variables not available for this study (e.g. boundary layer height) and local or long-range emissions (and emission sources) could play a more important role. Therefore, the remaining of this analysis will only deal with projections of future O_3 concentrations derived from an AOGCM. Moreover, as O_3 is highly dependent on seasonal changes in its relations with meteorological predictors, the O_3 regression model is run in a seasonal mode.

Prior to using the synoptic-regression based tool for downscaling of air quality levels from coarse AOGCM-output (with a typical resolution of 300 x 300 km^2), it needs to be tested whether the observed local relations between meteorological and air quality variables hold on a larger scale. Hence, the statistical downscaling tool is evaluated using low-resolution ECMWF data interpolated on the spectral T63 horizontal grid (similar to the ECHAM5-MPI/OM resolution) for the period 2005-2006. Using this data as input for the regression-based models leads to a slight decrease of the explained variance due to a lower variability of the meteorological predictors and model biases. Nevertheless, this approach can compete with other dynamical and statistical downscaling methods, which are often employed using observed time series, without being tested on low-resolution gridded data.

In a last step, the synoptic-regression based approach is applied on future ECHAM5-MPI/OM data in order to make estimates of future O_3 levels for the mid-latitude site of Cabauw. Thereby, explanatory meteorological predictor variables are taken from ECHAM5-MPI/OM for the present-day 1991-2000 period and 2 future periods 2051-2060 and 2091-2100 from three SRES scenarios A2, A1B and B1. As any information on biogenic and anthropogenic emissions is not explicitly taken into account, this research solely includes the influence of changes in meteorological variables, without taking into account future levels of biogenic and anthropogenic emissions.

The circulation pattern frequencies derived from ECHAM5-MPI/OM for the period 1991-2000 do not differ significantly compared to the reference circulation pattern frequencies. Moreover, the monthly frequency distribution over all patterns also does not differ significantly, except for the month of February. This allows a straightforward evaluation of the present-day and future downscaled versus observed O_3 levels in terms of the meteorological variables important for high ozone concentrations. Although the capabilities of the downscaling method on coarse-resolution data is tested extensively, the downscaled O_3 levels from ECHAM5-MPI/OM meteorological predictors are still underestimated compared to the observed concentrations for the present-day evaluation period of 1991-2000 (see section 8.3). Therefore, a bias correction

method is applied that takes into account the differences between the ECHAM5-MPI/OM downscaled O_3 and observed O_3 distribution quantities.

Under the various SRES scenarios, the overall maximum 8 hourly mean O_3 concentration increases with 2.5 to 6.5 µg/m³ and 6.1 to 10.9 µg/m³, for the 2051-2060 and 2091-2100 period respectively, against the present-day 10-year average of 55.2 µg/m³. This effect is enhanced when considering the summer season only, with a range of increase between the different future scenarios of 5.4 to 12.5 µg/m³ and 13.4 to 26 µg/m³ (for 2051-2060 and 2091-2100 respectively) against a present-day summer average of 73.5 µg/m³. An increase in maximum temperature and shortwave radiation, associated with a decrease in cloud cover under the various future scenario assumptions are the main drivers of ozone increase.

In order to verify whether these findings are physically plausible, our results are compared with the observed heat wave in August 2003, characterized by a poor air quality (especially in terms of O_3) and excess of mortalities in large parts of Western and Central Europe. In this respect, the summer of 2003 has been cited and shown in our analysis to be an example of how future European summers may look like under a changing climate. As observed in 2003, the increase in ozone in a future climate can pose a serious threat to human health and the natural environment in Western Europe. And although our results are from one individual AOCGM only, most other global models are in line with the projected conditions that are used here. It should, however, be noted that by taking into account only one GCM, the range of uncertainty might be underestimated. Therefore, a future task lies in the application of this tool on multiple AOGCMs and SRES climate scenarios (ENSEMBLES). This could provide a more in-depth understanding of future O_3 variability under different models and scenarios, creating the possibility to present more robust lower and upper boundaries of possible O_3 concentrations, comparable to the IPCC projections of future temperature levels and precipitation amounts.

8.2 Limitations of the synoptic-regression based approach

Section 8.1 descris how the synoptic-regression based approach is developed and to what extent it can be applied to estimate future O_3 concentrations for rural mid-latitude areas in The Netherlands. In the course of the above-mentioned analyses, we specifically mentioned the weaknesses (e.g. loss of the observed explained variance for a multiple regression, as referred to in Table 2.1) and strengths (e.g. easy physically interpretable, a valuable diagnostic tool for AOGCM evaluation) of the used methods. Nevertheless, it is worth mentioning

some additional limitations of the entire strategy (synoptic-regression based statistical downscaling) in order to put this research in a wider perspective.

As mentioned in the introduction, this dissertation follows a downscaling approach to bridge the gap between the information gained from AOGCMs and the (local-scale) information required by the impact assessors. Whereas the dynamical downscaling techniques are computationally expensive and time consuming, statistical downscaling is a computationally more efficient and practical approach in addressing the current needs of high-resolution climate modelling results for impact and assessment studies. From a physical point-of-view, the dynamical approach dynamically derives spatially distributed local (or regional) atmospheric variability from large-scale AOGCM forcing. Hence, the model itself resolves the physical properties of the atmosphere. In contrast, the statistical approach developed here derives quantitative relations between large-scale circulation indices and local climate or environmental variables from observations using statistical relationships. As a consequence, the latter is, in first instance, limited to the area for which the transfer functions are derived. Although our analysis shows that rural areas can be considered as spatially homogeneous in terms of air O_3 and PM_{10}, as is shown by Flemming et al. (2005), it does not provide a straightforward solution for other land covers (surban, urban, …). A possible strategy for this concern is addressed in appendix C.

Secondly, our statistical approach assumes that the present-day meteorology - air quality relations remain constant in the future. Nevertheless, the rates of the chemical reactions that form ozone are temperature-dependent, and will proceed more rapidly in a warmer environment. Also a decrease in relative humidity together with an increase of the photolysis rate, due to a decrease in cloud cover (Meleux et al., 2007), could lead to a lower production of OH radicals. Moreover, photolysis of ozone produces an oxygen atom which can either reform ozone via reaction with oxygen molecules or produce OH radicals via reaction with water vapor, the latter representing a sink for ozone. It is clear that these complex reactions cannot be solved by our statistical downscaling approach, as mentioned in Chapter 6. In this respect, (global) chemistry transport models provide a promising (albeit at present considerably more computationally expensive) tool for future air quality assessment studies. This is further addressed in section 8.4.

Climate change also has an indirect effect on future ozone concentrations. E.g., forests, shrubs, grasslands, and other sources of natural hydrocarbons (VOCs) emit greater quantities at higher temperatures. Soil microbial activity may also increase with warmer temperatures, leading to an increase in NO_x emissions. These higher natural emissions of VOCs and NO_x could lead to an increase in

tropospheric O_3. A further impact is through the increase of NO_x from lightning. While lightning is not a significant source of NO_x over industrial regions, it forms ozone over remote regions of the globe, thus contributing to the background concentrations of ozone. On the other hand, climate change could reduce O_3 concentrations. For example, a more vigorous hydrologic cycle could lead to an increase in cloudy days. More cloud cover, especially in the morning hours, could diminish reaction rates and thus lower O_3 formation. Moreover, future anthropogenic emissions are another source of uncertainty. To some extent, this is indirectly taken into account using meteorological information from the AOGCMs driven by future SRES scenarios. Nevertheless, the above-mentioned features are hard to cope with in statistical downscaling approaches, as the latter cannot take into account these (natural) changes in emissions because of constant air-quality and meteorology transfer functions that are based on present-day information. Nevertheless, these changes are not straightforward to implement in dynamical downscaling techniques as e.g., although explicitly resolving physical-chemical processes, a great deal of uncertainty exists at present with respect to the hydrological cycle and the effect of vegetation dynamics in (global) chemical transport models.

Because many (natural and anthropogenic) aspects of the earth system affect air quality, and most of these have been held constant in downscaling studies, the results of these studies should not be considered predictions of future air quality levels associated with climate change. Rather, they demonstrate the sensitivity of atmospheric air pollutants to changes in (in this study) specific meteorological variables. In this respect, the statistical method provided here remains relevant in the future air quality debate because of its simplicity, physical interpretability and computational efficiency. The latter is further addressed in section 8.5.

8.3 A need for AOGCM improvement

During the statistical downscaling analysis using low resolution meteorological variables and circulation patterns from operational ECMWF and future SRES ECHAM5-MPI/OM scenario data, it became clear that, next to the importance of the resolution, also deficiencies in the models play an important role in the correct representation of present-day downscaled O_3 compared to observed O_3 records. In first instance, model deficiencies appear in terms of a lower variability of the ECMWF and ECHAM5 meteorological variables compared to the observed variables. At present, confidence in climate models is founded in accepted physical principles and from their ability to reproduce observed features of current climate and past climate changes, particularly at continental scales and above. This confidence in model estimates is higher for some climate variables (e.g., temperature) than for others (e.g., precipitation), and for large-

scale feature compared to small-scale processes, which cannot be represented explicitly by the models (Randall et al., 2007). This explains why the mean properties of a specific variable are often well reproduced while significant discrepancies can be found in the tails of the variables' distribution functions. Precisely these statistical properties are important in air quality research and hence explain the discrepancies in some of the ECMWF and ECHAM5-MPI/OM surface meteorological variables found in this dissertation.

Secondly, significant differences were found in terms of ECHAM5-MPI/OM circulation pattern frequencies compared to the observed frequencies, especially in summer over the 40-year reference period (1961-2000). This is derived from the application of the objective Lamb classification method on a 40-year 20th Century control run (1961-2000) of the ECHAM5-MPI/OM model for Western and Central Europe, evaluated using the reference ECMWF-ERA40 reanalysis data. In general, ECHAM5-MPI/OM is able to reproduce the frequencies in directional circulation types, especially for the late autumn, winter and early spring period. For late spring, summer and early autumn of this 40-year period, significant differences are found for most of the directional types. In particular western types are significantly overestimated by ECHAM5-MPI/OM, while eastern types are underestimated. In contrast, these differences in frequencies are shown to be insignificant for the more recent 10-year period (1991-2000). This discrepancy is elaborated in more detail in Appendix B of this dissertation, whereby it is shown that differences in frequency occurrences between objective Lamb weather types are due to a large sensitivity of the circulation patterns to the grid configuration of the objective Lamb classification method and the time periods under consideration. Splitting the 40-year period into four 10-year sub periods reveals that the first two sub periods 1961-1970 and 1971-1980 have a larger variability in circulation patterns, which cannot fully be captured by the AOGCM, especially for the late spring and summer period. The periods 1981-1990 and 1991-2000 are characterized by smaller biases in frequency occurrences, except of the months June and February in the two periods respectively.

This research not only shows that the use of a circulation classification technique provides a rather simple methodology to detect changes and differences in circulation patterns on a synoptic time-scale, it also shows that the use of Lamb circulation patterns is an appropriate tool for AOGCM evaluation, in order to detect biases in the global model, which should be considered when the AOGCM is applied for specific impact studies, as was done in Chapter 7 of this dissertation. Here, the AOGCM mean is replaced by the observed mean, for the present-day climate, and a similar approach is used to correct for the future climate based on the present-day AOGCM results. Often a more straightforward and popular procedure for rapid impact assessment, such as "change factors" or

"perturbation factors", is used (Prudhomme et al., 2002; Wilby, 2004). In this approach, a reference climatology is established for a specific region and variable, for e.g. the climatological 1960-1990 daily maximum temperature average. Secondly, the changes in the relevant GCM grid box closest to this target site are calculated between a future and present-day climate from the AOGCM (e.g. a difference of 5°C). Third, this difference is simply added to each day in the reference climate. Although this provides an areal average climate change for the grid-box of the GCM, incorporating the details of the station observations, there are some problems with this method. This method assumes that only the minima, maxima and means of the future climate change, whereas all other properties (e.g. variability) remain constant. This procedure also assumes a constant future spatial pattern, similar as the one in the present-day climate, and furthermore, this method assumes a correct representation of the AOGCM for the present-day climate. Clearly, this approach should be considered with caution, as AOGCMs still show inconsistencies for some variables. Moreover, some processes are highly non-linear in time, space and physical properties, and should therefore be treated appropriately. As already stated above, in order to avoid additional non-physical uncertainties in the process of local climate assessment studies, this urges for a further and continuous improvement of the present-day state-of-the-art AOGCMs.

Furthermore, it is worth mentioning that the formulation of clear reasons for the model biases found in this dissertation is out of the scope of this work. This can only be done by detailed sensitivity experiments that focus on the models responses to changes in physical parameterizations, model resolution, coupling to ocean, etc…. Nevertheless, in order to address these questions, one has to know the biases. Therefore, we hope that our approach is useful to determine circulation pattern specific model biases and can be helpful to the modellers' community.

8.4 Issues in dynamical downscaling

It is important to stress that this dissertation only tackles the impact of global climate change on future O_3 levels, thereby not taking into account future changes in anthropogenic emissions and disregarding other feedbacks that could play an important role. Future regional-scale ozone increases for example appear to be related to a drying out of soils and vegetated surfaces, leading to a reduced destruction of ozone. Others suggested that increased temperatures could lead to increased biogenic volatile organic compound (VOC) emissions (e.g. isoprenes), strengthening the regional-scale ozone formation. As tropospheric ozone is, after all, the third most important man-made greenhouse gas after CO_2 and methane, joint efforts should be done first to develop an integrated model setup, in order

to improve the quantification of air quality levels under changing climate conditions. Attention should be paid to a combined role of changing future (biogenic and anthropogenic) emissions and climatological conditions in order to set-up appropriate emission reduction measures to achieve acceptable future ozone levels, both on local, regional and the global scale.

This integrated approach, taking into account emission changes, feedbacks and other physical processes can only be done using a dynamical downscaling approach, hence meaning the nesting of regional climate models in global climate models for regional impact assessment studies. Thereby, the errors in the large-scale AOGCM (as described in 8.2) are transferred to the RCM, which itself has biases that are not necessarily lower. In this respect, some sensitivity experiments are performed in order to improve ARPS' urban thermal characteristics. These features are of importance in air quality modelling and downscaling studies because of their influence on the diurnal boundary layer height development and the dispersion, hence the concentration, of various air pollutants. Based on the measurements from the ESCOMPTE campaign, the mesoscale model ARPS was first evaluated for the 20-23rd of June 2001 period, in the Marseille Berre-Pond region (France). ARPS is shown to be able to reproduce the diurnal cycle of temperature, wind speed and direction and water vapour, as well for urban as for rural areas. For all parameters, the modelled errors are within the error limits defined for air quality modelling purposes. Subsequently, simulated surface heat fluxes were confronted with measurements from Marseille Centre, Meyrargues and two scintillometer observation sites. Overall, the simulated fluxes agree fairly well with the measurements, except for the sensible heat flux over the centre of Marseille and the urban scintillometer sites, which were largely underestimated. Therefore, sensitivity simulations were executed in order to test the impact of different thermal roughness length parameterizations and various thermal surface parameter values on the simulated sensible heat flux over urban portions of the domain. The analysis of these sensitivity simulations showed that the Zilitinkevich et al. (1992) thermal roughness length parameterization scheme, in combination with intermediate values for thermal admittance, give the best results compared to the observations. Moreover, comparisons with more complex models as for e.g. the TEB/ISBA and LUMPS scheme over the same terrain, show that by using this simple approach, a similar magnitude of flux errors compared to observations are obtained.

Next to the thermal characteristics, many other aspects, for e.g. the initial and boundary conditions, the parameterizations and resolution, contribute to a correct representation of the surface meteorology. Moreover, the heterogeneity of the earths' surface makes it hard to draw any firm uniform conclusions on the

results described in chapter 3. The findings are representative for the simulation of specific characteristics in the Marseille Berre-Pond Region and a week in June 2001, governed by a high-pressure system without rain. Although we expect the use of similar values of thermal roughness lengths and a similar thermal parameterization scheme to be adequate for densely constructed old European cities (similar to Marseille), it is clear that more research is required to settle this for other regions or cities, time periods and meteorological conditions. A first step in this direction is the MUSTI (Measuring urban surfaces' thermal inertia) project (PRODEX-PX/8/EO/14). Thereby, the objective of the MUSTI project is to retrieve thermal coefficients that characterize urban surfaces using diurnal time series of surface temperature as measured by the SEVIRI instrument (Spinning Enhanced Visible and Infrared Imager) onboard the MSG platform (Meteosat Second Generation), together with surface temperatures simulated by the ARPS atmospheric model. The targeted parameters are thermal conductivity, heat capacity, and thermal roughness length.

Of course this research is only part of a continuous ongoing research trying to produce reliable meteorological conditions with mesoscale models that, afterwards, can serve as input for air dispersion models. More research is planned to be done in the CLIMAQS project which main objective is to develop a very broad and generic knowledge platform in advanced atmospheric modelling, thereby aiming at medium- to long-term applicability of ARPS and AURORA (Air quality modelling in Urban Regions using an Optimal Resolution Approach) for policy support in the areas of climate change impacts and urban/regional air pollution.

8.5 The relevance of dynamical versus statistical downscaling in future air quality applications

At present, mesoscale and global models continue to improve their results in comparison to present-day observed data, with an increasing horizontal and vertical resolution and growing (international coordinated) efforts towards an online coupled meteorological - air dispersion approach (e.g. COST 728 – www.COST728.org). In the near future, we believe that, due to an increase in computing power and an improved understanding of the physical processes governing specific air quality episodes, meteorological-air quality model systems are converging towards a high-resolution online coupled integrated system, in which the necessary feedbacks are provided from the chemical transport model to the meteorological model and vice versa. Nevertheless, due to the fact that this dynamical approach is at present still computationally expensive, we have opt to continue this research using on a statistical

downscaling approach that is computational less demanding, more easy applicable and rapidly interpretable in terms of the physical linkages.

Comparative studies applying both dynamical and statistical downscaling tools on downscaling surface meteorological or environmental variables found divergence between the methods under various climate change forcings, but without systematic explanations for the magnitude of divergence. These intercomparison studies state that it is not possible to bring forward one method that returns more “correct” responses to external forcings of a possible climate compared to the other. Generally, it was suggested that a regional assessment of a specific variable could be improved by assessing multiple (both statistical and dynamical) downscaling methods for the same AOGCM, and research programs are encouraged that lead to rigorous intercomparisons of statistical downscaling methods and nested regional climate modelling methods.

Therefore, we believe that this study provides insight in the meteorological elements contributing to high O_3 concentrations in present-day and future climate conditions. Further research based on a dynamical downscaling method and focusing on the ‘correct’ representation of these meteorological variables believed to be important for O_3 production, should provide insight in other, more complex processes that can result in even higher or lower O_3 concentrations. In this way, it is clear, that, as long AOGCMs and RCMs do not provide the physical evidence of being reliable and applicable (in terms of spatial and temporal resolution) in a specific climatological and (or) environmental field, it is interesting to perform both statistical and dynamical downscaling methods, as both methods are complementary.

References

Agirre-Basurko, E., Ibarra-Berastegi, G. and Madariaga, I., 2006. Regression and multilayer perceptron-based models to forecast hourly O-3 and NO2 levels in the Bilbao area. Environmental Modelling & Software 21, 430-446.

Ainslie, B. and Steyn, D. G., 2007. Spatiotemporal trends in episodic ozone pollution in the Lower Fraser Valley, British Columbia, in relation to mesoscale atmospheric circulation patterns and emissions. Journal of Applied Meteorology and Climatology 46, 1631-1644.

Al-Alawi, S. M., Abdul-Wahab, S. A. and Bakheit, C. S., 2008. Combining principal component regression and artificial neural networks for more accurate predictions of ground-level ozone. Environmental Modelling & Software 23, 396-403.

Alcamo, J., Moreno, J. M., Nováky, B., Bindi, M., Corobov, R., Devoy, R. J. N., Giannakopoulos, C., Martin, E., Olesen, J. E. and Shvidenko, A., 2007. Europe. Climate Change 2007: Impacts, Adaptation and Vulnerability. Contribution of Working Group II to the Fourth Assessment Report of the Intergovernmental Panel on Climate Change, M.L. Parry, O.F. Canziani, J.P. Palutikof, P.J. van der Linden and C.E. Hanson, Eds. Cambridge University Press, Cambridge, UK, 541-580.

Alexandersson, H. and Moberg, A., 1997. Homogenization of Swedish temperature data .1. Homogeneity test for linear trends. International Journal of Climatology 17, 25-34.

Anderson R.J., 1993. A study of wind stress and heat flux over the open ocean by the inertial dissipation method. Journal of physical oceanography 23: 2153 – 2161.

Andersson, C. and Langner, J., 2007a. Inter-anual variations of ozone and nitrogen dioxide over europe during 1958-2003 simulated with a regional CTM. Water Air Soil Pollution.

Andersson, C., Langner, J. and Bergström, R., 2007b. Interannual variation and trends in air pollution over Europe due to climate variability during 1958-2001 simulated with a regional CTM coupled to the ERA40 reanalysis. Tellus Series a-Dynamic Meteorology and Oceanography 59B, 77-98.

Arya, S., 2001. Introduction to micrometeorology. Academic Press, Second edition.

Avise, J., Chen, J., Lamb, B., Wiedinmyer, C., Guenther, A., SalathÃ©, E. and Mass, C., 2008. Attribution of projected changes in US ozone and PM2.5 concentrations to global changes. Atmos. Chem. Phys. Discuss. 8, 15131-15163.

Barrero, M. A., Grimalt, J. O. and Canton, L., 2006. Prediction of daily ozone concentration maxima in the urban atmosphere. Chemometrics and Intelligent Laboratory Systems 80, 67-76.

Barry, R. G. and Perry, A. H., 1973. Synoptic climatology. Methuen, London, UK.

Bärtsch-Ritter, N., Keller, J., Dommen, J., Prévôt, A.S.H., 2003. Effects of various meteorological conditions and spatial emission resolutions on the ozone concentration & ROG/No_x limitation in the Milan area (I). Atmospheric chemistry and physics discussion 3: 733-768.

Beljaars, A. C. M. and Bosveld, F. C., 1997. Cabauw data for the validation of land surface parameterization schemes. Journal of Climate 10, 1172-1193.

Beck, C., 2000. Zirkulationdynamische Variabilität im bereich Nordatlantik-Europa seit 1780. Würzburger Geografische arbeiten Heft 95.

Beck, C., Jacobeit, J. and Jones, P. D., 2007. Frequency and within-type variations of large-scale circulation types and their effects on low-frequency climate variability in Central Europe since 1780. International Journal of Climatology 27, 473-491.

Benvenuto, F. and Marani, A., 2000. Nowcasting of urban air pollutants by neural networks. Nuovo Cimento Della Societa Italiana Di Fisica C-Geophysics and Space Physics 23, 567-586.

Bernard, S. M. and Ebi, K. L., 2001a. Comments on the process and product of the health impacts assessment component of the national assessment of the potential consequences of climate variability and change for the United States. Environmental Health Perspectives 109, 177-184.

Bernard, S. M., Samet, J. M., Grambsch, A., Ebi, K. L. and Romieu, I., 2001b. The potential impacts of climate variability and change on air pollution-related health effects in the United States. Environmental Health Perspectives 109, 199-209.

Bessembinder, J., 2007. Inventarisatie regionale klimaatscenario's in omringende landen. KNMI/Klimaat voor ruimte. Project CS7, The Netherlands.

Best, M.J., 2005. Representing urban areas within operational numerical weather prediction models. Boundary layer meteorology, 114: 91-109.

Biner, S., Caya, D., Laprise, R. and Spacek, L., 2000. Nesting of RCMs by imposing large scales. Research activities in Atmospheric and Oceanic Modelling, WMO/TD No. 987, Report No. 30.

Boukhris, O. L. F., Willems, P. and Vanneuille, W., 2008. The impact of climate change on the hydrology in highly urbanised Belgian areas. Proceedings of The International Urban Water Conference, Heverlee, Belgium, 15-19 September, 2008: Water and Urban Development Paradigms Towards an Integration of Engineering, Design and Management Approaches, Feyen, J. et al. (Ed.), 271-276.

Bridgeman, H. and O'Connor, J., 2007. Relationships between air pollution and meteorology in Newcastle, Australia. Proceedings of the 6th international conference on Urban Air Quality.

Brunekreef, B. and Holgate, S. T., 2002. Air pollution and health. Lancet 360, 1233-1242.

Brutsaert, W., 1982. Evaporation into the Atmosphere. D. Reidel, 229 pp.

Buchanan, C. M., Beverland, I. J., Heal, M. R., 2002. The influence of weather-type and long-range transport on air particle concentrations in Edinburgh, UK. Atmospheric Environment 36: 5343-5354.

Buishand,A., Brandsma,T., 1997. Comparison of circulation classification schemes for predicting temperature and precipitation in The Netherlands. International Journal of Climatology 17: 875-889.

Burger, G., 1996. Expanded downscaling for generating local weather scenarios. Climate Research 7, 111-128.

Cahill, A.T., Parlange, M.B., Albertson, J.D., 1997. On the brutsaert temperature roughness length model for sensible heat flux estimation. Water resources research 33(10): 3215-2324.

Campbell, G. G., Kittel, T. G. F., Meehl, G. A.,Washington. W. M., 1995. Low-Frequency Variability and Co2 Transient Climate-Change .2. Eof Analysis of Co2 and Model-Configuration Sensitivity. Global and Planetary Change 10: 201-216.

Cannon, A. J., Whitfield, P. H. and Lord, E. R., 2002. Synoptic map-pattern classification using recursive partitioning and principal component analysis. Monthly Weather Review 130, 1187-1206.

Cavazos, T., 1999. Large-scale circulation anomalies conducive to extreme precipitation events and derivation of daily rainfall in northeastern Mexico and southeastern Texas. Journal of Climate 12, 1506-1523.

Chaloulakou, A., Grivas, G. and Spyrellis, N., 2003a. Neural network and multiple regression models for PM10 prediction in Athens: A comparative assessment. Journal of the Air & Waste Management Association 53, 1183-1190.

Chaloulakou, A., Kassomenos, P., Spyrellis, N., Demokritou, P. and Koutrakis, P., 2003b. Measurements of PM10 and PM2.5 particle concentrations in Athens, Greece. Atmospheric Environment 37, 649-660.

Chan, N. Y., Stacey, M. T., Smith, A. E., Ebi, K. L. and Wilson, T. F., 2001. An empirical mechanistic framework for heat-related illness. Climate Research 16, 133-143.

Chen, J. L., Avise, J., Lamb, B. K., Salathé, E., Mass, C. F., Guenther, A., Wiedinmyer, C., Lamarque, J. F., O'Neill, S., McKenzie, D. and Larkin, N., 2008. The effects of global changes upon regional ozone pollution in the United States. Atmospheric Chemistry and Physics Disscussion 8, 15165-15205.

Cheng, S. Q. and Lam, K. C., 2000. Synoptic typing and its application to the assessment of climatic impact on concentrations of sulfur dioxide and nitrogen oxides in Hong Kong. Atmospheric Environment 34, 585-594.

Cheng, C. S. Q., Campbell, M., Li, Q., Li, G. L., Auld, H., Day, N., Pengelly, D., Gingrich, S. and Yap, D., 2007a. A synoptic climatological approach to assess climatic impact on air quality in South-central Canada. Part I: Historical analysis. Water Air and Soil Pollution 182, 131-148.

Cheng, C. S. Q., Campbell, M., Li, Q., Li, G. L., Auld, H., Day, N., Pengelly, D., Gingrich, S. and Yap, D., 2007b. A synoptic climatological approach to assess climatic impact on air quality in South-central Canada. Part II: Future estimates. Water Air and Soil Pollution 182, 117-130.

Chernoff H, Lehmann E.L., 1954. The use of maximum likelihood estimates in χ^2 tests for goodness-of-fit. The Annals of Mathematical Statistics 25: 579-586

Christensen, J. H et al., 2007. 2007: Regional Climate Projections." Climate Change 2007: The Physical Science Basis. Contribution of Working Group I to the Fourth Assessment Report of the Intergovernmental Panel on Climate Change [Solomon, S., D. Qin, M. Manning, Z. Chen, M. Marquis, K.B. Averyt, M. Tignor and H.L. Miller (eds.)]. Cambridge University Press, Cambridge, United Kingdom and New York, NY, USA.

Civerolo, K., Hogrefe, C., Lynn, B., Rosenthal, J., Ku, J.Y., Solecki, W., Cox, J., Small, C., Rosenzweig, C., Goldberg, R., Knowlton, K., Kinney, P., 2007. Estimating the effect of increased urbanization on surface meteorology and ozone concentrations in the New York City metropolitan region. Atmospheric environment 41 (9): 1803-1818.

Cobourn, W. G., Dolcine, L., French, M. and Hubbard, M. C., 2000. A comparison of nonlinear regression and neural network models for ground-level ozone forecasting. Journal of the Air & Waste Management Association 50, 1999-2009.

Cobourn, W. G., 2007. Accuracy and reliability of an automated air quality forecast system for ozone in seven Kentucky metropolitan areas. Atmospheric Environment 41, 5863-5875.

Collier, C.G., Davies, F., Bozier, K.E., Holt, A.R., Middleton, D.R., Pearson, G.N., Siemen, S., Willetts, D.V., Upton, G.J.G., Young, R.I., 2005. Dual Doppler lidar measurements for improving dispersion models. Bulletin of the American Meteorological Society 86, 825–838.

Comrie, A. C. and Yarnal, B., 1992a Relationships between Synoptic-Scale Atmospheric Circulation and Ozone Concentrations in Metropolitan Pittsburgh, Pennsylvania. Atmospheric Environment Part B-Urban Atmosphere 26, 301-312.

Comrie, A. C., 1992b An enhanced synoptic climatology of ozone using a sequencing technique. Physical Geography 13, 53 - 65.

Comrie, A. C., 1997. Comparing neural networks and regression models for ozone forecasting. Journal of the Air & Waste Management Association 47, 653-663.

Conway, D., Jones, P. D., 1998. The use of weather types and air flow indices for GCM downscaling. Journal of Hydrology 213(1-4): 348-361.

Corte-Real, J., Qian, B. D. and Xu, H., 1998. Regional climate change in Portugal: Precipitation variability associated with large-scale atmospheric circulation. International Journal of Climatology 18, 619-635.

Cros, B., Durand, P, Cachier, H., Drobinski, P., Frejafon, E., Kottmeier, C., Perros, P. E., Peuch, V. H., Ponche, J. L., Robin, D., Said, F., Toupance, G., Wortham, H., 2004. The ESCOMPTE program: an overview. Atmospheric Research 69(3-4): 241-279.

D'Andrea, F., Tibaldi, S., Blackburn, M., Boer, G., Déqué, M., Dix, M.R., Dugas, B., Ferranti, L., Iwasaki, T., Kitoh, A., Pope, V., Randall, D., Roeckner, E., Straus, D., Stern, W., Van den Dool, H., Williamson, D., 1998. Northern Hemisphere atmospheric blocking as simulated by 15 atmospheric general circulation models in the period 1979-1988. Climate Dynamics 14(6): 385-407.

Davies, T. D., Kelly, P. M., Low, P. S. and Pierce, C. E., 1992a. Surface Ozone Concentrations in Europe - Links with the Regional-Scale Atmospheric Circulation. Journal of Geophysical Research-Atmospheres 97, 9819-9832.

Davies, T. D., Farmer, G., Kelly, P. M., Glover, G. M., Apsimon, H. M. and Barthelmie, R. J., 1992b. Surface Pressure Pattern Indicators of Mean Monthly Pollutant Concentrations in Southern Scandinavian Precipitation - a Test Using Case-Studies of Months with High and Low Concentrations of Nonmarine Sulfate and Nitrate. Atmospheric Environment Part a-General Topics 26, 261-278.

Davies, F., Middleton, D.R., Bozier, K.E., 2007. Urban air pollution and measurements of boundary layer height. Atmospheric environment 41: 4040 – 4049.

Davis, J. M. and Speckman, P., 1999. A model for predicting maximum and 8 h average ozone in Houston. Atmospheric Environment 33, 2487-2500.

Dawson, J.P., Adams, P.J., Pandis, S.N., 2007a. Sensitivity of ozone to summertime climate in the eastern USA: A modelling case study. Atmospheric environment 41: 1494-1511.

Dawson, J.P., Adams, P.J., Pandis, S.N., 2007b. Sensitivity of $PM_{2.5}$ to climate in the eastern US: A modelling case study. Atmospheric chemistry and physics 7: 4295-4309.

De Bruin, H. A. R., and Holtslag, A. A. M., 1982. A simple parameterization of surface fluxes of sensible and latent heat during daytime compared with the Penman–Monteith concept. Journal of Applied Meteorology, 21**,** 1610–1621.

De Bruin, H.A.R., Van den Hurk, B.J.J.M., Kohsiek, W., 1995. The scintillation method tested over a dry vineyard area. Boundary layer meteorology 76: 25-40.
Delcloo, A. W. and De Backer, H., 2005. Modelling planetary boundary layer ozone, using meteorological parameters at Uccle and Payerne. Atmospheric Environment 39, 5067-5077.

Delcloo, A. W. and De Backer, H., 2008. Five day 3D back trajectory clusters and trends analysis of the Uccle ozone sounding time series in the lower troposphere (1969–2001). Atmospheric Environment 42, 4419–4432.

De Ridder, K., Schayes, G., 1997. The IAGL Land Surface Model. Journal of applied meteorology 36: 167 - 182.

De Ridder, K., 2006. Testing Brutsaert's temperature roughness parameterization for representing urban surfaces in atmospheric models. Geophysical research letters 30.

Demuzere, M., Werner, M., van Lipzig, N. P. M. and Roeckner, E., 2008a. An analysis of present and future ECHAM5 pressure fields using a classification of circulation patterns. International Journal of Climatology 29.

Demuzere, M., Trigo, R. M., Vila-Guerau de Arellano, J. and van Lipzig, N. P. M., 2008b. The impact of weather and atmospheric circulation on O3 and PM10 levels at a mid-latitude site. Atmos. Chem. Phys. Discuss. 8, 21037-21088.

Demuzere, M., van Lipzig, N.P.M., 2008c. A new method to assess air quality levels using a synoptic-regression approach. Part I: Present-day analysis for O_3 and PM_{10}. Atmopsheric environment (submitted).

Demuzere, M., van Lipzig, N.P.M., 2008d. A new method to assess air quality levels using a synoptic-regression approach. Part II: Future O_3 projections. Atmopsheric environment (submitted).

Deque, M., Jones, R. G., Wild, M., Giorgi, F., Christensen, J. H., Hassell, D. C., Vidale, P. L., Rockel, B., Jacob, D., Kjellstrom, E., de Castro, M., Kucharski, F. and van den Hurk, B., 2005. Global high resolution versus Limited Area Model climate change projections over Europe: quantifying confidence level from PRUDENCE results. Climate Dynamics 25, 653-670.

Dickinson, R. E., Errico, R. M., Giorgi, F. and Bates, G. T., 1989. A Regional Climate Model for the Western United-States. Climatic Change 15, 383-422.

Domonkos, P., Kysely, J., Piotrowicz, K., Petrovic, P. and Likso, T., 2003. Variability of extreme temperature events in South-Central Europe during the 20th century and its relationship with large-scale circulation. International Journal of Climatology 23, 987-1010.

EEA, 1995. CORINE Land Cover project, published by the Commission of European Communities.

Enke, W. and Spekat, A., 1997. Downscaling climate model outputs into local and regional weather elements by classification and regression. Climate Research 8, 195-207.

European Commission, 1994. CORINE land Cover Technical Guide. EUR 12585 EN, OPOCE Luxembourg.

Europan Union, 1999. Council Directive 1999/39/EC of 22 April 1999 regulating to limit values for sulphur dioxide, nitrogen dioxide and oxides of nitrogen, particulate matter and lead in ambient air. Official Journal of the European Communities L163 0041-0060.

European Union, 2005. The communication on Thematic strategy on air pollution and the directive on ambient air quality and cleaner air for Europe. Commission of the Europenian Union, Brussels.

European Union, 2008. Directive 2008/50/EC of the European Parliament and of the council of 21 May 2008 on ambient air quality and cleaner air for Europe. Official Journal of the European Union L 152/1.

Fan, H., Sailor, D.J., 2005. Modeling the impacts of anthropogenic heating on the urban climate of Philadelphia: a comparison of implementations in two PBL schemes. Atmospheric Environment 39 (2005) 73–84.

Flemming, J., Stern, R. and Yamartino, R. J., 2005. A new air quality regime classification scheme for O-3, NO2, SO2 and PM10 observations sites. Atmospheric Environment 39, 6121-6129.

Fowler, H.J., Kilsby, C.G., 2002. A weather-type approach to analyzing water resource drought in the Yorkshire region from 1881 to 1998. Journal of Hydrology 262: 177 – 192.
Garratt, J. R., 1992. The atmospheric boundary. University Press, Cambridge, 316 pp.

Gachon, P. and Dibike, Y., 2007. Temperature change signals in northern Canada: convergence of statistical downscaling results using two driving GCMs. International Journal of Climatology 27, 1623-1641.

Gardner, M. W. and Dorling, S. R., 1998. Artificial neural networks (the multilayer perceptron) - A review of applications in the atmospheric sciences. Atmospheric Environment 32, 2627-2636.

Gardner, M. W. and Dorling, S. R., 1999. Neural network modelling and prediction of hourly NOx and NO2 concentrations in urban air in London. Atmospheric Environment 33, 709-719.

Gardner, M. W. and Dorling, S. R., 2000. Meteorologically adjusted trends in UK daily maximum surface ozone concentrations. Atmospheric Environment 34, 171-176.

Garratt, J. R., 1992. The Atmospheric Boundary. 316pp., Univ. Press, Cambridge.

Gerstengarbe, F. W., Werner, P. C. and Rüge, U., 1999. Katalog der Grosswetterlagen Europas (1881-1998) nach Paul Hess unde Helmuth Brezowsky. Potsdam, Offenbach, a.M. (Germany) (http://www.pik-potsdam.de/~uwerner/gwl/welcome.htm).

Giorgi, F. and Meleux, F., 2007. Modelling the regional effects of climate change on air quality. Comptes Rendus Geoscience 339, 721-733.

Goodess, C.M. 2000. The construction of daily rainfall scenarios for Mediterranean sites using a circulation-type approach to downscaling. Ph.D. Thesis, University of East Anglia, pp486.

Goyal, P., Chan, A. T. and Jaiswal, N., 2006. Statistical models for the prediction of respirable suspended particulate matter in urban cities. Atmospheric Environment 40, 2068-2077.

Graedel, T. E., Bates, T. S., Bouwman, A. F., Cunnold, D., Dignon, J., Fung, I., Jacob, D. J., Lamb, B. K., Logan, J. A., Marland, G., Middleton, P., Pacyna, J. M., Placet, M. and Veldt, C., 1993. A Compilation of Inventories of Emissions to the Atmosphere. Global Biogeochemical Cycles 7, 1-26.

Grell, G. A., Peckham, S. E., Schmitz, R., McKeen, S. A., Frost, G., Skamarock, W. C., Eder, B., 2005. Fully coupled "online" chemistry within the WRF model. Atmospheric Environment 39 (37): 6957-6975.

Grimmond, S., Cleugh, H. A., Oke, T.R., 1991. An objective heat storage model and its comparison with other schemes. Atmospheric Environment., 25B**,** 311–326.

Grimmond, C.S.B. , Oke, T.R., 1999. Heat storage in urban areas: local-scale observations and evaluation of a simple model. Journal of applied meteorology 38: 922-940.

Grimmond, C.S.B. and T.R. Oke 2002. Turbulent heat fluxes in urban areas: Observations and local-scale urban meteorological parameterization scheme (LUMPS). Journal of Applied Meteorology, 41: 792-810.

Grimmond, C.S.B, Salmond, J.A., Oke, T.R., Offerle, B., Lemonsu, A., 2004. Flux and turbulence measurements at a densely built-up site in Marseille: Heat, mass (water and carbon dioxide) and momentum. Journal of Geophysical Research – Atmosphere 109(D24).

Grivas, G. and Chaloulakou, A., 2006. Artificial neural network models for prediction of PM10 hourly concentrations, in the Greater Area of Athens, Greece. Atmospheric Environment 40, 1216-1229.

Guicherit, R. and Van Dop, H., 1977. Photochemical production of ozone in western Europe (1971-1975) and its relation to meteorology. Atmospheric Environment 11, 145-155.

Gutman, G., Ignatov, A., 1998. Derivation of green vegetation fraction from NOAA/AVHRR for use in weather prediction models. International Journal of Remote Sensing, 19: 1533-1543.

Hafner, J. and Kidder, S.Q., 1999. Urban heat island monitoring in conjunction with satellite-derived surface/soil parameters. Journal of applied meteorology 38: 448-465.

Hamdi, R., Schayer, G., 2005, Validation of the Martilli's Urban Boundary Layer Scheme with measurements from two mid-latitude European cities. Atmospheric chemistry and physics Discussion, 5, 4257–4289.

Harrison, R. M., Deacon, A. R., Jones, M. R. and Appleby, R. S., 1997. Sources and processes affecting concentrations of PM10 and PM2.5 particulate matter in Birmingham (UK). Atmospheric Environment 31, 4103-4117.

Hartogensis, O., K., C. J. Watts, C.J., Rodriguez, J. C., De Bruin, H. A. R., 2003. Derivation of an Effective Height for Scintillometers: La Poza Experiment in Northwest Mexico. Journal of meteorology 4: 915-928.

Hayhoe, K., Cayan, D., Field, C. B., Frumhoff, P. C., Maurer, E. P., Miller, N. L., Moser, S. C., Schneider, S. H., Cahill, K. N., Cleland, E. E., Dale, L., Drapek, R., Hanemann, R. M., Kalkstein, L. S., Lenihan, J., Lunch, C. K., Neilson, R. P., Sheridan, S. C. and Verville, J. H., 2004. Emissions pathways, climate change, and impacts on California. Proceedings of the National Academy of Sciences of the United States of America 101, 12422-12427.

Heald, C. L., Henze, D. K., Horowitz, L. W., Feddema, J., Lamarque, J. F., Guenther, A., Hess, P. G., Vitt, F., Seinfeld, J. H., Goldstein, A. H. and Fung, I., 2008. Predicted change in global secondary organic aerosol concentrations in response to future climate, emissions, and land use change. Journal of Geophysical Research-Atmospheres 113, -.

Hewitt, C. D. and Griggs, D., 2004. Ensembles-based Predictions of Climate Changes and their Impacts. Eos 85, 566.

Hoerling, M. P., Hurrell, J. W.,Xu, T. Y., 2001. Tropical origins for recent North Atlantic climate change. Science 292: 90-92.

Hooyberghs, J., Mensink, C., Dumont, G., Fierens, F. and Brasseur, O., 2005. A neural network forecast for daily average PM10 concentrations in Belgium. Atmospheric Environment 39, 3279-3289.

Hooyberghs, J., Mensink, C., Dumont, G., Fierens, F., 2006. Spatial interpolation of ambient ozone concentrations from sparse monitoring points in Belgium. Journal of Environmental Monitoring 8:1129-1135.

Hope, P. K., 2006. Projected future changes in synoptic systems influencing southwest Western Australia. Climate Dynamics 26, 765-780.

Hu, Z. Z.,Wu, Z., 2004. The intensification and shift of the annual North Atlantic Oscillation in a global warming scenario simulation. Tellus Series a-Dynamic Meteorology and Oceanography 56: 112 - 124.

Hubbard, M. C. and Cobourn, W. G., 1998. Development of a regression model to forecast ground-level ozone concentration in Louisville, KY. Atmospheric Environment 32, 2637-2647.

Hurrell, J. W. and VanLoon, H., 1997. Decadal variations in climate associated with the north Atlantic oscillation. Climatic Change 36, 301-326.

Huth, R., 1999. Statistical downscaling in central Europe: evaluation of methods and potential predictors. Climate Research 13, 91-101.

Huth, R., Kysely, J. and Dubrovsky, M., 2001. Time structure of observed, GCM-simulated, downscaled, and stochastically generated daily temperature series. Journal of Climate 14, 4047-4061.

Huth, R., Kliegrova, S. and Metelka, L., 2008. Non-linearity in statistical downscaling: does it bring an improvement for daily temperature in Europe? International Journal of Climatology 28, 465-477.
Huth, R., Beck, C., Philipp, A. Demuzere, M. Ustrnul, Z., Cahynová, M., Kyselý, K., Tveito, O.E., 2008. Classifications of atmospheric circulation patterns: recent advances and applications, Annals of the New York Academy of sciences (in press).

Hurrell, J.W., 1995. Decadal trends in the North Atlantic Oscillation and relationships to regional temperature and precipitation. Science 269: 676-679.

Hurrell, J. W., Hoerling, M. P., Phillips, A. S., Xu, T., 2004. Twentieth century North Atlantic climate change. Part 1: assessing determinism. Climate Dynamics 23 (3-4): 371-389.

Huth, R., 1997, Continental-scale circulation in the UKHI GCM. Journal of Climate: 10: 1545-1561.

Huth, R., 2000. A circulation classification scheme applicable in GCM studies. Theoretical and Applied Climatology 67(1-2): p. 1-18.

Huth, R., 2001. Disaggregating climatic trends by classification of circulation patterns. International Journal of Climatology 21, 135-153.

Huth, R., Kliegrova, S. and Metelka, L., 2008b. Non-linearity in statistical downscaling: does it bring an improvement for daily temperature in Europe? International Journal of Climatology 28, 465-477.

Ichinose, T., Shimodozono, K., Hanaki, K., 1999. Impact of anthropogenic heat on urban climate in Tokyo. Atmospheric Environment, 33(24 – 25), 3897– 3909.

Incropera, F. P. and DeWitt, D. P., 1990. Introduction to Heat Transfer. John Wiley & Sons.

IPCC, 1996. Revised 1996 IPCC Guidelines for national greenhouse gas inventories.

IPCC, 2001. Climate Change 2001: Synthesis Report. A Contribution of Working Groups I, II, and III to the Third Assessment Report of the Integovernmental Panel on Climate Change [Watson, R.T. and the Core Writing Team (eds.)]. Cambridge University Press, Cambridge,United Kingdom, and New York, NY, USA, 398 pp.

Intergovernmental Panel on Climate Change (IPCC), 2007. the Physical Science Basis, Contribution of Working Group I to the Fourth Assessment Report of the IPCC, 2007, Available online from http://www.ipcc.ch.

Isaaks, E.H., Srivastava, R.M., 1989. An introduction to applied geostatistics. Oxford university Press, New York.

Jacobson, M. Z., 2008. On the causal link between carbon dioxide and air pollution mortality. Geophysical Research Letters 35, -.

Janssen, S., Dumont, G., Fierens, F., Mensink, C, 2008. Spatial interpolation of air pollution measurements using CORINE land cover data. Atmospheric Environment 42:4884-4903.

Jenkins, G. J., Perry, M. C. and Prior, M. J., 2007. The climate of the United Kingdom and recent trends. Met Office Hadley Centre, Exeter, UK.

Jenkinson, A.F., Collison, F.P., 1977. An initial climatology of gales over the North Sea. Synoptic Climatology Branch Memorandum 62: Meteorological Office, London.

Jol, A., Kielland, G. (Eds.), 1997. Air Pollution in Europe 1997, European Environment Agency, Copenhagen.

Jones, P.D., Hulme, M., Briffa, K.R., 1993. A comparison of Lamb circulation types with an objective classification scheme. International Journal of Climatology 13, 655-663.

Jones, P.W., 1999. First- and second-order conservative remapping schemes for grids in spherical coordinates. Monhtly weather review, 127, 2204-2211.

Jungclaus, J. H., Keenlyside, N., Botzet, M., Haak, H., Luo, J. J., Latif, M., Marotzke, J., Mikolajewicz, U. and Roeckner, E., 2006. Ocean circulation and tropical variability in the coupled model ECHAM5/MPI-OM. Journal of Climate 19, 3952-3972.

Kalkstein, L. S. and Corrigan, P., 1986. A Synoptic Climatological Approach For Geographical Analysis: Assessment of Sulfur Dioxide Concentrations. Annals of the Association of American Geographers 76, 381-395.

Kalkstein, L. S., Nichols, M. C., Barthel, C. D. and Greene, J. S., 1996. A new spatial synoptic classification: Application to air-mass analysis. International Journal of Climatology 16, 983-1004.

Kanda, M., Kawai, T., Kanega, M., Moriwaki, R., Narita, K., Hagishima, A., 2005. A simple energy balance model for regular building arrays. Boundary layer meteorology, 16: 423 – 443.

Karl, T. R., Wang, W. C., Schlesinger, M. E., Knight, R. W. and Portman, D., 1990. A Method of Relating General-Circulation Model Simulated Climate to the Observed Local Climate .1. Seasonal Statistics. Journal of Climate 3, 1053-1079.

Kassomenos, P. A., Sindosi, O. A., Lolis, C. J. and Chaloulakou, A., 2003. On the relation between seasonal synoptic circulation types and spatial air quality characteristics in Athens, Greece. Journal of the Air & Waste Management Association 53, 309-324.

Kato, S., Yamaguchi, Y, 2005. Analysis of urban heat-island effect using ASTER and ETM+ Data: Separation of anthropogenic heat discharge and natural heat radiation from sensible heat flux. Remote Sensing of the environment 99(1-2): 44-54.

Keevallik, S. and Russak, V., 2001. Changes in the amount of low clouds in Estonia (1955-1995). International Journal of Climatology 21, 389-397.

Khaliq, M. N., and Ouarda, T. B. M. J., 2007. On the critical values of the standard normal homogeneity test (SNHT). International Journal of Climatology *27*:681-687.

Kruskal, H. and Wallis, W. A., 1952. Use of ranks in one-criterion variance analysis. Journal of the American Statistical Association 47, 583-621.

Kukkonen, J., Partanen, L., Karppinen, A., Ruuskanen, J., Junninen, H., Kolehmainen, M., Niska, H., Dorling, S., Chatterton, T., Foxall, R. and Cawley, G., 2003. Extensive evaluation of neural network models for the prediction of NO2 and PM10 concentrations, compared with a deterministic modelling system and measurements in central Helsinki. Atmospheric Environment 37, 4539-4550.

Kunkel, K. E., Huang, H. C., Liang, J. Y., Lin, J. T., Wuebbles, D. J., Tao, Z., Williams, A., Caughey, M., Zhu, J. and Hayhoe, K., 2007. Sensitivity of future ozone concentrations in the northeast USA to regional climate change. . Mitig. Adapt. Strat. Glob. Change. doi:10.1007/s11027-007-9137-y.

Kysely, J., 2002. Temporal fluctuations in heat waves at Prague-Klementinum, the Czech Republic, from 1901-97, and their relationships to atmospheric circulation. International Journal of Climatology 22, 33-50.

Kysely, J. and Domonkos, P., 2006. Recent increase in persistence of atmospheric circulation over Europe: Comparison with long-term variations since 1881. International Journal of Climatology 26, 461-483.

Kysely, J. and Huth, R., 2006. Changes in atmospheric circulation over Europe detected by objective and subjective methods. Theoretical and Applied Climatology 85, 19-36.

Kysely, J., 2007. Implications of enhanced persistence of atmospheric circulation for the occurrence and severity of temperature extremes. International Journal of Climatology 27, 689-695.

Lagouarde, J. P., Irvine,M., Bonnefond, J.M., Grimmond, C. S. B., Long, N., Oke, T. R., Salmond, J., Offerle, B., 2002. Sensible heat flux estimated over the city of Marseille, using a LAS scintillometer. Preprints, Fourth Symp. on the Urban Environment, Norfolk, VA, Amer. Meteor. Soc., 215–216.

Lamb, H. H., 1972. British Isles Weather Types and a Register of Daily Sequence of Circulation Patterns, 1861-1971. Geophysical Memoir 116: HMSO, London (UK),

85 pp.

Lasry, F., Coll, I. and Buisson, E., 2005. An insight into the formation of severe ozone episodes: modeling the 21/03/01 event in the ESCOMPTE region. Atmospheric Research 74, 191-215.

Latif, M., Arpe, K.,Roeckner, E., 2000. Oceanic control of decadal North Atlantic sea level pressure variability in winter. Geophysical Research Letters 27: 727-730.

Leathers, D. J. and Ellis, A. W., 1996. Synoptic mechanisms associated with snowfall increases to the Lee of Lakes Erie and Ontario. International Journal of Climatology 16, 1117-1135.

Lemonsu, A., Grimmond, C. S. B., Masson, V., 2004. Modelling the Surface Energy Balance of an Old Mediterranean City Core. Journal of Applied Meteorology: 43, 312–327.

Li, X. S. and Sailor, D., 2000. Application of tree-structured regression for regional precipitation prediction using general circulation model output. Climate Research 16, 17-30.

Liao, H., Chen, W. T. and Seinfeld, J. H., 2006. Role of climate change in global predictions of future tropospheric ozone and aerosols. Journal of Geophysical Research-Atmospheres 111, -.

Lin, J. T., Patten, K. O., Hayhoe, K., Liang, X. Z. and Wuebbles, D. J., 2008. Effects of future climate and biogenic emissions changes on surface ozone over the United States and China. Journal of Applied Meteorology and Climatology 47, 1888-1909.

Loptien, U., Ruprecht, E., 2005. Effect of synoptic systems on the variability of the North Atlantic Oscillation. Monthly Weather Review 133: 2894-2904.

Lu, H. C., Hsieh, J. C. and Chang, T. S., 2006. Prediction of daily maximum ozone concentrations from meteorological conditions using a two-stage neural network. Atmospheric Research 81, 124-139.

Ma, J., Daggupaty, S. M., 2000. Using all observed information in a variational approach to measuring *z0m* and *z0t*. Journal of applied meteorology, 39: 1391-1401.

Mahmud, A., Tyree, M., Cayan, D., Nehzat, M. and Kleeman, M. J., 2008. Statistical downscaling of climate change impacts on ozone concentrations in California. Journal of Geophysical Research 113,

Mahrt, L., Sun, J., MacPherson, J. I., Jensen, N. O., Desjardins, R. L., 1997, Formulation of surface heat flux: Application to BOREAS. Journal of Geophysical Research 102: 29641-29649.

Mahrt, L., Vickers, D., 2002. Relationship of area-averaged carbon dioxide and water vapour fluxes to atmospheric variables. Agriculture and forest meteorology 112, 195-202.

Makar, A., Gravel, S., Chirkov, V., Strawbridge, K.B., Froude, F., Arnold, J., Brook, J., 2006. Heat flux, urban properties, and regional weather, Atmospheric Environment, 40, 2750-2766.

Marshall, J., Kushnir, Y., Batisti, D., Chang, P., Czaja, R., Dicson, R., Hurrell, J., McCartney, M., Saravanan, R., Visbeck, M., 2001. North Atlantic climate variability: phenomena, impacts and mechanisms. Journal of Climatology 21: 1863-1898.

Marsland, S. J., Haak, H., Jungclaus, J. H., Latif, M., Röske, F., 2003. The Max-Planck-Institute global ocean/sea ice model with orthogonal curvilinear coordinates. Ocean Modelling 5 (2): 91-127.

Martilli, A., Clappier, A., Rotach, M.W., 2002. An urban surface exchange parameterisation for mesoscale models. Boundary-Layer Meteorology 104(2): 261-304.

Masson, V., Grimmond,, C.S.B., Oke, T.R., 2002. Evaluation of the Town Energy Balance (TEB) scheme with direct measurements from dry districts in two cities. Journal of Applied Meteorology 41(10): 1011-1026.

McAneney, K.J., Green, A.E., Astill, M.S., 1995. Large-aperture scintillometry: the homogenous case. Agricultural and forest meteorology 76: 149-162.

Mckendry, I. G., 1994. Synoptic Circulation and Summertime Ground-Level Ozone Concentrations at Vancouver, British-Columbia. Journal of Applied Meteorology 33, 627-641.

McKendry, I.G., Stahl, K., Moore, R.D., 2006. Synoptic sea-level pressure patterns generated by a general circulation model: comparison with the types derived from NCEP/NCAR re-analysis and implications for downscaling. International Journal of Climatology 26, 1727-1736.

Mearns, L. O., Giorgi, F., Whetton, P., Pabon, D., Hulme, M. and Lal, M., 2003. Guidelines for use of climate scenarions developed from regional climate model experiments. Data distribution centre of the international panel of climate change, 38 pp. Available from IPCC-DCC: http://www.ipcc-data.org,

Medina, S., Plasencia, A., Ballester, F., Mucke, H. G., Schwartz, J. and group, A., 2004. Apheis: public health impact of PM10 in 19 European cities. Journal of Epidemiology and Community Health 58, 831-836.

Mestayer, P. G., Durand, P., Augustin, P., Bastin, S., Bonnefond, J. M., Benech, B., Campistron, B., Coppalle, A., Delbarre, H., Dousset, B., Drobinski, P., Druilhet, A., Frejafon, E., Grimmond, C. S. B., Groleau, D., Irvine, M., Kergomard, C., Kermadi, S., Lagouarde, J. P., Lemonsu, A., Lohou, F., Long, N., Masson, V., Moppert, C., Noilhan, J., Offerle, B., Oke, T. R., Pigeon, G., Puygrenier, V., Roberts, S., Rosant, J., Said, F., Salmond, J., Talbaut, M., Voogt, J., 2005. The urban boundary-layer field campaign in Marseille (UBL/CLU-ESCOMPTE): Set-up and first results. Boundary-Layer Meteorology: 114, 315-365.

Michou, M.P., Laville, P., Serca, D., Fotiadi, A., Bouchou, P., Peuch, V. H., 2005. Measured and modelled dry deposition velocities over the ESCOMPTE area. Atmospheric Research 74, 89-116.

Mondal, R., Sen, G. K., Chatterjee, M., Sen, B. K. and Sen, S., 2000. Ground-level concentration of nitrogen oxides (NOx) at some traffic intersection points in Calcutta. Atmospheric Environment 34, 629-633.

Murphy, A. H., 1988. Skill scores based on the mean square error and their relationship to the correlation coefficient. Monthly weather review 116, 2417-2424.

Nolte, C. G., Gilliland, A. B., Hogrefe, C. and Mickley, L. J., 2008. Linking global to regional models to assess future climate impacts on surface ozone levels in the United States. Journal of Geophysical Research-Atmospheres 113.

Norusis, M. J., 2002. SPSS 11.0 guide to data analysis. Upper saddle River, NJ: Prentice Hall.

NRC, 1991. Human exposure assessment for airborne pollution: advances and opportunities. Washington DC National Acadamy Press.

Nunnari, G., Nucifora, A. F. M. and Randieri, C., 1998. The application of neural techniques to the modelling of time-series of atmospheric pollution data. Ecological Modelling 111, 187-205.

Oanh, N. T. K., Chutimon, P., Ekbordin, W. and Supat, W., 2005. Meteorological pattern classification and application for forecasting air pollution episode potential in a mountain-valley area. Atmospheric Environment 39, 1211-1225.

Offerle, B., Grimmond, C.S.B, Fortuniak, K., Klysik, K., Oke, T.R., 2006. Temporal variations in heat fluxes over a central European city. Theoretical and applied climatology 84: 13-115.

Oke, T.R., 1987. Boundary Layer Climate. 2nd edition, Methuen, London.

Osborn, T.J., Briffa, K.R., Tett, S. F. B., Jones, P.D., Trigo, R.M., 1999. Evaluation of the North Atlantic Oscillation as simulated by a coupled climate model. Climate Dynamics 15: 685-702.

Oshima, N., Kato, H. and Kadokura, S., 2002. An application of statistical downscaling to estimate surface air temperature in Japan. Journal of Geophysical Research-Atmospheres 107, -.

Otte, T. L., 2005. Linking the Eta Model with the Community Multiscale Air Quality (CMAQ) Modeling System to build a National Air Quality Forecasting System (vol 20, pg 367, 2005). Weather and Forecasting 20, 700-700.

Papalexiou, S., Moussiopoulos, N., 2006. Wind flow and photochemical air pollution in Thessaloniki, Greece. Part II: Statistical evaluation of European Zooming Model's simulation results. Environmental Modelling & Software 21: 1752-1758.

Papanastasiou, D. K., Melas, D. and Kioutsioukis, I., 2007. Development and assessment of neural network and multiple regression models in order to predict PM10 levels in a medium-sized mediterranean city. Water Air and Soil Pollution 182, 325-334.

Perez, P., Trier, A. and Reyes, J., 2000. Prediction of PM2.5 concentrations several hours in advance using neural networks in Santiago, Chile. Atmospheric Environment 34, 1189-1196.

Perez, P., 2001. Prediction of sulfur dioxide concentrations at a site near downtown Santiago, Chile. Atmospheric Environment 35, 4929-4935.

Pigeon, G., Legain, D., Durand, P., Masson, V., 2007. Anthropogenic heat release in an old European agglomeration (Toulouse, France). International Journal of Climatology, 27: 1969-1981.

Piringer, M., Joffre, S., 2005. The urban surface energy budget and mixing height in European cities: data, models, and challenges for urban meteorology and air quality. In: Piringer, M., Joffre, S. (Eds.), Final Report of Working group 2 of COST 715 Action. Demetra Ltd. Publishers, Bulgaria, p. 216.

Post, P., Truija, V., Tuulik, J., 2002. Circulation weather types and their influence on temperature and precipitation in Estonia. Boreal Environmental. Research 7: 281 – 289.

Priestley, C.H.B., 1959. Turbulent transfer in the lower atmosphere. Chicago, University of Chicago Press.
Prudhomme, C., Reynard, N. and Crooks, S., 2002. Downscaling of global climate models for flood frequency analysis: where are we now? Hydrological Processes 16, 1137-1150.

Pye, H. O. T., Liao, H., Wu, S., Mickley, L. J., Joacob, D. J., Henze, D. K. and Seinfeld, J. H., (in press). Effects of changes in climate and emissions of future sukfate-nitrate-ammonium aerosol levels in the United States. Journal of Geophysical Research-Atmospheres

Racherla, P. N. and Adams, P. J., 2006. Sensitivity of global tropospheric ozone and fine particulate matter concentrations to climate change. Journal of Geophysical Research-Atmospheres 111, -.

Racherla, P. N. and Adams, P. J., 2008. The response of surface ozone to climate change over the Eastern United States. Atmospheric Chemistry and Physics 8, 871-885.

Racsko, P., Szeidl, L. and Semenov, M., 1991. A Serial Approach to Local Stochastic Weather Models. Ecological Modelling 57, 27-41.

Raible, C.C., Blender, R., 2004. Northern hemisphere midlatitutde cyclone variability in GCM simulations with different ocean representations. Climate Dynamics 22: 239-248.

Raible, C. C., Stocker, T. F., Yoshimori, M., Renold, M., Beyerle, U., Casty, C., Luterbacher, J., 2005. Northern hemispheric trends of pressure indices and atmospheric circulation patterns in observations, reconstructions, and coupled GCM simulations. Journal of climate 18: 3968-3982.

Raible, C. C., 2007. On the relation between extremes of midlatitude cyclones and the atmospheric circulation using ERA40, Geophysical Research Letters 34: 1-6.

Randall, D. A., Wood, R. A., Bony, S., Colman, R., Fichefet, T., Fyfe, J., Kattsov, V., Pitman, A., Shukla, J., Srinivasan, J., Stouffer, R. J., Sumi, A. and Taylor, K. E., 2007. Climate Models and Their Evaluation. In: Climate Change 2007: The Physical Science Basis. Contribution of Working Group I to the Fourth Assessment Report of the Intergovernmental Panel on Climate Change [Solomon, S., D. Qin, M. Manning, Z. Chen, M. Marquis, K.B. Averyt, M.Tignor and H.L. Miller (eds.)]. Cambridge University Press, Cambridge, United Kingdom and New York, NY, USA.

Reich, S. L., Gomez, D. R. and Dawidowski, L. E., 1999. Artificial neural network for the identification of unknown air pollution sources. Atmospheric Environment 33, 3045-3052.

Reis, S., Simpson, D., Friedrich, R., Jonson, J. E., Unger, S. and Obermeier, A., 2000. Road traffic emissions - predictions of future contributions to regional ozone levels in Europe. Atmospheric Environment 34, 4701-4710.

Richardson, C. W., 1981. Stochastic Simulation of Daily Precipitation, Temperature, and Solar-Radiation. Water Resources Research 17, 182-190.

Roberts, S.M., Oke, T.R., Grimmond, C.S.B., Voogt, J.A., 2006. Comparison of four methods to estimate urban heat storage. Journal of applied meteorology and climatology 45: 1766-1781.

Roeckner, E., Bäuml, G., Boneventura, L., Brokopf, R., Esch, M., Girogetta, M., Hagemann, S., Kirchner, I., Kornblueh, L., Manzini, E., Schlese, U., Schulzweida, U. and Tompkins, A., 2003. The atmospheric general circulation model ECHAM5 part I: Model Description. [available from Max Planck Institute for Meteorology, Bundesstr. 53, 20146, Hamburg, Germany].

Roeckner, E., Brokopf, R., Esch, M., Girogetta, M., Hagemann, S., Kornblueh, L., Manzini, E., Schlese, U. and Schulzweida, U., 2004. The atmospheric general circulation model ECHAM5 part II: Sensitivity of simulated climate to horizontal and vertical resolution. Report no. 354, Hamburg (Germany).

Roeckner, E., Brokopf, R., Esch, M., Giorgetta, M., Hagemann, S., Kornblueh, L., Manzini, E., Schlese, U. and Schulzweida, U., 2006a. Sensitivity of simulated climate to horizontal and vertical resolution in the ECHAM5 atmosphere model. Journal of Climate 19, 3771-3791.

Roeckner, E., Brasseur, G.P., Giorgetta, M., Jacob, D., Jungclaus, J., Reick, C. and Sillmann., J., 2006b. Climate projections for the 21st century. Max Planck Institute for Meteorology, Internal Report, 28 pp [available from Max Planck Institute for Meteorology, Bundesstr. 53, 20146, Hamburg, Germany].

Rogers, J.C., 1997. North Atlantic storm track variability and its association to the North Atlantic Oscillation and climate variability of Northern Europe. Journal of Climate 10: 1635-1647.

Sabins, F. F., 1997. Introduction to Remote Sensing. W. H. Freeman & Co.

Sailor, D. J., Lu, L., 2004. A top-down methodology for developing diurnal and seasonal anthropogenic heating profiles for urban areas. Atmospheric Environment, 38(17), 2737–2748.

Santer, B. D., Wigley, T. M. L., Boyle, J. S., Gaffen, D. J., Hnilo, J. J., Nychka, D., Parker, D. E. and Taylor, K. E., 2000. Statistical significance of trends and trend differences in layer-average atmospheric temperature time series. Journal of Geophysical Research-Atmospheres 105, 7337-7356.

Sarrat, C., A. Lemonsu, A., Masson, V., Guedalia , D., 2006. Impact of urban heat island on regional atmospheric pollution. Atmospheric Environment 40: 1743-1758.

Satsangi, G. S., Lakhani, A., Kulshrestha, P. R. and Taneja, A., 2004. Seasonal and diurnal variation of surface ozone and a preliminary analysis of exceedance of its critical levels at a semi-arid site in India. Journal of Atmospheric Chemistry 47, 271-286.

Schaap, M., Apituley, A., Koelemeijer, R. B. A., Timmermans, R. M. A., Schoemaker, R., Mathijssen, J. and de Leeuw, G., 2008. On the relation between aerosol optical depth and PM2.5 in the Netherlands. SATLINK final report, Report 555034003, AH Bilthoven, 2008

Schar, C., Vidale, P. L., Luthi, D., Frei, C., Haberli, C., Liniger, M. A., Appenzeller, C., 2004. The role of increasing temperature variability in European summer heatwaves. Nature 427: 332-336.

Scherrer, S. C., Croci-Maspoli, M., Schwierz, C., Appenzeller, C. 2006. Two-dimensional indices of atmospheric blocking and their statistical relationship with winter climate patterns in the Euro-Atlantic region. International Journal of Climatology 26(2): 233-249.

Schlink, U., Herbarth, O., Richter, M., Dorling, S., Nunnari, G., Cawley, G. and Pelikan, E., 2006. Statistical models to assess the health effects and to forecast ground-level ozone. Environmental Modelling & Software 21, 547-558.

Schlünzen, H., Katzfey, J.J., 2003. Relevance of sub-grid-scale land-use effects for mesoscale models. Tellus 55A: 232-246.

Schwierz, C., Appenzeller, C., Davies, H.C., Liniger, M.A., Muller, W., Stocker, T. F., Yoshimori, M., 2006. Challenges posed by and approaches to the study of seasonal-to-decadal climate variability. Climatic Change 79 (1-2): 31-63.

Seaman, N.L., 2000. Meteorological modeling for air-quality assessments. Atmospheric environment 34: 2231-2259.

Seaman, N.L., 2003. Future directions of meteorology to air-quality research. Environmental International 29: 245-252.

Seinfeld, J. H. and Pandis, S. N., 1998. Atmospheric chemistry and physics from air pollution to climate change. New York: John Wiley & Sons, Inc.

Semazzi, F., 2003. Air quality research: perspective from climate change modelling research. Environment International 29, 253-261.

Serreze, M.C., Carse, F., Barry, R.G., Rogers, J.C., 1997. Icelandic low cyclone activity: climatological features, linkages with the NAO, and relationships with recent changes in the Northern Hemisphere circulation. Journal of Climate 10: 453-464.

Sickmöller, M., Blender, R., Fraedrich, K., 2000. Observed winter cyclone tracks in the Northern Hemisphere in re-analyzed ECMWF-data. Quaternary Journal of the Royal Meteorology Society 126: 591-620.

Sillman, S., 1999. The relation between ozone, NOx and hydrocarbons in urban and polluted rural environments. Atmospheric Environment 33, 1821-1845.

Sillman, S. and He, D. Y., 2002. Some theoretical results concerning O-3-NOx-VOC chemistry and NOx-VOC indicators. Journal of Geophysical Research-Atmospheres 107, -.

Skelly, W. C. and Henderson-Sellers, A., 1996. Grid box or grid point: What type of data do GCMs deliver to climate impacts researchers? . International Journal of Climatology 16, 1079-1086.

Sliggers, S., Kakebeeke, W. e. and Europe, U. N. E. C. f., 2004. Clearing the air: 25 years of the Convention on Long-range Transboundary Air Pollution. United Nations, Geneva, Switzerland.

Slini, T., Kaprara, A., Karatzas, K. and Moussiopoulos, N., 2006. PM10 forecasting for Thessaloniki, Greece. Environmental Modelling & Software 21, 559-565.

Smith, R. L., Davis, J. M., Sacks, J., Speckman, P. and Styer, P., 2000. Regression models for air pollution and daily mortality: analysis of data from Birmingham, Alabama. Environmetrics 11, 719-743.

Sousa, S. I. V., Martins, F. G., Alvim-Ferraz, M. C. M. and Pereira, M. C., 2007. Multiple linear regression and artificial neural networks based on principal components to predict ozone concentrations. Environmental Modelling & Software 22, 97-103.

Stadlober, E., Hormann, S. and Pfeiler, B., 2008. Quality and performance of a PM10 daily forecasting model. Atmospheric Environment 42, 1098-1109.

Styer, P., Mcmillan, N., Gao, F., Davis, J. and Sacks, J., 1995. Effect of Outdoor Airborne Particulate Matter on Daily Death Counts. Environmental Health Perspectives 103, 490-497.

Taha, H., 1997. Urban climates and heat islands: Albedo, evapotranspiration and anthropogenic heat. Energy buildings 25: 99-103.

Taha, H., 1999. Modifying a mesoscale meteorological model to better incorporate urban heat storage: a bulk-parameterization approach. Journal of Applied Meteorology 38, 466–473.

Tarasova, O. A., Brenninkmeijer, C. A. M., Jockel, P., Zvyagintsev, A. M. and Kuznetsov, G. I., 2007. A climatology of surface ozone in the extra tropics: cluster analysis of observations and model results. Atmospheric Chemistry and Physics 7, 6099-6117.

Taylor, K. E., 2007. Climate Models and Their Evaluation. In: Climate Change 2007: The Physical Science Basis. Contribution of Working Group I to the Fourth Assessment Report of the Intergovernmental Panel on Climate Change [Solomon, S., D. Qin, M. Manning, Z. Chen, M. Marquis, K.B. Averyt, M.Tignor and H.L. Miller Sliggers, Kakebeeke and Europe,]. Cambridge University Press, Cambridge, United Kingdom and New York, NY, USA.

Thode, H., 2002. Testing for normality. Marcel Dekker, New York.

Tibaldi, S., 1993. Low frequency variability and blocking as diagnostic tools for global change models. In: Shukla J (ed) Prediction of Interannual Climate Variations. NATO-ASI series 1 6: Springer-Verlag, Berlin Heidelberg New York, pp 173-182

Trigo, R.M., Dacamara, C.C., 2000. Circulation weather types and their influence on the precipitation regime in Portugal. International Journal of Climatology 20: 1559–1581.

Trigo, R. M. and Palutikof, J. P., 2001. Precipitation scenarios over Iberia: A comparison between direct GCM output and different downscaling techniques. Journal of Climate 14, 4422-4446.

Trigo, R.M., Osborn, T.J., Corte-Real, J.M., 2002. The North Atlantic Oscillation influence on Europe: climate impacts and associated physical mechanisms. Climate Research 20, 91-17.

Trigo, R. M., Trigo, I. F., DaCamara, C. C.,Osborn, T. J., 2004. Climate impact of the European winter blocking episodes from the NCEP/NCAR Reanalyses. Climate Dynamics 23: 17-28.

Troufleau, D. Lhomme, J. P., Monteny, B., Vidal, A., 1997. Sensible heat flux and radiometric surface temperature over sparse Sahelian vegetation. I. An experimental analysis of the *kB-1* parameter. Journal of Hydrology 188-189: 815-838.

Tulet, P., Crassier, V. and Rosset, R., 2000. Air pollution modelling at a regional scale. Environmental Modelling & Software 15, 693-701.

Ulbrich, U., Christoph, M., 1999. A shift in the NAO and increasing storm track activity over Europe due to anthropogenic greenhouse gas. Climate Dynamics 15: 551-559.

Unger, N., Shindell, D. T., Koch, D. M., Amann, M., Cofala, J. and Streets, D. G., 2006. Influences of man-made emissions and climate changes on tropospheric ozone, methane, and sulfate at 2030 from a broad range of possible futures. Journal of Geophysical Research-Atmospheres 111, -.

Uppala, S. M., Allberg, K., Simmons, P. W., Andrae, A. J., Da Costa, U., Bechtold, V., Fiorino, M., Gibson, J. K., Haseler, J., Hernandez, A., Kelly, G. A., Li, X., Onogi, K., Saarinen, S., Sokka, N., Allan, R. P., Andersson, E., Arpe, K., Balmaseda, M. A., Beljaars, A. C. M., Van De Berg, L., Bidlot, J., Bormann, N., Caires, S., Chevallier, F., Dethof, A.,

Dragosavac, M., Fisher, M., Fuentes, M., Hagemann, S., H´olm, E., Hoskins, B. J., Isaksen, L., Janssen, P. A., E. M., Jenne, R., Mcnally, A. P., Mahfouf, J.-F., Morcrette, J.-J., Rayner, N. A., Saunders, R., W., Simon, P., Sterl, A., Trenberth, K. E., Untch, A., Vasiljevic, D., Viterbo, P., Woollen, J., 2005. The ERA-40 re-analysis. Quaternary Journal of the Royal Meteorological Society 131: 2961-3012.

van der Wal, J. T. and Janssen, L. H. J. M., 2000. Analysis of spatial and temporal variations of PM 10 concentrations in the Netherlands using Kalman filtering. Atmospheric Environment 34, 3675-3687.

van Ulden, A. P. and van Oldenborgh, G. J., 2006. Large-scale atmospheric circulation biases and changes in global climate model simulations and their importance for climate change in Central Europe. Atmospheric Chemistry and Physics, 6: 863-881.

Van Weverberg, K., De Ridder, K. and Van Rompaey, A., 2008. Modeling the contribution of the brussels heat island to a long temperature time series. Journal of Applied Meteorology and Climatology 47, 976-990.

Verstraeten, G., Poesen, J., Demarée, G., Salles, C., 2006. Long-term (105 years) variability in rain erosivity as derived from 10-min rainfall depth data for Ukkel (Brussels, Belgium): Implications for assessing soil erosion rates. Journal of Geophysical Research 111: 1-11.

Vicente-Serrano, S. M. and Lopez-Moreno, J. I., 2006. The influence of atmospheric circulation at different spatial scales on winter drought variability through a semi-arid climatic gradient in Northeast Spain. International Journal of Climatology 26, 1427-1453.

Von Storch, H., 1999. On the Use of ‘‘Inflation’’ in Statistical Downscaling. Journal of Climate 12, 3505-3506.

von Storch, H., Langenberg, H. and Feser, F., 2000. A spectral nudging technique for dynamical downscaling purposes. Monthly weather review 128, 3664-3673.

Voogt J.A., Grimmond, C.S.B., 2000. Modeling surface sensible heat flux using surface radiative temperatures in a simple urban area. Journal of Applied Meteorology 39, 1679-1699.

Vukovich, F. M., 1995. Regional-Scale Boundary-Layer Ozone Variations in the Eastern United-States and Their Association with Meteorological Variations. Atmospheric Environment 29, 2259-2273.

Vukovich, F. M., 1998. Aspects of subregional ozone variations in the SOS region. Atmospheric Environment 32, 3881-3889.

Vukovich, F. M. and Sherwell, J., 2003. An examination of the relationship between certain meteorological parameters and surface ozone variations in the Baltimore-Washington corridor. Atmospheric Environment 37, 971-981.

Wagner, D., 1999. Assessment of the probability of extreme weather events and their potential effects in large conurbations. Atmospheric Environment 33, 4151-4155.

Warneck, P., 1998. Chemistry of the Natural Atmosphere. 2nd ed., International Geophysics Series Vol.71, Academic Press, New York
Welty, J. R., 1974. Engineering Heat Transfer. Wiley.

Werner, P. C., Gerstengarbe, F. W., Fraedrich, K. and Oesterle, H., 2000. Recent climate chance in the North Atlantic/European sector. International Journal of Climatology 20, 463-471.

Wilby, R. L. and Wigley, T. M. L., 1997. Downscaling general circulation model output: a review of methods and limitations. Progress in Physical Geography 21, 530-548.

Wilby, R. L., Hay, L. E. and Leavesley, G. H., 1999. A comparison of downscaled and raw GCM output: implications for climate change scenarios in the San Juan River basin, Colorado. Journal of Hydrology 225, 67-91.

Wilby, R. L., Charles, S. P., Zorita, E., Timbal, B., Whetton, P. and Mearns, L. O., 2004. Guidelines for use of climate scenarios developed from the statistical downscaling methods. available from the DDC of IPCC TGCIA, 27 pp. Available from: IPCC-DDC: http://www.ipcc-data.org,

Wilks, D. S., 1995. Statistical Methods in the Atmospheric Sciences. Academic Press, San Diego.

Willmott, C.J, 1981. On the validation of models. Physical Geography, 2(2), 184-194.

Willmott, C.J, 1982. Some comments on the evaluation of model performance. Bulletin of the American Meteorological Society, **63(**11), 1309-1313.

Willmott, C.J., Matsuura, K., 2005., Advantages of the mean absolute error (MAE) over the root mean square error (RMSE) in assessing average model performance. Climate Research, 30(1), 79-82.

Wise, E. K. and Comrie, A. C., 2005. Meteorologically adjusted urban air quality trends in the Southwestern United States. Atmospheric Environment 39, 2969-2980.

Wittich K-P, Hansing, O., 1995. Area-averaged vegetative cover fraction estimated from satellite data. International Journal of Biometeorology 38: 209–215.

WHO, 2000. Air quality guidelines for Europe. 2nd ed. Copenhagen, World Health Organization Regional Office for Europe, 2000 (WHO Regional Publications, European Series No. 91).

WHO, 2005. World Health Organisation air quality guidelines for particulate matter, ozone, nitrogen dioxide and sulfur dioxide, global update 2005, Summary of risk assessment. World Health Organization Regional Office for Europe.

Xue, M., Droegemeier, K. K., Wong, V., 2000. The Advanced Regional Prediction System (ARPS) - A multi-scale nonhydrostatic atmospheric simulation and prediction model. Part I: Model dynamics and verification. Meteorology and atmospheric physics 75 (3-4): 161-193.

Xue, M., Droegemeier, K. K., Wong, V., Shapiro, A., Brewster, K., Carr, F., Weber, D., Liu, Y., Wang, D., 2001. The Advanced Regional Prediction System (ARPS) - A multi-scale nonhydrostatic atmospheric simulation and prediction model. Part II: Model physics and applications. Meteorology and atmospheric physics 76 (3-4): 143-165.

Yarnal, B., 1993. Synoptic climatology in environmental analysis. London: Belhaven Press

Zeng, X.B., Dickinson, R.E., 1998. Effect of subsurface sublayer on surface skin temperature and fluxes. Journal of climate 11(4): 537-550.

Zhang, F. Q., Bei, N. F., Nielsen-Gammon, J. W., Li, G. H., Zhang, R. Y., Stuart, A. and Aksoy, A., 2007. Impacts of meteorological uncertainties on ozone pollution predictability estimated through meteorological and photochemical ensemble forecasts. Journal of Geophysical Research-Atmospheres 112, -.

Zilitinkevich, S.S., 1970. Dynamics of the Atmospheric boundary layer. Leningrad Gidrometeor, 291 pp.

Zilitinkevich, S.S., Fedorevich, E.E., Shabalova, M.V., 1992. Numerical-Model of a Nonsteady Atmospheric Planetary Boundary-Layer, Based on Similarity Theory. Boundary-Layer Meteorology 59(4): 387-411.

Zorita, E. and von Storch, H., 1999. The analog method as a simple statistical downscaling technique: Comparison with more complicated methods. Journal of Climate 12, 2474-2489.

Yarnal, B., 1993. Synoptic climatology in environmental analysis. London: Belhaven Press.